IMAGING OF PLATELET ACTIN NODULE DYNAMICS WITH HIGH SPATIAL AND TEMPORAL RESOLUTION

By

Amy Davies

UNIVERSITY OF BIRMINGHAM

A thesis submitted to the University of Birmingham for the degree of

DOCTOR OF PHILOSOPHY

PSIBS Doctoral Training Centre

School of Chemistry

College of Physical Sciences

University of Birmingham

September 2013

ABSTRACT

Platelets play a critical role in haemostasis and through platelet adhesion and aggregation ensure the integrity of the cardiovascular system is maintained in the event of an injury. The actin cytoskeleton plays a pivotal role in mediating the massive shape change involved in platelet spreading, aggregation and clot retraction at sites of injury. The formation of actin structures, such as filopodia, lamellipodia and stress fibres, are well characterised in platelets but little is known about the role of a recently characterised actin structure, referred to as the actin nodule. Investigating the actin nodules relied on fixed cell studies but live cell studies would greatly enhance our understanding of the role of actin nodules in platelets. However, introduction of fluorescent actin labels to human platelets for live cell imaging studies is currently not possible. Therefore, the aims of this thesis are to characterise the actin nodule and elucidate their role in platelet spreading. To achieve this, platelets from the Lifeact-GFP transgenic mouse were used. For human platelets, the intracellular delivery of the actin label, Lifeact, into human platelets using pH (low) insertion peptide was investigated. Additionally, the use of fluorescent labels and luminescent europium coated gold nanoparticles is explored as potential labels for multimodal imaging of human platelet actin nodule dynamics.

Through live cell imaging studies of Lifeact-GFP mouse platelets, I have characterised actin nodules in mouse platelets as a transient, surface-proximal, stationary actin structure which requires actin polymerisation downstream of SFK activity and the presence of Arp 2/3 complex. Additionally, their co-localisation with αIIb staining and, from previous work in our lab, with vinculin, talin and paxillin suggest a role for the actin nodule in platelet adhesion.

I have also demonstrated that pHLIP is able to deliver Lifeact and luminescent europium coated gold nanoparticles into the cytoplasm of human platelets. Once delivered, Lifeact was able to label the actin cytoskeleton and consequently this represents a step forward in the ability to image actin dynamics in human platelets. Finally, I have shown that gold nanoparticles can be functionalised with multiple moieties and that they are suitable as labels for multiple imaging modalities.

Publications arising from work presented in this thesis:

Davies, A., Lewis, D. J., Watson, S. P., Thomas, S. G. & Pikramenou, Z. 2012. pH-controlled delivery of luminescent europium coated nanoparticles into platelets. *Proceedings of the National Academy of Sciences,* 109**,** 1862-1867.

Work from this thesis was presented at the following conferences:

UK Platelet Meeting, Nottingham. June 2010

"Application of TIRF Microscopy to Study Platelet Spreading"

(Poster)

Actin 2010, Bristol. December 2010

"Integrin αIIbβ3 and actin nodule dynamics: using Lifeact and TIRFM to study platelet spreading"

(Poster)

Conference on Methods and Applications of Fluorescence: Spectroscopy, Imaging and Probes, Strasbourg. September 2011

"Delivery of luminescent gold nanoparticles into human platelets using a pH-controlled strategy"

(Poster)

Royal Society of Chemistry Younger Members Symposium 2012, Nottingham. June 2012

"Delivery of luminescent gold nanoparticles into human platelets using a pH-controlled strategy"

(Talk)

Irène Joliot-Curie Conference, Warwick. October 2012

"Delivery of luminescent gold nanoparticles into human platelets using a pH-dependent method"

(Poster)

ACKNOWLEDGEMENTS

Firstly I would like to thank my supervisors Dr Steve Thomas and Prof Zoe Pikramenou for their support, encouragement and guidance throughout my PhD. I would also like to thank Prof Steve Watson for his encouragement and guidance. Additionally, I would like to thank all the staff involved in PSIBS Doctoral Training Centre.

I would also like to thank the University of Birmingham for providing lab space and the Physical Sciences of Imaging in the Biomedical Sciences (PSIBS) Engineering and Physical Sciences Research Council (EPSRC) Doctoral Training Centre for funding. Equipment funding was also received through Birmingham Science City: Innovative Uses for Advanced Materials in the Modern World (West Midlands Centre for Advanced Materials Project 2), with support from Advantage West Midlands (AWM) and part funded by the European Regional Development Fund (ERDF). The Nikon A1R confocal / TIRF microscope used in this research was obtained, through Birmingham Science City Translational Medicine Clinical Research and Infrastructure Trials Platform, with support from Advantage West Midlands (AWM).

I would like to thank all the members of the platelet group, past and present, especially those who donated blood, took blood and bled the mice for me, which greatly facilitated my research. I enjoyed working in the lab and/or office with you all. I also want to thank all the members of the Pikramenou group, both past and present. I had a lot of fun working in the group and also enjoyed group coffee breaks and nights out, including the chemistry balls. Finally, I would like to thank the many members of PSIBS. Everyone is friendly and encouraging of each other's work. Without you, my PhD would not have been the same.

I would like to thank all my friends for their support. Most especially, I would like to thank Jen. Doing our PhD's at the same time may have made for a slightly strange and stressed out house but I loved every minute of it. The "legendary" parties that were often followed by sofa-bound hangovers, film nights and moaning about work helped to balance out the many peaks and troughs of a PhD. I'd like to thank Dave, a great friend who has supported me and looked out for me throughout my PhD.

I am grateful for all the support I received from all of my family. In particular, I would like to thank my sister Francine and my brothers Rhys and Trystan for all their love and support throughout my many years at university. You will all be pleased to know that I'm finally done "collecting" degrees! I'd also like to thank my nieces, Jamie and Eleri, although they are too young at present to understand, they never fail to cheer me up and their curiosity inspires me. Finally, Mam and Dad: without your love, support, encouragement and belief in me, I would not be where I am today, thank you. To you both, I dedicate this thesis.

CONTENTS

LIST OF FIGURES

LIST OF TABLES

ABBREVIATIONS

aa	Amino acid
ABP140	Actin Binding Protein 140
ACD	Acid citrate dextrose
ADP	Adenosine diphosphate
ATP	Adenosine triphospate
AuNP	13 nm gold nanoparticles
CPP	Cell-penetrating peptide
CRM	Confocal reflection microscopy
DMF	Dimethylformamide
DMSO	Dimethylsulphoxide
ECM	Extracellular matrix
ERM proteins	Ezrin, radixin and moesin proteins
Eu	Europium
EuL	Luminescent europium complex
EuL•AuNP	EuL coated gold nanoparticles
F-actin	Filamentous actin
FAM	Carboxyflourescein
G-actin	Globular actin
GFP	Green fluorescent protein
HPLC	High-performance liquid chromatography
ICP-OES	Inductively coupled plasma optical emission sectrometry
Lifeact	17 amino acid actin binding protein

Lifeact•AuNP	Lifeact coated gold nanoparticles
MALDI	Matrix-assisted laser desorption/ ionisation
PBS	Phosphate buffered saline
PGI_2	Prostacyclin
pHLIP	pH (low) insertion peptide
pHLIP•AuNP	pHLIP coated gold nanoparticles
pHLIP•EuL•AuNP	pHLIP and EuL coated gold nanoparticles
pHLIP-Lifeact	pHLIP conjugated to Lifeact-FAM via a disulphide bond
pHLIP-Lifeact•AuNP	pHLIP-Lifeact coated gold nanoparticles
PRP	Platelet rich plasma
ROCK	Rho-associated protein kinase
SFK	Src family kinases
SPDP	*N*-succinimidyl 3-(2-pyridyldithio)propionate
SPR	Surface plasmon resonance
TCEP	Tris(2-carboxyethyl)phosphine hydrochloride
TIRF microscopy	Total internal reflection fluorescence microscopy
UV-Vis	Ultraviolet – Visible light
VWF	von Willebrand factor
WASp	Wiskott Aldrich Syndrome proteins

CHAPTER 1

GENERAL INTRODUCTION

1.1 INTRODUCTION

Delivery of substances, drugs, proteins, DNA, imaging probes to name but a few, into cells is of great interest to many areas of the life sciences. Whether the interest is in the area of treating illnesses, such as cancer, by effective and targeted delivery of drugs or in elucidating the many functions of a given cell type via biochemical assays and various imaging modalities, they all share a similar end in requiring a suitable method of delivery to perform the desired task. There are many different types of delivery systems available or under investigation, from the complex polymer spheres enabling cell targeting or time-dependent release in whole organisms to the simple method of membrane permeablisation of *ex vivo* or *in vitro* cell cultures. This work is concerned with delivery of imaging agents into cells, in particular platelets, to enable imaging of platelet dynamics with high spatial and temporal resolution.

1.2 PLATELETS

1.2.1 Platelet Overview

Platelets are small (0.5 – 3 μm), anucleate cells that circulate in the peripheral blood and play a critical role in haemostasis. Their small size means they are marginalised to the the edge of the vessel by the red blood cells. Their position next to the endothelium enables them to quickly respond to damage, arresting any or further blood loss. As well as their role in thrombosis formation, platelets are also implicated in other processes including, inflammation, bacteria removal and metastasis of cancer through their interaction with neutrophils (Weksler, 1983, Bazzoni et al., 1991, Tang et al., 2002, Wong et al., 2013, Jurasz et al., 2004, Takagi et al., 2013).

Platelets are produced in the bone marrow by their multi-nucleated precursor cells, megakaryocytes, which are descended from haematopoietic stem cells (Hartwig and Italiano, 2003). The cells produce long protrusions referred to as pro-platelets from which platelets bud. The process of platelet release from pro-platelets is not fully understood but it is believed that pro-platelet formation occurs in the osteobalstic niche. The pro-platelets protrude through the endothelial cells, enabling release of platelets directly into the vasculature. Each cell generates 2000 - 3000 platelets.

Due to their anucleate state, these cells have a short lifespan, 7 – 10 days, in the circulating blood and have very limited protein synthesis (Watson and Harrison, 2007). Platelets contain many signalling proteins and surface receptors which result in high sensitivity of platelets to external stimulus. This enables fast activation and subsequent rapid aggregation and clot

formation, following vessel wall damage (Figure 1.2.1). Consequently, arresting blood loss through the damaged vessel.

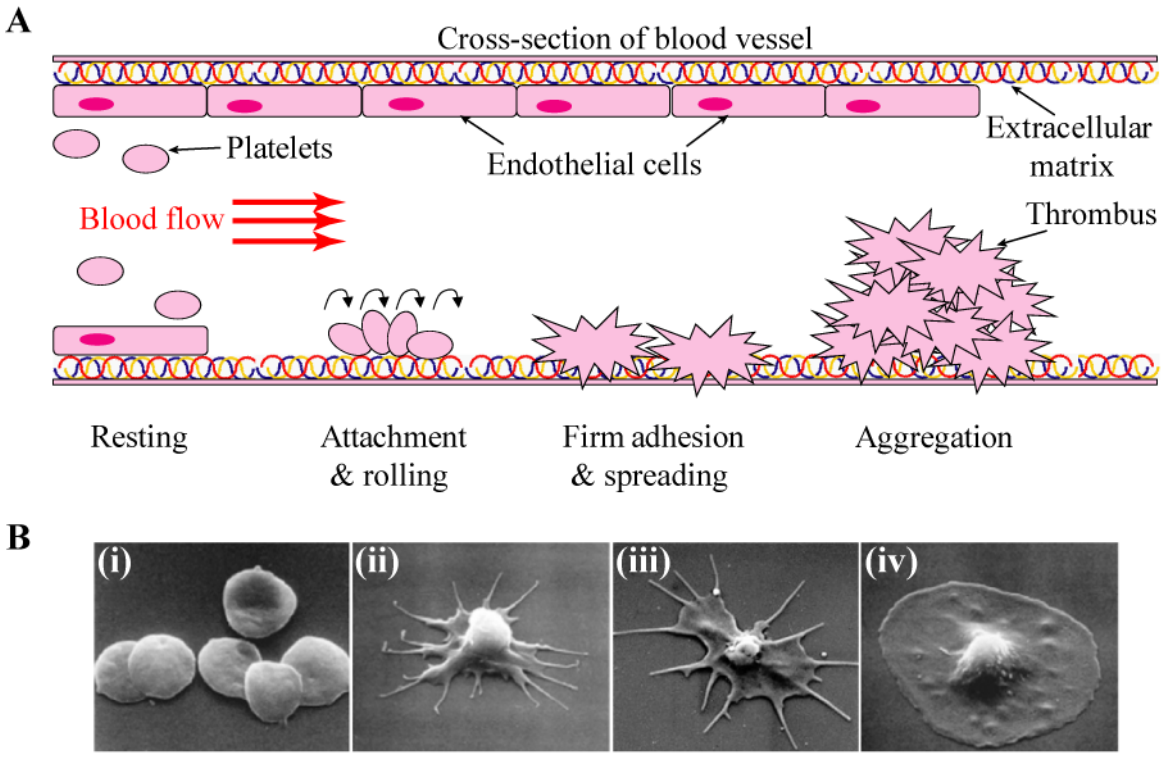

Figure 1.2.1. Platelet function. (A) Schematic representation of platelet activation upon blood vessel damage. (B) Representative scanning electron microscopy images of platelets at various stages; (i) resting, (ii) attachment, (iii) firm adhesion and spreading and (iv)fully spread. Images adapted from; (i, ii, iv) – (Vallenius, 2004) and (iii) - www.acbd.monash.org

1.2.2 Platelet structure

The megakaryocyte produces all the platelet-specific proteins, organelles and membrane systems found in platelets. The platelet contains many of the same organelles as most cells, including lysosymes, mitochondria and actin filaments and tubules of the cytoskeleton but they do not contain a nucleus (Figure 1.2.2). They also contain dense granules, α-granules and an open canalicular system.

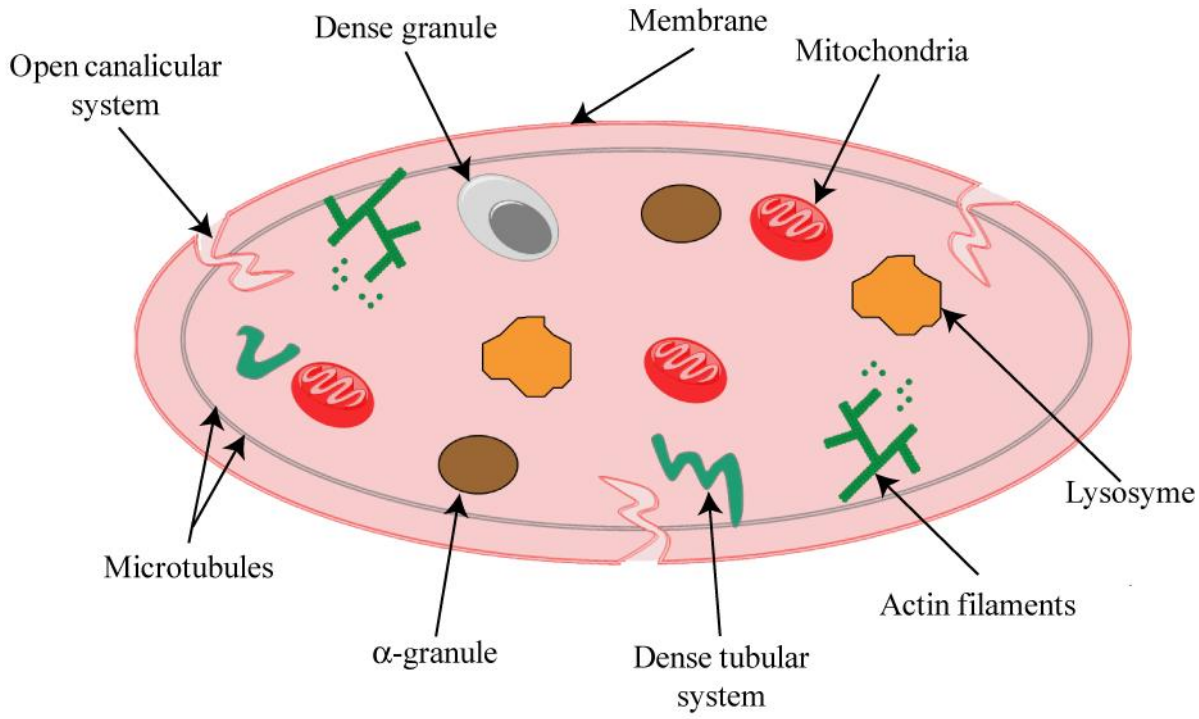

Figure 1.2.2. Schematic representation of the platelet structure.

Each human platelet contains; a few lysosomes, 50 to 80 α-granules, which contain more than 300 secretable proteins, including adhesion molecules, such as P-selectin, chemokines, cytokines, fibrinolytic regulators, immunologic modulators and a variety of coagulation, compliment, growth, proangiogenic and antiangiogenic factors and three to eight dense (δ-) granules, these contain mostly small molecules, including calcium, magnesium, polyphosphate, ATP, ADP, GTP, GDP, and serotonin (Kahr, 2009).

Platelets have an open canalicular system (OCS) which is a reservoir of membrane that is evaginated when the platelet spreads, as such, contributing to the increase in surface area to volume ratio of the platelets (White and Clawson, 1980). This membrane is a series of interconnected tubes that are in contact with the external environment.

1.2.3 Platelet activation and thrombus formation

The platelet membrane contains many receptor proteins to multiple agonists (Figure 1.2.3). These surface receptor proteins transmit signals from the extracellular environment to the cell interior. In platelets there are two categories of surface receptors; G protein-coupled receptors, GPCRs, and tyrosine kinase-linked receptors:

GPCR receptors. The seven transmembrane proteins in the GPCR class induce platelet activation through a G protein. Included in this class of proteins are; $P2Y_{12}$, protease activated receptor 1, PAR1, thromboxane A_2 receptor, TxA_2R, and prostacyclin receptor, PGI_2R which bind ADP, thrombin, TxA_2 and PGI_2, respectively.

Tyrosine kinase-linked receptors. The platelet receptors in the tyrosine kinase-linked receptors category signal through activation of tyrosine kinases such as Src and Syk. Included in this class of proteins are; GPVI and GPIb-IX-V which bind collagen and von Willebrand factor, VWF, respectively, and integrins, including αIIbβ3 and α2β1. αIIbβ3 is the most prolific membrane protein on the platelet and mediates binding of fibrinogen and VWF and α2β1 is the main platelet collagen receptor (Phillips et al., 2001, Clemetson and Clemetson, 2001).

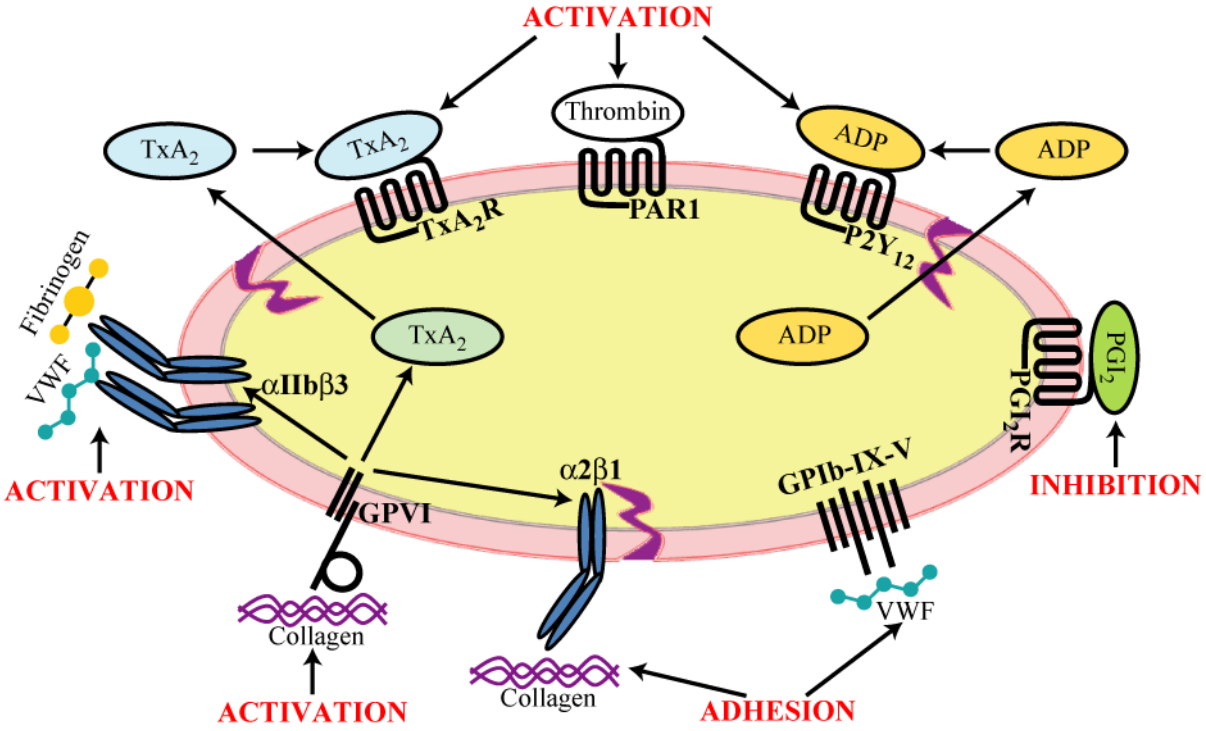

Figure 1.2.3. Schematic representation of platelet activation through various platelet surface receptors.

While circulating in the blood, the platelets are kept in their resting state by the production and release of nitric oxide, NO, heparin and prostacyclin, PGI_2, by the endothelial cells of the blood vessels. These inhibitors prevent activation and binding of platelets to the healthy endothelium. Damage to the endothelium exposes the basement membrane which contains matrix proteins including, collagen and laminin. Collagen is considered to be the most thrombogenic constistuent of vessel wall. Activation of platelets leads to occlusion of the exposed subendothelial matrix, consequently preventing further blood loss. Platelet activation occurs via a defined sequence of events (Figure 1.2.4) (Varga-Szabo et al., 2008, Rivera et al., 2009).

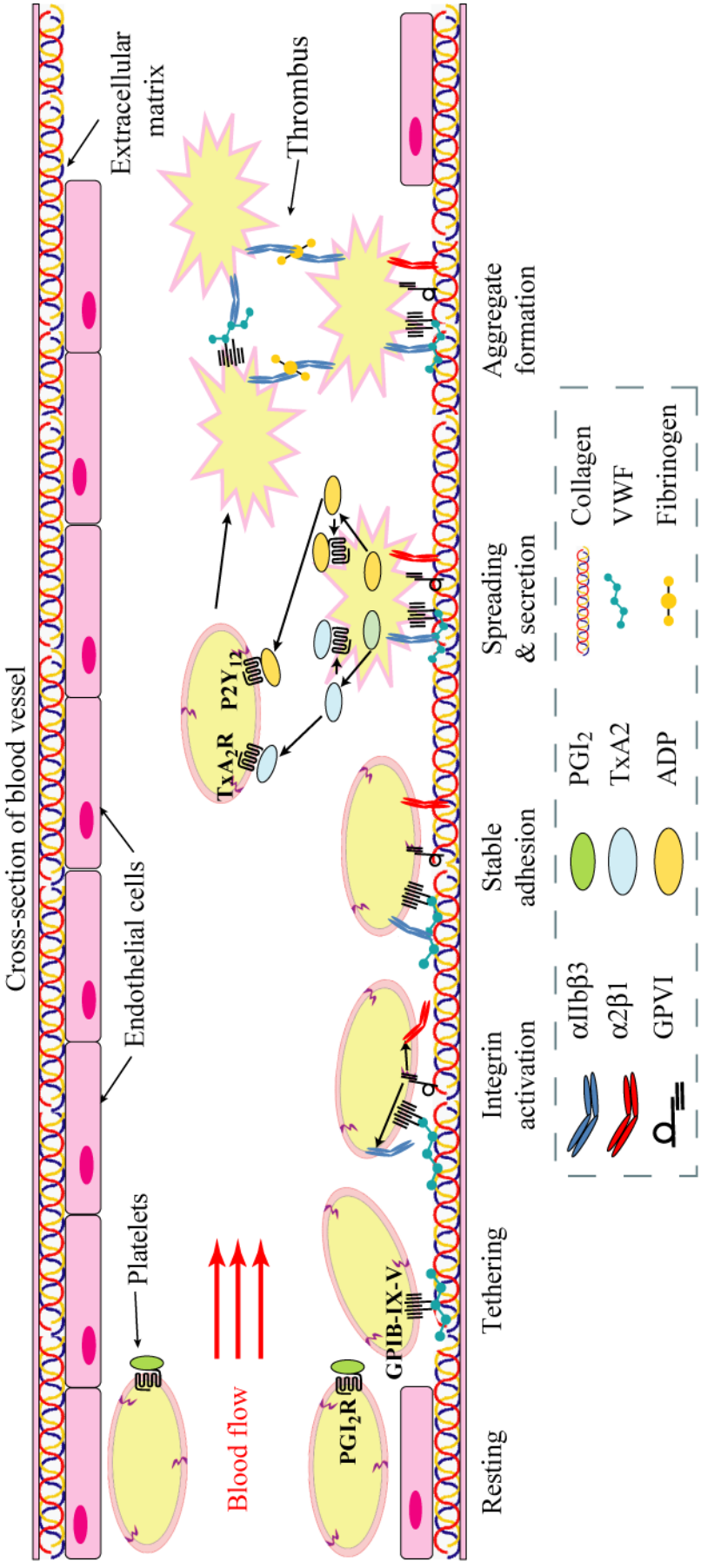

Figure 1.2.4. Schematic representation of platelet activation and thrombus formation. The GPIb-IX-V interaction with VWF mediates platelet tethering thereby enabling GPVI interaction with collagen. This leads to activation of integrins, αIIbβ3 and α2β1 and stable adhesion of the platelet to the ECM via their interaction with VWF and collagen, respectively. The platelet spreads and secretes the contents of it α- and δ-granules, including ADP and TxA2, which activate circulating platelets and fibrinogen. Platelet aggregation occurs by binding of αIIbβ3 to fibrinogen.

1. **Tethering:** the receptors and mechanisms of platelet tethering and adhesion are dependent upon the rheological conditions in the vessel. In the venous system, for instance, where shear rate is low, the platelet integrin α2β1 binds to the collagen, tethering the platelet to the exposed surface. However, this interaction has a slow on/off rate, so does not occur in vessels with high shear rates. Instead, the platelet tethering occurs through binding of VWF which has been immobilised on the exposed collagen, to the platelets GPIb-IX-V complex (Berndt et al., 2001). This interaction has a fast on/off rate resulting in transient association between VWF and GPIb-IX-V and causes platelets to roll along the exposed matrix until stable adhesion occurs.
2. **Integrin activation and stable adhesion:** The interaction of VWF with GPIb-IX-V enables binding of the low affinity collagen receptor GPVI to collagen. This interaction activates the platelet integrins α2β1 and αIIbβ3 which bind collagen and VWF, respectively. This inside-out activation of the integrins leads to stable adhesion of the platelet to the exposed surface as a consequence of the high affinity and slow dissociation rates of the integrins for their ligands.
3. **Spreading:** Following stable adhesion, massive reorganisation of the actin cytoskeleton leads to a characteristic set of morphological changes of the platelet. This includes the formation of filopodia and lamellipodia in a process referred to as platelet spreading. Platelet spreading causes an increase in the platelet surface area, further strengthening the platelet adhesion.
4. **Procoagulant activity:** Platelet activation causes exposure of the membrane phospholipid phosphatidylserine, PS, which provides a procoagulant surface to support thrombin formation. The presence of thrombin results in activation of additional platelets via binding to protease activated receptor 1, PAR1.

5. **Clot retraction:** Thrombin also cleaves fibrinogen, thus enabling generation of a fibrin mesh. The fibrin mesh helps to further block the gap in the endothelium and further strengthens the thrombus through clot retraction. Clot retraction is mediated by the interaction of fibrin with the actin cytoskeleton via their binding to αIIbβ3.

1.2.4 Platelet shape change

Platelet activation involves a characteristic set of morphological changes (Figure 1.2.2 *B*) leading to formation of filopodia, lamellipodia, actin nodules and stress fibres, in a process known as spreading (Calaminus et al., 2008). This change in shape is driven by an increase in the rate of polymerisation of the platelet actin cytoskeleton, downstream of a signalling cascade initiated by binding of surface receptors to an agonist.

While circulating in the blood, the platelet has a discoid shape. This shape is preserved by the platelet cytoskeleton which involves a spectrin-based membrane skeleton, a tightly coiled, circumambient band of microtubules and a rigid actin filament network. Upon activation of or adhesion of platelets, they undergo dramatic morphological changes, with the formation of filopodia protrusions, followed by lamellipodia formation before the platelet is fully spread, adopting a 'fried-egg' shape (Fig. 1.2.2 *B*). These morphological changes are as a result of the breakdown of the ring of microtubules and of polymerisation, branching and depolymerisation of the actin cytoskeleton, driving the formation of a variety of actin structures including, filopodia, actin nodules, lamellipodia and stress fibres.

Signalling across platelet receptors leads to the rapid activation of molecules that induce reorganization of the cytoskeleton. This, in turn, allows platelet aggregation, contraction, or spreading at sites of injury. A further function of the cytoskeleton is to bind these signalling molecules and recruit them to the required location for activation (Fox, 2001).

1.3 ACTIN CYTOSKELETON

The actin cytoskeleton plays a vital role in maintaining the shape and integrity of the platelet in the high shear environment of the vascular system and mediating shape change once activated (Kobsar and Eigenthaler, 2006). While circulating in the blood, the platelet's characteristic discoid shape is preserved by a rigid network of actin filaments throughout the cytoplasm (Boyles et al., 1985). When the platelet adheres to the extracellular matrix, ECM, the platelet shape change is induced by the massive reorganisation of the actin cytoskeleton (Hartwig, 1992).

1.3.1 Actin

Actin, a 42 kDa protein, is the most profuse protein in platelets, with approximately 2 million copies per cell and 40 % of which exists in a polymerised form consisting of 2000-5000 actin filaments (Hartwig and Italiano, 2006, Hartwig and Kwiatkowski, 1991). The rest remains in its monomeric form, globular (G-) actin, in the cytoplasm. Polymerisation of G-actin to filamentous (F-) actin is controlled by many actin binding and signalling proteins (Figure 1.3.1). The type of actin structure formed with F-actin is dependent on the type of proteins present.

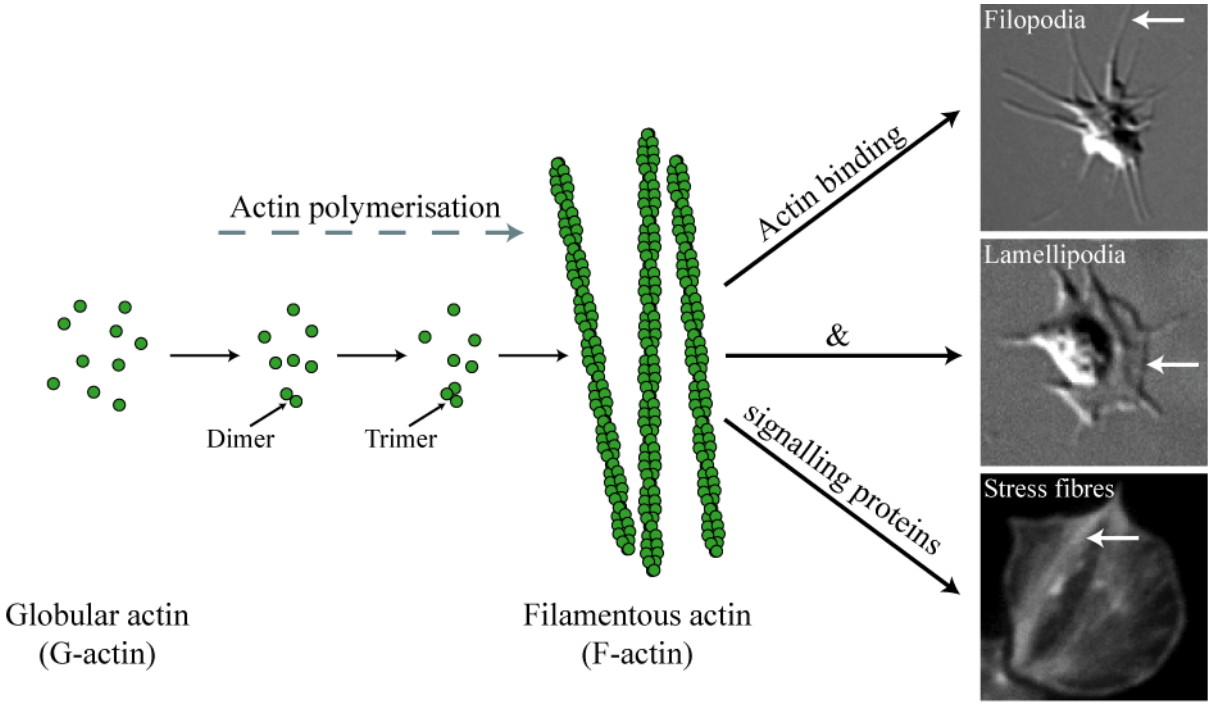

Figure 1.3.1. Schematic representation of actin polymerisation. Globular (G-) actin polymerises to form filamentous (F-) actin. The presence of actin binding and signalling proteins determine the actin structure formed, e.g. filopodia, lamellipodia or stress fibres (*arrows*) in platelets.

1.3.2 Actin polymerisation & depolymerisation

G-actin binds to ATP or ADP. The conformation of the actin monomer is controlled by the process of ATP hydrolysis. Binding of ATP to G-actin, is not required for actin polymerisation but the conformation induced by ATP binding results in ATP-actin polymerising more readily than ADP-actin. Initiation of actin polymerisation is a spontaneous process wherein G-actin oligomerises, to form a trimer, if the monomer concentration is above the critical concentration (Carlier and Pantaloni, 1997). These initial actin filaments are highly unstable and require the presence of additional proteins for efficient nucleation and assembly of actin filament networks. These proteins include capping protein, ADP/cofilin, profilin, formins and Arp2/3 complex (Dos Remedios et al., 2003)

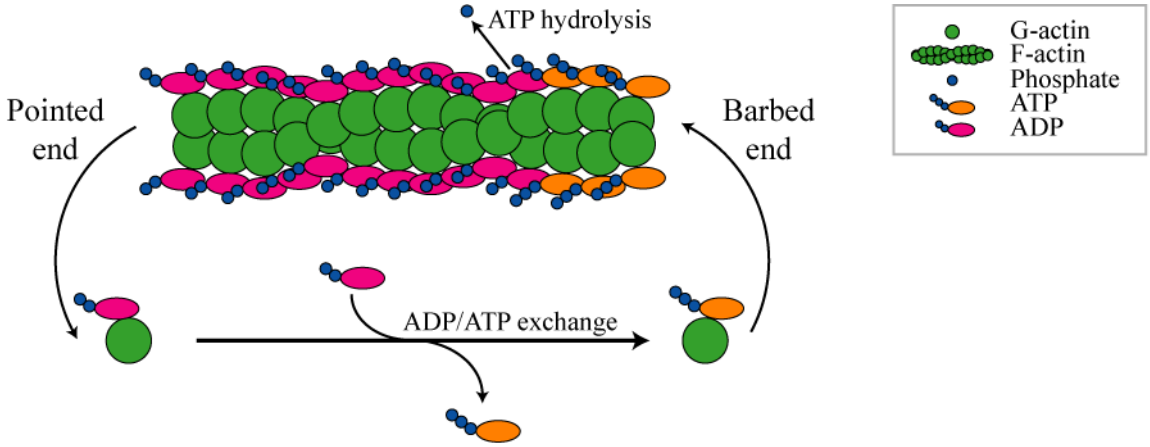

Figure 1.3.2. Schematic representation of actin treadmilling. ATP bound actin associates with the rapidly growing barbed end of the F-actin microfilament and the ATP is hydrolysed to ADP. ADP bound actin dissociates from the pointed end of F-actin. Treadmilling occurs when G-actin concentrations are between the critical concentrations for the barbed or pointed ends and results in a balance between the net dissociation and net association of G-actin. Adapted from (Cooper, 2000).

F-actin is polarised and its polarity is visualised via electron microscopy and is a result of myosin bound to the filaments which gives the appearance that it is coated with arrowheads that all align in one direction (Begg et al., 1978). This gives rise to their names as the pointed and barbed ends of the actin filament. The barbed end is bound with capping protein (Isenberg et al., 1980, Narita et al., 2006). The barbed end is arranged toward the plasma membrane while the pointed end is toward the cell interior. Actin filaments are polymerised by the addition of ATP-actin to the barbed end, as a result, the barbed end has a high concentration of ATP. Following polymerisation, the ATP is hydrolysed to ADP. Although dissociation of monomers occurs at both ends of F-actin, ADP-actin dissociates more readily than ATP-actin. As a result there is a net effect of depolymerisation at the pointed end. In a resting cell, stable actin filaments undergo continuous polymerisation and depolymerisation with a constant treadmilling of G-actin from the pointed end to the barbed end (Figure 1.3.2) (Bugyi and Carlier, 2010). To maintain this equilibrium, the pool of ATP actin is replenished by binding

of ADP-actin to profilin, a nucleotide exchange factor. Conversely, to ensure that not all of the ADP-actin is incorporated into F-actin, excess ADP-actin also binds to thymosin-β4 thereby preventing nucleotide exchange (Carlier et al., 1993).

When the cell is stimulated, there is an increase in barbed end formation brought about by uncapping or severing existing filaments and by *de novo* nucleation. This has the effect of increasing the rate of actin polymerisation. Actin binding proteins such as, profilin, cofilin, Arp2/3 and many others, together promote and rapid turnover of actin filaments and influence remodelling of the actin cytoskeleton required for cell motility and/ or shape change.

1.3.3 Actin structures

The remodelling of the actin cytoskeleton results in the formation of different actin structures. These actin structures include filopodia, lamellipodia, stress fibres, membrane ruffles, focal adhesions, podosomes, invadapodia and the platelet actin nodule. The structure formed is influenced by a variety of signalling pathways in response to stimulation of the cell.

Filopodia

Filopodia are thin membrane protrusions and consist of parallel bundles of 10-30 actin microfilaments which are held together by the actin binding proteins, such as fascins while ezrin, radixin and moesin (ERM) proteins link the cytoskeleton to the membrane (Figure 1.3.3 *A*) (Mattila and Lappalainen, 2008). Filopodia are implicated in many different cellular processes, including cell migration, adhesion to the ECM, wound healing, neurite growth and as a sensor of chemoattractants, guiding the cell towards them (Faix and Rottner, 2006).

Within the filopodia structure, the F-actin is arranged with the barbed end at the membrane. As a result, actin polymerisation occurs at the tip of the filopodium and is most likely driven by formins (Mellor, 2010).

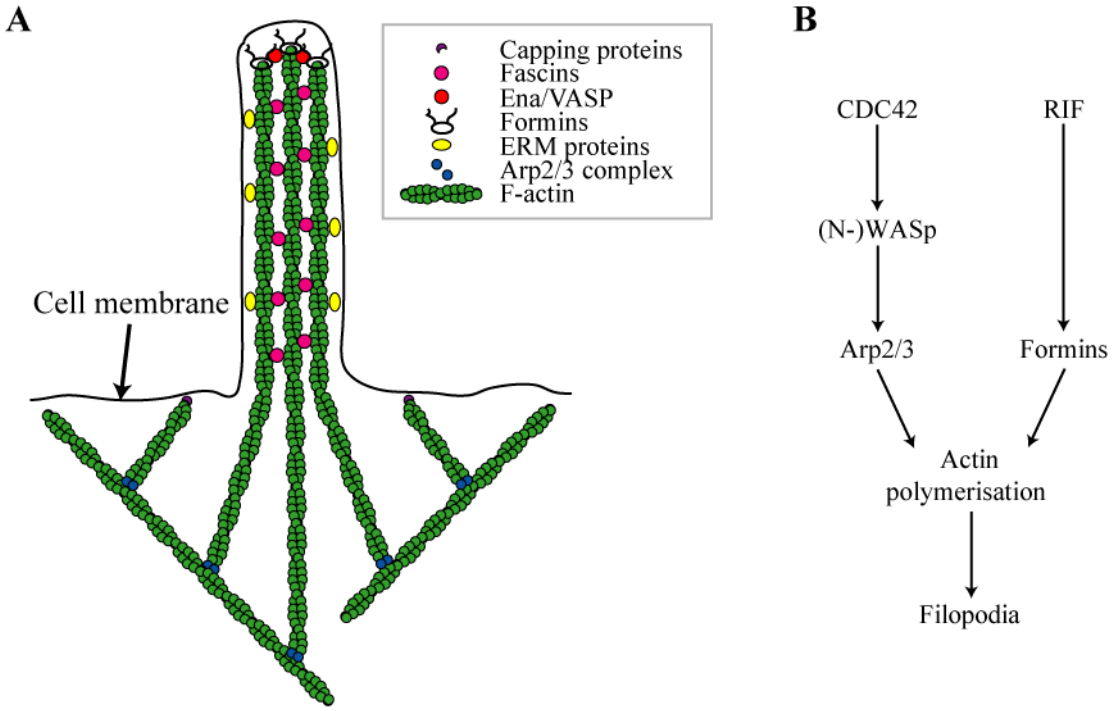

Figure 1.3.3. Schematic representation of filopodia structure and formation. (A) Schematic representation of the F-actin and actin-associated proteins that form the filopodia structure. Adapted from (Mellor, 2010). (B) Signalling pathways that lead to the the formation of filopodia.

Filopodia formation in platelets is driven by the Rho GTPases (Figure 1.3.3 *B*) in particular via CDC42 activation of Wiskott Aldrich Syndrome protein, WASp/ Arp2/3 pathway (Carlier et al., 1999). However, filopodia still form in WASp-/- platelets (Gross et al., 1999, Falet et al., 2002). Alternatively RIF activation of the formin mDia1 has been proposed as a CDC42-independent pathway (Goh et al., 2011). In platelets, pathways other than Rif-mDia1 may play a role in filopodia formation (Goggs et al., 2013). Both pathways result in downstream actin polymerisation and hence filopodia formation.

Lamellipodia

Lamellipodia consists of highly branched, short actin filaments and form a sheet-like structure in the gaps between filopodia (Figure 1.3.4 *A*) (Vinzenz et al., 2012). The 3D layer of cross-linked actin filmaments is essential for cell spreading and motility. The branching is as a result of binding of Arp2/3 complex to F-actin, enabling nucleation of new actin filaments in that branch-off from existing filaments. The presence of Arp2/3 in cells is crucial for lamellipodia formation (Wu et al., 2012).

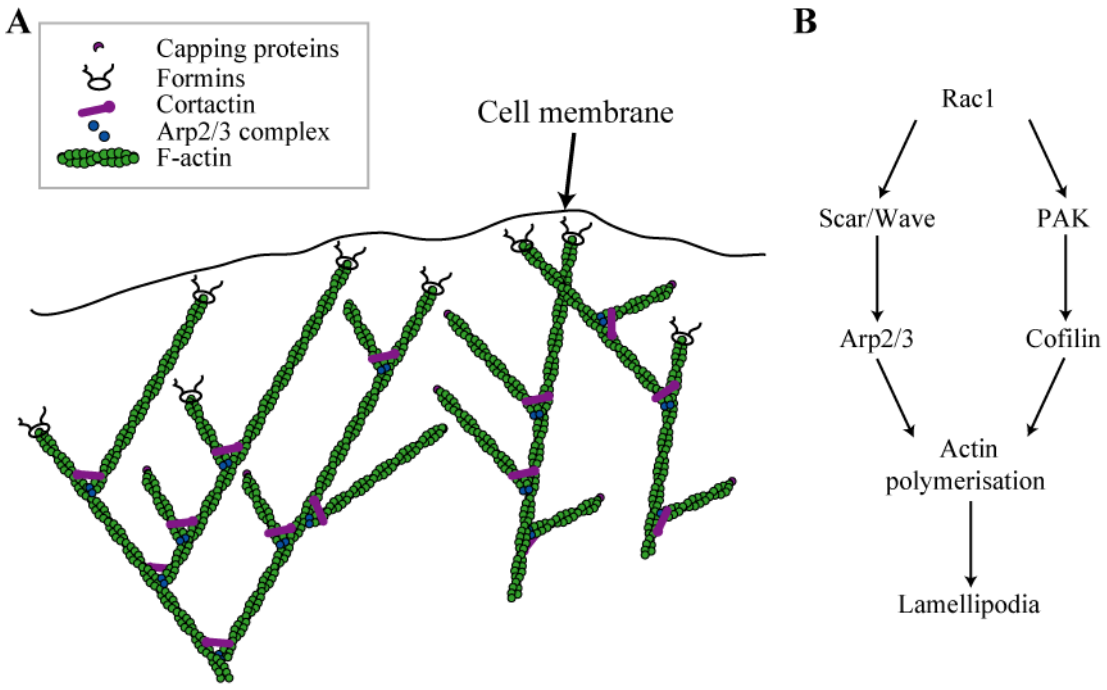

Figure 1.3.4. Schematic representation of lamellipodia structure and formation. (A) Schematic representation of the F-actin and actin-associated proteins that form the lamellipodia structure. Adapted from (Cosen-Binker and Kapus, 2006). (B) Signalling pathways that lead to the the formation of lamellipodia.

Similar to filopodia formation, lamellipodia formation in platelets is driven by Rho GTPases (Figure 1.3.4 *B*). Unlike filopodia, the main Rho GTPase implicated in lamellipodia formation is Rac1 which is activated by several platelet agonists, including, thrombin, fibrinogen,

collagen and ADP (McCarty et al., 2005). This results in actin polymerisation via downstream activation of Scar/Wave and Arp2/3 or via PAK and cofilin (Ibarra et al., 2005, Spence et al., 2012, Aslan et al., 2013)

Stress Fibres

Stress fibres have a similar structural organisation to sarcomeres in muscle cells and contain non-muscle versions of proteins such as actin and myosin II (Figure1.3.5 *A*) (Pellegrin and Mellor, 2007). F-actin is cross-linked by binding of myosin II and α-actinin to form parallel microfilaments (Peterson et al., 2004). Stress fibres are implicated in tail retraction in migrating cells and also have a major role in generating contractile forces in tissues. Within the stress fibre, the orientation of F-actin is dependent upon the contractile properties required in the cells (Cramer et al., 1997).

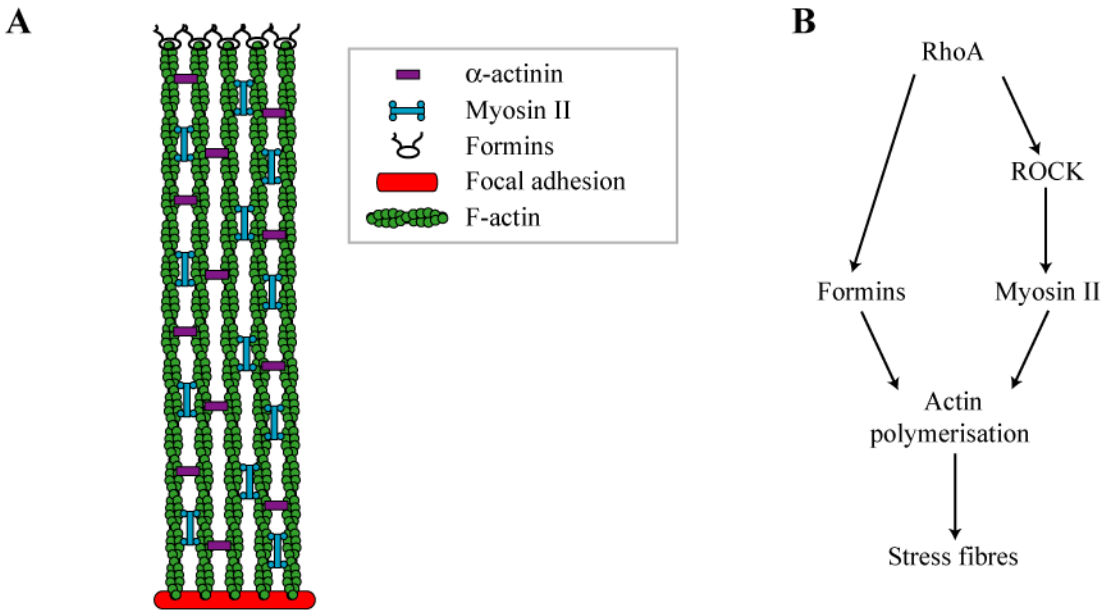

Figure 1.3.5. Schematic representation of stress fibre structure and formation. (A) Schematic representation of the F-actin and actin-associated proteins that form the stress fibre. (B) Signalling pathways that lead to the the formation of stress fibres.
Adapted from (Pellegrin and Mellor, 2007).

Stress fibre formation in platelets is driven by the Rho GTPase RhoA. This either affects actin polymerisation via the formin mDia1 or Rho-associated protein kinase, ROCK/myosin II activation pathways (Figure 1.3.5 *B*) (Gao et al., 2009, Katoh et al., 2001). Both pathways result in polymerisation of actin and formation of stress fibres.

Other specialised actin structures

Other actin structures have also been described in spreading cells including, dorsal and peripheral ruffles, focal adhesions, podosomes and invadapodia (Figure 1.3.6):

Dorsal and peripheral ruffles are similar to lamellipodia (Figure 1.3.6 *A*). The difference between ruffles and lamellipodia is that lamellipodia are forward-protruding structures that are weakly adhered to the substratum while ruffles protrude away from and are not adhered to the substratum (Abercrombie, 1980). There are two types of membrane ruffles; dorsal and peripheral ruffles (Abercrombie et al., 1970). Dorsal ruffles are found behind the lamellipodia leading edge and are often associated with receptor internalisation (Hoon et al., 2012). Peripheral ruffles are usually found at the leading edge of lamellipodia and play a role in cell motility (Suetsugu et al., 2003). However, neither peripheral nor dorsal ruffles have been reported in platelets.

Focal adhesions are actin-rich structures which connect stress fibres to the substratum and as such contain many actin associated proteins linking the stress fibres to the substratum via integrins (Figure 1.3.6 *B*). These proteins include vinculin, talin, paxillin and focal adhesion kinase, FAK (Kanchanawong et al., 2010). They are often located at stress fibre termini.

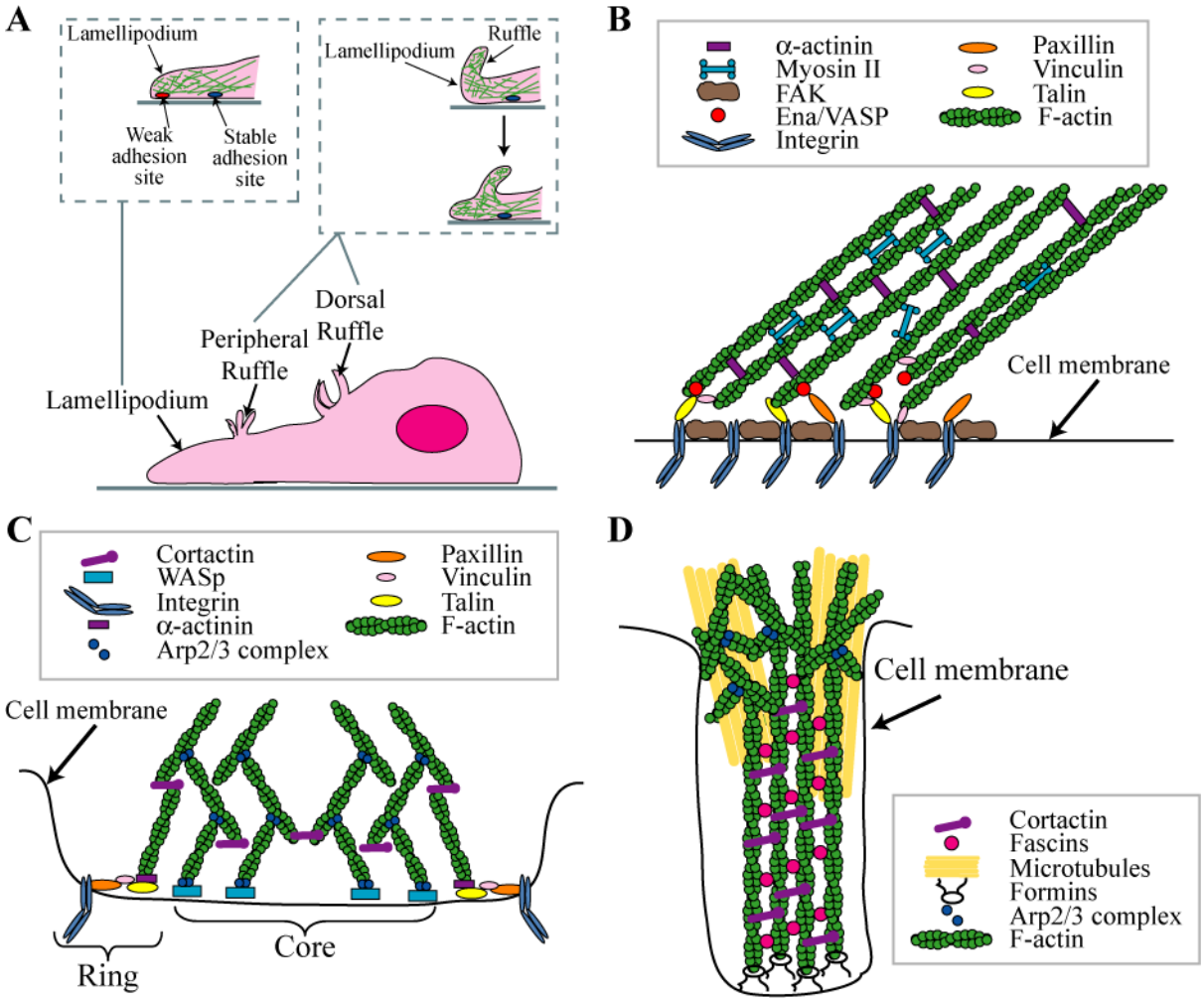

Figure 1.3.6. Schematic represntation of other specialised actin structures. Schematic representation of: (A) Dorsal and peripheral ruffles have a similar morphology and actin structure to lamellipodia. (B) Focal adhesions. Adapted from (Kanchanawong et al., 2010). (C) Podosomes. Adapted from (Linder and Aepfelbacher, 2003). (D) Invadopodia. Adapted from (Linder et al., 2011).

Focal adhesions serve as a point from which the cell can transmit internally generated force to the extracellular matrix, ECM, and vice versa (Wang and Suo, 2005). The presence of force, generated by the actin cytoskeleton, inside the cell drives the formation of the focal adhesion complexes. Focal adhesions have been reported in platelets spread on fibrinogen and glass (Leng et al., 1998, Cerecedo et al., 2006)

Podosomes are actin-rich structures involved in adhesion which were first identified in osteoclasts (Marchisio et al., 1984). They are a punctate actin structure which consists of an actin core surrounded by a ring of actin-associated proteins linking the actin filaments to integrins and consequently to the ECM (Figure 1.3.6 *C*). These proteins include, vinculin, talin and paxillin (Linder and Kopp, 2005). Super-resolution technology has found that the podosomes are polygonal in shape (Cox et al., 2012). The podosomes are often found grouped together in large numbers, forming a rosette structure.

Podosomes are adhesive structures and are comprised of many of the same proteins that are found in focal adhesions, including talin, vinculin, paxillin and Src family kinases, SFKs. However, the presence of Wiskott Aldrich Syndrome protein, WASp, is unique to podosomes and therefore distinguishes them from other actin structures (Block et al., 2008). Podosomes are also thought to play a role in cell invasion via matrix degradation through secretion of matrix metalloproteins, MMPs, from the podosome core (Gawden-Bone et al., 2010, Linder, 2007, Schachtner et al., 2013). Although podosomes are found in the platelet precursor, the megakaryocyte, they have not been identified in platelets.

Invadopodia are actin-rich structures which protrude from the cell. They consist of a F-actin core, microtubules and several actin associated proteins including, formins, cortactin and fascins (Figure 1.3.6 *D*) (Schoumacher et al., 2010, Linder, 2007). The invadopodia base has a similar branched actin structure to podosomes from which parallel bundles of actin, similar to those in filopodia, protrude.

Similarly to podosomes, invadopodia degrade ECM by secretion of MMPs (Linder et al., 2011). However, unlike podosomes, they are mainly found in cancer cells, its elongated protrusions project in to the ECM and they are more efficient at degrading the substratum (Linder, 2007). However, invadopodia have not been reported in platelets.

Actin nodules

While filopodia, lamellipodia, and stress fibres have been well described in platelets, the actin nodule was first described in 2008 by Calaminus *et al* (Calaminus et al., 2008). The actin nodules are punctate areas of actin staining, present in the early stages of platelet spreading but absent in fully spread platelets with stress fibres (Figure 1.3.7 *A*-*B*). Actin polymerisation is required for nodule formation. Immunohistochemistry studies revealed that the actin nodules co-localised with many of the proteins involved in regulating the actin cytoskeleton including Rac, Fyn, Arp2/3 complex, cortactin, talin, and β1 and β3-integrin subunits. Additional proteins that were found to co-localise with actin nodules include, adhesion- and degranularion-promoting adapter protein, ADAP, and vinculin (Kasirer-Friede et al., 2010). Although, in ADAP$^{-/-}$ platelets nodules still formed but they did not co-localise with vinculin. Vinculin deficient platelets still formed actin nodules which suggest that vinculin is not required for actin nodule formation but its presence may help maintain the interaction between the cytoskeleton and the ECM when exposed to mechanical forces (Mitsios et al., 2010).

Focal adhesions and podosomes have a similar circular appearance to that of the actin nodule; however, it is not thought that the actin nodule represents either of these actin structures:

While focal adhesions form at the ends of stress fibres, the actin nodule is not present in platelets with stress fibres. Moreover, the rosette structure and presence of an enriched actin core and outer ring, the main characteristics of a podosome, are not apparent in actin nodules. Consequently, the actin nodule appears to be a novel platelet actin structure.

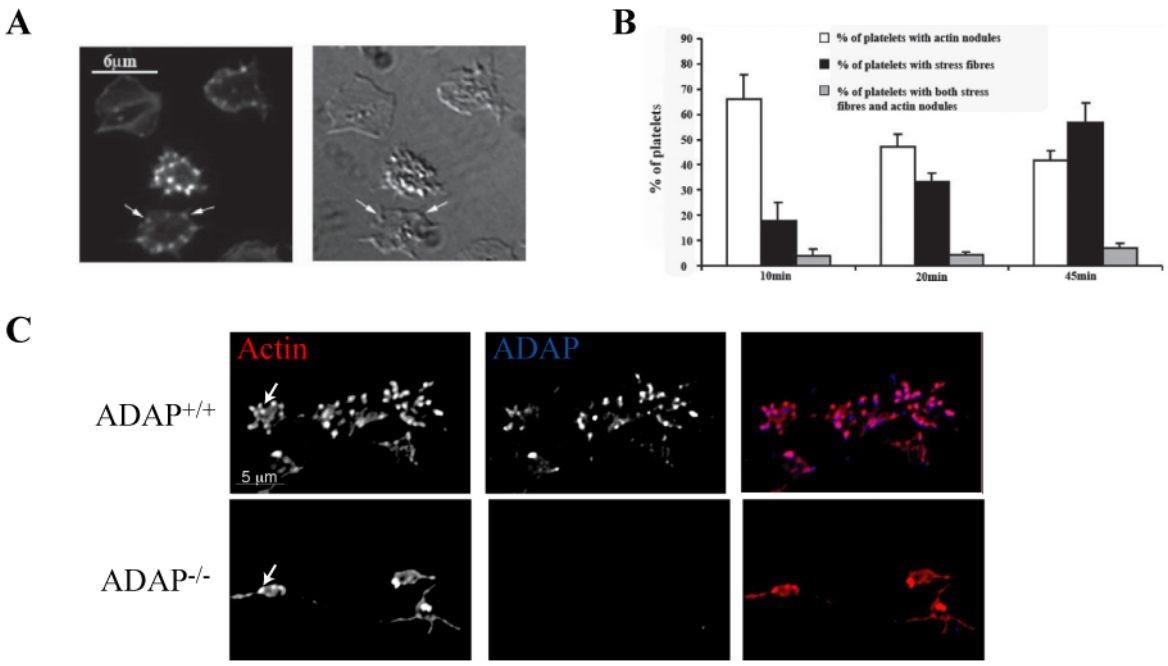

Figure 1.3.7. The platelet actin nodule. (A) Fluorescence and DIC images of human platelets allowed to spread on fibrinogen for 45 minutes prior to fixation and staining with FITC-phalloidin. Arrows indicate the location of actin nodules which are visible in both fluorescent and DIC images. (B) Percentage of actin nodule containing platelets decreased as cells spread and stress fibres appeared. (C) Fluorescence images of platelets adhered to fibrinogen under flow condtions. Actin nodules (*arrows*) are present in platelets under shear stress and co-localise with ADAP when present. Images taken from (Calaminus et al., 2008, Kasirer-Friede et al., 2010).

The actin nodules appear to be unrelated to filopodia formation since filopodia are found in platelets with or without actin nodules. However, the authors propose that the time course and the type of proteins that associate with the actin nodule allude to it playing a part in the process of lamellipodia formation (Calaminus et al., 2008). Additionally, it is supposed that

the actin nodules may play an important function in the actin dynamics of early spreading platelets

Although it was found that Src did not co-localise with nodules, Kasirer-Friede *et al*, found that the nodules co-localised with activated Src under flow conditions (Calaminus et al., 2008, Kasirer-Friede et al., 2010). Furthermore, under shear stress they noted that nodules were persistent throughout the cells, even when fully spread but lacking stress fibres (Figure 1.3.7 *C*). Thus suggesting the nodules may have a further role in anchoring the platelets to a surface when under shear stress.

1.4 VISUALISATION OF THE ACTIN CYTOSKELETON

Fixed cell imaging studies have provided a great deal of information about platelet shape change but the role of actin, and in particular that of the actin nodule, in this can only be thoroughly studied through live-cell imaging. Reliable visualisation of the actin cytoskeleton has historically been achieved by injection of fluorescently labelled actin or fluorescently labelled phalloidin. The development of fluorescent proteins, most notably the green fluorescent protein, GFP and its colour analogues, enabled expression of GFP fusion proteins in transfected cells. These fusion proteins included actin and actin binding proteins such as moesin and utrophin.

1.4.1 Phallotoxins

Phalloidin is a naturally occuing bicyclic heptapeptide found in death cap mushrooms (*Amanita phalloides*). It binds with high affinity (~30 pM) to F-actin (Faulstich et al., 1977), although, this affinity is somewhat reduced when phalloidin is fluorescently labelled (~270 nM) (Wulf et al., 1979). In particular it binds at the interface between F-actin subunits, effectively locking them together (Vandekerckhove et al., 1985). This binding inhibits ATP hydrolysis and prevents depolymerisation of F-actin which has the effect of stabilising actin filaments (Barden et al., 1987). This stabilisation of F-actin is irreversible and leads to cell death, therefore it is more suited for use with fixed cells. Phalloidin is cell impermeant so uptake into cells has relied on membrane permeablisation, microinjection, electroporation or scrape loading (Small et al., 1999). However, cell permeant versions are now available. The use of phalloidin for live cell imaging is limited to injectable large cells. Phalloidin injected into live cells was found to disrupt actin dynamics consequently affecting cell growth and

motility (Wehland et al., 1977). However, when used in low concentrations, it can be used to visualise actin in living cells (Wehland and Weber, 1981).

1.4.2 Fluorescent proteins

The discovery and development of fluorescent proteins, most notably the green fluorescent protein, GFP, drastically improved the ability to label proteins in intact cells. GFP is a 238 aa, 26.9 kDa protein derived from the *Aequorea victoria* jellyfish (Shimomura et al., 1962). It exhibits bright green fluorescence upon exposure to blue light. Since it was first cloned and expressed in cultured cells it has become one of the most widely used proteins in cell biology (Prasher et al., 1992, Chalfie et al., 1994). Its most common use is as a fusion tag to proteins of interest to monitor their cellular localisations. GFP has been targetted to every major cell organelle and its size and shape nor the differing environments within cells and their organelle appear to affect GFP. Additionally GFP has been expressed ubiquitously in whole animal models (Okabe et al., 1997). However use of GFP fusion proteins is limited to cells which can be transfected or can undergo microinjection.

Actin-GFP

Expression of GFP-actin fusion protein has been used to study live cell actin dynamics (Choidas et al., 1998, Calaminus et al., 2008). Although GFP-actin enables labelling of the actin cytoskeleton, it has several disadvantages. This includes the requirement for low expression levels to reduce background staining by GFP-actin monomers and to provide a large pool of non-labelled actin to compensate for the impairment in functionality of GFP-

actin (Westphal et al., 1997, Yamada et al., 2005). Additionally, the expression of GFP-actin has been shown to affect cellular actin dynamics (Feng et al., 2005, Deibler et al., 2011).

Actin binding proteins/ domains

In place of GFP-actin fusion protein, other GFP-fusion proteins have been utilised to study live cell actin dynamics. Actin binding proteins or binding domains GFP-fusions used have included, moesin, LimeE, ABP120, ABP140 and utrophin (Edwards et al., 1997, Bretschneider et al., 2004, Socol et al., 2010, Pang et al., 1998, Yang and Pon, 2002, Burkel et al., 2007). While all have successfully been used to monitor actin dynamics in live cells, the fusion proteins may still affect actin dynamics because of their larger size and the likely competition for binding with their unlabelled, endogenous homologue. While all have successfully been used to monitor actin dynamics in live cells, the fusion proteins may still affect actin dynamics because of their larger size and the likely competition for binding with their unlabelled, endogenous homologue.

1.4.3 Lifeact

Total internal reflection fluorescence, TIRF, microscopy studies of the actin binding capabilities of Actin Binding Protein 140, ABP140, revealed that the protein's first 17 amino acids were all that were required to efficiently bind to actin (Riedl et al., 2008). The peptide sequence of those first 17 amino acids, referred to as 'Lifeact', were found to be absent from other organisms despite being highly conserved among close relatives of *Saccharomyces cerevisiae*. Riedl *et al* assert that its small size and lack of endogenous analogous sequences make it an attractive alternative for actin labelling in higher eukaryotic cells (Riedl et al.,

2008). Additionally, Lifeact was found to have a lower affinity for F-actin (1.3 μM) than phalloidin (30 pM) which may attribute to Lifeact appearing to leave actin polymerisation and depolymerisation unaffected (Riedl et al., 2008, Faulstich et al., 1977). Although over expression of Lifeact has been shown to adversely affect actin dynamics, when compared with cells expressing actin-GFP, actin dynamics are dramatically less affected by its presence (van der Honing et al., 2011, Deibler et al., 2011)

Phalloidin has been used extensively in platelets to image the actin cytoskeleton of fixed cells. Additionally, GFP-actin and GFP-lifeact have been used to study live cell actin dynamics in platelets from mouse models expressing the GFP fusion proteins (Calaminus et al., 2008, Schachtner et al., 2012). However, these labelling methods have fundamental drawbacks for studying actin dynamics in spreading human platelets: Firstly, human platelets are anucleate, so it is not possible to transfect the cells which rules out the possibility of using the fluorescent protein fusion proteins. Secondly, the platelet membrane is extremely sensitive to external stimuli. Therefore, introduction of fluorescent labels via techniques such as microinjection, scrape loading or detergent induced membrane permeablisation would not be possible.

Instead this project aims to introduce fluorescently labelled Lifeact peptide into human platelet using an intracellular delivery moiety, in order to study actin nodule dynamics. The small size of the Lifeact peptide makes it relatively easy and cheap to manufacture. Additionally, access to platelets from Lifeact-GFP mouse model would serve as a suitable

comparison; firstly for validation of successful cellular uptake and nodule labelling and secondly for fundamental studies on the actin nodule and its role in platelet function.

1.5 INTRACELLULAR DELIVERY OF MOLECULES

There are many different methods of introducing imaging labels, such as Lifeact, or other molecules into cells. Methods of achieving this include; transfection, microinjection, membrane permeablisation, exploitation of the cells natural endocytic pathways, cell penetrating peptides, nanoparticles or liposomes.

1.5.1 Overview in platelets

Due to the platelet's anucleate state and reactivity to external stimuli, the use of transfection or microinjection to deliver imaging labels are not suitable. Even though transgenic mouse models which express GFP fusion proteins, including GFP-Lifeact, are available, they are costly and time consuming to generate and murine cells are not always suitable substitutes for human cells (Okabe et al., 1997, Riedl et al., 2010, Lin, 2008). Consequently, in platelets, membrane permeablisation is the main method of introducing imaging labels to cells. However, permeablisation of platelets results in rapid loss of intracellular contents as a result of the high surface area to volume ratio so is reserved for fixed cell samples only (Flaumenhaft, 2004).

1.5.2 Other methods

In the fields of drug delivery and diagnostics a number of other intracellular delivery methods are being investigated to facilitate delivery of drugs or imaging agents including nanoparticles, liposomes and cell penetrating peptides.

Nanoparticles

There are many different types of nanoparticles including polymers, dendrimers, micelles, liposomes and metallic. These nanoparticles either encapsulate the therapeutic or imaging agent or provide a surface for their attachment. Cellular uptake of these nanoparticles is most likely via endocytosis although passive uptake of nanoparticles is also thought to occur (Treuel et al., 2013, Verma et al., 2008, Lin et al., 2010). Additionally, it is proposed that in cancerous tumours, the increased permeability of the cells membranes enables non-endocytic uptake of nanoparticles (Maeda et al., 2013, Maruyama, 2011, Wang et al., 2012, Wolinsky et al., 2012, Haley and Frenkel, 2008).

Nanoparticles have been shown to enter a variety of cells on a timescale of 2 – 48 hours of incubation (Bickford et al., Chung et al., Li et al., 2010, Wang et al., 2009). Nanoparticle carriers which are taken up via endocytosis, result in the imaging label or drug residing in vesicles outside of the cytoplasm. Those that passively move across the cell membrane into the cytoplasm can result in disruption to the cell membrane (Leroueil et al., 2008). Therefore, there is a lot of scepticism towards the use of nanoparticles as intracellular, cytoplasmic delivery vectors (Nativo et al., 2008).

Nanoparticles have been used to label whole platelets or to induce platelet aggregation following interaction with the platelet membrane (Woolley et al., 2013, Dobrovolskaia et al., 2012). Additionally, nanoparticles are increasingly explored for diagnostic and drug delivery potential, their interaction with and their effect on the blood cells, including platelets requires investigation (Semberova et al., 2009, Lacerda et al., 2011, Ali et al., 2013, Ilinskaya and Dobrovolskaia, 2013a, Ilinskaya and Dobrovolskaia, 2013b). However, they are unlikely to be

suitable to deliver imaging labels, such as Lifeact, into the cytoplasm of human platelets without affecting the cell.

Cell-penetrating peptides

Another approach is to utilise the membrane penetrating properties of some peptides. These peptides are most commonly referred to as cell-penetrating peptides, CPP, but are also known as protein transduction domain, PTD, or membrane translocatting sequence, MTS. CPPs usually consist of fewer than 30 aa residues and are able to deliver cargo molecules into cells (Lundberg and Langel, 2003). There are many types of CPP currently under investigation (Jones and Sayers, 2012) but the most studied are HIV-Tat peptide (Chauhan et al., 2007), penetratin (Derossi et al., 1994) which is also known as pAntp, transportan (Pooga et al., 1998) and poly-L-lysine or poly-L-arginine, PLL and PLA, respectively (Futaki et al., 2007, Reuter et al., 2009, Schmidt et al., 2010). . Although, initially assumed that direct transport of these peptides across the lipid bilayer was the mechanism of their uptake, it is now thought their uptake may be by endocytosis (Richard et al., 2003, Chauhan et al., 2007, Futaki et al., 2007). A range of cargo molecules have been delivered using CPPs including small peptides, oligonucleotides and nanoparticles (Abes et al., 2007, Liu et al., 2013, Zhang et al., 2013, Zhang et al., 2011, Schwarze et al., 1999). In platelets CPPs have been used to deliver inhibitors or actually inhibit platelet receptors (Bernard et al., 2009, Covic et al., 2002a, Covic et al., 2002b, David et al., 2006, Dimitriou et al., 2009)

1.5.3 pH (low) insertion peptide

Recently another method of cellular delivery has been reported, in the form of a peptide called pH (low) insertion peptide, pHLIP (Reshetnyak et al., 2006). pHLIP spontaneously inserts itself into the lipid bilayer upon a decrease in pH, thereby translocating its cargo molecules into the cell. It is not clear at present if pHLIP would be categorised as a CPP (Jones and Sayers, 2012).

pHLIP, is derived from the C-helix of the transmembrane bacteriorhopsin, BR, protein. The C-helix, unlike the other six helices of BR, was found to have unique properties, including its solubility and pH controlled membrane insertion (Hunt et al., 1997a). Transmembrane helices are ordinarily characterised by their sequences of approximately twenty hydrophobic amino acids giving rise to water insolubility, the C-helix, however, was found to be both soluble in an aqueous and lipid environment (Reshetnyak et al., 2007, Hunt et al., 1997b). The modification of the peptides hydrophobicity by pH is due to the presence of two aspartic acid residues. In the native BR, these residues play a key role in proton transport, with one residue acting as the donor and the other, the acceptor (Bousche et al., 1991a, Bousche et al., 1991b, Bousche et al., 1992). However, Hunt *et al* found that the protonation of one or both of these residues, in a mildly acidic environment, resulted in enhancement of the peptide hydrophobicity, thereby enabling spontaneous membrane insertion (Hunt et al., 1997b, Hessa et al., 2005). Furthermore, it was found that this pH-dependent alteration in solubility is also strictly dependent on the presence of phospholipids.

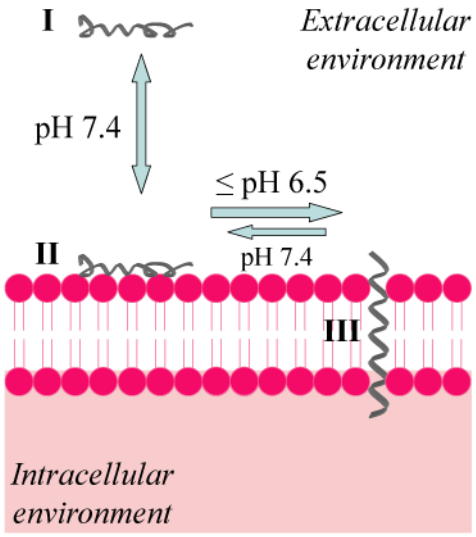

Figure 1.5.1. Schematic representation of pH-dependent membrane insertion of pH (low) insertion peptide. pHLIP exists in three states; At neutral pH, pHLIP is in solution (**I**) or loosely associated with lipid membranes (**II**) but upon reduction in pH to <6.5, pHLIP is inserted across membrane (**III**). Insertion is reversed upon restoration of neutral pH.

At neutral or slightly alkaline pH (pH 7 - pH 8), BR C-helix and pHLIP exist as an unstructured peptide both in solution (State I) and when it associates with lipid membranes (State II) (Figure 1.5.1). At acidic pH (<pH 6.5), pHLIP forms an α-helix and spontaneously inserts itself, unidirectionally, across the lipid bilayer (State III). Whereby, pHLIP's polar *C*-terminus is moved into the cytoplasm while its *N*-terminus remains outside (Reshetnyak et al., 2007). In all three states pHLIP is monomeric at concentrations less than 7 μM (Reshetnyak et al., 2007). The insertion process is completely reversible upon restoration of neutral pH (Reshetnyak et al., 2006).

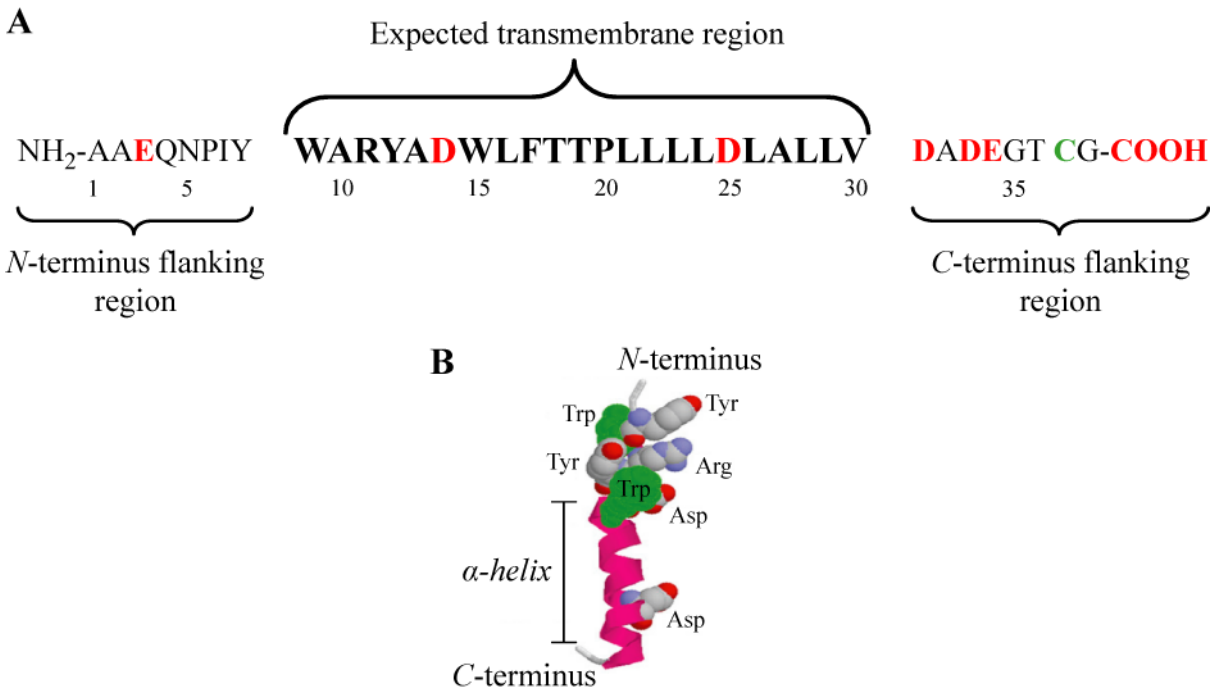

Figure 1.5.2. Structure of pH (low) insertion peptide. (A) pHLIP amino acid sequence; the expected transmembrane sequence of pHLIP is highlighted in bold, the position of the acidic residues in red and a cysteine residue, present in the C-terminus to enable attachment of cargo molelcules via a disulphide bond, is highlighted in green. (B) An atomic representation of the transmembrane α-helix of pHLIP. Adapted from (Reshetnyak et al., 2007).

pHLIP is a 38 amino acid peptide that consists of 22 amino acids from the transmembrane section of the BR C-helix and two flanking sequences (Figure 1.5.2) (Andreev et al., 2009). It is relatively rich in acidic residues (four aspartic acid (Asp) and two glutamic acid (Glu) residues and the *C*-terminal carboxy group) and their combined negative charge forms a large energy barrier (~22 kcal/mol) to peptide insertion (Barrera et al., 2011). Binding to the lipid membrane and subsequent peptide insertion, at low pH, are accompanied by energy release (~6-7 kcal/mol and ~1.8 kcal/mol, respectively) suggesting that a large proportion of these groups need to be protonated in order for insertion to occur. It has been found that the two transmembrane Asp residues (Asp14 and 25) are protonated first inducing deeper penetration of the peptide in the membrane, accompanied by α-helix formation (Figure 1.5.3) (Musial-

Siwek et al., 2010, Karabadzhak et al., 2012). This agrees with an earlier finding that 1.5 - 1.8 protons are involved in the protonation step (Reshetnyak et al., 2008). However, the other charged residues at the *C*-terminus are unlikely to be protonated at the same time, thus opposing the peptide insertion and driving formation of intermediate structures observed by Andreev *et al* (Andreev et al., 2010). Karabadzhak *et al*, propose that this rate limiting step could be overcome in order to relieve the instability and tension that the partial insertion exhibits on the lipid bilayer (Karabadzhak et al., 2012).

Removal of pHLIP from the lipid bilayer is via a different mechanism which occurs more rapidly than insertion (Figure 1.5.3) (Andreev et al., 2010). Increasing the extracellular pH results in deprotination of the charged residues buried deep in the membrane hydrophobic core thus destabilising the helix (Barrera et al., 2011). The energy from the destabilising process fuels removal of pHLIP from the membrane. In the lipid palmitoyl oleyl phosphatidyl choline, POPC, vesicles, the removal process is complete in approximately 100 ms (Andreev et al., 2010).

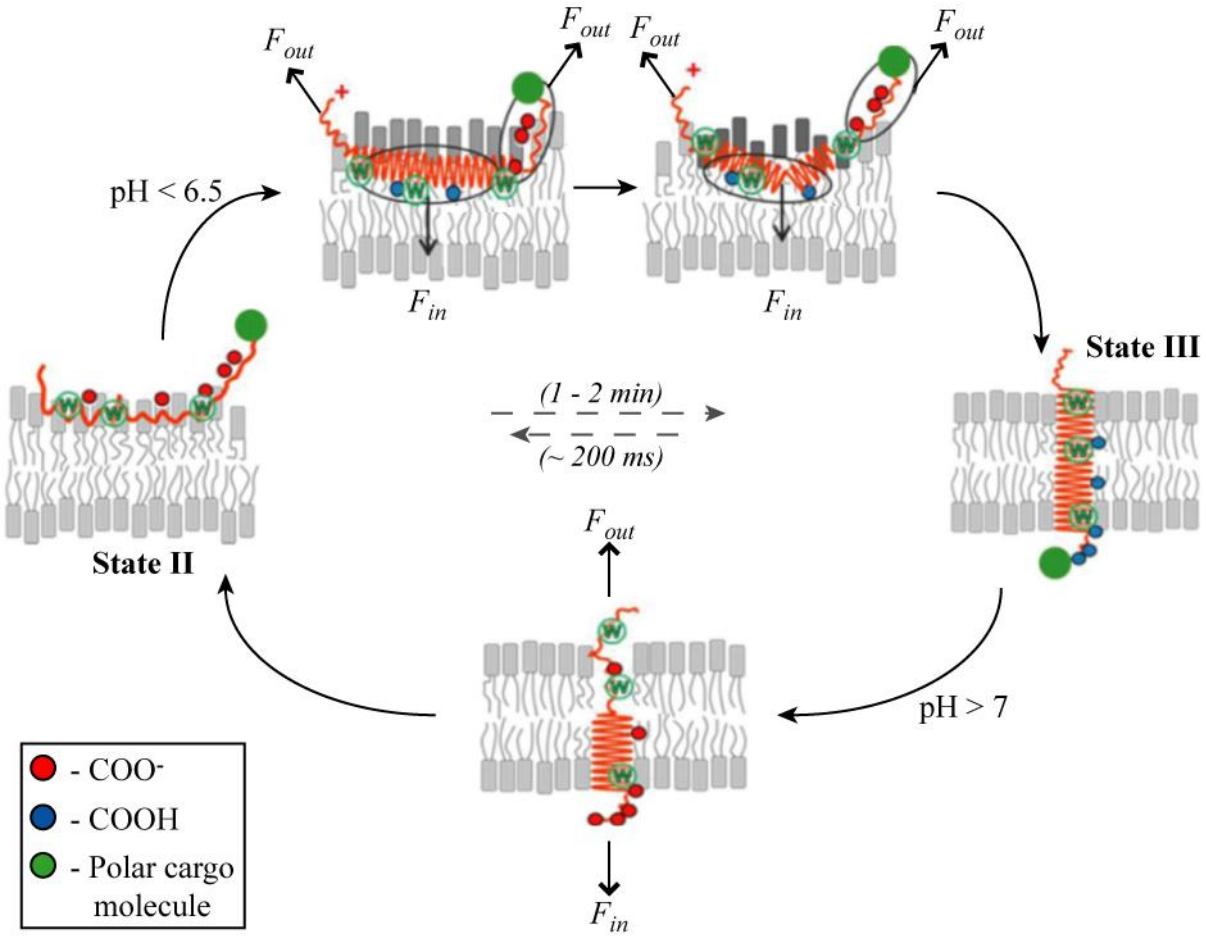

Figure 1.5.3. Schematic representation of membrane-associated folding/ insertion and unfolding/ exit of pHLIP. The formation of intermediate structures during pHLIP insertion into membranes is driven by the differing protonation rates of the acidic residues (red/ blue circles). Membrane distortion during this process is represented by lipids with darker head groups. pHLIP unfolding and exit occurs more rapidly than insertion. Adapted from (Karabadzhak et al., 2012).

pHLIP has dual cargo delivery properties: Cargo molecules attached to its *N*-terminus are delivered to the cell surface and then tethered there in low pH conditions (Figure 1.5.4 *A*). This is particularly useful for enabling imaging of cell membranes or tissue margins and has been shown to have potential diagnostic possibilities for positron emission tomography (PET) and near-infrared (NIR) imaging technologies (Reshetnyak et al., 2011, Segala et al., 2009, Andreev et al., 2007, Vavere et al., 2009, Mata et al., 2007). Additionally, attachment of cargo molecules to the *C*-terminus of pHLIP enables cytoplasmic delivery of cargo molecules

(Figure 1.5.4 *B*). If that cargo molecule is conjugated to pHLIP via a disulphide bond, the reducing environment of the cell cleaves the bond, releasing the cargo into the cell (Reshetnyak et al., 2006). *C*-terminally conjugated cargo enables cytoplasmic delivery and release of molecules such as drugs, inhibitors or molecular labels (Moshnikova et al., 2013, Wijesinghe et al., 2011, An et al., 2010). Thus pHLIP can be used as both an intracellular cargo/drug delivery system and for labelling cell/ tissue margins.

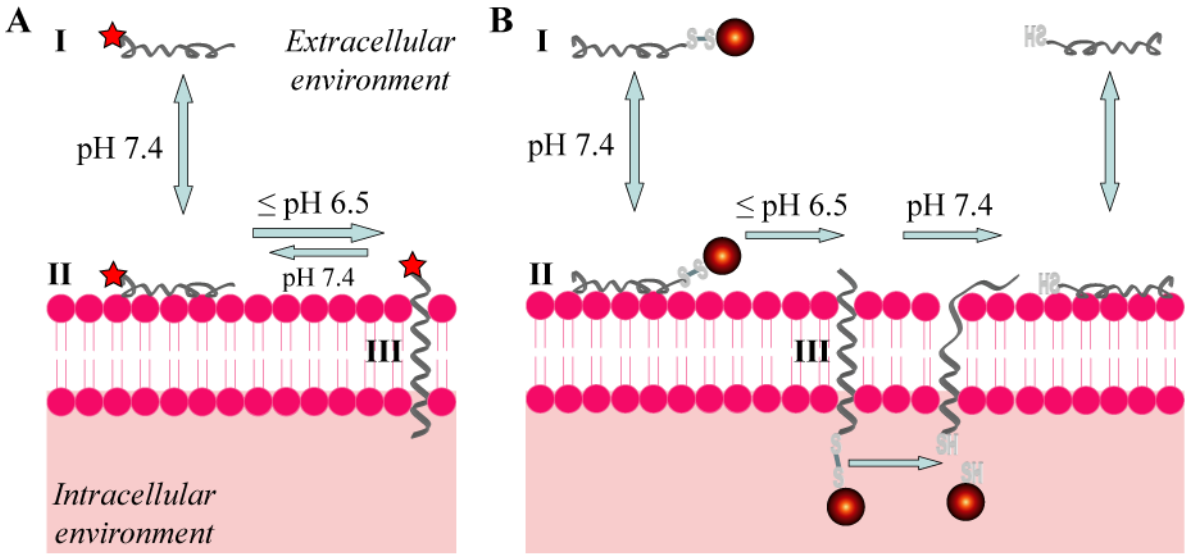

Figure 1.5.4. Schematic representation of the dual cargo delivery properties of pHLIP. (A) Cargo molecules conjugated to pHLIP's *N*-terminus are delivered then tethered to the surface of cells in a low pH extracellular environment. (B) While cell-impermeable cargo molecules conjugated to pHLIP's *C*-terminus via a disulphide bond are translocated across the cell membrane in to the cytoplasm. Release of cargo molecules is achieved by the reduction of the disulphide bond in the reducing environment inside the cell. I, II and III represent the three states that pHLIP adopts; - in solution, associated with the lipid membrane and inserted across the lipid membrane, respectively. The low pH induced insertion is completely reversed upon restoration of neutral pH.

As a cell labelling mechanism, many different types of imaging labels have been conjugated to pHLIP's *N*-terminus which demonstrates its suitability for a variety of medical imaging techniques. These have included; near-infrared, NIR, labels such as Cy5.5 and Alexa750

(Segala et al., 2009, Reshetnyak et al., 2011), ^{64}Cu-DOTA and [^{18}F] for positron emission tomography, PET, (Vavere et al., 2009, Daumar et al., 2012), gold nanoparticles or fluorescent labels for optical imaging of tissue sections (Yao et al., 2012, Sosunov et al., 2013) and ^{99}Tc labels for single photon emission computed tomography (Macholl et al., 2012, Weerakkody et al., 2013).

pHLIP has been shown to deliver a variety of molecules into cells, including peptide nucleic acid, PNA, (~2.5 kDa), cyclic peptides (<850 Da), fluorescent dyes such as dansyl, α-amanitin and phalloidin (Reshetnyak et al., 2006, Thevenin et al., 2009). However, the type of *C*-terminus conjugated cargo for cytoplasmic delivery is limited by the cargo's hydrophobicity. The more hydrophobic the cargo molecule, the more likely it will be translocated across the lipid bilayer by pHLIP. For instance, phallocidin is a highly polar molecule (logP = -1.6) but was not delivered to the cytoplasm of cells when conjugated via a disulphide bond to the *C*-terminus of pHLIP (Wijesinghe et al., 2011). Upon modulation of the polarity of phallacidin by addition of hydrophobic side chide chains of varying carbon length, increased cellular uptake of phallacidin was observed (30% for logP = -0.74, 70% for logP = -0.09). These results demonstrate the importance of the cargo polarity when selecting potential molecules for cytosolic delivery by pHLIP. To enable delivery of polar molecules, liposomes, which are composed of lipids conjugated to pHLP's *N*-terminus, take advantage of the ability of pHLIP to interact with lipid membranes and as a result promote fusion of liposomes to the cell membrane (Yao et al., 2013).

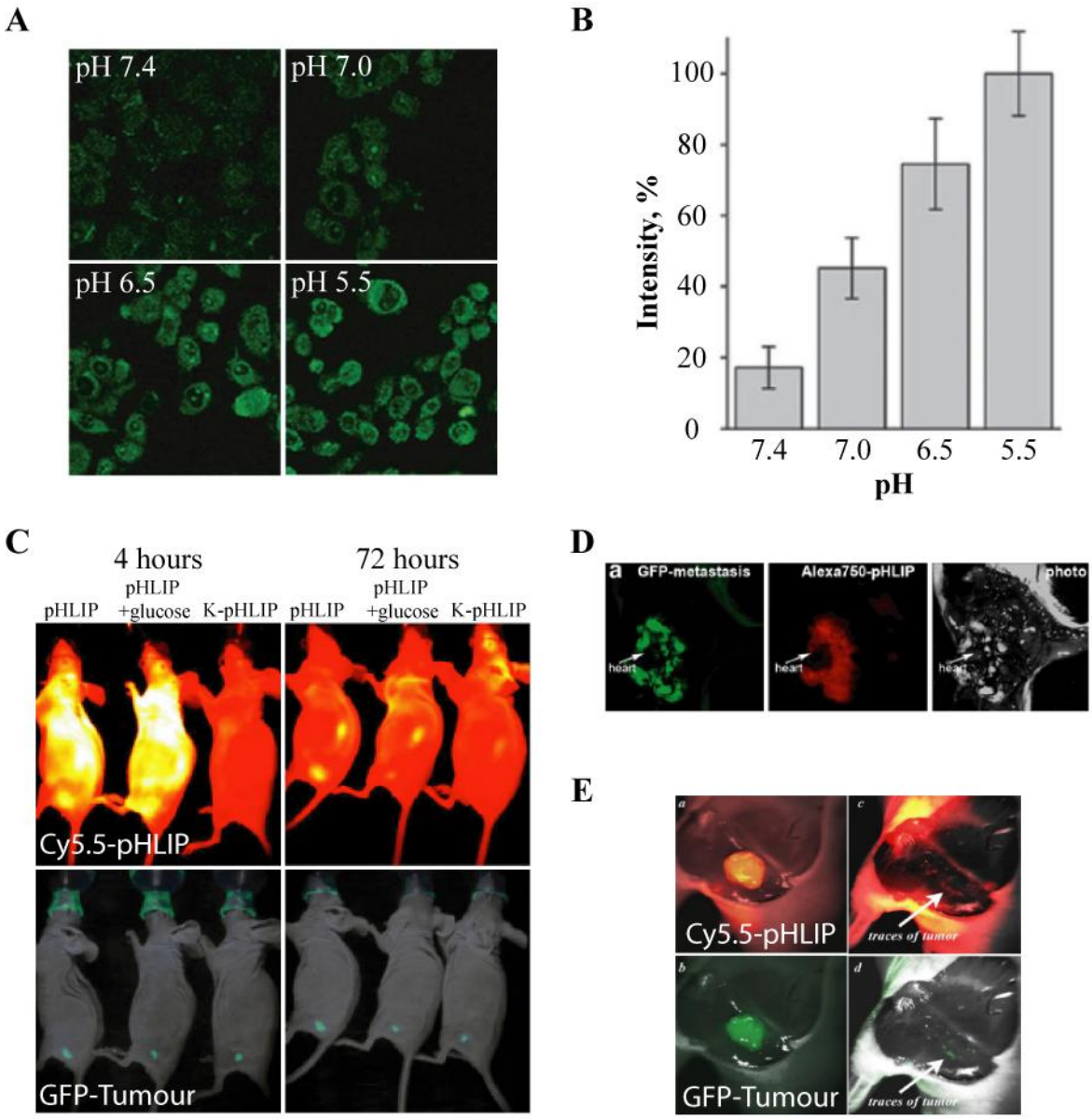

Figure 1.5.5. Biological applications of pHLIP. (A) pHLIP-mediated delivery of dansyl in HeLa cells at various pH values and (B) quantification of the fluorescence which demonstrates increasing uptake with decreasing pH (Reshetnyak et al., 2006). *In vivo* applications of pHLIP have been directed at targeting the intrinsic low pH associated with tumours: (C) Within 4 hours post injection of Cy5.5-pHLIP, Cy5.5 fluorescence is localised to established GFP-tumours. This localisation is maintained upto 72 hours post injection (Reshetnyak et al., 2011). (D) Fluorescently labelled pHLIP localises to metastasis aswell as established tumours (Reshetnyak et al., 2011). (E) pHLIP labelling enables visualisation of traces of tumour remaining after tumour excision (Segala et al., 2009).

Biological applications of pHLIP have focused on exploiting the low pH conditions that arise as a symptom of some pathological diseases (Figure 1.5.5). Such diseases include cancerous tumours (Stubbs et al., 2000), atherosclerotic plaques (Naghavi et al., 2002), ischemia (Cobbe and Poole-Wilson), inflammation (Kellum et al., 2004), infection (Kielian and Jungerwirth, 1990) and trauma-induced tissue damage (Johansson et al., 2012). The pH-dependent insertion properties of pHLIP make it an ideal diagnostic tool and drug delivery system for treating such conditions. Successful detection of cancerous tumours, metastases, ischemic tissue and H1N1 virus damaged alveolar has been demonstrated in a variety of mouse models (Reshetnyak et al., 2011, Segala et al., 2009, Vavere et al., 2009, Sosunov et al., 2013, Daumar et al., 2012, Moshnikova et al., 2013, Li et al., 2013). Retention of pHLIP in normal tissues, excluding the kidneys, is minimal (Andreev et al., 2007). Although, membrane disruption of red blood cells by pHLIP in neutral conditions was observed. The sequence of pHLIP has been tuned to increase targeting efficiency and reduce retention in non-target cells and tissues (Weerakkody et al., 2013).

pHLIP uptake on a cellular level has been investigated for cell cultures with artificially lowered environmental pH (Reshetnyak et al., 2006, An et al., 2010, Yao et al., 2012, Moshnikova et al., 2013). These studies have demonstrated that pHLIP is able to deliver cargo molecules and label cells. Additionally, the effect of pHLIP on cells was determined to be minimal; no leakage of cell contents which is indicative of retention of membrane integrity and no apparent effect on cell numbers (Reshetnyak et al., 2006).

Its properties, including small size, solubility, pH-dependent membrane insertion and its formation of a transmembrane helix, make it an attractive moiety for studying transmembrane protein properties. Additionally, this peptide has the potential to act as a delivery system for drug molecules, imaging probes or other cargo molecules targeting low pH environments which can be generated artificially or found in pathological conditions. pHLIP has the further advantage that cargo uptake would not be reliant on endocytic pathways which are required for the many other delivery systems discussed above. These properties of pHLIP make it an attractive delivery method for use in platelets. To date, pHLIP has not been used as a delivery agent for assisting in further understanding of cellular workings or to enable elucidation of roles of structures or protein complexes inside cells. This project aims to develop pHLIP as a delivery vector to deliver a variety of imaging labels to enable imaging of actin nodule dynamics in human platelets.

1.6 IMAGING MODALITIES

1.6.1 Epifluorescence microscopy

Epifluorescence microscopy is an optical microscopy technique which exploits the phenomenon of fluorescence or phosphorescence. Fluorescence occurs when a fluorophore absorbs a photon and then emits a photon of lower energy and therefore, higher wavelength than the excitation light. This red-shift enables the separation of the excitation and emission light through the use of filters. A schematic diagram of the principle of epifluorescence microscopy is shown below (Figure. 1.6.1).

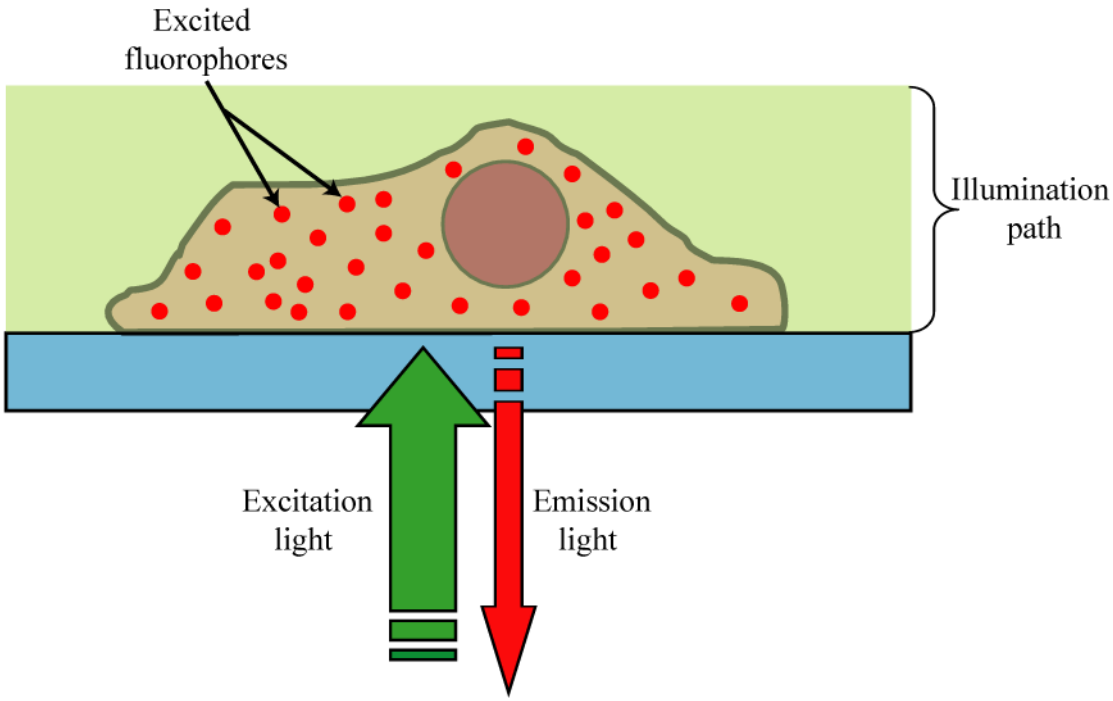

Figure 1.6.1. Schematic representation of the principles of epifluorescence microscopy. For epifluorescence microscopy in an inverted microscope system, exctiation light is transmitted through the sample, exciting fluorophores in the illuminated region throughout the cell. The fluorescence emission is collected via the use of filters to separate the excitation and emission wavelengths.

Epifluorescence microscopy is widely used for imaging fluorescent labels in cells and is suitable for both live cell and fixed cell samples. However, its main disadvantage is the inability to differentiate between fluorophores in different focal planes. Consequently, two different fluorophores which are in different focal planes appear to originate from the same point and could be misinterpreted as being co-localised.

1.6.2 Confocal fluorescence and reflection microscopy

Confocal fluorescence microscopy has similar illumination principles as fluorescence microscopy, except it is able to eliminate out-of-focus emitted light through the use of a pinhole, thereby enabling imaging in a variety of focal planes (Figure 1.6.2). Imaging in different focal planes allows for three dimensional reconstruction of the sample. There are several types of confocal microscope, namely laser scanning confocal microscope, LSCM, and spinning disk confocal microscope, SDCM. LSCM is the most commonly used type, where by a laser is scanned across a sample, while SDCM has a rotating array of microlenses to focus the beam and a simultaneous rotating array of pin holes (Stephens and Allan, 2003). SDCM enables rapid live cell imaging, with markedly reduced photobleaching but it is slow to change between limited laser lines, reducing its use in two colour studies, and it cannot be used for techniques such as fluorescence recovery after photobleaching, FRAP, both of which can be done using LSCM.

LSCM also enables confocal reflection microscopy (CRM), a technique whereby light reflected from ~10 nm either side of the excitation wavelength. Due to the interference pattern of incidence and reflected light, areas which are closer to the surface of the coated coverslip

appear dark while those further away are lighter (Curtis, 1964, Radler et al., 1995). Specialist microscopes are available which suppress stray reflections enabling imaging of ultrathin optical sections of approximately 5 nm (Filler and Peuker, 2000).

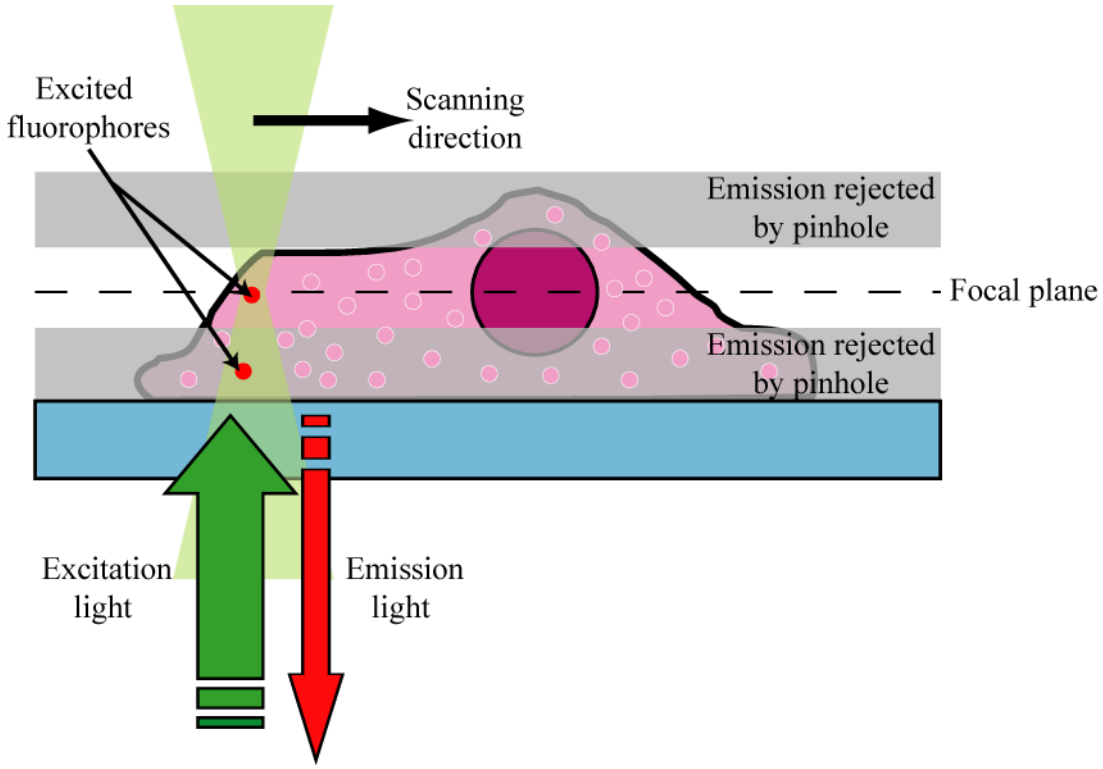

Figure 1.6.2. Schematic representation of the principles of laser scanning confocal microscopy. For laser scanning confocal fluorescence microscopy in an inverted microscope system, exctiation light is transmitted through the sample, exciting fluorophores in the illuminated region throughout the cell. The presence of an illumination pinhole focuses the excitation light into a beam which is scanned across the sample. Additionally a pinhole before the detector enables elimination of fluorescence from out-of-focus fluorophores. The fluorescence emission is collected via the use of filters to separate the excitation and emission wavelengths.

This technique can therefore be used to image membrane morphology at the interface between the membrane and the coverslip (Limozin and Sengupta, 2009, Verschueren, 1985). It has been previously used to determine close platelet/surface contact areas of platelets under static and flow conditions (Lee et al., 2012, Kasirer-Friede et al., 2010). Additionally, this technique

enables simultaneous visualisation of the whole platelet via CRM and the fluorescence image. Thereby providing more accurate cellular localisation of the fluorescence signal in platelets than would otherwise be achieved using a conventional LSCM with transmitted light imaging capabilities.

A further application of CRM is imaging of gold nanoparticles. Gold nanoparticles of ~13 nm diameter have been shown to scatter light of around 600 nm. Using CRM with 633 nm laser can enable imaging of nanoparticles in cells and has been demonstrated in fixed cell samples (Kah et al., 2008, Bickford et al., 2010).

1.6.3 Total internal reflection fluorescence microscopy

Total internal reflection fluorescence (TIRF) microscopy permits imaging at the cell membrane–coverslip interface. This is possible because the excitation light is angled such that the light will be reflected back from the interface between the glass coverslip and the cell medium, this phenomenon is known as total internal reflection. Since light cannot become discontinuous at a boundary, an evanescent wave of light is generated which exponentially decays with distance travelled (Figure 1.6.3). This provides illumination at a distance of between 100 nm and 200 nm from the coverslip (Millis, 2012). The angle required for total internal reflection to occur is greater than the critical angle, θc. The critical angle is dependent on the refractive indexes of the two surfaces, the glass coverslip and the cell medium, and defined as:

$$\sin \theta c = \frac{n2}{n1}, \qquad where\ n1\ > n2$$

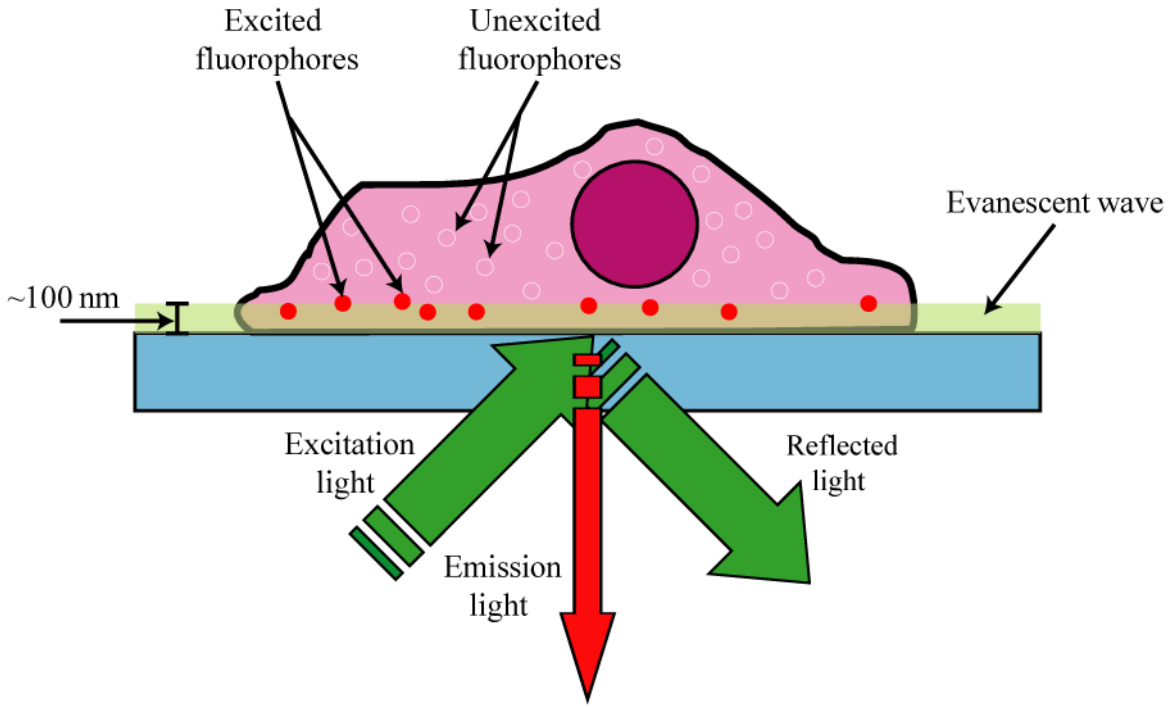

Figure 1.6.3. Schematic representation of the principles of total internal reflection fluorescence microscopy. Excitation light is reflected from the glass coverslip resulting in the generation of an evanescent wave at the interface between the coverslip and the cell. Only fluorophores in the path of the evanescent wave are illuminated.

This technique has the advantage of only illuminating fluorophores at less than 100 nm from the coverslip, therefore, removing the out-of-focus light that is usually present in fluorescent microscopy techniques. TIRF also permits imaging events at the cell surface, including cell motility and attachment events. It has also been reported that by adjusting the illumination angle enables imaging events at both the basal and the apical membrane (Fan and Jin, 2007). This is a particularly useful technique for imaging platelet spreading dynamics which involve adhesion to the surface and spreading across the surface mediated by surface receptor binding events (Schoenwaelder et al., 2010, Okamura et al., 2011).

Additionally TIRF microscopy can be combined with other imaging techniques such as confocal or epifluorescence microscopy to enable imaging of events occurring at the cell

surface and throughout the rest of the cell (Pitkeathly et al., 2012). The combination of TIRF and epifluorescence microscopy, either simultaneously or sequentially, has proven useful in studying endocytosis event enabling tracking of vesicles and their constituents from the cell membrane into the cell (Merrifield et al., 2002, Lee et al., 2006).

1.6.4 Transmission electron microscopy

Transmission electron microscopy (TEM) enables high resolution imaging of fixed samples using an electron beam to generate the image. High energy electrons are fired at ultra thin specimens interacting with the sample as they are transmitted through it. It is this interaction that is used to generate an image. The resolution achieved can be as low as ~50 pm (Erni et al., 2009). TEM has applications across many disciplines, including in cell biology and in the determination of nanoparticles size distribution.

Biological samples for TEM have to undergo a long and complex preparation process, in comparison to light microscopy samples. It includes fixation, dehydration, embedding, sectioning, mounting on grids and staining with heavy metals such as uranyl acetate or lead citrate to provide contrast.

TEM has several disadvantages, including preparation required, it can only be used for fixed samples, is more expensive than light microscopy techniques, only a small field of view so samples may not be characteristic of the whole sample and potential of damaging biological samples by the high energy beam. Despite these drawbacks, the high resolution afforded by the use of TEM makes it an attractive imaging modality for elucidating cellular structures

such as the open canalicular system and the cytoskeletal system in platelets (White and Clawson, 1980, Loftus et al., 1984, Yoshikawa, 1991). Immunogold labelling has enabled imaging of localisation of cellular proteins due to the high contrast provided by the gold label bound to an antibody of choice.

As such TEM will allow for determination of, firstly, the presence of gold nanoparticles in cell, demonstrating the ability of pHLIP as a delivery agent. Secondly, it will enable imaging, with high spatial resolution the localisation of these nanoparticles inside the cell and, as a result, direct measurement of the localisation of the protein and or structure the nanoparticles have been synthesised to bind to, for instance the actin cytoskeleton if coated with Lifeact.

1.7 MICROSCOPY LABELS

1.7.1 Fluorescent & luminescent labels

Organic fluorophores such as, fluorescein and Rhodamine, are widely used as labels in fluorescence microscopy. However, their fluorescence is often quenched following conjugation to proteins, is pH sensitive and they are not particularly photostable (Brunner et al., 1998, Singer and Johnson, 1997). This has led to the synthesis of other dyes such as Alexa dyes which are more stable, pH insensitive, exhibit more intense fluorescence and have wide variety of colours which are suitable for common excitation sources (Panchuk-Voloshina et al., 1999).

Lanthanide ions are usually referred to as luminescent rather that fluorescent labels. This is because fluorescence refers to spin allowed singlet-to-singlet emission taking 10^{-6} to 10^{-12} seconds. However, lanthanide emission is as a result of *f-f* transitions which are forbidden resulting in lifetimes in the μs to ms range. As a result, direct excitation of the lanthanide ion is inefficient so excitation is usually achieved through complexation with a ligand.

The type of complex used can be used to tune the coordination and photophysical properties of a lanthanide (Charbonniere et al., 2008, Charbonniere et al., 2007, Andreiadis et al., 2009). Since the coordination chemistry of the lanthanides is similar across the group, the lanthanide can be altered to suit the required electromagnetic or paramagnetic properties (Lewis et al., 2012). For instance, Sm^{3+}, Eu^{3+}, Tb^{3+} and Dy^{3+} emit in the visible range while Pr^{3+}, Nd^{3+}, Ho^{3+}, Er^{3+} and Yb^{3+} emit in the near-infra red, NIR, and Gd^{3+} is highly paramagnetic. The conjugation to a ligand also helps to prevent quenching of lanthanide luminescence in aqueous solutions. Furthermore, these complexes can be designed to facilitate targeting of the

lanthanide complexes to specific organelle and to signal information about the environment (Montgomery et al., 2009).

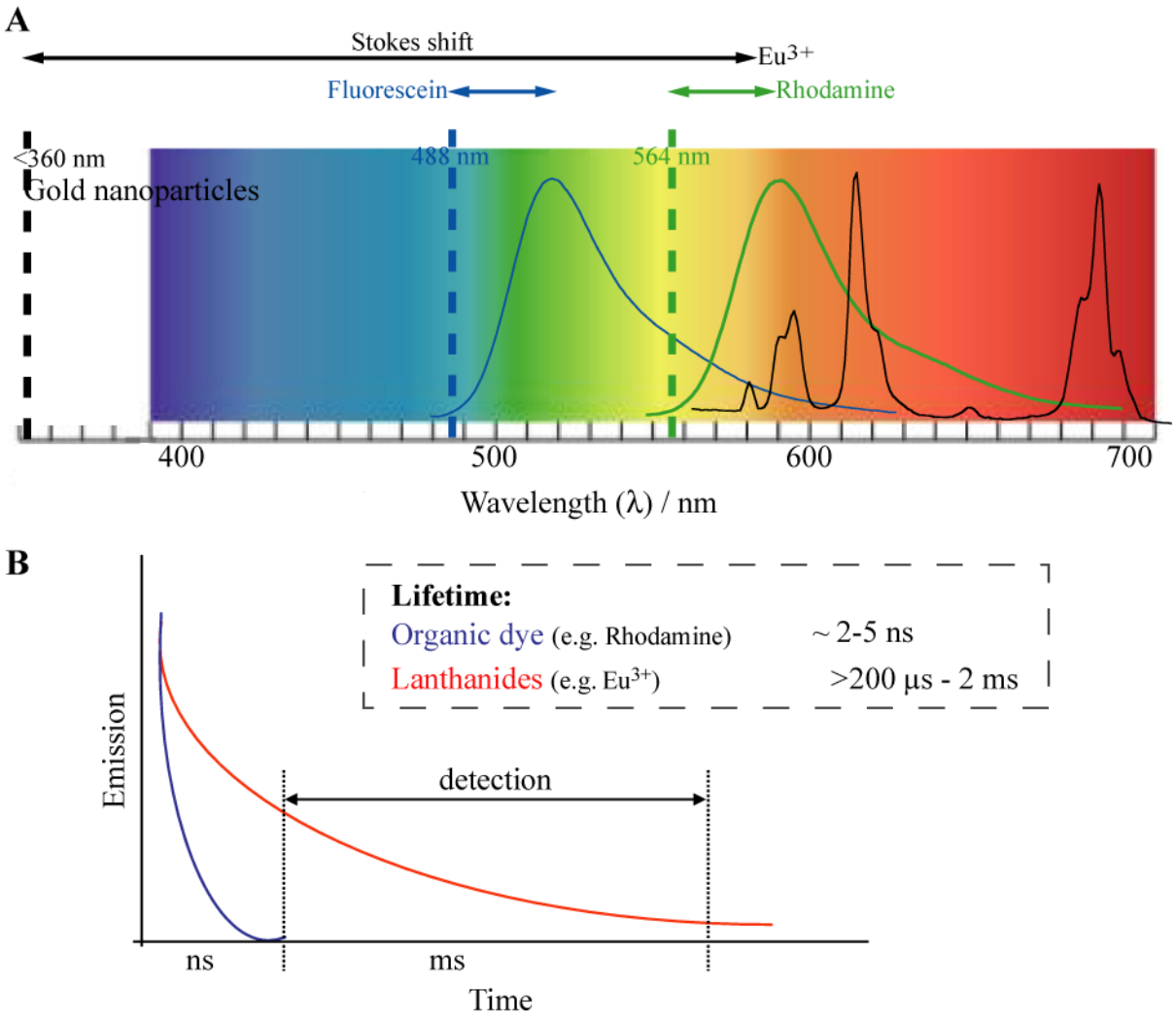

Figure 1.7.1. Electromagetic properties of organic fluorophores and luminescent lanthanide ions. (A) Emission spectra for the organic fluorophores, fluorescein (blue) and rhodamine (green), and Eu^{3+} (black). Their respective excitation wavelengths are indicated. (B) Representation of emission lifetimes for organic fluorophores and luminescent lanthanide ions.

The advantage of using lanthanides over organic fluorophores include, their visible, narrow band-width luminescence, large stokes shifts and long lifetimes (Figure 1.7.1). In addition, emission can be turned by utilising different lanthanides, which can also tune the magnetic

properties of the label. The long lifetimes make them suitable for time-gated fluorescence imaging which enables elimination of autofluorescence signals. However, they have limited brightness and excitation and emission ranges often mean they are not suitable for use with conventional microscope systems.

1.7.2 Gold nanoparticles

Gold nanoparticles, AuNP, are attractive for use in biological and biomedical applications due to their optical properties, their bioinertness and they are not toxic (Ghosh et al., 2010). Their potential applications include drug carriers, labelling and tracking agents, vectors for gene therapy and magnetic resonance imaging (MRI) contrast agents (Thanh and Green, 2010).

Formation of gold colloids involves the reduction of tetrachloroauric acid, usually following one of three methods: (1) Turkevich citrate method, (2) citrate-tannic acid method and (3) Brust-Schiffrin alkane-thiols method (Turkevich et al., 1951, Brust et al., 1994, Mühlpfordt, 1982). The simplest method is the Turkevich method which involves the reduction of tetrachloroauric acid with trisodium citrate, the mechanisms of which have been investigated widely (Grabar et al., 1995, Kimling et al., 2006, Frens, 1973). Nanoparticle size is controlled by the amount of reducing agent used (Kumar et al., 2007).

The tuneable size and electron density of AuNPs make them attractive for single particle detection in electron microscopy, thereby providing greater spatial resolution. Additionally, they provide a large surface area which behaves as a scaffold, enabling attachment of multiple

moieties. This tailoring of the monolayers formed on AuNPs mean that they are suitable for many different applications.

AuNPs can be functionalised as optical probes via the addition of fluorophores, thus enabling introduction of multiple fluorophores to a single probe. This will result in an increase in the fluorescent signal for an individual probe and, as such, facilitate single molecule imaging. This has been achieved with a variety of fluorescent molecules including organic and inorganic dyes (Hong et al., 2006, Goutayer et al., 2010, Evans et al., 2010, Wang et al., 2010, Lewis et al., 2006, Hallett et al., 2009, Dasary et al., 2008). Functionalisation of nanoparticles usually arises as a result of gold-sulphur bond formation (Chung et al., 2012, Zhong et al., 1999, Jaccob et al., 2012).

Furthermore, as optical probes, gold and silver nanoparticles are known to scatter coloured light when illuminated with white light. An increase in diameter from 40 nm results in a change in colour from green to red and are easily distinguishable in cells (Yguerabide and Yguerabide, 1998). AuNPs with smaller diameters of around 13 nm have potential for scattering light at around 600 nm (Kah et al., 2008). This enables imaging of cells treated with AuNPs using confocal reflectance microscopy using a standard 633 nm laser.

Nanoparticles have been shown to enter a variety of cells on a timescale of 2 – 24 hours of incubation usually via endocytosis or use of surfactants (Bickford et al., 2010, Chung et al., 2008, Li et al., 2010, Wang et al., 2009). Of particular interest, one study reported silver nanoparticles entered platelets within two hours of incubation (Chung et al., 2008). However,

other research suggests that gold nanoparticles may cause platelet aggregation (Wiwanitkit et al., 2009).

The delivery of gold nanoparticles in to cells without in a very short time scale ~<1 hour would be a big improvement on the current uptake times. Conjugation to pHLIP will enable this fast uptake, thereby allowing imaging of platelet and nanoparticles dynamics. In fixed cells the presence of the gold nanoparticles provide a probe when imaging with electron microscopy, and when coated with fluorophores such as a luminescent lanthanide complex that can bind to AuNP via the formation of a gold-sulphur bond, enable fluorescence microscopy in real-time.

1.8 THESIS AIMS

The overall aim of this thesis is to investigate the delivery of imaging labels into human platelets in order to further the understanding of the role of the actin nodule in platelets. This can be divided into the following objectives:

1. Investigate the role of the actin nodule in Lifeact-GFP mouse platelets.
2. Examine the suitability of pHLIP as a molecular delivery agent for human platelets.
3. Develop pHLIP as a delivery vector, in human platelets, to deliver a range of labels including, Lifeact peptide and gold nanoparticles. Thus facilitating live cell imaging of human platelet actin dynamics.

CHAPTER 2

MATERIALS & METHODS

2.1 REAGENTS

Fluorescently-conjugated antibodies for αIIb and α2 were purchased from BD Biosciences (Oxford, UK). FITC rat anti-mouse CD41 (0.5 $mgmL^{-1}$, in aqueous buffered solution containing ≤0.09 % sodium azide), PE rat anti-mouse CD41 (0.2 $mgmL^{-1}$, in aqueous buffered solution containing ≤0.09 % sodium azide) and FITC mouse anti-human CD49b (0.5 $mgmL^{-1}$, in aqueous buffered solution containing ≤0.09 % sodium azide). Antibodies were used as received, stored at 4 °C.

pHLIP and Lifeact were prepared and Lifeact labelled by Alta Biosciences. The peptide sequences were:

pHLIP: AAEQNPIYARYADWLFTPLLLLDLALLVDADEGTC(Thiopyridyl)-G

Lifeact: CMGVADLIKKFESISKEEK

The Lifeact peptide was labelled with carboxyfluorescein, FAM. Purity was checked by the supplier with high-performance liquid chromatography, HPLC, and matrix-assisted laser desorption/ionisation, MALDI, mass spectrometry where a peak observed at *m/z* 4349 is assigned to $[M-H]^-$ for pHLIP and 2557 is assigned to $[M-H]^-$ for Lifeact-FAM.

pHLIP was dissolved in a sodium phosphate buffer (0.1 M, pH 7.0) with 75 % v/v DMSO to give a 10 mM stock solution and Lifeact-FAM was dissolved in a sodium phosphate buffer (0.1 M, pH 7.0) with 37 % v/v DMF to give a 5 mM stock solution. The peptides were stored at -20 ºC.

DyLight 550 Antibody Labelling Kit was purchased from Pierce. FM4-64FX lipophilic styryl dye was purchased from Invitrogen.

EuL was prepared by D. J. Lewis as previously described (Davies et al., 2012). PlasmaCal Calibration standards for europium and gold were purchased from SCP science.

N-succinimidyl 3-(2-pyridyldithio) propionate, SPDP, and Tris(2-carboxyethyl)phosphine hydrochloride, TCEP, was purchased from Pierce.

Unless otherwise stated, all chemicals were purchased from Sigma-Aldrich. Solvents were purchased from Sigma-Aldrich or Fisher. Deuterated solvents were purchased from Goss Scientific or Sigma-Aldrich and used as received. HPLC grade solvents were used in photophysical studies. Water was deionised using an Elgar Option 3 water purifier.

2.2 METHODS

2.2.1 Platelet preparation

2.2.1.1 Preparation of murine platelets.

All solutions were warmed to 37 °C prior to use. Fresh murine blood was obtained from CO_2 terminally anaesthetised mice by cardiac puncture and taken into acid-citrate-dextrose (ACD; 100 µL 10% v/v, 85 mM sodium citrate, 110 mM glucose, 80 mM citric acid). Modified Tyrode's buffer (200 µL, 134.0 mM NaCl, 2.90 mM KCl, 0.34 mM Na_2HPO_4:$12H_2O$, 12.0 mM $NaHCO_3$, 20.0 mM Hepes, 1.0 mM $MgCl_2$, pH 7.3) containing glucose (5.0 mM) was added to the blood and the resulting suspension centrifuged for 5 minutes (200 x g) at room temperature. 700 µL was removed from the top of the suspension and centrifuged for 6 minutes (200 x g) to obtain the yellow supernatant (platelet rich plasma - PRP). Washed platelets were prepared via centrifugation of PRP for 6 minutes (1000 x g) in the presence of PGI_2 (0.1 μgmL^{-1}). The pellet was resuspended in modified Tyrode's buffer to a concentration of 2×10^8 $cellsmL^{-1}$ and allowed to rest for 30 minutes.

2.2.1.2 Isolation of human platelet rich plasma

All solutions were warmed to 37 °C prior to use. Fresh human blood was obtained into sodium citrate (10% v/v) by venipuncture. Acid-citrate-dextrose (ACD, 10% v/v; 85 mM sodium citrate, 110 mM glucose, 80 mM citric acid) was added to the blood and the resulting suspension transferred to polypropylene tubes and centrifuged for 20 minutes (200 × g) at room temperature. The yellow supernatant (platelet rich plasma - PRP) was collected.

2.2.1.3 Preparation of washed human platelets. PGI_2 (0.1 μgmL^{-1}) was added to the PRP and the suspension centrifuged for 10 minutes (1,000 × g). The resulting supernatant was removed and the pellet resuspended in modified Tyrode's buffer (25 mL, 134.0 mM NaCl, 2.90 mM KCl, 0.34 mM Na_2HPO_4:$12H_2O$, 12.0 mM $NaHCO_3$, 20.0 mM Hepes, 1.0 mM $MgCl_2$, pH 7.4) containing glucose (5.0 mM) and ACD (3 ml). PGI2 (0.1 μgmL^{-1}) was added and suspension was centrifuged for 10 minutes (1000 x g). The resultant supernatant was removed and the pellet resuspended in modified Tyrode's buffer containing glucose and ACD as previous. The platelet suspension was diluted to 2×10^8 $cellsmL^{-1}$ and allowed to rest for 30 minutes.

2.2.1.4 Preparation of human platelets for treatment with pHLIP/ pHLIP-Lifeact/ pHLIP•AuNP samples.

As described above (**2.2.1.2**), PRP was collected, PGI_2 (0.1 μgmL^{-1}) was added and the suspension centrifuged for 10 minutes (1,000 × g). The resulting supernatant was removed and the pellet resuspended in modified Tyrode's buffer (25 mL, 134.0 mM NaCl, 2.90 mM KCl, 0.34 mM Na_2HPO_4:$12H_2O$, 12.0 mM $NaHCO_3$, 20.0 mM Hepes, 1.0 mM $MgCl_2$, pH 6.5 (or pH 7.4, as required)) containing glucose (5.0 mM) to a concentration of 2×10^8 $cellsmL^{-1}$ and allowed to rest for 30 minutes.

2.2.2 Platelet functional assays

2.2.2.1 Platelet spreading.

Glass coverslips were coated with fibrinogen (100 μgmL^{-1} in PBS) at 4 °C overnight. Uncoated glass was blocked by denatured BSA (5 $mgmL^{-1}$ in PBS, 1 hour at room temperature). Platelet suspensions were diluted to 2×10^7 $cellsmL^{-1}$ with modified Tyrode's buffer (at pH 6.5 or pH 7.4, as required).

For live cell imaging, platelets were allowed to spread on the coverslips in a live cell imaging chamber. The microscopes were fitted with an environment chamber and heated to 37 °C prior to imaging.

For fixed cell samples, platelets were allowed to spread on the coverslips at 37 °C for 45 minutes in a humidified chamber (37 °C, 5% CO_2) prior to fixation with 10% formalin for 10 minutes. Residual formalin was quenched with NH_4Cl_2 (50 mM) for 10 minutes at room temperature. Coverslips were washed three times with PBS and once with deionized water and mounted on glass slides using Hydromount and stored at 4 °C until imaged.

2.2.2.2 Platelet inhibitor assays

In separate experiments, platelet suspensions were treated with Cytochalasin D (10 µM), Latrunculin A (3 µM), Jasplakinolide (5 µM), Y27632 (20 µM), PP2 (10 µM), BAPTA-AM (10 µM), CK-666 (20 µM) for 10 min prior to spreading. Solvent control samples were treated with DMSO (0.1 % *v/v*), likewise.

2.2.2.3 Antibody staining.

Platelets were incubated with fluorescently labelled antibodies (1 % v/v) for 10 minutes prior to spreading.

2.2.2.4 Fixed cell actin staining.

Following fixation and quenching with NH_4Cl_2, coverslips were washed three times with PBS. Triton X-100 (0.1 % in PBS) was added to cells for 5 minutes, washed with PBS and fluorescently labelled phalloidin (6.6 pM; in PBS containing BSA), Lifeact (5 pM; in PBS containing BSA) or Lifeact•AuNP (30 pM; in PBS) added. Samples were left in the dark for 30 minutes, then washed with PBS and water and mounted as previously described.

2.2.2.5 pHLIP/ pHLIP-Lifeact treatment of human platelets.

Unless otherwise stated, Lifeact/ pHLIP/ 550-pHLIP/ pHLIP-Lifeact/ 550-pHLIP-Lifeact was added to platelet suspension (2×10^8 cellsmL^{-1}) for 40 minutes (room temperature). The suspension was then diluted with modified Tyrode's buffer (at pH 6.5 or pH 7.4, as required) containing glucose to2×10^7 cellsmL^{-1} prior to spreading.

2.2.2.6 AuNP treatment of human platelets

Unless otherwise stated, pHLIP•EuL•AuNP, pHLIP•AuNP, EuL•AuNP or citrate-stabilized AuNP (approximately 8,000 NPs⁄cell or approximately 40,000 NPs⁄cell for TEM and light microscopy, respectively) were added to the platelet suspension (2×10^8 cellsmL^{-1} or 3.2×10^8 cellsmL^{-1} for light microscopy and TEM, respectively) for 10 minutes (room temperature). The suspension was then diluted with modified Tyrode's buffer (at pH 6.5 or pH 7.4, as required) containing glucose to2×10^7 cellsmL^{-1} prior to spreading or platelet suspension fixed for TEM.

2.2.2.7 Variable pH platelet experiment.

Following treatment with pHLIP/ pHLIP-Lifeact/ pHLIP•AuNP samples, modified Tyrode's buffer (pH 6.5 for pH 6.5 samples or 7.4, and pH 6.5 to 7.4 and pH 7.4 samples) was added to cell suspension to a concentration of 1×10^8 cellsmL^{-1} and allowed to rest for 10 minutes. PGI_2 (0.1 μgmL^{-1}) was added and the suspension centrifuged for 10 minutes (1,000 × g). The resulting supernatant was removed and the pellet resuspended in modified Tyrode's buffer (pH 6.5 for pH 6.5 samples or 7.4, and pH 6.5 to 7.4 and pH 7.4 samples) to a concentration of 2×10^7 cellsmL^{-1} and allowed to rest for 20 minutes prior to spreading.

2.2.2.8 Platelet leakage assay.

Washed human platelets were loaded with Oregon-Green BAPTA-1 AM (1 μM) in the presence of $CaCl_2$ (200 μM) and Apyrase (2 UmL^{-1}) for 45 minutes at 37 °C. ACD (12 μlmL^{-1}) and PGI_2 (0.1 μgmL^{-1}) were added and the cells centrifuged for 20 minutes (700 × g). The resulting supernatant was removed and the pellet resuspended in modified Tyrode's buffer (pH 6.5). pHLIP•EuL•AuNP (approximately 8;000 NPs⁄cell), saponin (10 μgmL^{-1}) or modified Tyrode's buffer (pH 6.5) were added to the platelet suspension for 10 minutes at room temperature. The platelets were centrifuged for 20 minutes (700 × g) in the presence of PGI_2 (0.1 μgmL^{-1}) and the resulting supernatants retained. $CaCl_2$ (50 μM final) was added to the supernatants and the emission of Oregon-Green BAPTA-1 AM between 510 nm and 600 nm was recorded following excitation at 480 nm. The area under the curve was determined for each sample to determine fluorescence intensity.

2.2.2.9 Labelling of the platelet membrane with FM4-64FX.

Labelling of the platelet membrane with FM4-64FX lipophilic styryl dye was undertaken as per manufacturer's instructions. All solutions were kept on ice and staining procedure was

carried out on ice. Essentially, FM4-64FX (100 μg) was dissolved in water (100 μL) to give a stock solution of 1 $mgmL^{-1}$ and stored at -20 °C. Washed platelets (2×10^{7} $cellsmL^{-1)}$ were allowed to spread on fibrinogen (100 $mgmL^{-1}$ in PBS) coated coverslips for 45 minutes. A working solution of dye (5 μgmL^{-}) in PBS was prepared a few minutes prior to staining. Coverslips were removed from Tyrode's buffer and quickly immersed in the staining solution for 1 minute. Platelets were then fixed with 10 % formalin for 10 minutes. Residual formalin was quenched with NH_4Cl_2 (50 mM) for 10 minutes at room temperature. Coverslips were washed three times with PBS and once with deionized water and mounted on glass slides using Hydromount and stored at 4 °C until imaged.

2.2.2.10 Platelet Preparation for TEM.

Following treatment with nanoparticles, treated or untreated platelet samples were centrifuged (10 minutes, 1,000 × g) in the presence of PGI_2 (0.1 μgmL^{-1}) and resuspended in gluteraldehyde (2.5% v/v, 0.5 M PBS). Samples were subsequently placed in 1% osmium tetroxide solution and gradually dehydrated with alcohol and propylene oxide. The platelets were embedded in resin and ultrathin sections (50 — 150 nm) obtained which were mounted onto copper electron microscope grids (Formvar film). Samples were contrasted with uranyl acetate and lead citrate.

2.2.3 Preparation of pHLIP conjugates

2.2.3.1 pHLIP-Lifeact conjugation.

Lifeact-FAM (5 mM; 37 % v/v in sodium phosphate buffer, pH 7) was added in 8 equal aliquots to pHLIP (5 mM; 75 % v/v in sodium phosphate buffer, pH 7) to give a final ratio of 8 parts Lifeact to 10 parts pHLIP. The conjugation reaction occurred at room temperature and in the dark to prevent bleaching of fluorescein. When necessary the peptide conjugate was diluted using ultrapure water.

Reverse phase high performance liquid chromatography, HPLC, was used to determine conjugation of Lifeact-FAM to pHLIP.

2.2.3.2 Labelling pHLIP with Dylight 550.

The labelling of the *N*-terminus of pHLIP was achieved using Dylight Antibody labelling kit (Pierce), as per manufacturer's instructions. Essentially, pHLIP (2 mg) was dissolved in sodium borate buffer (0.05 M in PBS, 1 mL). Borate buffer (0.67 M, 40 μL) was added to peptide solution (0.5 mL). The peptide solution (0.5 mL) was added to vial containing Dylight Reagent and vortexed gently. The reaction mixture was incubated for 60 minutes at room temperature protected from light. Purification resin (250 μL) was added to two spin columns and centrifuged for 1 minute (1000 x g) to remove storage solution. Peptide solution (250 μL) was added to each of the spin columns and vortexed to enable mixing of the resin and peptide solution prior to centrifugation for 1 minute (1000 x g). The eluents were collected and combined. The absorbance at 280 and 557 nm was measured using Nanodrop UV-Vis spectophotometer (Thermo Scientific) and the protein concentration and moles dye/mole protein calculated as 0.34 mM and 0.045 moles dye/mole protein, respectively (ε_{pHLIP} = 13,940 M^{-1} cm^{-1}, (Reshetnyak et al., 2006)).

2.2.3.3 Synthesis of citrate-stabilised gold nanoparticles, AuNP.

Gold colloids were prepared as per Grabar *et al* (Grabar et al., 1995). Essentially, all glassware used in this preparation were initially washed with aqua regia (3:1 HCl/HNO_3) and water and dried in an oven. Hydrogen tetrachloroaurate (0.17 g, 0.5 mM) was dissolved in deionised water (500 mL) and brought to the boil with vigorous stirring. Sodium citrate (0.57 g, 1.9 mM) in water (50 mL) was then added rapidly to the vortex, initiating a slow colour change from yellow to burgundy. The resulting solution was kept at the boil for a further 10 minutes. The solution was then allowed to cool to room temperature and stirring was continued for 15 minutes. The resulting AuNP were characterised using UV-Vis absorption spectroscopy and TEM to confirm the presence of approximately 13 nm spherical nanoparticles.

2.2.3.4 Preparation and characterisation of pHLIP•EuL•AuNP.

The preparation of pHLIP•EuL•AuNP was monitored by the changes of the shifts in the characteristic nanoparticle SPR band during titration of pHLIP and EuL using UV-Vis absorption spectroscopy. Ten aliquots of pHLIP (2 μL, 10 mM in sodium phosphate buffer (0.1 M) with 75% v/v DMSO) were added to citrate gold nanoparticles, AuNP (2.5 mL, 9.4 nM in water) up to a final peptide concentration of 80 μM where no further shift of the SPR was observed. Subsequent titration of seven aliquots of EuL (12 μL, 10 mM in methanol) led to further shifts of the SPR up to a final EuL concentration of 0.33 mM. The solution was purified by size-exclusion chromatography on superfine Sephadex G25 and eluted with distilled water. The red band was collected and stored at 4 °C and the UV-Vis spectrum was repeated to ensure no changes on the SPR band following chromatography. The dilution

effect after the column was examined by UV-Vis spectroscopy and the final nanoparticle concentration was estimated to be 7.4 nM. This sample was used to treat the platelets. Excitation and emission spectra were acquired for diluted samples, as indicated, to avoid inner filter effects. Characteristic UV-Vis (H_2O) λ_{max} = 527 nm. TEM results indicate mono-disperse nanoparticles of 13 nm diameter. Zeta potential (4.9 nM) = −29 (±1) mV.

2.2.3.5 Preparation and characterisation of pHLIP•AuNP.

The shifts of the SPR band were monitored upon addition of aliquots of pHLIP (20 μL, 10 mM in 0.1 M sodium phosphate buffer with 75% v/v DMSO) to AuNP (2.5 mL, 9.4 nM) to reach a final peptide concentration of 80 μM. The solution was purified by size-exclusion chromatography as described for pHLIP•EuL•AuNP, and a final concentration of 7.4 nM was used to treat the platelets. Characteristic UV-Vis (H_2O) λ_{max} = 523 nm. Zeta potential (4.9 nM) = −21 (±1) mV.

2.2.3.6 Preparation and characterisation of EuL•AuNP.

The shifts of the SPR band were monitored upon addition of aliquots of EuL (30 μL, 10 mM in methanol) to AuNP in water (2.5 mL, 9.4 nM) to a final concentration of 0.12 mM. The suspension was purified by size-exclusion chromatography, as described for pHLIP•EuL•AuNP, and a final concentration of 7.4 nM was used to treat the platelets. Characteristic UV-Vis (H_2O) λ_{max} = 526 nm. TEM results indicate mono-disperse nanoparticles of 13 nm diameter. Zeta potential (4.9 nM) = −14 (±2) mV.

2.2.3.7 Preparation and characterisation of Lifeact•AuNP.

The preparation of Lifeact•AuNP was monitored by the changes of the shifts in the characteristic nanoparticle SPR band during titration of Lifeact using UV-Vis absorption spectroscopy. Eight aliquots of Lifeact (1 μL, 5 mM in sodium phosphate buffer (0.1 M) with 37% DMSO) were added to citrate gold nanoparticles, AuNP (2.5 mL, 9.4 nM in water) up to a final peptide concentration of 16 μM where no further shift of the SPR was observed. The solution was purified by size-exclusion chromatography on superfine Sephadex G25 and eluted with distilled water. The red band was collected and stored at 4 °C and the UV-Vis spectrum was repeated to ensure no changes on the SPR band following chromatography. The dilution effect after the column was examined by UV-Vis spectroscopy and the final nanoparticle concentration was estimated to be 6.3 nM. This sample was used to label platelets or for further synthetic steps. Emission spectra were acquired for diluted samples, as indicated, to avoid inner filter effects. Characteristic UV-Vis (H2O) λmax = 525 nm.

2.2.3.8 Preparation and characterisation of SPDP-Lifeact•AuNP. The preparation of SPDP-Lifeact•AuNP was monitored by the changes in the nanoparticle SPR band following the addition of SPDP using UV-Vis absorption spectroscopy. As similarly described by manufacturers instructions and Lee *et al*, SPDP (400 μL, 3 mM in PBS with 10 % DMSO) was added to Lifeact•AuNP (400 μL, 30 nM in PBS) and stirred vigorously for 45 minutes at room temperature (Lee et al., 2009). Unconjugated SPDP was removed by repeated centrifugation for 30 minutes (13,000 rpm, 4 °C), supernatant removed and the nanoparticles re-dispersed in PBS (three times). After removal of supernatant following final washing step, the nanoparticles were re-dispersed in sodium borate buffer (400 μL). The UV-Vis spectrum was repeated to ensure no changes on the SPR band following washing.

2.2.3.9 Preparation and characterisation of pHLIP-Lifeact•AuNP. pHLIP-SH (16 μM, in sodium phosphate buffer with 37 % DMF) was added to SPDP-Lifeact•AuNP (15 nM, in sodium borate buffer or PBS) and incubated for 18 hours at room temperature.

2.2.3.10 Reduction of disulphide bond on pHLIP, pHLIP-SH. The disulphide bond on the *C*-terminus of pHLIP was reduced by addition of TCEP (4.28 μL, 3.8 mM in PBS) to pHLIP (46 μL, 10 mM in sodium phosphate buffer (0.1 M) with 75 % DMF). The reaction was allowed to proceed at room temperature for 1 hour then the peptide was stored at 4 °C for several days before use. Prior to use pHLIP-SH was diluted with sodium phosphate buffer to a concentration of 5 mM.

2.2.3.11 Lifeact•AuNP buffer compatibility. Lifeact•AuNP (6.3 nM in water) was centrifuged for 30 minutes (13,000 rpm, 4 °C). The supernatant was removed and the nanoparticles were re-dispersed in PBS, PBS-EDTA (100 mM sodium phosphate, 150 mM NaCl, 1 mM EDTA, 0.02 % *w/v* sodium azide, pH 7.5) or sodium borate buffer (0.1 M; 50 mM boric acid, 20 mM sodium tetraborate, pH 7.5) to a Lifeact•AuNP concentration of 9.3 nM. The UV-Vis spectrum was repeated to ensure no changes on the SPR band following buffer change.

2.3 INSTRUMENTATION

2.3.1 Confocal reflection and fluorescence microscopy.

Samples were imaged using the 488 nm laser line (Ar/ArKr laser), 543 nm and 633 nm laser line (He/Ne laser) on a Leica DMIRE 2 laser scanning confocal microscope with 63×, 1.4 N/A. oil objective. Reflected light was collected at 478 – 498 nm and 623 – 643 nm for excitation of 488 nm and 633 nm, respectively. Fluorescence emission was collected at 500 - 550 nm for GFP and FAM, 580 - 650 nm for PE and DyLight 550 and 645 – 850 for FM4-64FX. Images were acquired using the Leica TSC SP2 software.

2.3.2 Total internal reflection fluorescence microscopy.

Live samples were imaged using the Olympus IX81 Inverted microscope with a 60x Plan Apo 1.49 NA oil-immersion objective and a Hammamatsu ORCA-R2 C10600 12-bit CCD. Fluorescein was excited with a 491-50 Diode type laser and PE with a 561-50 DPSS type laser. Images were acquired using Xcellence Advanced Live Cell Imaging System 1.1.

TIRF microscopy undertaken in the Machesky lab (Beatson Institute for Cancer Research, Glasgow) (Figure 3.15) was performed on a Nikon Eclipse TE 2000-U microscope equipped with a 60x and a 100x 1.45 NA Nikon TIRF oil immersion objectives. The Nikon Epi-fluorescence condenser was replaced with a custom condenser in which laser light was introduced into the illumination pathway directly from the optical fibre output oriented parallel to the optical axis of the microscope. The light source for evanescent wave illumination was a 473 nm diode laser or 561 laser (Omicron), with each laser line coupled into the condenser separately in order to allow individual TIRF angle adjustments. The lasers were controlled by a DAC 2000 card or a uniblitz shutter operated by MetaMorph (Molecular

Devices). A green/red dual filterblock (ET-GFP/mcherry, AHF Analysentechnik, Germany) was used for dual colour excitation 473 and 561 excitation. A Multi-Spec dual emission splitter (Optical Insights, NM) with a 595nm dichroic and two bandpass filters (510-565 for green and 605-655nm for red) was used to separate both emissions. All imaging was performed with a Cascade 512F EMCCD camera (Photometrics UK).

Live human platelets labelled with antibody for FITC-α2 (Figure 3.18) were imaged using the Nikon A1R inverted confocal/TIRF microscope with CFI Plan Apo TIRF 60x 1.49 N.A oil objective. The excitation used was, Exciter S490/20x with Dichroic 86100bs and the emission was collected using Emitter S528/38m for FITC. Images were acquired using NIS Elements AR Software Advanced Research.

2.3.3 Transmission electron microscopy.

Samples were imaged using Jeol 1200EX TEM with an operating voltage of 80 keV and Gatan multiscan camera. Images were acquired using DigitalMicrograph 1.8 (Gatan, CA, USA).

2.3.4 Luminescence microscopy and spectroscopy.

Samples were imaged using an Olympus IX71 inverted fluorescent microscope with a LUCPLFLN 40×, 0.60 N/A: objective coupled to an Edinburgh Instruments FLS920 spectrophotometer. Excitation at 340 nm was achieved by a 450 W Xe lamp and EuL emission (>510 nm) was detected by a Hamamatsu EMCCD C9100-13. Excitation and emission wavelengths were controlled using Edinburgh Instruments v6.8 PC software. Images

were acquired using Cell^M 3.2 (Olympus Soft Imaging Solutions GmBH). Emission spectra were acquired using Edinburgh Instruments F900 v6.8 PC software.

Steady-state luminescence experiments were carried out using an Edinburgh instruments FLS900 system equipped with a 450 W Xenon lamp, double excitation and emission monochromators. Detection of emitted photons was achieved by the use of a cooled Hamamatsu R928 (Vis-red sensitive) photomultiplier tube. Emission lifetimes were recorded on the same system using an Edinburgh Instruments μF microsecond flashlamp (1–1000 Hz) as excitation source and using the multichannel scaling, MCS, single photon counting method. Detector saturation was avoided in all circumstances by using minimal signal rate intensities combined with extended data collection times. Lifetime data were fitted to - decays using Edinburgh Instruments F900 PC software using the exponential tail fit option. Instrument response for lifetime data collected using the IX-71 microscope was measured using erythrosine in water.

2.3.5 UV-Vis absorption spectroscopy.

UV-Vis absorption spectra were recorded using a Varian Cary 5000 dual beam spectrometer.

2.3.6 Inductively Coupled Plasma Optical Emission Spectroscopy, ICP-OES.

ICP-OES analysis was run at the University of Warwick using a Perkin-Elmer 5300DV ICP-OES system. Concentrations of europium and gold in nanoparticle samples were determined using linear calibration curves constructed from purchased standards, with $R^2 > 0.999$ in all cases.

2.3.7 Zeta-potential measurements.

Zeta potentials were acquired using a Beckman-Coulter DelsaNano C instrument. All samples studied were at 4.9 nM concentration of particles.

2.4 ANALYSIS OF RESULTS

2.4.1 Analysis of live cell mouse platelet images

Individual platelets which were observed to settle and start spreading during imaging were cropped to enable visualisation and analysis of platelet actin nodule dynamics.

2.4.2 Analysis of number of nodules per platelet

The number of nodules per platelet was counted for each time frame and recorded. Additionally, the number of frames that each individual nodule was present in was counted and multiplied by the time between frames to give a value for the nodule lifetime in the cell.

2.4.3 Platelet area/ nodule size.

The mean platelet surface area or mean nodule size (μm^2) of individual platelets or nodules was quantified using ImageJ software.

2.4.4 Analysis of nodule displacement

The coordinates of the approximate centre of nodules was recorded for each individual nodule at each time point. The displacement at each time point was calculated from the difference between the first recorded coordinates and the coordinate at the time point of interest.

2.4.5 Statistics.

Where applicable, results are shown as ± standard error mean, s.e.m. Statistical significance of differences between means was ascertained by Student's *t*-test or one-way analysis of variance, ANOVA, as indicated, using GraphPad Prism v4.03 for Windows (GraphPad Software, San Diego California, USA, www.graphpad.com). If means were determined to be

significantly different with ANOVA, further multiple comparisons were undertaken using a Tukey test. For all results, probability values of $P < 0.05$ were considered to be statistically significant

CHAPTER 3

IMAGING OF LIFEACT-GFP MOUSE PLATELETS TO ELUCIDATE THE ROLE OF ACTIN NODULES IN PLATELET ADHESION AND SPREADING

3.1 INTRODUCTION

Actin nodules were first described by Calaminus *et al* as a novel actin-rich structure in platelets which appear prior to lamellipodia and stress fibre formation during platelet spreading (Figure 3.1) (Calaminus et al., 2008). The nodules were also labelled with antibodies for various actin regulatory proteins, including Rac, Fyn, cortactin, talin, Arp2/3 complex, β1- and β3-integrin subunits, and under flow and shear stress conditions, with activated Src (Calaminus et al., 2008, Kasirer-Friede et al., 2010). From these findings, it has been conjectured that the nodules may have a role in driving formation of the later forming actin structures, such as lamellipodia and stress fibres, while also involved in surface anchoring in shear stress conditions.

However, this work was done using fixed human platelets stained with phalloidin or mouse platelets expressing actin-GFP, neither of which are suitable methods for imaging actin nodule dynamics. Firstly, phalloidin can only be used in fixed platelets due to its inability to permeate the cell membrane and the stabilising effect that phalloidin has on actin filaments (Wulf et al., 1979). Although, incredibly useful for imaging actin in fixed cells, fixed cells imaging does not provide temporal information about the nodule's appearance, disappearance or what it does in between. Thus live-cell imaging is a far more useful approach to

understanding what an actin nodule is and its role in platelet spreading. Secondly, although cells expressing actin-GFP enable live cell imaging, the actin fusion proteins have been shown to alter the actin dynamics (Feng et al., 2005, Deibler et al., 2011).

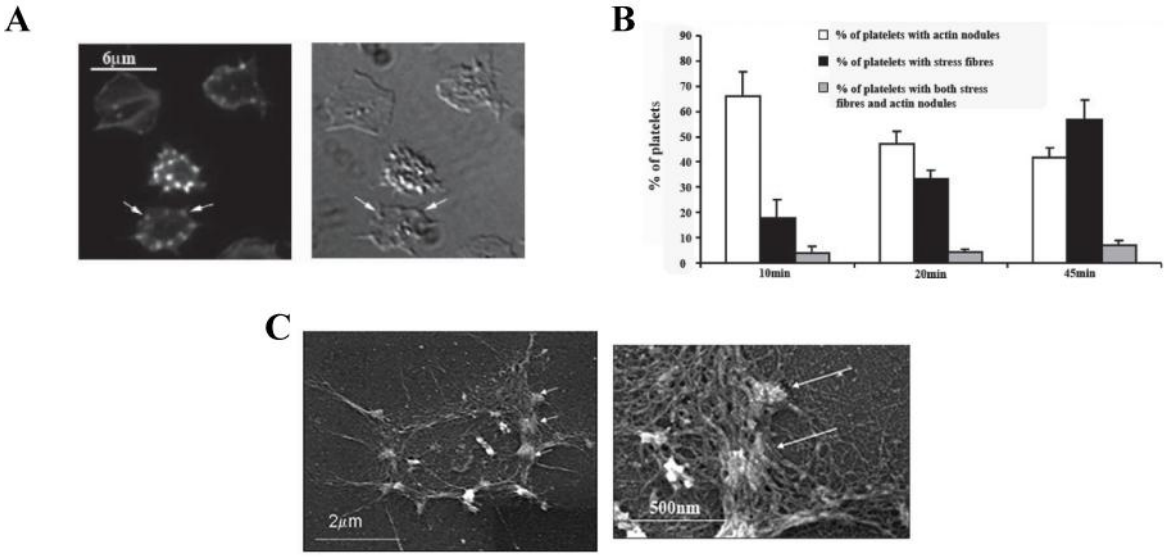

Figure 3.1. Identification of the platelet actin nodule. (A) Fluorescence and DIC images of human platelets allowed to spread on fibrinogen for 45 minutes prior to fixation and staining with FITC-phalloidin. Arrows indicate the location of actin nodules which are visible in both fluorescent and DIC images. (B) Percentage of actin nodule containing platelets decreased as cells spread and stress fibres appeared. (C) Scanning electron microscopy of platelets allowed to spread on fibrinogen for 45 minutes in the presence of blebbistatin. Arrows indicate the position of actin nodules from which actin filaments appear to spread out from. Images taken from (Calaminus et al., 2008).

A mouse model expressing Lifeact-GFP has been developed (Riedl et al., 2010). Lifeact, an actin binding protein, has been shown to bind transiently with F-actin and, as such, it does not appear to interfere with actin dynamics to the same extent as actin-GFP (Riedl et al., 2008, Deibler et al., 2011). Furthermore, in a conditionally-inducible Lifeact-GFP mouse model, platelets appear unaffected by the presence of Lifeact-GFP and spread normally (Schachtner et al., 2012). Therefore, use of platelets from Lifeact-GFP mice will enable live cell imaging of platelet spreading and consequently the study of actin nodules.

It is the aim of the work in this chapter to utilise platelets from GFP-Lifeact mice to study the actin nodule dynamics in order to elucidate the role of the actin nodule during platelet spreading.

3.2 RESULTS & DISCUSSION

3.2.1 Characterisation of actin nodule dynamics

Actin nodule dynamics were first imaged using platelets from actin-GFP mice which suggested that these actin structures were dynamic (Calaminus et al., 2008). Live cell TIRF imaging of Lifeact-GFP mouse platelets confirmed the dynamic and transient nature of actin nodules in spreading platelets (Figure 3.2).

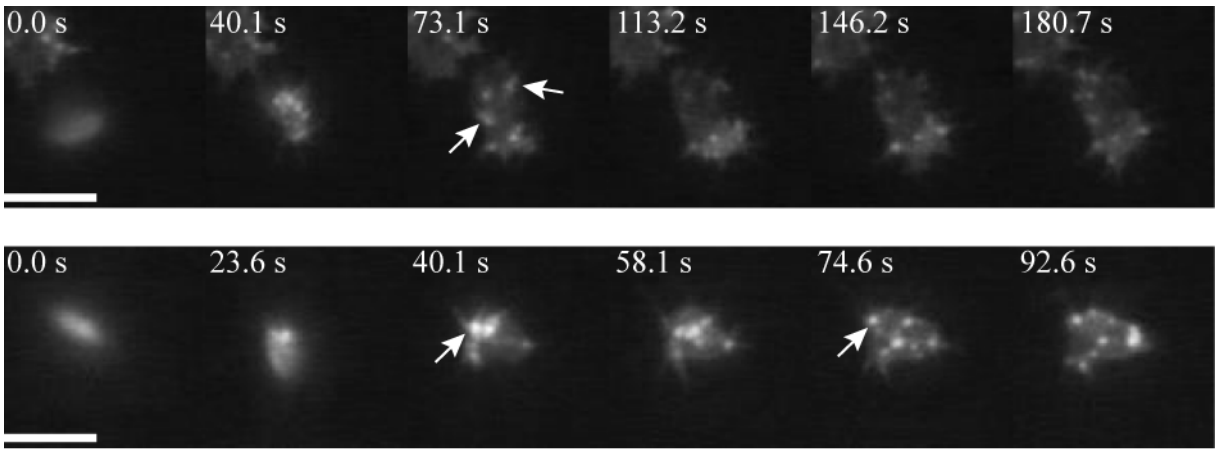

Figure 3.2. Time course of actin nodule dynamics in Lifeact-GFP mouse platelets. Washed Lifeact-GFP mouse platelets (2×10^7 mL^{-1}) were allowed to spread on fibrinogen (37 °C). Platelet spreading was monitored using real-time TIRF microscopy, with an image acquired every 1.5 s. Time course of two individual platelets (*top/ bottom*) at indicated time points demonstrate the changes in platelet shape and nodule number during platelet spreading. Images are representative of more than three expreiments. Scale bar = 5 μm.

TIRF microscopy enables imaging of the nodules at the basal cell membrane, however any nodules which are not present within 100 nm of the coverslip would not be seen. Therefore, to investigate whether there are nodules present in the platelet which are outside of the evanescent field, platelets were image in TIRF and epifluorescence illumination (Figure 3.3 *A*). Epifluorescence microscopy enables imaging of events throughout the cell.

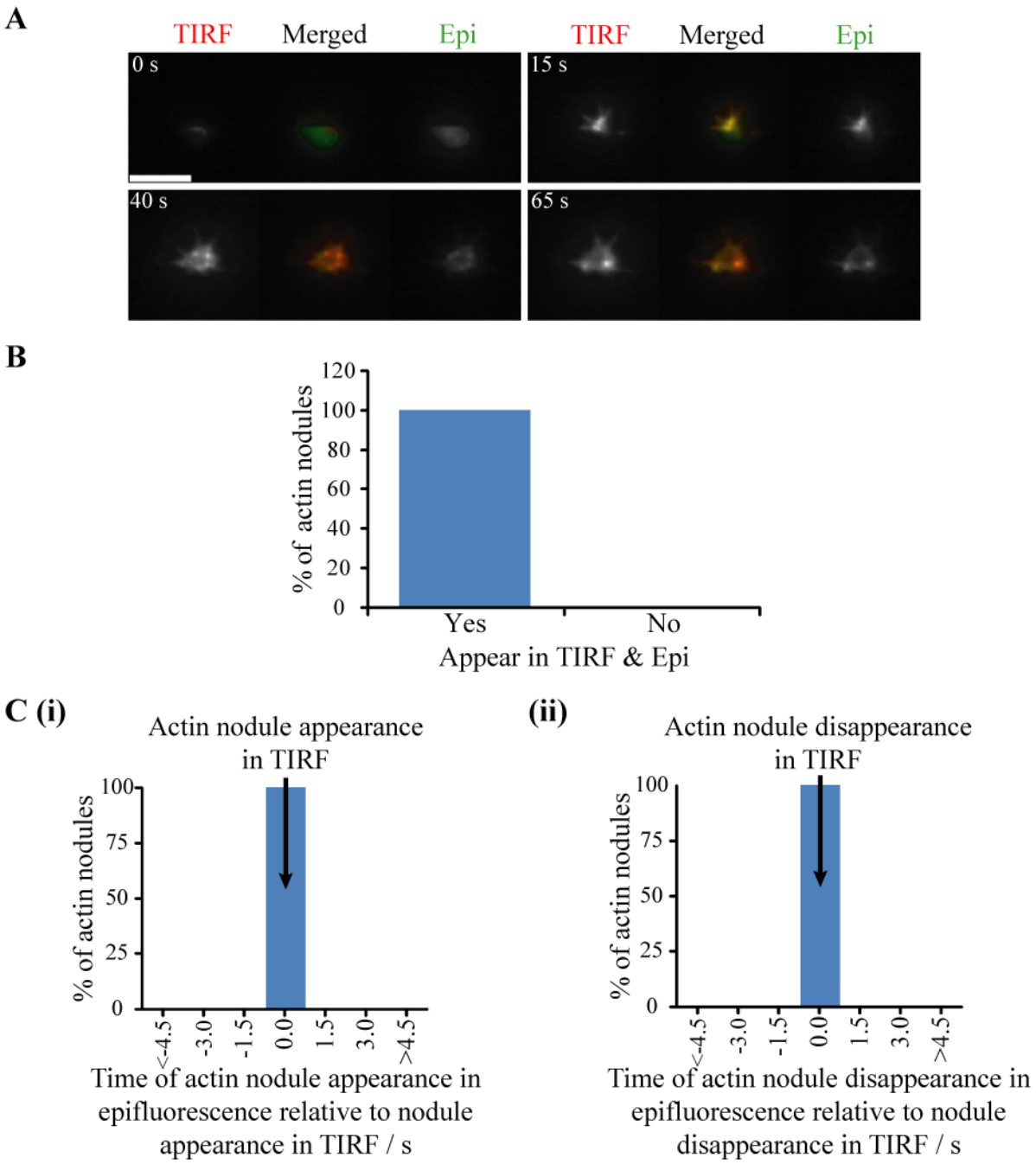

Figure 3.3. Appearance of actin nodules in TIRF and epifluorescence microscopies. Washed Lifeact-GFP mouse platelets (2 x 10^7 mL^{-1}) allowed to spread on fibrinogen (37 °C). Platelet spreading was monitored using real-time TIRF and epifluorescence microscopy, with a TIRF and epifluorescence image acquired every 1.5 s. (A) Time course of one individual platelet, at indicated time points, spreading in TIRF and epifluorescence. Images are representative of more than three expreiments. Scale bar = 5 µm. (B) The amount of actin nodules which appear in both TIRF and epi images. (C) Distribution of the timing of actin nodule appearance and disappearance in epifluorescence relative to actin nodule formation and disappearance in TIRF (at 0 s), (i) and (ii), respectively. These demonstrate that nodules appear in TIRF and epifluorescence at the same time. A minimum of 15 platelets (with ~ 30 nodules/platelet) were analysed per experiment.

All nodules that were present in epifluorescence were also present in TIRF (Figure 3.3 *B*). Additionally, nodule appearance and disappearance occurred at the same time in both TIRF and epifluorescence (Figure 3.3 *C*). This suggests that all nodules in the cell are at the basal membrane and that TIRF microscopy is suitable for imaging nodule dynamics.

All platelets contained actin nodules with their first appearance a matter of seconds after the platelet adheres to the fibrinogen surface (Figure 3.4 *A*-*B*). The number of nodules in a platelet rapidly increases in the first 30 seconds of spreading to an average of 5 nodules and thereafter the numbers remain fairly constant. Although nodule numbers remain steady, the individual nodules continually turn-over, with nodules displaying a range of lifetimes from 3 seconds to greater than 150 seconds. On average the nodule lifetime is 31.2 (± 1.53) seconds with the vast majority of nodules (86 %) persistent for less than 50 seconds (Figure 3.4 *C*). The maximum observed displacement of individual actin nodules was less than 0.4 μm. This value is equivalent to three pixels. Given that the nodules were 2-3 pixels wide and the centre of the was approximated by eye it is unlikely that the nodules moved and the displacement due to errors in determination of the centre of nodules. Consequently, the nodules were not found to be mobile but instead remained in the same location, at which they first appeared, for their entire lifetime (Figure 3.4 *D*). Additionally, the fluorescent area of the nodules was determined which showed that it fluctuates throughout the nodule lifetime (Figure 3.4 *Ei*) but the overall trend is for the fluorescent area to increase in the first 50 % of its lifetime and then decrease until it disappears (Figure 3.4 *Eii*).

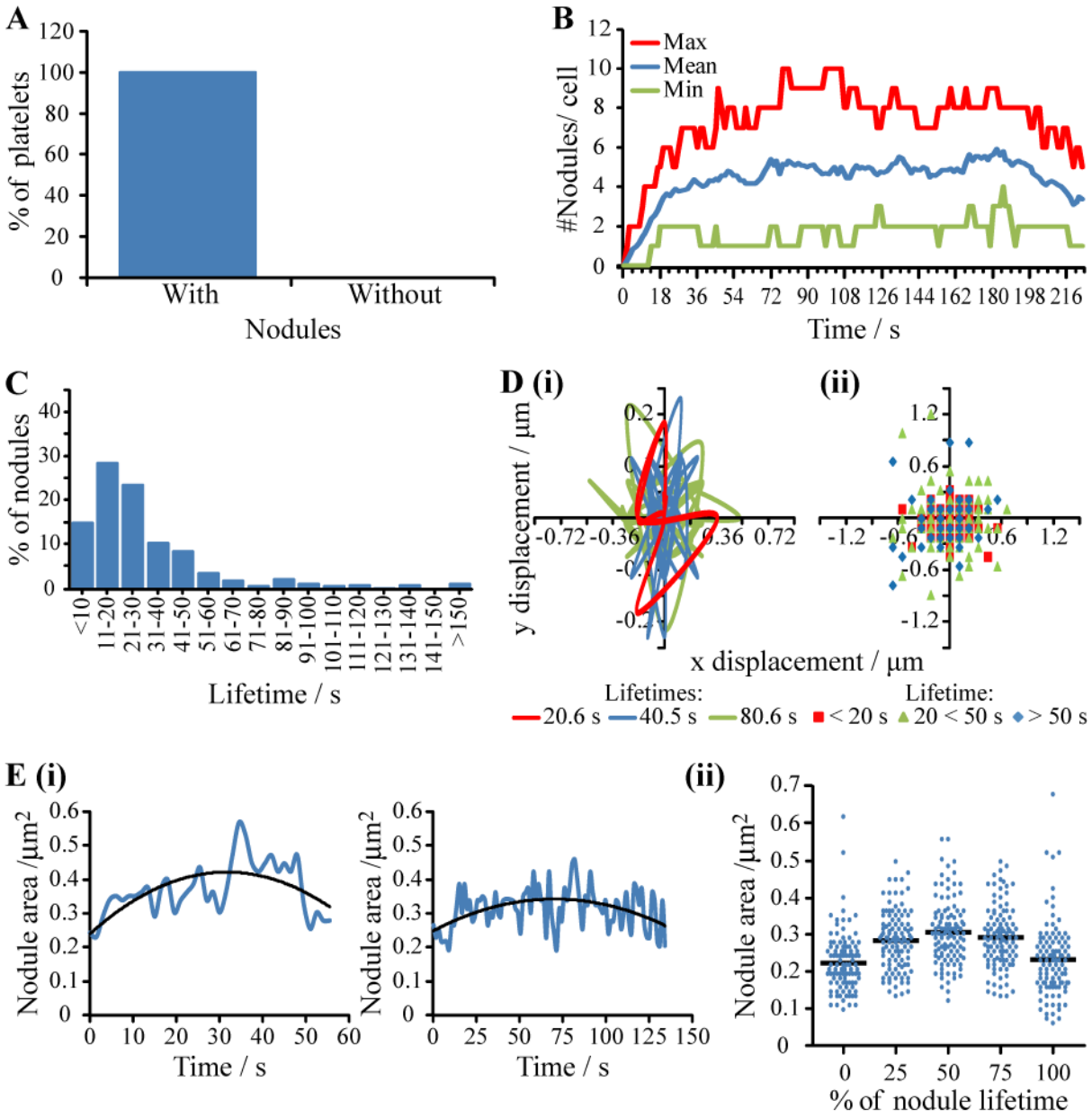

Figure 3.4. Characterisation of actin nodule dynamics in Lifeact-GFP mouse platelets. Washed Lifeact-GFP mouse platelets (2 x 10^7 mL^{-1}) were allowed to spread on fibrinogen (37 °C). Platelet spreading was monitored using real-time TIRF microscopy, with an image taken every 1.5 s. (A) Platelets containing actin nodules were counted. (B) Time course for the number of actin nodules per platelet during spreading. (C) Distribution of nodule lifetimes (Mean lifetime = 31.2 s) . (D) Nodule displacement; (i) Path of nodule movement representative of nodules with short, medium and long lifetimes. (ii) Final displacement of nodules relative to their point of origin. (E) The fluorescent area of nodules was determined; (i) Representative graphs of the nodule fluorescent area (—) for two nodules of different lifetimes. (— = second order polynomial trend line). (ii) Distibution of nodule fluorescent areas a various points in the nodule lifetime. A minimum of 15 platelets (with ~30 nodules/platelet) were analysed per experiment. The results are from more than three experiments.

Nodules were localised throughout the platelet and assigned one of the following categories; (1) “periphery” when localised to the platelet edge, (2) “centre” when localised within the main body of the cell, (3) “filopodia base” when localised to the area from which a filopod protrudes and (4) “filopodia” when found along the filopodia structure (Figure 3.5 *A*). The majority of nodules were found to be localised to the cell periphery (Figure 3.5 *B*). The localisation of the nodules in the platelet does not appear to affect the lifetime of a nodule (Figure 3.5 *C*).

The actin nodule is a dynamic actin structure which is present in all platelets within seconds of adhesion which suggests that the actin nodule may not have a role in initial platelet adhesion events. However, the nodules appear prior to the formation of the main platelet actin structures, filopodia, lamellipodia and stress fibres, so it may have a role in initial platelet spreading events. Each nodule remains stationary and persists for approximately 30 s but is quickly replaced by another nodule, as evidenced by the number of nodules per cell remaining fairly constant. The nodules are present throughout the cell volume and distributed across the cell. Their presence at the cell periphery and at the base of filopodia may indicate a role in platelet adhesion or in the formation of filopodia and lamellipodia which protrude from the cell periphery.

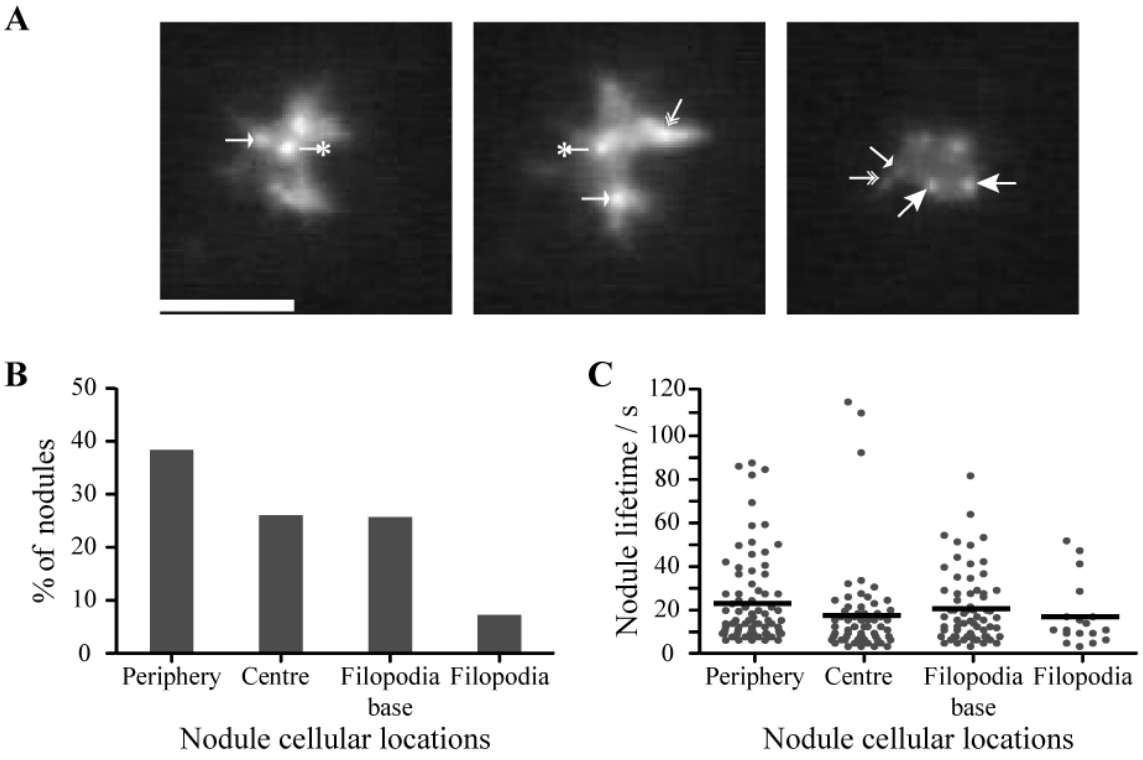

Figure 3.5. Localisation of actin nodules in Lifeact-GFP mouse platelets. Washed Lifeact-GFP mouse platelets (2 x 10^7 mL^{-1}) were allowed to spread on fibrinogen (37 °C). Platelet spreading was monitored using real-time TIRF microscopy, with an image taken every 1.5 s. (A) TIRF microscopy images of platelets. ➔ indicates nodules at cell periphery, . ➙ indicates nodules in centre of cell, → indicates nodules at base of filopodia and . ↠ .indicates nodules in the filopodia. Images are representative of more than three experiments. Scale bar = 5 µm. (B) Nodules were localised to the cell periphery, the central region of the platelet, at the base of a forming filopodia and within the filopodia structure. (C) Distribution of nodule lifetimes in relation to their cellular localisation. A minimum of 15 platelets (with ~ 30 nodules/platelet) were analysed per experiment.

3.2.2 Actin polymerisation is required for nodule formation

Previous work suggested that the actin nodule was a dynamic structure which relied on actin polymerisation for their formation and stability (Calaminus et al., 2008). However, this relied on stained, fixed platelets. Live-cell TIRF microscopy of spreading of Lifeact-GFP mouse platelets treated with Cytochalasin D demonstrated the inability of the platelets to spread properly upon a fibrinogen-coated surface, failing to produce filopodia (Figure 3.6 *A*).

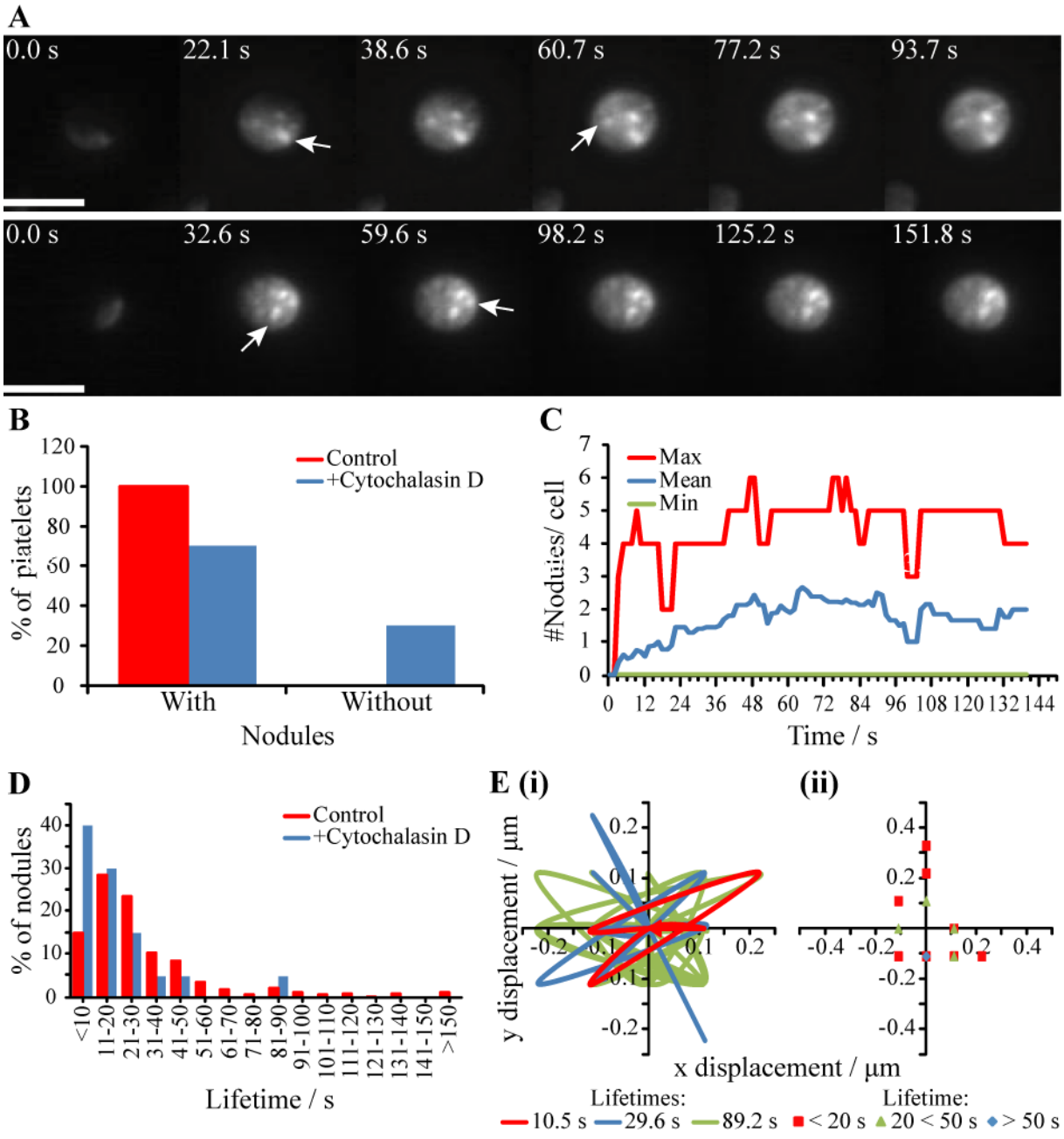

Figure 3.6. The effect of Cytochalasin D on actin nodules. Washed Lifeact-GFP mouse platelets (2 x 10^7 mL^{-1}) were incubated with DMSO (0.1 % *v/v*) or Cytochalasin D (10 µM) 10 minutes prior to spreading on fibrinogen (37 °C). Platelet spreading was monitored using real-time TIRF microscopy, with an image taken every 1.5 s. (A) Time course of two individual platelets (*top/ bottom*), at indicated time points. Arrows indicate the location of actin nodules. Images are representative of three experiemnts. Scale bar = 5 µm. (B) Platelets containing actin nodules were counted. (C) Time course for the number of actin nodules per platelet during spreading. (D) Distribution of nodule lifetimes (Mean lifetime = 18.9 s). (E) Nodule displacement in platelets treated with Cytochalasin D; (i) Path of nodule movement representative of nodules with short, medium and long lifetimes. (ii) Final displacement of nodules relative to their point of origin. A minimum of 15 platelets (with ~ 7 nodules/platelet) were analysed per experiments.

However, the majority (70 %) of the rounded platelets contained at least one actin nodule (Figure 3.6 *B*) with platelets exhibiting a mean of 2 nodules/cell for >50 % of the imaging time (Figure 3.6 *C*), a decrease on the figure seen for control samples. The mean nodule lifetime (18.9 s ± 4.40) is significantly decreased compared with control samples and 95 % of nodules have a lifetime less than 50 s (Figure 3.6 *D*). The nodules remained immobile throughout their lifetime (Figure 3.6 *E*).

Lifeact-GFP mouse platelets were treated with Latrunculin A, before spreading on fibrinogen coated coverslips and imaged live using TIRF microscopy. These platelets did not spread normally, instead remained rounded without the appearance of filopodia (Figure 3.7). Furthermore, no nodules were present in any platelets.

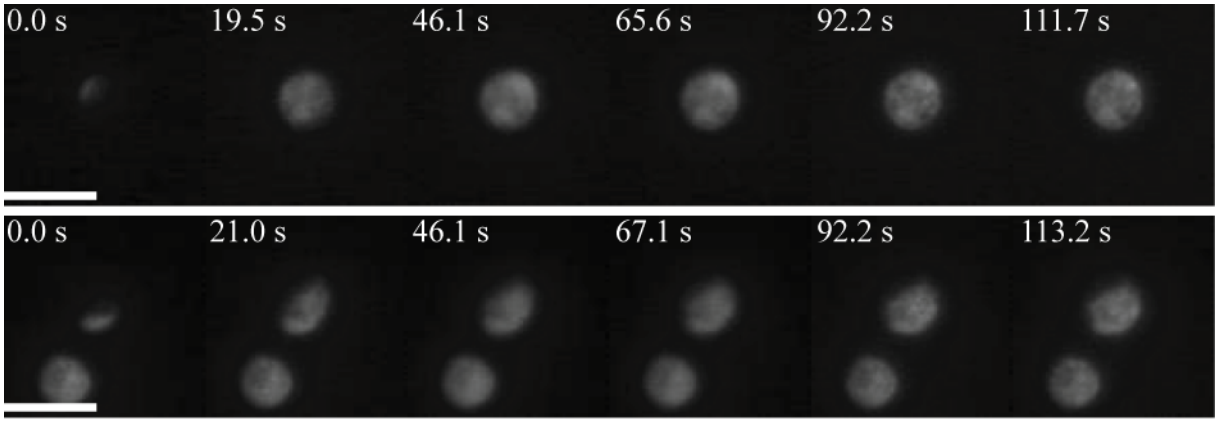

Figure 3.7. The effect of Latrunculin A on actin nodule dynamics. Washed Lifeact-GFP mouse platelets (2 x 10^7 mL^{-1}) were incubated with Latrunculin A (3 μM) for 10 minutes prior to spreading on fibrinogen (37 °C). Platelet spreading was monitored using real-time TIRF microscopy, with an image taken every 1.5 s. Time course of two individual platelets (*top/ bottom*), at indicated time points. Images are representative of three experiments. Scale bar = 5 μm.

Lifeact-GFP mouse platelets were treated with Jasplakinolide, before spreading on fibrinogen coated coverslips and imaged live using TIRF microscopy. These platelets did not spread normally, instead remained rounded without the appearance of filopodia (Figure 3.8). Furthermore, no nodules were present in any platelets. These rounded platelets had a reduced contact surface area compared with other rounded platelet samples, Latrunculin A or Cytochalasin D.

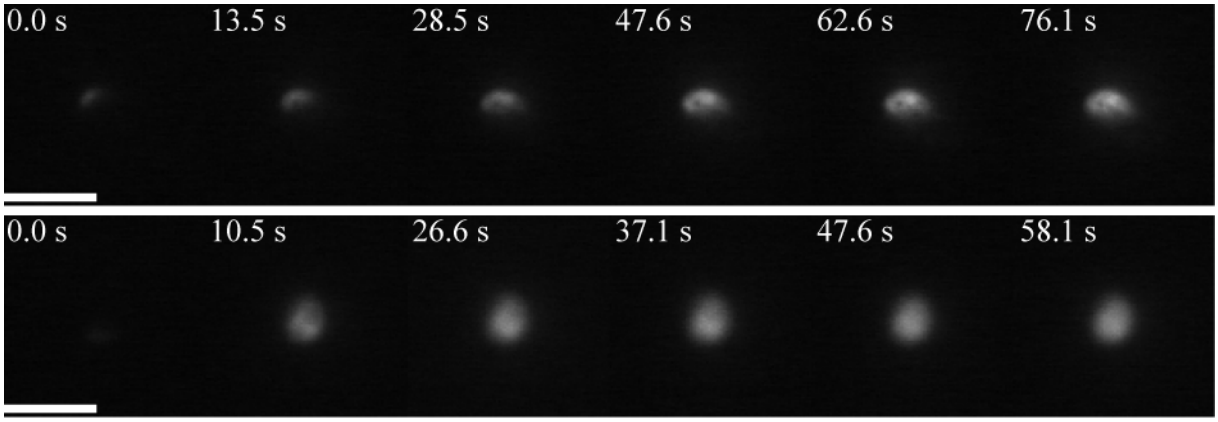

Figure 3.8. The effect of Jasplakinolide on actin nodules. Washed Lifeact-GFP mouse platelets (2 x 10^7 mL^{-1}) were incubated with Jasplakinolide (5 μM) for 10 minutes prior to spreading on fibrinogen (37 °C). Platelet spreading was monitored using real-time TIRF microscopy, with an image taken every 1.5 s. Time course of two individual platelets (*top/ bottom*) at indicated time points. Images are representative of three experiments. Scale bar = 5 μm.

While addition of Latrunculin A resulted in loss of nodules, treatment with Cytochalasin D did not. Unexpectedly nodule turnover remained reasonably dynamic in Cytochalasin D treated platelets. Additionally no nodules were present in platelets treated with Jasplakinolide. Since Jasplakinolide is a potent inducer of actin polymerisation (Bubb et al., 1994) and prevents depolymerisation, it would be expected that if nodules were present in platelets prior to activation, they would still be present in the activated platelets. Since there are no actin

nodules present, the platelets may instead be filled with a disorganised soup of actin filaments preventing the platelet from forming the organised actin structures which enable the platelet to spread. Therefore, these results suggest that nodules are formed immediately upon activation of the platelet as a result of actin polymerisation.

3.2.3 Actin nodule turnover correlated with ROCK activity

Previous work by Calaminus *et at* showed that addition of the ROCK inhibitor, Y27632 (50 μM), to human platelets resulted in inhibition of stress fibre formation and a doubling of the number of actin nodule containing platelets (80 %) compared with the DMSO control (45 %) (Calaminus et al., 2008). To further investigate the role of ROCK in actin nodules, live cell imaging of Lifeact-GFP mouse platelets treated with Y27632 (20 μM) was undertaken (Figure 3.9 *A*). This revealed that all platelets contained at least one actin nodule at some point during their lifetime (Figure 3.9 *B*-*C*). The number of actin nodules is increased in Y27632 treated platelets with cells exhibiting a mean of 6 nodules/cell for >50 % of the time the platelets were imaged for. However, the mean nodule lifetime was significantly decreased (20.2 s ± 0.79) with 95 % of nodules having a lifetime of less than 50 s (Figure 3.9 *D*). Similarly to control samples, nodules in Y27632 treated platelets were stationary (Figure 3.9 *E*).

These results support the previous hypothesis that ROCK is not required for actin nodule formation. Furthermore, the increased nodule turn over, as inferred by the decrease in nodule lifetimes and increase in the number of nodules per cell, suggests that ROCK may play a role

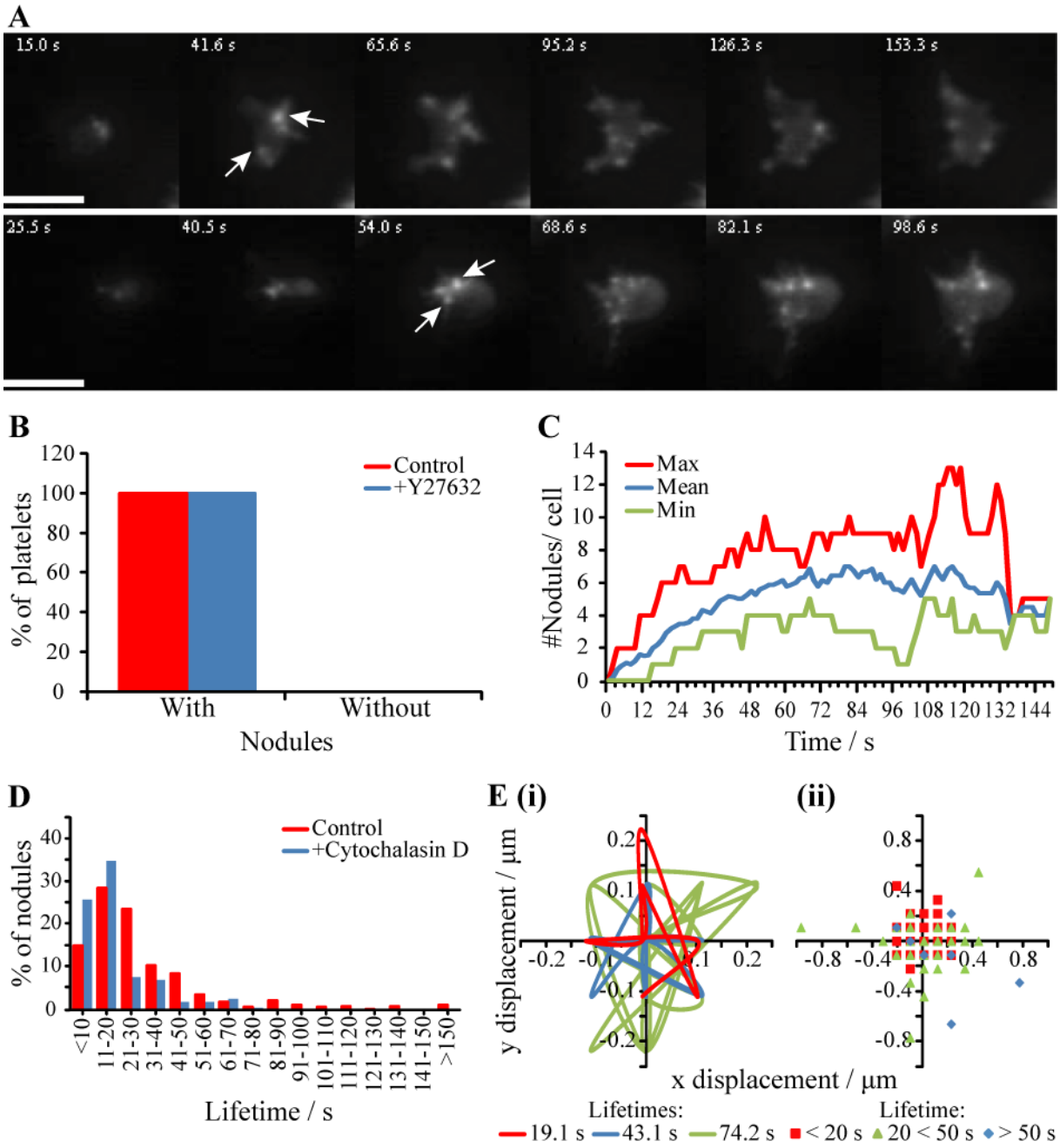

Figure 3.9. The effect of ROCK inhibitor Y27632 on actin nodules. Washed Lifeact-GFP mouse platelets (2 x 10^7 mL^{-1}) were incubated with DMSO (0.1 % *v/v*) or Y27632 (20 µM) 10 minutes prior to spreading on fibrinogen (37 °C). Platelet spreading was monitored using real-time TIRF microscopy, with an image taken every 1.5 s. (A) Time course of two individual platelets (*top/ bottom*) at indicated time points. Arrows indicate location of actin nodules. Images are representative of three experiments. Scale bar = 5 µm. (B) Platelets containing actin nodules were counted. (C) Time course for the number of actin nodules per platelet during spreading. (D) Distribution of nodule lifetimes (Mean lifetime = 20.2 s). (E) Nodule displacement in platelets treated with Y27632; (i) Path of nodule movement representative of nodules with short, medium and long lifetimes. (ii) Final displacement of nodules relative to their point of origin. A minimum of 15 platelets (with ~ 30 nodules/platelet) were analysed per experiment.

in the stability of the nodules. In particular, it may be that disappearance of nodules may be as a result of actin depolymerisation.

3.2.4 Src family kinase activity and actin nodule dynamics

The original work describing nodules investigated the role of Src kinase activity in human platelets on actin nodules using the Src kinase inhibitor, PD0173952. They found that actin nodules were absent in PD0173952 treated platelets and conclude that the formation and stability of actin nodules required continuous actin polymerisation downstream of Src kinases (Calaminus et al., 2008). To investigate the role of Src kinase activity on actin nodule dynamics, Lifeact-GFP mouse platelets were treated with another SFK inhibitor, PP2, before spreading on fibrinogen coated coverslips and imaged live using TIRF microscopy. These platelets did not spread normally, instead remained rounded without the appearance of filopodia (Figure 3.10 *A*). Also, the nodules were different in appearance to those seen for control samples and instead appear less well defined and fuzzy. All platelets had at least one nodule present per cell at some point during the experiment window (Figure 3.10 *B*-*C*). These nodules had a highly significant reduction in mean lifetime (8.2 s ± 0.42) compared with control platelets (31.2 s ± 1.53) with 100 % of nodules having a lifetime of less than 40 seconds (Figure 3.10 *D*). Again, nodules were immobile (Figure 3.10 *E*).

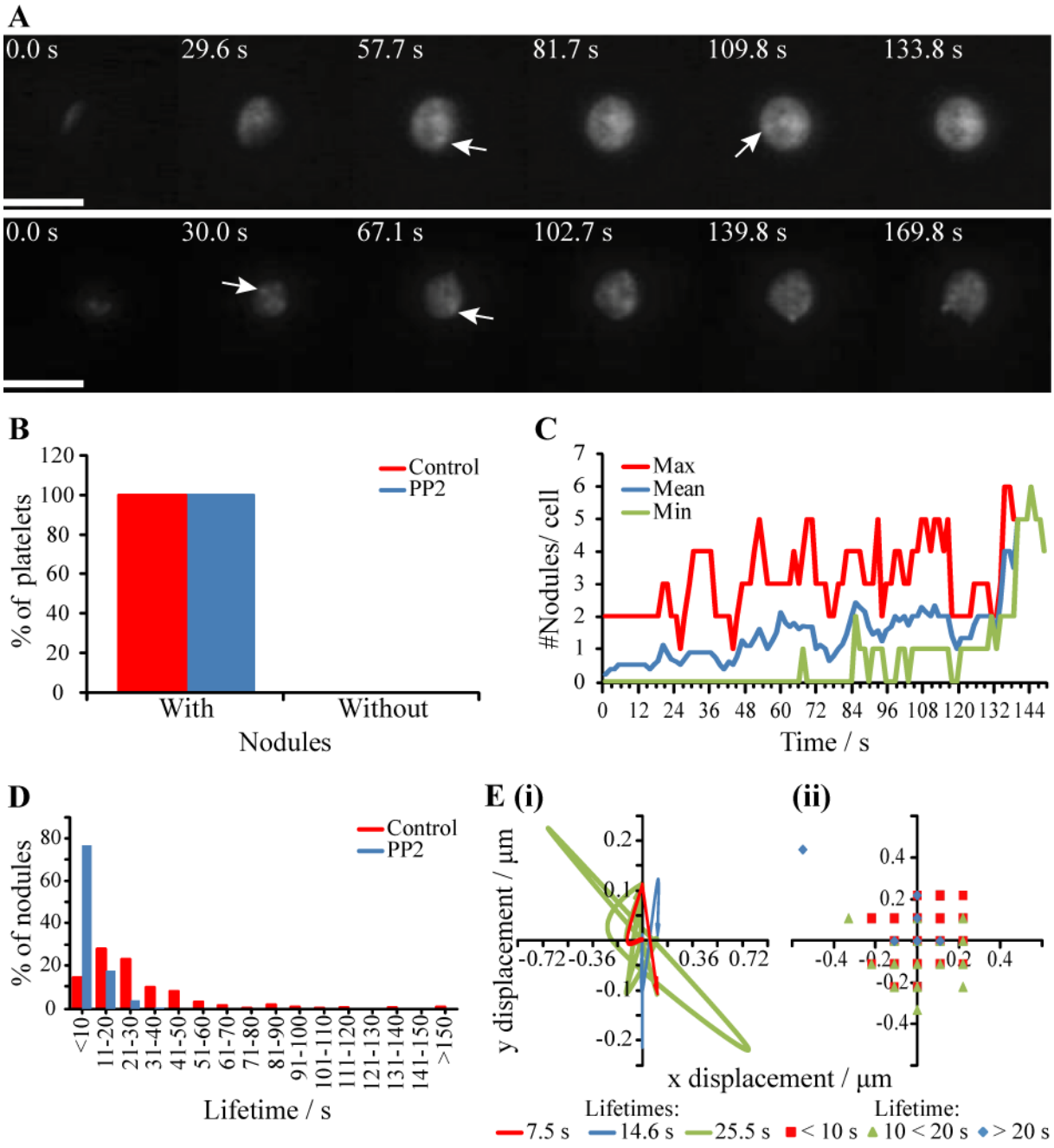

Figure 3.10 The effect of PP2 on actin nodules. Washed Lifeact-GFP mouse platelets (2 x 10^7 mL^{-1}) were incubated with DMSO (0.1 % *v/v*) or PP2 (10 µM) 10 minutes prior to spreading on fibrinogen (37 °C). Platelet spreading was monitored using real-time TIRF microscopy, with an image taken every 1.5 s. (A) Time course of two individual platelets (*top/ bottom*) at indicated time points. Arrows indicate location of actin nodules. Images are representative of three experiments. Scale bar = 5 µm. (B) Platelets containing actin nodules were counted. (C) Time course for the number of actin nodules per platelet during spreading. (D) Distribution of nodule lifetimes (Mean lifetime = 8.2 s). (E) Nodule displacement in platelets treated with PP2; (i) Path of nodule movement representative of nodules with short, medium and long lifetimes. (ii) Final displacement of nodules relative to their point of origin. A minimum of 15 platelets (with ~ 20 nodules/platelet) were analysed per experiment.

To further investigate which of the Src family kinases (SFK) have a role in actin nodules, platelets from loss-of-function mouse mutants for the Src family kinases, $Lyn^{-/-}$, $Lyn^{-/-}/Fyn^{-/-}$ and $Src^{-/-}/Fyn^{-/-}$ (Severin et al., 2012) and their wild type (WT) controls were allowed to spread on fibrinogen coated coverslips for 45 minutes prior to fixation and staining with phalloidin-488. Platelets from all mouse models appeared to spread normally (Figure 3.11 *A*), however, there was a highly significant decrease in the number of spread platelets for $Lyn^{-/-}/Fyn^{-/-}$and $Src^{-/-}/Fyn^{-/-}$ (Figure 3.11 *B*). The percentage of nodule containing cells for $Lyn^{-/-}$ platelets was similar to WT platelets but a significant decrease was observed for $Lyn^{-/-}/Fyn^{-/-}$ and $Src^{-/-}/Fyn^{-/-}$ (Figure 3.11 *C*). However, in platelets that did contain actin nodules, the distribution of the number of nodules per cell was similar (Figure 3.11 *D*).

These results support the previous hypothesis that actin nodule formation and stability requires Src kinase activity. Loss of Lyn, Lyn and Fyn or Src and Fyn did not appear to affect the number of actin nodules per platelet which suggests that other SFK's may be involved instead of/ as well as Lyn, Fyn and Src in nodule formation and dynamics.

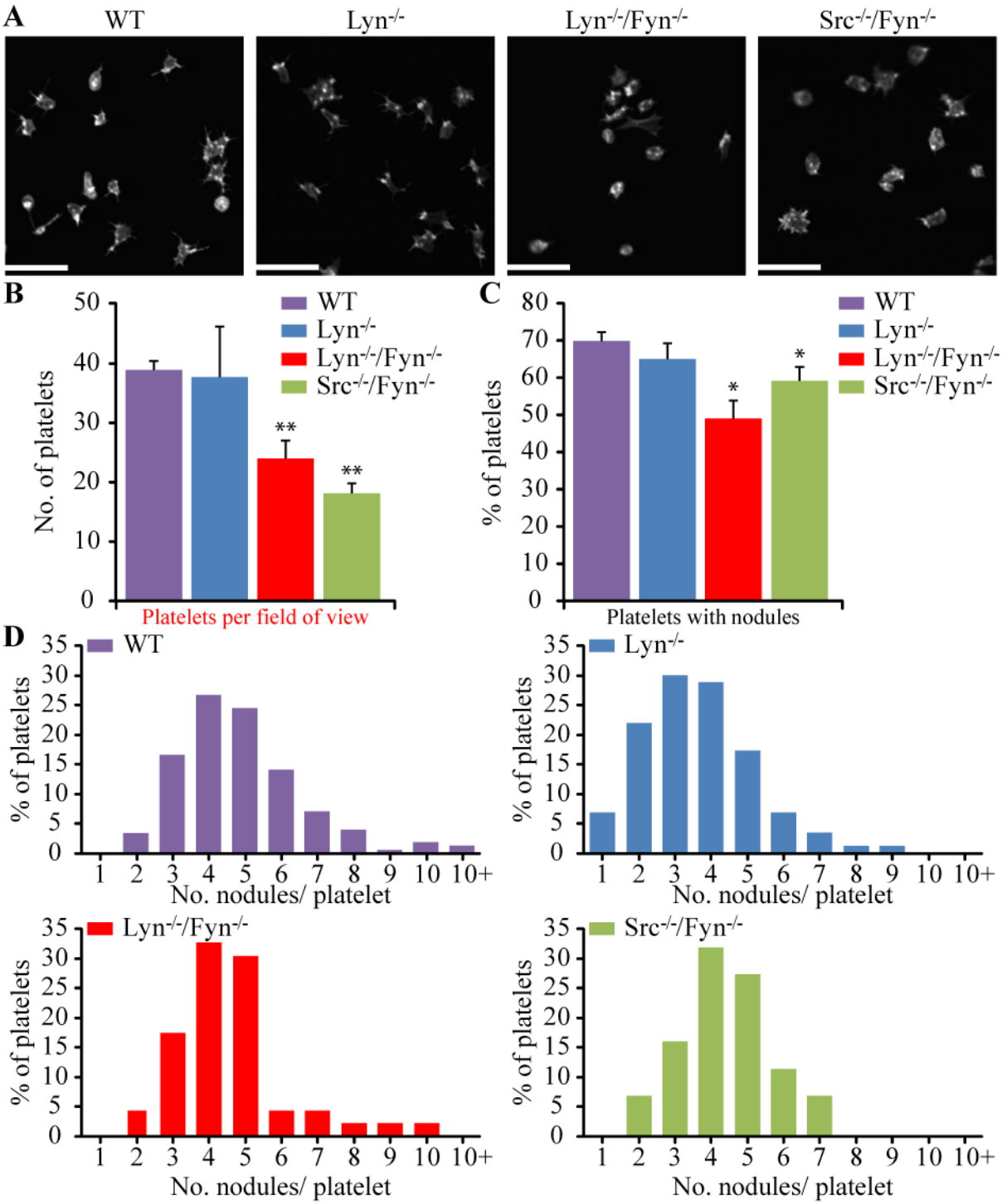

Figure 3.11. Comparison of actin nodule numbers in SFK KO mouse platelets. Washed mouse platelets (2 x 10^7 mL^{-1}) from various KO models were allowed to spread on fibrinogen for 45 min (37 °C, CO_2). Platelets were fixed, permeablised with Triton X-100 (0.1 % in PBS) and stained with 488-phalloidin (2 µM). (A) Confocal fluorescence microscopy images of fixed platelet samples. Images are representative of three experiments. Scale bar = 10 µm. (B) Mean number of spread platelets per field of view. (C) Platelets containing actin nodules were counted. (C) Percentage distribution of actin nodule numbers per platelet. A minimum of 100 platelets were analysed per experiment. Values are shown ± s.e.m. *P < 0.05 and **P < 0.01 is relative to wild-type control.

3.2.5 The role of calcium in actin nodule dynamics

Changes in local concentrations of $[Ca^{2+}]_i$ are implicated in the reorganisation of the actin cytoskeleton and subsequent platelet shape change. There are several Ca^{2+}-dependent signalling pathways and actin regulatory proteins, such as gelsolin, which bind Ca^{2+} that are involved in regulation of the actin cytoskeleton (Ariyoshi and Salzman, 1996, Yin and Stossel, 1979, Furukawa et al., 2003). Additionally, a rise in $[Ca^{2+}]_i$ is observed at the point from which filopodia and lamellipodia form, suggesting a role for Ca^{2+} in regulating their formation (Ariyoshi and Salzman, 1996, Hartwig, 1992).

Live-cell TIRF microscopy of spreading of Lifeact-GFP mouse platelets treated with BAPTA-AM demonstrated the inability of the platelets to spread properly upon a fibrinogen-coated surface (Figure 3.12 *A*). Platelets remained mostly rounded with only one or two abnormally long filopodia formed. The majority of cells (85 %) produced at least one actin nodule during the experiment window (Figure 3.12 *B*). Furthermore the time from cell attachment to nodule appearance (~36 s) was noticeably longer than for control samples (3 s). Platelets exhibited a mean of 2 nodules/cell for >50 % of the imaging time, representing a 50 % decrease on the figure seen for control samples (Figure 3.12 *C*). These nodules have a similar mean lifetime of 24.2 s (± 1.73) to the control platelets, with 91% of nodules having a lifetime less than 50 s (Figure 3.12 *D*). Nodule position remained constant throughout nodule lifetime (Figure 3.12 *E*).

The abnormally long filopodia have been previously observed in platelets treated with Quin-2, which suggested that calcium has a role in cytoskeletal reorganisation (Hartwig, 1992). The

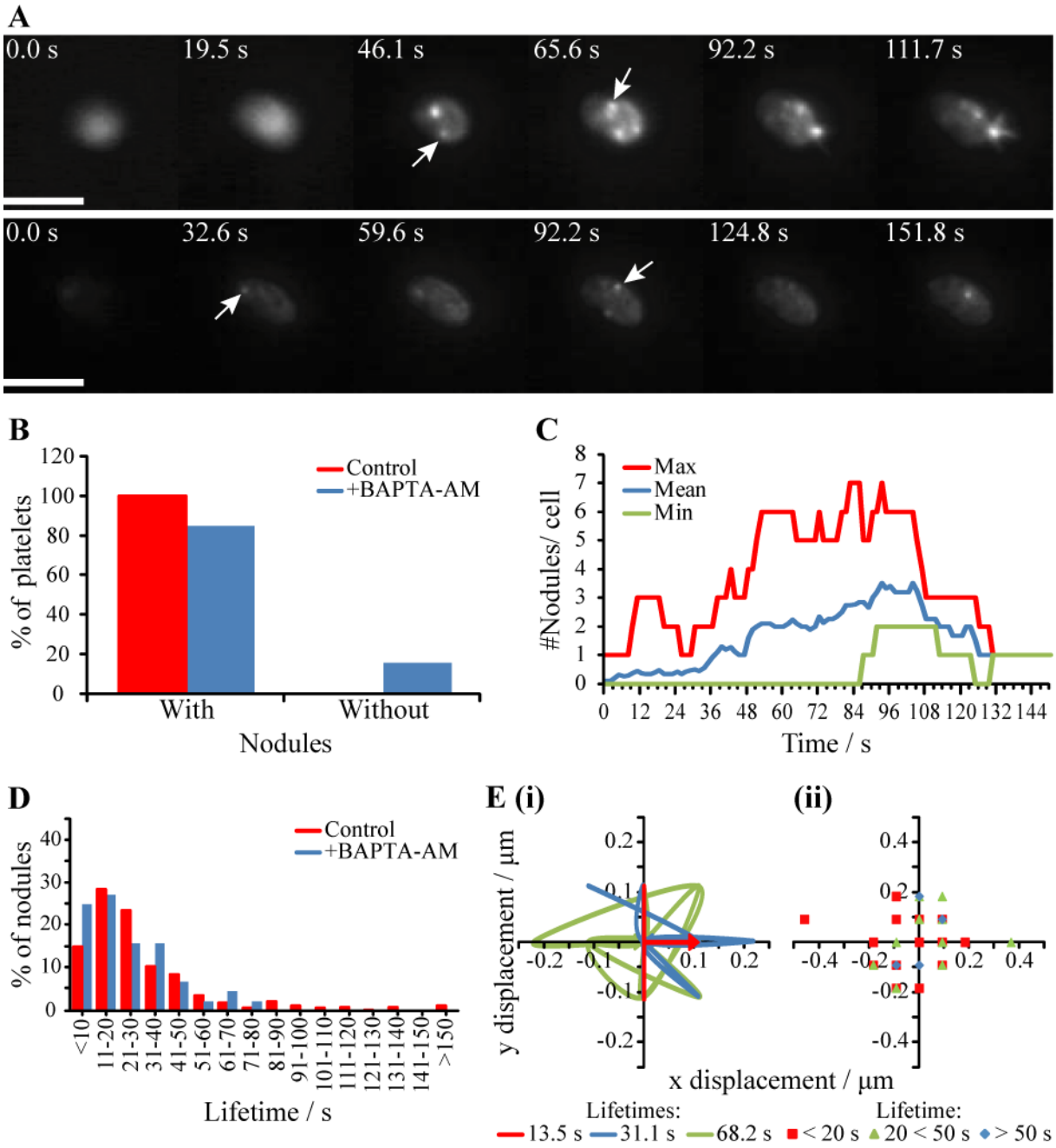

Figure 3.12. The effect of BAPTA-AM on actin nodules. Washed Lifeact-GFP mouse platelets (2 x 10^7 mL^{-1}) were incubated with DMSO (0.1 % *v/v*) or BAPTA-AM (10 µM) 10 min prior to spreading on fibrinogen (37 °C). Platelet spreading was monitored using real-time TIRF microscopy, with an image taken every 1.5 s. (A) Time course of two individual platelets (*top/ bottom*) at indicated time points. Arrows indicate location of actin nodules. Images are representative of three experiments. Scale bar = 5 µm. (B) Platelets containing actin nodules were counted. (C) Time course for the number of actin nodules per platelet during spreading. (D) Distribution of nodule lifetimes (Mean lifetime = 24.2 s). (E) Nodule displacement in platelets treated with BAPTA-AM; (i) Path of nodule movement representative of nodules with short, medium and long lifetimes. (ii) Final displacement of nodules relative to their point of origin. A minimum of 15 platelets (with ~ 15 nodules/platelet) were analysed per experiment.

decrease in the number of nodules per platelet when incubated with the Ca^{2+} chelating agent, BAPTA-AM, suggests that Ca^{2+} may also play a role in the cytoskeletal reorganisation required for actin nodule formation.

3.2.6 The role of Arp2/3 complex in actin nodule dynamics

Actin nodules have previously been reported to co-localise with Arp2/3 complex in immunohistochemistry studies (Calaminus et al., 2008). To further investigate the role of Arp2/3 in actin nodule formation and dynamics, live cell imaging of Lifeact-GFP mouse platelets treated with CK-666 (20 μM) was undertaken (Figure 3.13). These platelets did not spread normally, instead remained rounded without the appearance of filopodia. Furthermore, no nodules were present in any platelets. The complete lack of nodules upon inhibition of Arp2/3 suggests that it is required for actin nodule formation in platelets.

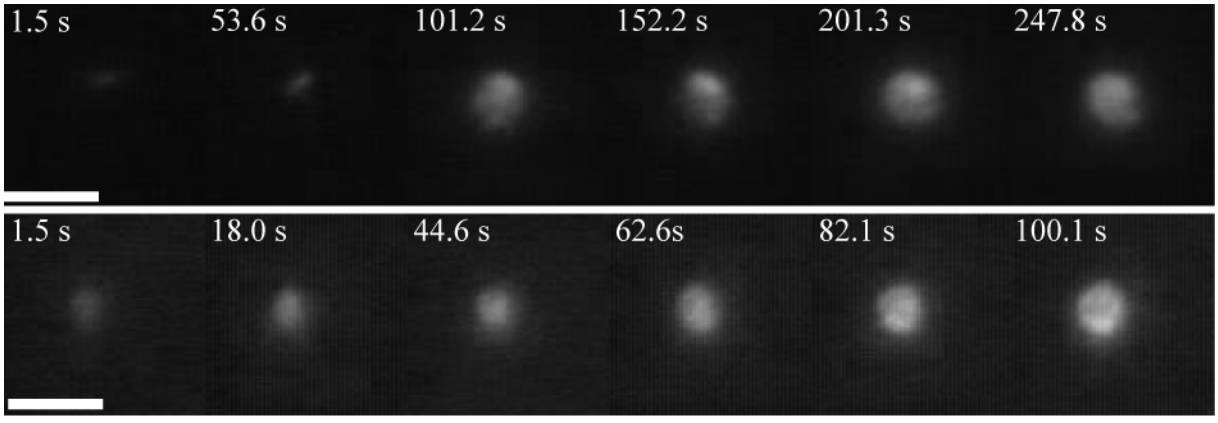

Figure 3.13. The effect of Arp2/3 inhibitor CK-666 on actin nodules. Washed Lifeact-GFP mouse platelets (2 x 10^7 mL^{-1}) were incubated with CK-666 (20 μM) 10 minutes prior to spreading on fibrinogen (37 °C). Platelet spreading was monitored using real-time TIRF microscopy, with an image taken every 1.5 s. Time course of two individual platelet (*top/ bottom*) at indicated time points. Images are representative of three experiments. Scale bar = 5 μm.

3.2.7 Spatial and temporal relationship between actin nodule formation and filopodia emergence

As apparent from Figure 3.5, a quarter of nodules in a platelet are localised to the base of a filopodia structure. This together with the nodule being the first actin structure apparent in spreading platelets suggests that there may be a relationship between nodule formation and filopodia formation. The following section of work investigates if there is such a relationship.

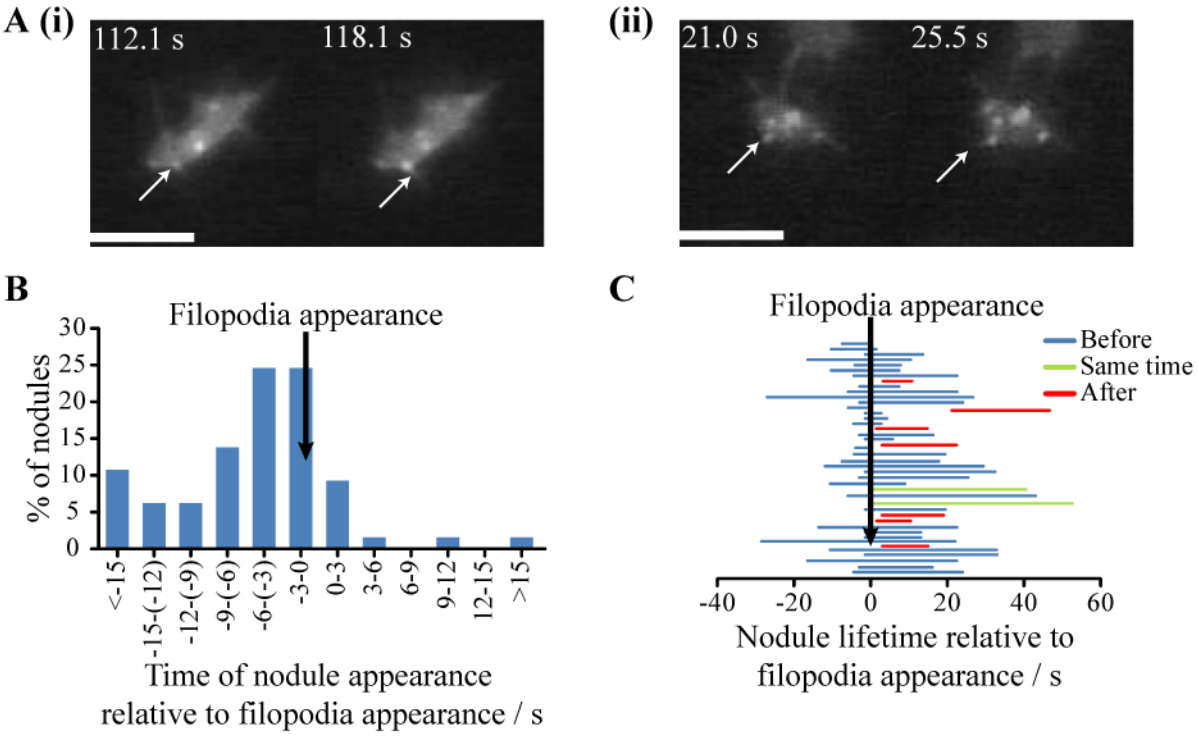

Figure 3.14. Relationship between actin nodules and filopodia formation. Washed Lifeact-GFP mouse platelets (2 x 10^7 mL^{-1}) were allowed to spread on fibrinogen (37 °C). Platelet spreading was monitored using real-time TIRF microscopy, with an image taken every 1.5 s. (A) Time course of two individual platelets (i/ ii) at indicated time points. Arrows indicate the position of actin nodules (*left image*) and then the filopodia which emerge from it (*right image*). Images are representative of three experiments. Scale bar = 5 µm. (B) Distribution of the timing of nodule appearance relative to filopodia appearance Arrow indicates filopodia appearance taken as 0 s. (C) Distribution of representative actin nodule lifetimes, that are localised to the base of filopodia, relative to the appearance of the filopodia. Arrow indicates filopodia appearance taken as 0 s. — represents nodules which appear prior to filopodia emergence, — represents nodules which appear simultaneously with filopodia and — represents nodules that appear after filopodia appearance. A minimum of 15 platelets (with ~ 30 nodules/platelet) were analysed per experiment.

Nodules which localised to the filopodia base were tracked and the temporal relationship between the nodule appearance and filopodia appearance was determined (Figure 3.14 *A*). 86 % of nodules appeared before or concurrently with filopodia emergence (Figure 2.14 *B*). 63 % of nodules appeared less than 9 seconds before filopodia appearance which is early in the lifetime of an average actin nodule (Figure 3.14 *C*).

Since filopodia formation occurs both before and after actin nodule appearance it is unlikely that the actin nodule is required for filopodia formation. This is further supported by the observation that not all filopodia have an actin nodule at their base. However, the prevalence of actin nodule appearance at the base of filopodia suggests there may be a relationship between actin nodules and filopodia dynamics.

3.2.8 Spatial and temporal relationship between actin nodules and platelet surface receptors

Among the actin regulatory proteins found to co-localise with actin nodules were the β1- and β3-integrin subunits (Calaminus et al., 2008). The co-localisation of these integrin subunits insinuates a role in actin nodule dynamics. The two most abundant platelet integrins each contain one of the β subunits, the fibrinogen receptor, αIIbβ3, and the collagen receptor, α2β1. Since both fibrinogen and collagen play a role in platelet spreading, investigating the dynamics of their respective integrins in relation to the actin nodule will further enhance our understanding of the function of actin nodules in platelets.

Relationship between actin nodules and the fibrinogen receptor, αIIbβ3 integrin

Work undertaken during a visit to the Machesky lab (Beatson Institute for Cancer Research, Glasgow) utilised their Lifeact-RFP mouse model to preliminarily assess the TIRF microscopy potential of platelets from a Lifeact mouse model. Platelets were also labelled with FITC-conjugated antibody for the αIIb-integrin subunit to examine the possibility of live-cell dual-labelling studies. The punctate pattern of integrin labelling appeared to co-localise with the actin nodules (Figure 3.15). Pearson's correlation analysis was performed to

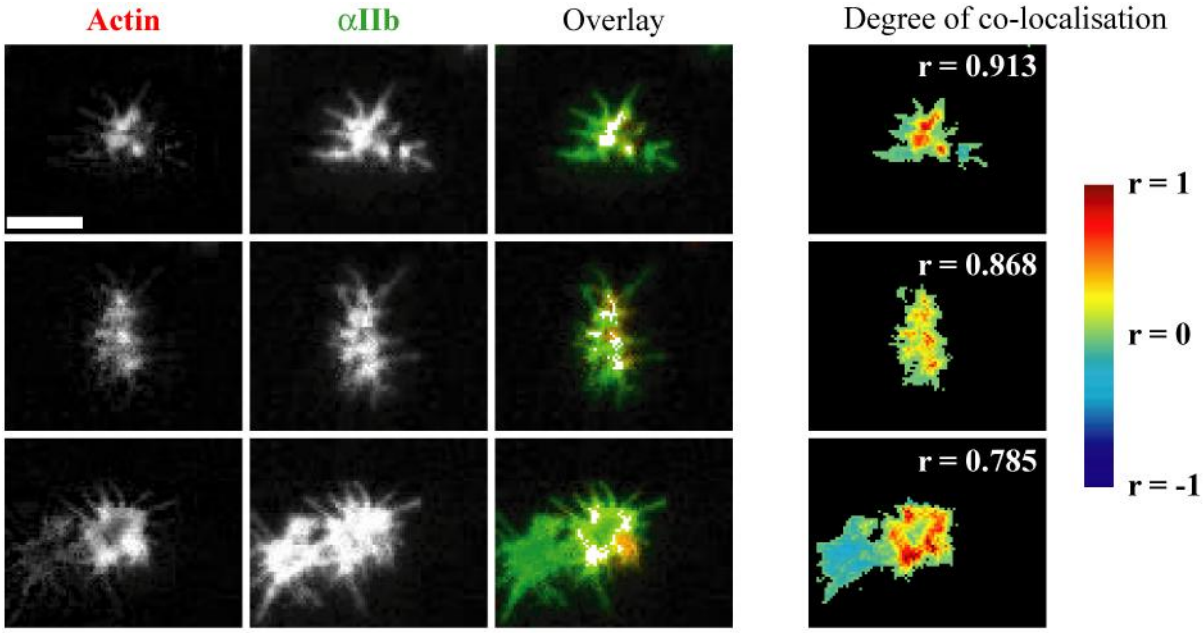

Figure 3.15. Co-localisation of actin nodules with αIIb-integrin subunit. Washed Lifeact-RFP mouse platelets (2 x 10^7 mL^{-1}) were incubated with a FITC-conjugated antibody for αIIb (1 % *v/v*) and allowed to spread on fibrinogen (37 °C). Platelet spreading was monitored using real-time TIRF microscopy. Images of actin and antibody staining were overlayed and the Pearson's correlation coefficient, r, was determined. The colour bar illustrates the degree of co-localisation where 1 is perfectly co-localised and -1 is mutually exclusive. Images are representative of three experiments. Scale bar = 5 µm.

gauge the degree of correlation between the actin staining and integrin labelling. The correlation coefficient, r, was 0.83 (± 0.05) which indicates a high degree of co-localisation

since r = 1 represents perfectly co-localised imaged and r = -1 represents mutually exclusive images (Bolte and Cordelières, 2006, Purbhoo et al., 2010).

Having ascertained the viability of live-cell dual-labelling TIRF microscopy studies for Lifeact mouse platelets and established a potential relationship between nodules and the integrin, further work was undertaken using platelets from Lifeact-GFP mice. This work aims to study the nature of the interactions and dynamics of the actin nodule and the αIIb-integrin subunit using a PE-conjugated antibody for αIIb.

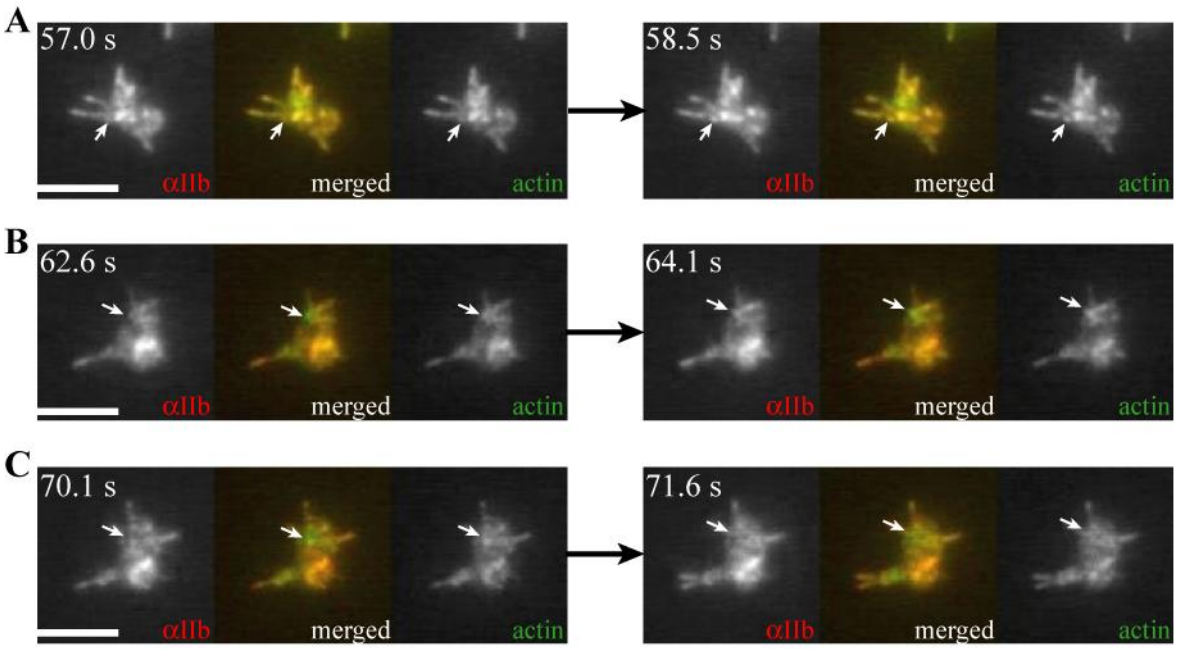

Figure 3.16. Dynamics of actin nodules and αIIb-integrin subunit. Washed Lifeact-GFP mouse platelets (2 x 10^7 mL^{-1}) were incubated with a PE-conjugated anitbody for αIIb (1 % v/v) for 10 minutes prior to spreading on fibrinogen (37 °C). Platelet spreading was monitored using real-time two-colour TIRF microscopy, with an image taken every 1.5 s. TIRF image sequences showing: (A) Actin nodule forms at same time as corresponding αIIb-rich structure. (B) Actin nodule forms prior to appearance of αIIb-rich structure. (C) Disappearance of actin nodule and αIIb-rich structure. Arrows indicate site of nodule appearance/ disappearance. Images are representative of more than three experiments. Scale bar = 5 μm.

Rapid, sequential, two-colour, real-time TIRF microscopy of GFP-Lifeact platelets labelled with a PE-conjugated antibody for αIIb enabled imaging of the relationship between actin nodule dynamics and αIIb integrin (Figure 3.16). It may be possible that the interaction with the antibody and αIIb-integrin subunit may inhibit the interaction of αIIb with fibrinogen. However, platelets appeared to spread normally, with nodule numbers and turnovers similar to untreated platelets, suggesting that at this concentration, the interaction with the antibody and αIIb-integrin subunit does not affect platelet spreading or nodule formation. All actin nodules co-localised with αIIb-rich structures (Figure 3.17 *A*). The majority of the actin nodules (> 75 %) appeared and disappeared concurrently with αIIb integrin cluster appearance. When broken down by cellular localisation of nodules and their associated integrin clusters, there was a decrease in the percentage of nodules which appeared concurrently with the integrin clusters for nodules which were localised to the centre of the cells (Figure 3.17 *B*). Although the integrin clusters mostly disappeared at the same time as the actin nodule disappearance, an integrin cluster did not always remain associated with an actin nodule (Figure 3.17 *C*). Instead for approximately 20 % of nodules the initial integrin cluster, disappeared and a second integrin cluster associated with the actin nodules. This turnover of the integrin-rich structures occurred more frequently for nodules at the base of filopodia (Figure 3.17 *D*). Additionally, these integrin-rich structures were only present when co-localised with actin nodules.

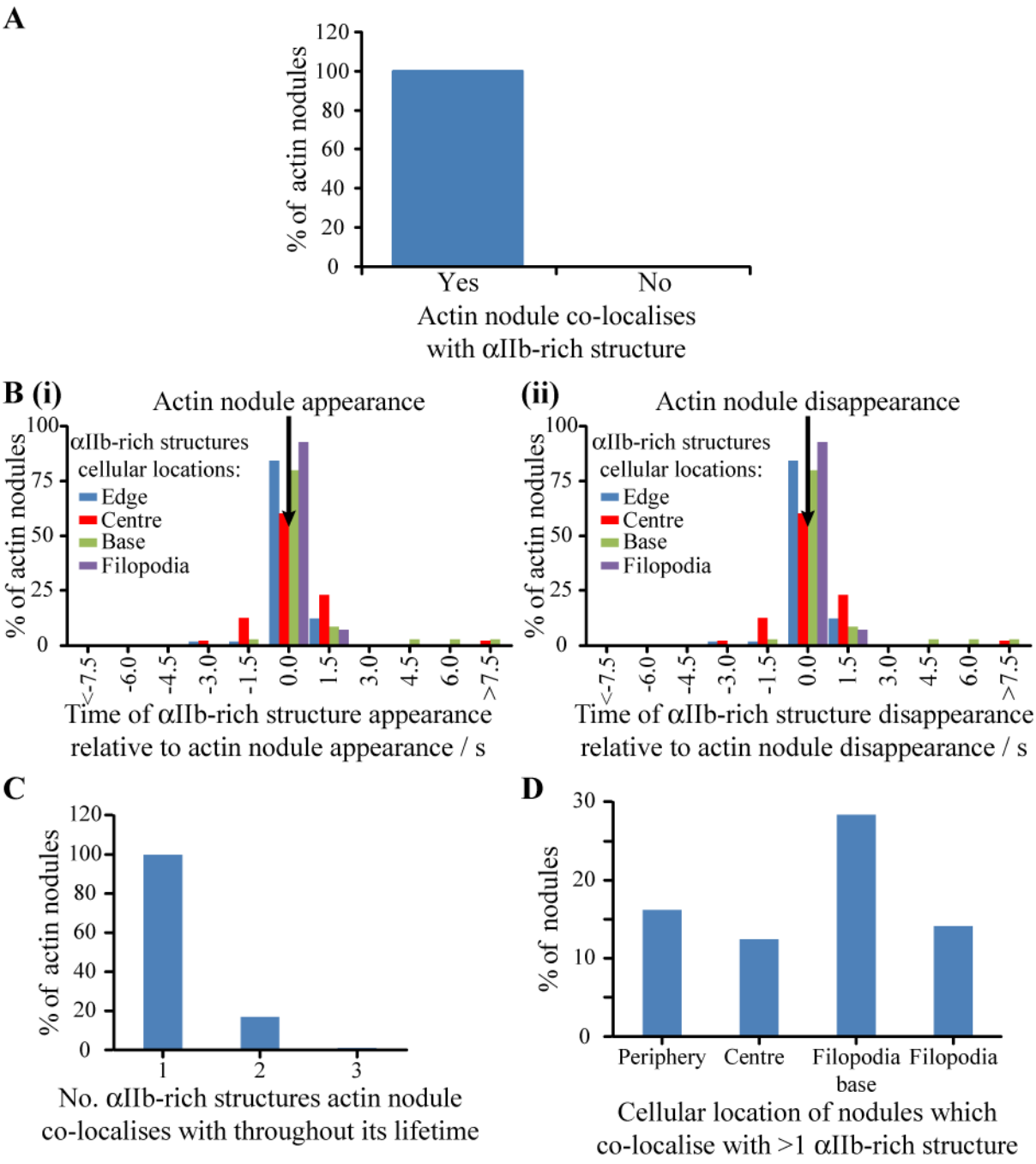

Figure 3.17. Co-localisation dynamics of actin nodules and αIIb-integrin subunit. Washed Lifeact-GFP mouse platelets (2 x 10^7 mL^{-1}) were incubated with a PE-conjugated antibody for αIIb (1 % v/v) for 10 min prior to spreading on fibrinogen (37 °C). Platelet spreading was monitored using real-time two-colour TIRF microscopy, with an image taken every 1.5 s. (A) The number of actin nodules which co-localise with αIIb. (B) Distribution of the timing of αIIb-rich structures appearance and disappearance relative to actin nodule formation and disappearance, (i) and (ii), respectively, for αIIb-rich structures at different cellular locations. (C) Turnover of αIIb-rich structures during actin nodule lifetime. (D) Cellular localisation of nodules which exhibit turnover of αIIb-rich structures. A minimum of 15 platelets (with ~ 30 nodules/platelet) were analysed per experiment. The results are from more than three experiments.

Relationship between actin nodules and the collagen receptor, α2β1 integrin

Although α2β1 is the most abundant collagen receptor on the platelet surface, there are only approximately 2000 copies per cell (Clemetson and Clemetson, 2001, Best et al., 2003). αIIbβ3 has far more copies per cell, in the region of 50,000 – 80,000 (Wagner et al., 1996). This difference in copies per cell would result in a decrease in the number of fluorescently labelled antibodies bound to the cell and consequently a decrease in the fluorescent signal. Therefore to test whether it is possible to image the integrin dynamics on platelets, human platelets were incubated with a fluorescently conjugated antibody for α2 prior to spreading on collagen coated coverslips. Platelet spreading was monitored in real time using TIRF microscopy (Figure 3.18).

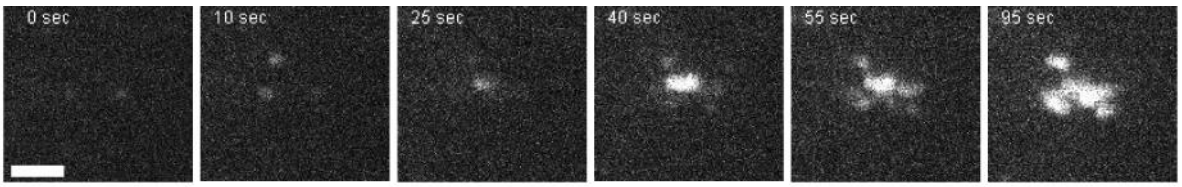

Figure 3.18. Dynamics of α2-integrin subunit in human platelets. Washed human platelets (2×10^7 mL^{-1}) were incubated with FITC-conjugated antibody for α2 (1 % *v/v*) for 10 minutes prior to spreading on collagen (37 °C). Platelet spreading was monitored using real-time TIRF microscopy, with an image taken every 5 s. Time course of α2-rich structure dynamics in human platalets. Images are representative of two experiments. Scale bar = 5 μm.

Unlike with αIIb labelling, the whole cell is not visible. Instead discrete clusters of fluorescence are visible as the platelet adheres to the surface. The number of clusters increase as the platelet spreads. These results demonstrate that it is possible to image α2 integrin dynamics on the platelet surface.

Unfortunately, it was not possible to image actin dynamics of Lifeact-GFP mouse platelet spreading on a collagen surface using TIRF microscopy due to the unevenness of the collagen surface. The uneven surface meant that not all of the platelet was visible within the evanescent field. However based on previous observations that actin nodules co-localised with β1, it may be that those α2-rich integrin clusters localised to actin nodules and two-colour TIRF studies similar to that used for αIIb are needed to determine if this is the case.

The co-localisation of actin nodules with αIIb throughout the nodule lifetime and the position of all nodules near the basement membrane (See **3.2.1**) suggest that nodules may be involved in adhesion. Other adhesion actin structures such as podosomes and focal adhesions both contain integrins enabling linking of the cytoskeleton to the ECM (Block et al., 2008). Previous work has found that actin nodules also co-localise with talin, vinculin and paxillin which are present in both focal adhesions and podosomes (Calaminus et al., 2008, Barnes, 2011). However, it is unlikely that the nodules represent either structure because they differ structurally from podosomes, for instance, no inner core of actin and they do not form rosette structures, and unlike focal adhesions they do not co-localise with pFAK and disappear prior to stress fibre formation (Calaminus et al., 2008, Barnes, 2011). Instead the actin nodule may represent a different adhesion structure in platelets.

3.3 CONCLUSIONS

Live-cell TIRF microscopy of Lifeact-GFP mouse platelets has enabled further research of the role of actin nodules in platelet spreading (Figure 3.19). The actin nodule is a transient actin rich structure which forms within seconds of platelet adhesion to matrix proteins. The actin nodules are localised to the basal membrane, throughout the platelet, and remain stationary during their lifetime which is on average 31 s. Actin nodule formation requires actin polymerisation downstream of SFK activity and the presence of Arp2/3 complex, while ROCK appears to play a role in nodule stability. Additionally actin nodule formation and disappearance are associated with formation and disappearance of αIIb-rich structures which co-localise with the actin nodule.

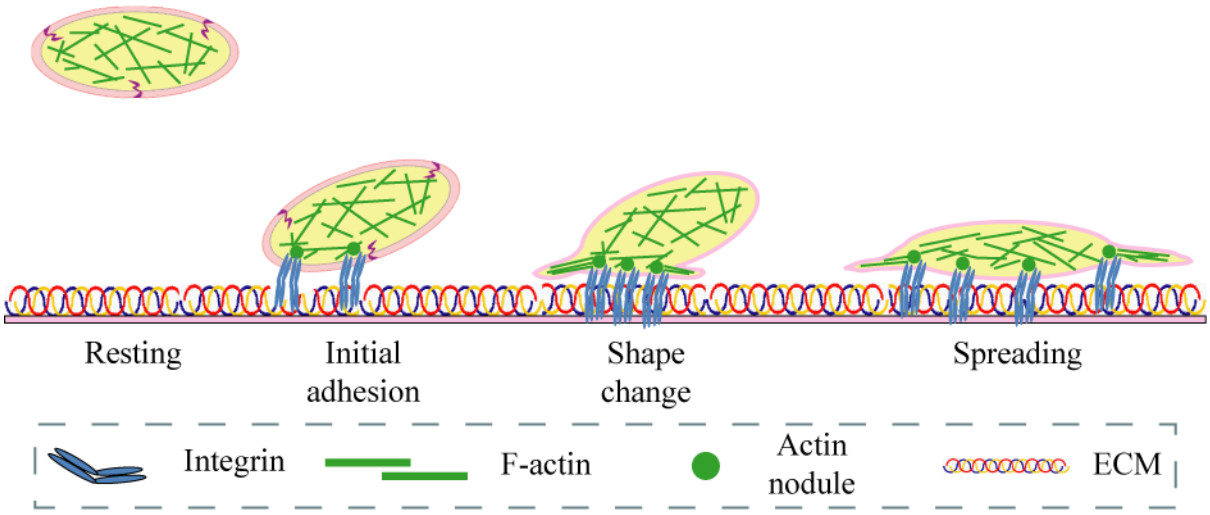

Figure 3.19. Schematic representation actin nodules in spreading platelets. Resting platelets contain a disorganised pool of F-actin. Upon platelet activation following initial adhesion, actin polymerisation and reorganisation results in formation of actin nodules which form concurrently with clustering of integrins. As the platelet continues to spread, forming filopodia and lamellipodia, the actin nodule and the integrin-rich structures increase in number and are constantly replaced with new ones.

The stationary nature of the actin nodule, its localisation to the basal membrane and its co-localisation with actin associated proteins which are present in podosomes and focal adhesions, suggest that the actin nodules may play a role in platelet adhesion. Their disappearance prior to formation of stress fibres suggest that their involvement is in initial adhesion events but not necessarily in stable adhesion. Therefore, the actin nodule may represent a novel adhesion structure in platelets.

CHAPTER 4

DELIVERY OF THE ACTIN BINDING PROTEIN, LIFEACT, INTO HUMAN PLATELETS USING pH (LOW) INSERTION PEPTIDE

4.1 INTRODUCTION

Reliable visualisation of the actin cytoskeleton is essential for further understanding of platelet actin dynamics, in particular, the actin nodule. In order to do this fluorescently labelled actin or actin binding proteins are required to label the actin. The discovery of GFP and its analogues and their incorporation into fusion proteins which can be expressed in other organisms, enabled the generation of GFP-actin fusion proteins (Shimomura et al., 1962, Tsien, 1998, Era et al., 2009, Yoon et al., 2002). Previously, this had mostly been achieved via injection of fluorescently labelled actin or addition of fluorescently labelled phalloidin. However, all of these methods have their drawbacks, including; phalloidin's cytotoxicity and GFP-actin fusions impair actin function (Cooper, 1987, Feng et al., 2005). This led to the exploration of actin binding domains as GFP fusion protein labels.

Due to the high sensitivity of platelet membranes and their lack of a nucleus, fluorescent label injection and cell transfection are not viable for use with human platelets. As a result, staining of fixed cells with fluorescently labelled phalloidin is the most prevalent technique for human platelets (Thomas et al., 2007, Calaminus et al., 2008, Mori et al., 2012). However, the use of fluorescently labelled actin binding domains, in particular Lifeact, has potential as an actin label in live human platelets (Riedl et al., 2008). Lifeact is derived from the first 17 amino acids of ABP140 in *Saccharomyces cerevisiae*. Its small size and its lower affinity for actin

than phalloidin (actin-phalloidin; 30 pM and actin-Lifeact; 1.3 μM), means that it does not appear to affect actin polymerisation or depolymerisation (Riedl et al., 2008, Deibler et al., 2011, Wulf et al., 1979, Faulstich et al., 1977). This has proved useful for looking at actin dynamics in platelets (**Chapter 3**) and their precursor megakaryocyte cells in GFP-Lifeact mouse models (Schachtner et al., 2012, Schachtner et al., 2013). However, Lifeact has mostly been used as a transgenicly expressed protein in cells or have been introduced via 'scrape loading', neither are suitable for human platelets (Riedl et al., 2008, Riedl et al., 2010, Munsie et al., 2009, Bottcher et al., 2009, Lizarraga et al., 2009, Li et al., 2008).

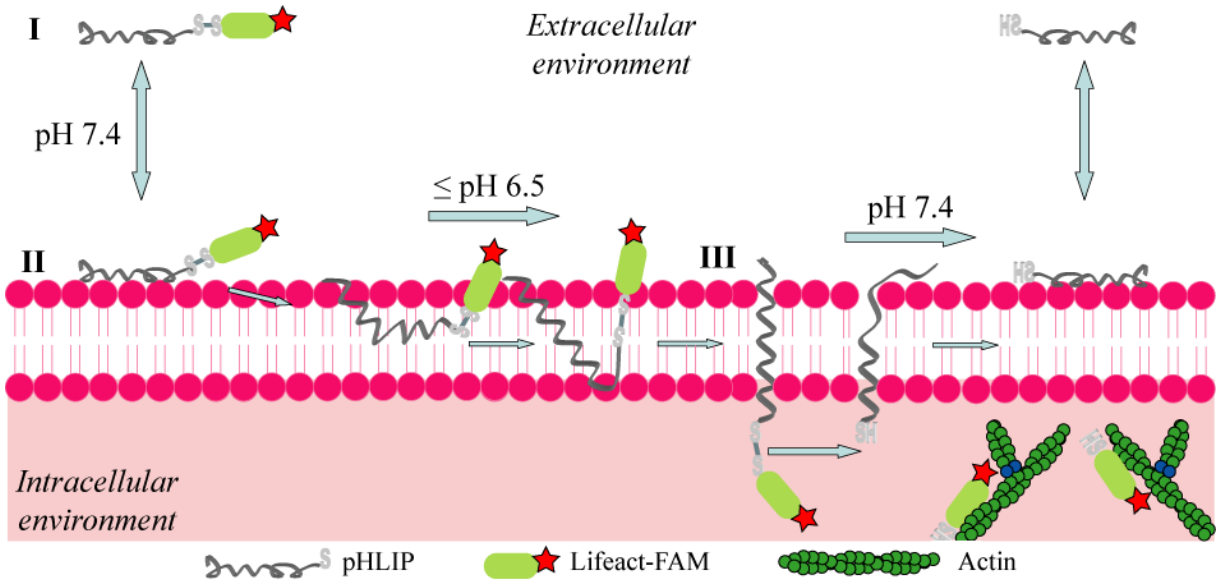

Figure 3.1. Schematic representation of pHLIP mediated cellular delivery of fluorescently labelled Lifeact. I, II and III represent the three states that pHLIP adopts; - in solution, associated with the lipid membrane and inserted across the lipid membrane, respectively. Lifeact, conjugated to pHLIP's *C*-terminus via a disulphide bond, is translocated across the cell membrane in to the cytoplasm. Reduction of the disulphide bond in the reducing environment inside the cell releases Lifeact into the cytoplasm. Thus enabling Lifeact to label of the actin cytoskeleton. The low pH induced insertion is completely reversed upon restoration of neutral pH.

Instead, this work introduces the use of pH (low) insertion peptide, pHLIP, to facilitate the delivery of Lifeact into human platelets. A 38 amino acid peptide, pHLIP has delivered a

variety of cell impermeable compounds, including phalloidin, into the cytoplasm of cells when conjugated via a disulphide bond to the peptide's *C*-terminus (Reshetnyak et al., 2006, An et al., 2010, Reshetnyak et al., 2011). The mechanism for pHLIP's cytoplasmic delivery of cargo is pH-dependent (Figure 4.1). Essentially; at neutral pH, pHLIP exists as an unstructured monomer and loosely associates with the lipid membrane (State I-II). Upon a reduction in pH to 6.5 or lower, pHLIP forms an α-helix and spontaneously inserts itself, *C*-terminus first across the lipid membrane (State III) (Karabadzhak et al., 2012). Thereby, translocating any cargo molecules bound to its *C*-terminus across the lipid membrane. The reducing environment of the cell cleaves the disulphide bond between pHLIP and its cargo, thereby releasing it into the cell (An et al., 2010, Wijesinghe et al., 2011, Moshnikova et al., 2013). Increasing the pH back to neutral results in the removal of pHLIP from its transmebrane situation (Andreev et al., 2010).

The work in this chapter aims to explore the suitability of Lifeact as an actin label and pHLIP as a delivery vector in human platelets. Fluorescently labelled Lifeact is conjugated to pHLIP's *C*-terminus via a disulphide bond, thereby releasing the translocated Lifeact peptide into the cytoplasm to label F-actin. Consequently, delivery of Lifeact into live cells will enable live cell imaging of actin dynamics in human platelets and facilitate research into the dynamics of the platelet actin nodule.

4.2 RESULTS & DISCUSSION

4.2.1 Lifeact as an actin label in human platelets

Lifeact peptide was synthesised following the sequence described by Riedl *et al* (Riedl et al., 2008) but with the addition of two extra amino acids; a cysteine residue was added to the *N*-terminus to enable conjugation to pHLIP via a disulphide bond and an additional lysine added to the *C*-terminus to enable addition of a fluorescent label. For this work Lifeact was labelled with carboxyfluorescein, FAM. Lifeact was dissolved in DMF (37 % v/v in sodium phosphate buffer (0.1 M, pH 7.0)).

Spread and fixed human platelets were permeablised and stained with 488-phalloidin or Lifeact-FAM (Figure 4.2). Comparable labelling of actin structures, including nodules, filopodia, lamellipodia and stress fibres, by phalloidin and a range of Lifeact concentrations is apparent in various representative stages of platelet spreading. The transient nature and relatively low F-actin affinity of Lifeact does not appear to affect actin labelling as evidenced by comparable actin labelling by Lifeact at various concentrations and that of phalloidin. However, the Lifeact labelled actin appears “fuzzier” than actin labelled with phalloidin, this may be as a result of the transient binding nature of Lifeact to actin, resulting in the presence of both actin bound and unbound label (Riedl et al., 2008, Riedl, 2011).

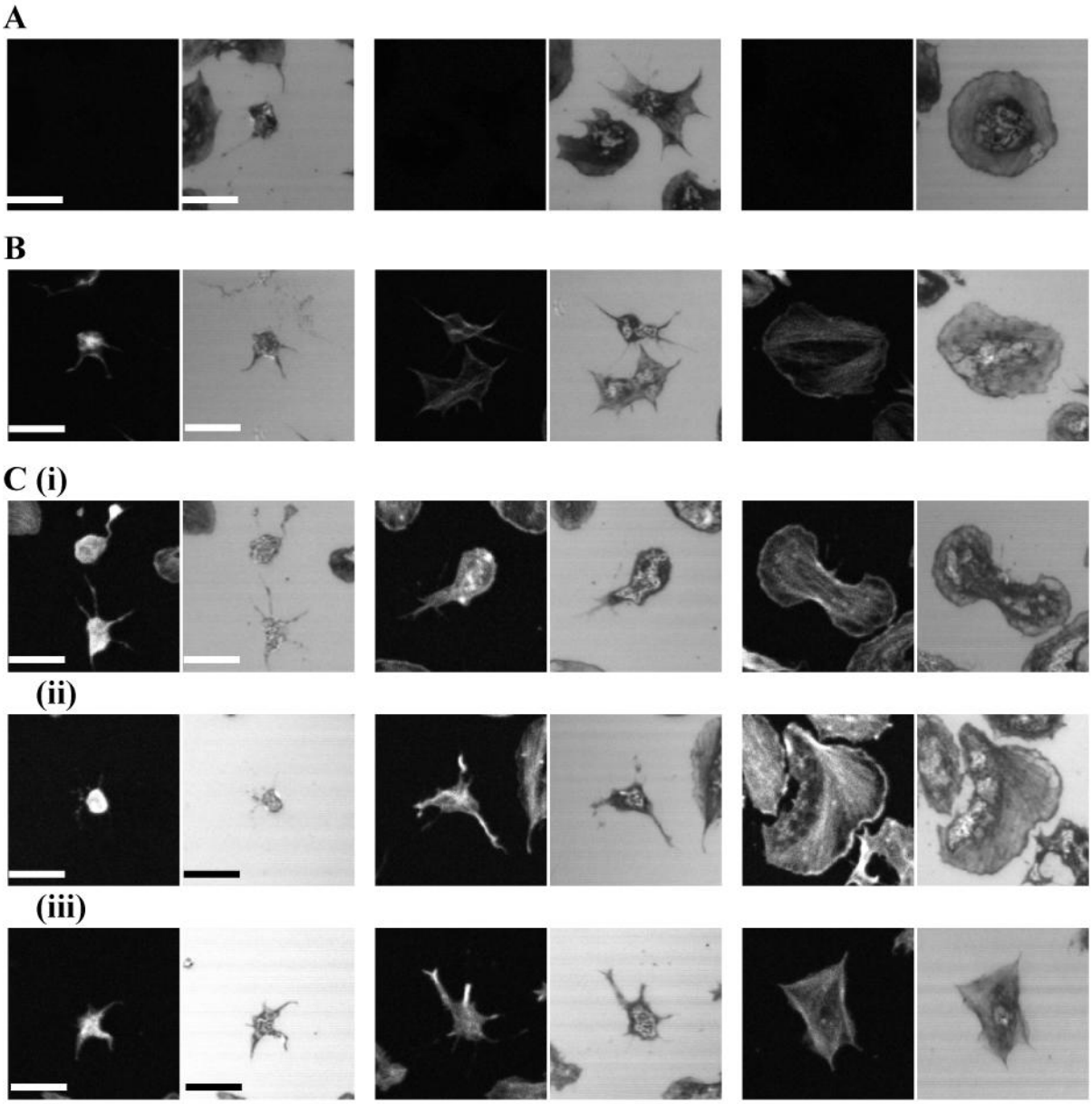

Figure 4.2. Confocal fluorescence and reflection microscopy of human platelets stained for actin. Washed human platelets (2 x 10^7 mL^{-1}) were allowed to spread on fibrinogen for 45 min (37 °C, CO_2) prior to fixation, permeablisation with Triton X-100 (0.1 % in PBS) and actin labelling. Representative fluorescence (*left*) and reflection (*right*) images of: (A) Unlabled platelets. (B) 488-phalloidin (6.6 pM) labelled platelets. (C) Platelets labelled with (i) 5 pM, (ii) 6.7 pM or (iii) 10 pM Lifeact-FAM. Images are representative of three experiments. Scale bar = 5 µm.

In spread, fixed and permeablised cells 6.6 pM Lifeact is sufficient to label the platelet actin cytoskeleton. However, in non-permeablised cells molecules are not able to enter the cells as easily, if at all, so increasing the concentration of Lifeact in cell solution would increase the likelihood of uptake, if Lifeact is able to permeate the membrane. Human platelets were incubated with Lifeact-FAM for 40 minutes in various pH conditions prior to spreading on fibrinogen and fixation (Figure 4.3) to assess whether Lifeact-FAM is able to enter non-permeablised platelets on its own. Although, there was some labelling, it was very faint and may be due to fixation related membrane permeability.

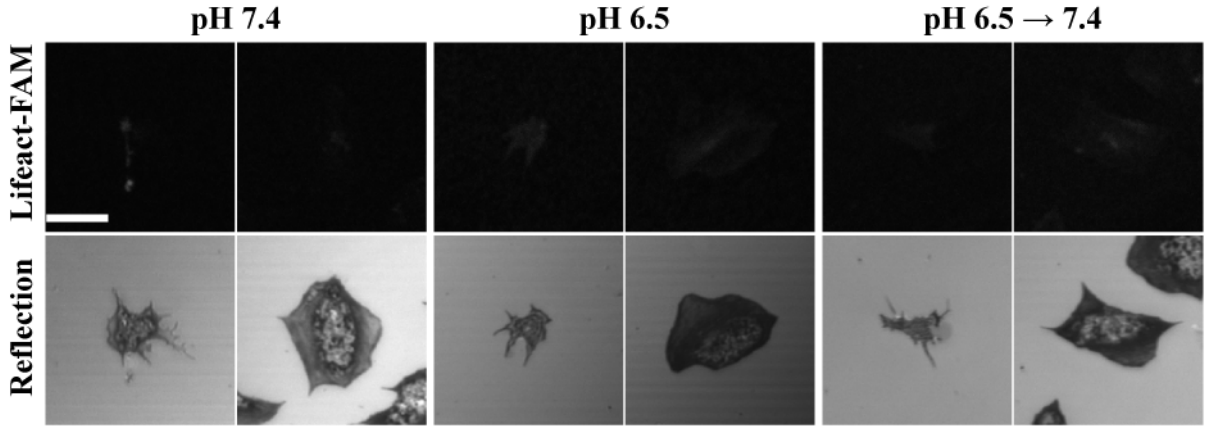

Figure 4.3. Uptake of Lifeact peptide into non-permeablised human platelets. Human platelets (2 x 10^8 mL^{-1}) were resuspended in Tyrode's buffer at pH 6.5 or pH 7.4, as indicated, and treated with Lifeact-FAM (8.8 μM, in 0.1 M sodium phosphate buffer with 37 % *v/v* DMF) for 40 minutes. The platelet suspension was diluted with Tyrode's buffer to 2 x 10^7 mL^{-1}, the pH was kept constant or increased to pH 7.4 and the platelets were allowed to spread on fibrinogen for 60 minutes prior to fixation. Confocal fluorescence (*top*) and reflection (*bottom*) images of platelets treated at pH 7.4, pH 6.5 or at pH 6.5 and increased to pH 7.4. . Images are representative of three experiments. Scale bar = 5 μm.

Lifeact peptide is able to label actin in permeablised platelets and appears to be unable to permeate the cell membrane on its own. Therefore, fluorescently labelled Lifeact is an ideal

candidate for cellular delivery using pHLIP in order to label the actin cytoskeleton of live human platelets.

4.2.2 pHLIP as a delivery agent for human platelets

The *C*-terminal of pHLIP, when inserted into a lipid membrane, is found in the cytoplasm of the cell and, as such, is the target for cargo molecule conjugation. In order to achieve this pHLIP was synthesised as per the sequence described by Reshetnyak *et al* but with the addition of a thiopyridyl group added to the *C*-terminus cysteine residue (Reshetnyak et al., 2006). The presence of the thiopyridyl group prevents disulphide bonds forming between cysteine residues of other pHLIP molecules and it also enables disulphide exchange with a cysteine residue of the cargo molecule. Consequently, allowing efficient conjugation of pHLIP to a cargo molecule such as Lifeact. pHLIP was dissolved in DMSO (75 % v/v in sodium phosphate buffer (0.1 M, pH 7.0)).

The effect of pHLIP on platelets in suspension was investigated. Following treatment of platelets with various concentrations of pHLIP at pH 6.5 for 10 minutes the number of platelets in the suspension was counted (Figure 4.5). At 10 μM pHLIP there was a highly significant decrease in the platelet number relative to 0.0 μM pHLIP control sample but not for any other concentration. This suggests that at pHLIP concentrations of 10 μM or more pHLIP affects cell viability. Therefore, pHLIP will be used at concentrations less than 10 μM.

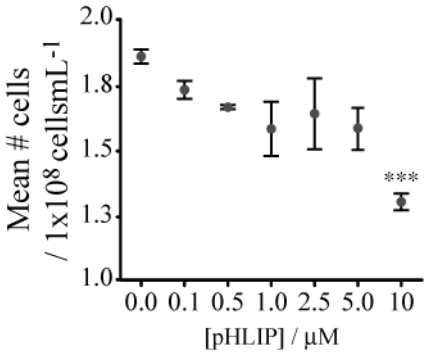

Figure 4.4. Effect of pHLIP on human platelet suspensions. Human platelets (2 x 10^{-8} mL^{-1}) were resuspendend in Tyrode's buffer (pH 6.5) and treated, in suspension, with various concentrations of pHLIP (in 0.1 M sodium phosphate buffer with 75 % *v/v* DMSO) for 10 minutes. Following treatment the number of cells in the platelet suspension was counted. Reduction in the number of platelets in suspension was observed for increasing concentrations of pHLIP. The results are from three experiments. Values are shown ± s.e.m. ***$P < 0.001$ is relative to 0.0 µM pHLIP.

Following the protocol used by An *et al.*, for calculating amount of phalloidin that needs to be delivered, using pHLIP, per cell when treating HeLa cells (An et al., 2010), human platelets were incubated with pHLIP (6.6 µM), under various pH conditions, for 40 minutes prior to spreading on fibrinogen and fixation. The platelets were then imaged using confocal reflection microscopy to assess platelet spreading (Figure 4.5 *A*). There was no significant difference in the mean cell density of spread platelets, mean platelet area or in the distribution of platelets at various spreading stages for platelets in any pH conditions when compared with their respective solvent control samples (Figure 4.5 *B-D*). Therefore, incubation with pHLIP at 6.6 µM does not appear to affect platelet spreading.

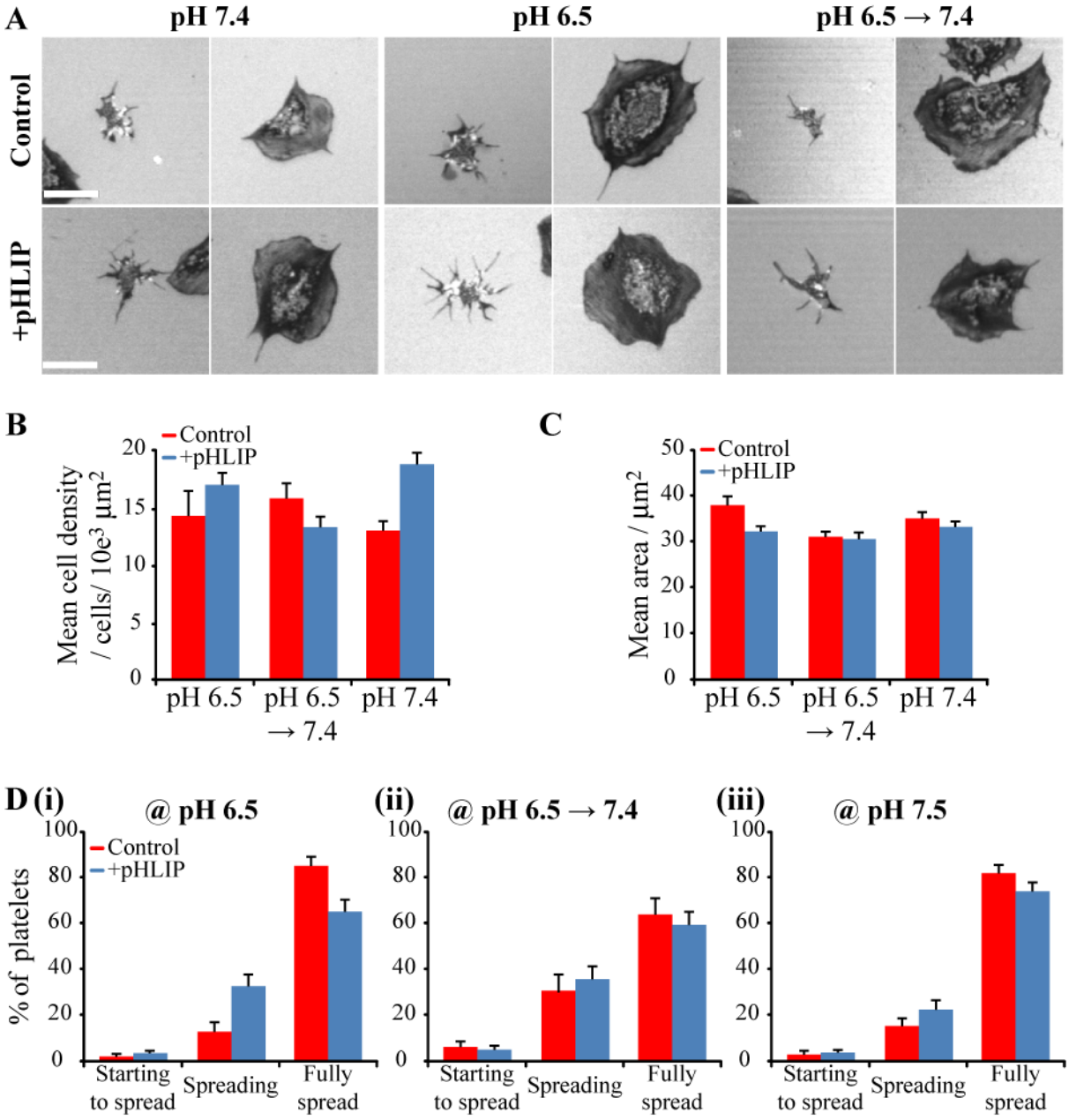

Figure 4.5. Effect of pHLIP on spreading of human platelets. Human platelets (2 x 10^8 mL^{-1}) were resuspended in Tyrode's buffer at pH 6.5 or pH 7.4, as indicated, and treated with DMSO (0.05 % *v/v*) or pHLIP (6.6 µM, in 0.1 M sodium phosphate buffer with 75 % *v/v* DMSO) for 40 minutes. The platelet suspension was diluted with Tyrode's buffer to 2 x 10^8 mL^{-1}, the pH was kept constant or increased to pH 7.4 and the platelets were allowed to spread on fibrinogen for 60 min (37 °C, 5 % CO_2) prior to fixation. (A) Confocal reflection microscopy images of control (*top*) and pHLIP treated (*bottom*) platelets. Images are representative of three experiments. Scale bar = 5 µM. (B) Mean cell density. (B) Mean platelet area. (C) Percentage of platelets at various stages of spreading; (i) at pH 6.5, (ii) at pH 6.5 and increased to pH 7.4 and (iii) at pH 7.4. A minimum of 30 platelets were analysed per experiment. Values are shown ± s.e.m.

The *N*-terminal of pHLIP was labelled with a DyLight 550 fluorescent label to enable visualisation of pHLIP on/in the platelet membrane. Dye to peptide ratio was calculated to be 0.04 moles of DyLight 550 per mole of pHLIP, indicating a labelling efficiency of 4 %. The final peptide concentration was determined to be 0.34 mM.

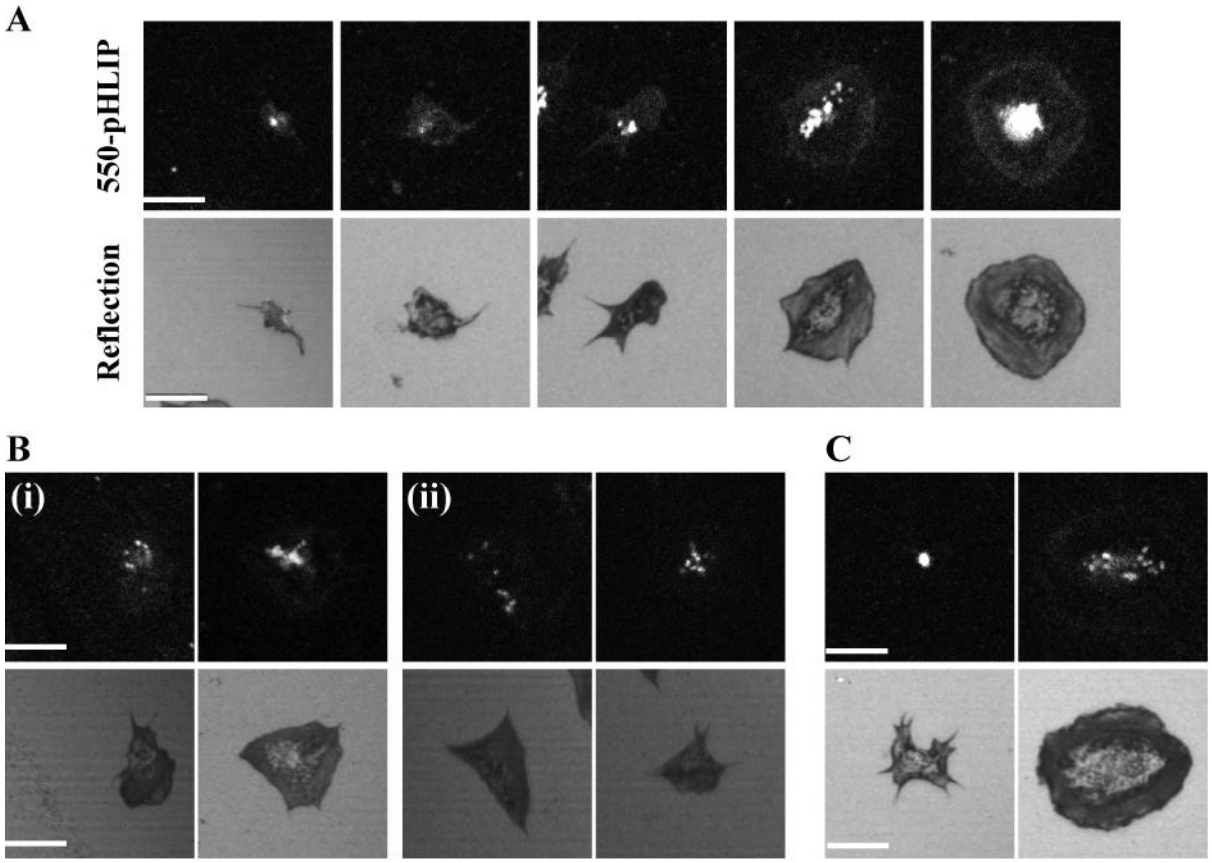

Figure 4.6. Confocal fluorescence and reflection microscopy of human platelets treated with 550-pHLIP. Human platelets (2 x 10^8 mL^{-1}) were resuspended in Tyrode's buffer at pH 6.5 or pH 7.4, as indicated, and treated with 550-pHLIP (8.8 μM, in 0.05 M borate buffer) for 40 minutes. The platelet suspension was diluted with Tyrode's buffer to 2 x 10^8 mL^{-1}, the pH was kept constant or increased to pH 7.4 and the platelets were allowed to spread on fibrinogen for 60 min (37 °C, 5 % CO_2) prior to fixation. Confocal fluorescence (*top*) and reflection (*bottom*) images of platelets treated at (A) pH 6.5, (B) pH 6.5 and increased to pH 7.4 and (C) at pH 7.4. The entire cell is labelled for platelets treated at pH 6.5 or only the centre for pH 7.4 conditions. A mixture of both entire cell (B(i)) or centre only (B(ii)) labelling was apparent when the pH was increased following treatment. Images are representative of three experiments. Scale bar = 5 μm.

pHLIP labelled with DyLight 550, 550-pHLIP, was added to human platelets at various pH conditions for 40 minutes prior to spreading on fibrinogen and fixation. The platelets were then imaged using confocal reflection and fluorescence microscopy (Figure 4.6). The majority of cells treated with 550-pHLIP exhibited fluorescence regardless of the pH conditions during treatment (Figure 4.7 *A*). However, the cellular localisation of this fluorescence differed with pH (Figure 4.7 *B*). All labelled cells had pronounced labelling in the centre of the cell, while for platelets treated at pH 7.4 the majority of cells (92 %) displayed only central labelling, the entire of the cell surface was labelled for the majority of platelets (89 %) treated at pH 6.5. Platelets treated at pH 6.5 but then the pH increased to pH 7.4, were evenly split between the proportion of cells entirely labelled (44 %) and only labelled in the cell centre (56 %).

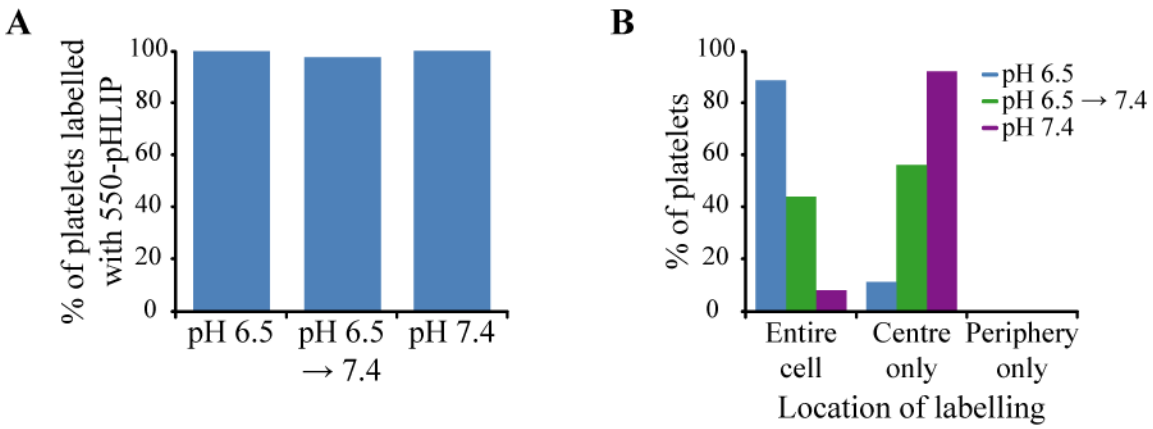

Figure 4.7. Platelets treated with 550-pHLIP. Human platelets (2 x 10^8 mL^{-1}) were resuspended in Tyrode's buffer at pH 6.5 or pH 7.4, as indicated, and treated with 550-pHLIP (8.8 µM, in 0.05 M borate buffer) for 40 min. The platelet suspension was diluted with Tyrode's buffer to 2 x 10^8 mL^{-1}, the pH was kept constant or increased to pH 7.4 and the platelets were allowed to spread on fibrinogen for 60 min (37 °C, 5 % CO_2) prior to fixation. (A) Percentage of platelets labelled with 550-pHLIP. (B) Cellular localisation of 550-pHLIP platelet labelling. A minimum of 30 platelets were analysed per experiment. the results are from three experiments. Values are shown ± s.e.m.

In all pH conditions there was a large concentration of pHLIP in the central region of the platelet. Since pHLIP binds to/inserts across the cell membrane, 550-pHLIP is a membrane label so the greater concentration in the centre of platelets could be as a result of increased membrane area from the open canalicular system. To assess whether this was the case platelets were labelled with FM4-64FX lipophilic styryl dye to label the platelet membrane (Figure 4.8). The fluorescence signal from the dye was very weak; however the membrane dye shows an increased concentration in the centre of the platelets, while the rest of the platelet surface is also labelled. The increased concentration in the centre of cells is similar to that of 550-pHLIP at pH 6.5. This suggests that the greater labelling of the cell centre may be due to increased membrane surface area.

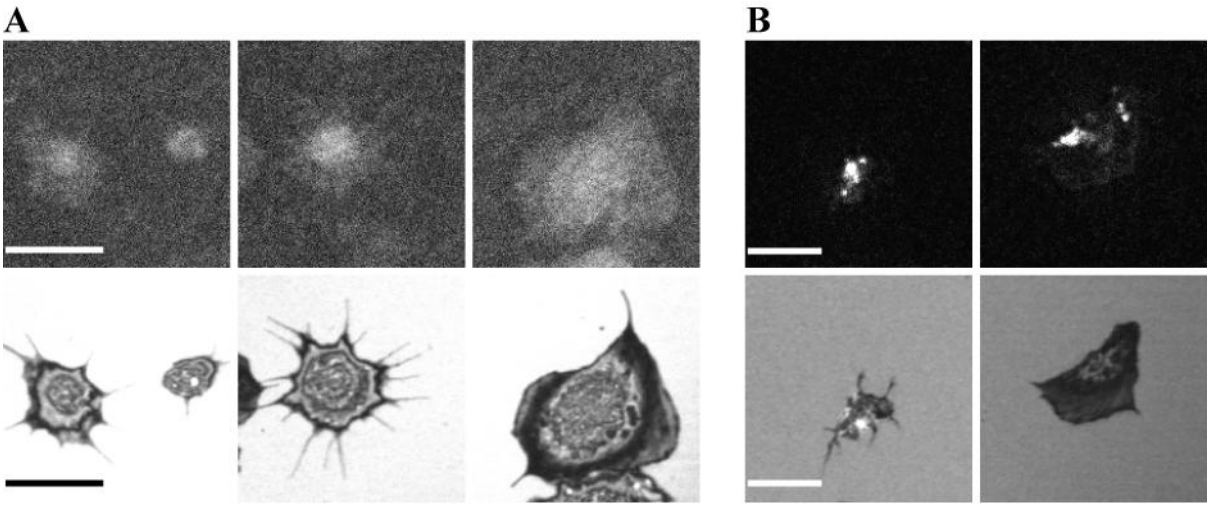

Figure 4.8. Labelling of the human platelet membrane. Human platelets (2 x 10^8 mL^{-1}) were resuspendend in Tyrode's buffer (pH 6.5) and left untreated or treated with 550-pHLIP (8.8 µM, in 0.05 M borate buffer) for 10 min. Platelet suspensions were diluted with Tyrode's buffer (pH 6.5) to 2 x 10^7 mL^{-1} and allowed to spread on fibrinogen for 45 min (37 °C, 5% CO_2) prior to fixation. The untreated sample was labelled with FM4-64FX (5 μgmL^{-1}, in water) for 1 min prior to fixation. Confocal fluorescence (*top*) and reflection (*bottom*) images of platelets with; (A) FM4-64FX membrane dye or (B) 550-pHLIP. Images are representative of three experiments. Scale bar = 5 µm.

Addition of pHLIP to platelets in various pH conditions and at the various concentrations tested does not appear to affect platelet spreading on fibrinogen, thus demonstrating the potential suitability of pHLIP for use as a delivery agent in human platelets. The labelling of pHLIP with 550 DyLight enabled visualisation of the distribution of pHLIP on the platelet. The difference in the fluorescence pattern between platelets treated at pH 6.5 and at pH 7.4 corresponds well with the model for pHLIP properties; at pH 7.4, pHLIP is loosely bound to the membrane so it is expected that less pHLIP would be associated with the membrane than at pH 6.5. When the platelets were treated at pH 6.5 and then the pH increased to 7.4, there was a reduction in the amount of entirely labelled cells corresponding with the removal of pHLIP from the membrane.

4.2.3 Conjugation and characterisation of pHLIP-Lifeact

Conjugation of pHLIP to Lifeact via formation of a disulphide bond between cysteine residue of Lifeact and cysteine-thiopyridyl of pHLIP will result in the release of pyridine 2-thione, P2T, (Figure 4.9). P2T produces an absorbance at around 343 nm (Zhao et al., 2002). So assaying for the presence of P2T using UV-Vis absorbance spectroscopy would be an indicator of conjugation of Lifeact to pHLIP. However, this assay was unsuccessful due to the very low concentration of P2T produced which was not detectable.

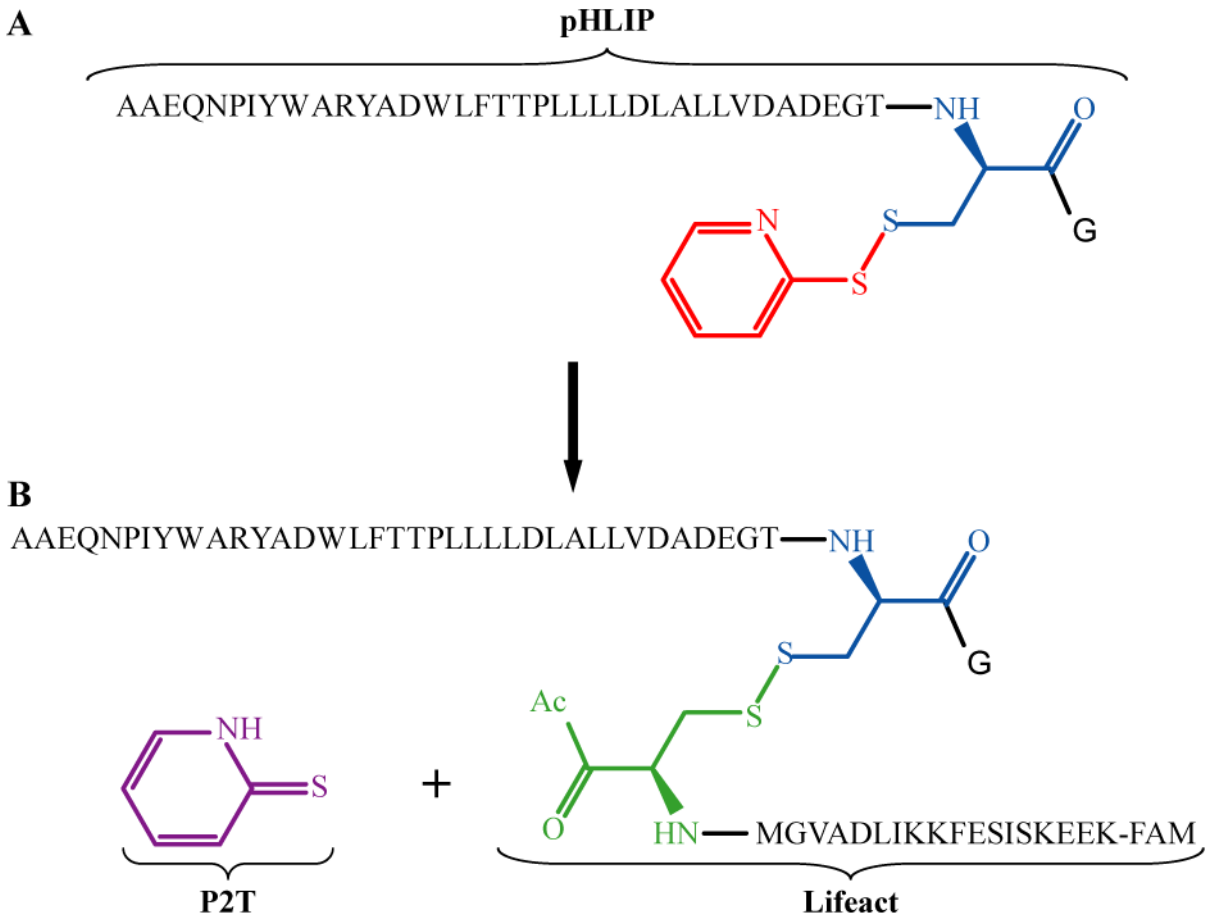

Figure 4.9. Schematic representation of pHLIP-Lifeact conjugation. (A) The *C*-terminus cysteine residue of pHLIP (blue) has been modified by the addition of a thiopyridyl group (red). (B) Upon addition of fluorescently labelled Lifeact, Lifeact-FAM, a disulphide exchange occurs resulting in formation of a disulphide bond between pHLIP's cysteine and the *N*-terminus cysteine residue of Lifeact-FAM (green) releasing pyridine 2-thione, P2T, (purple).

Instead, reverse phase HPLC was utilised to determine whether conjugation occurred. Lifeact-FAM eluted at 21.6 minutes, pHLIP at 27.4 minutes and there was a third absorbance peak that eluted at 25.9 minutes that following MS analysis proved to be pHLIP-Lifeact (Figure 4.10 *A*). Although quantification of how much pHLIP-Lifeact was formed is not possible from this HPLC technique, the optimum conjugation conditions were determined via monitoring of the increases/ decreases in the area of the absorbance peak for each of the three peptides (Figure 4.10 *B*). The actual percentages are not important or useful in this situation

due to differences in the absorbance of 215 nm light by each peptide. However, for each peptide after addition of 6 parts Lifeact-FAM to 10 parts pHLIP, the values plateaued suggesting that no further conjugation occurred. Therefore, to ensure maximum amount of conjugation eight times 1 part Lifeact-FAM was added to 10 parts pHLIP.

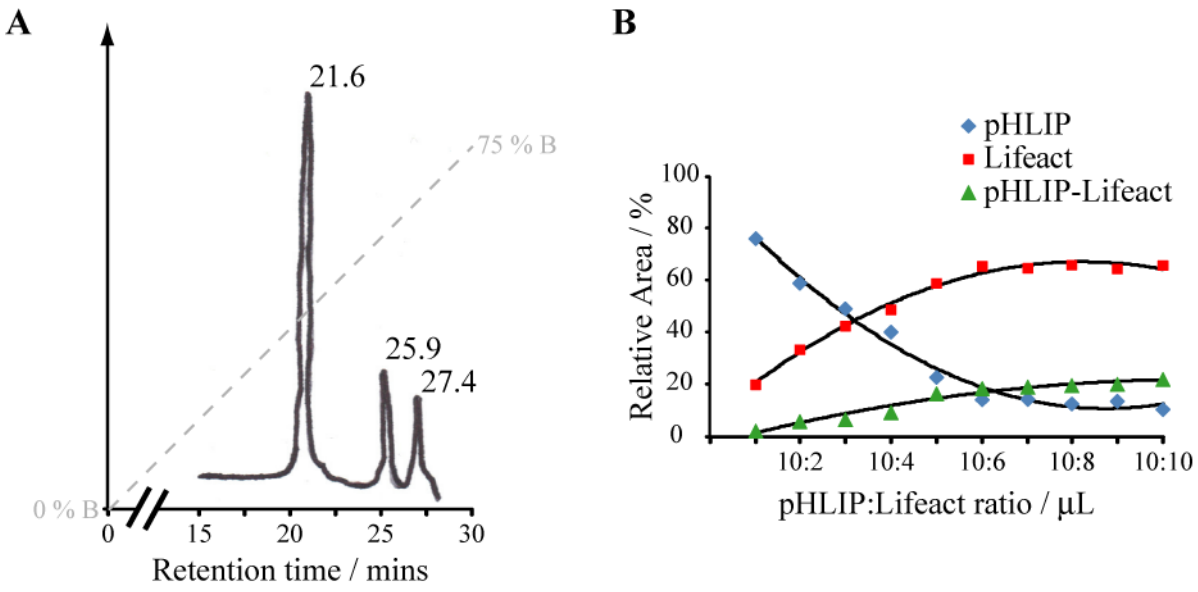

Figure 4.10. Conjugation of pHLIP-Lifeact. Conjugation of Lifeact to pHLIP was monitored using reverse phase HPLC. (A) Elution of Lifeact-FAM (21.6 mins), pHLIP-Lifeact (25.9 mins) and pHLIP (27.4 mins) using a water (A; 0.05 % TFA) to 100% MeCN (B; 0.05 % TFA) solvent gradient (dashed line). λ = 215 nm. (B) The relative area under the absorption peak for each peptide was determined for addition of each aliquot (1 µL) of Lifeact (1 mM, in 0.1 M sodium phosphate buffer with 7.4 % *v/v* DMF) to pHLIP (10 µL, 1 mM, in 0.1 M sodium phosphate buffer with 7.5 % *v/v* DMSO).

4.2.4 Treatment of human platelets with pHLIP-Lifeact

Human platelets were incubated with pHLIP-Lifeact (6.6 µM) in various pH conditions for 40 minutes. The pH was either kept constant or increased to pH 7.4 to remove excess, untranslocated pHLIP-Lifeact prior to spreading on fibrinogen (Figure 4.11). Platelets incubated with pHLIP-Lifeact at pH 7.4 displayed faint membrane labelling, if any, but there

is labelling in the centre of the cell, as was previously noticed for 550-pHLIP treated platelets. When platelets were treated at pH 6.5, labelling of the actin cytoskeleton is apparent. In samples where the pH was increased to remove excess or untranslocated pHLIP-Lifeact from the platelet membrane, there is a reduction in the amount of labelling as indicated by the decreased fluorescence intensity (Figure 4.15 *F*) but there is still clear actin labelling. In both samples, labelling of the central platelet region was present.

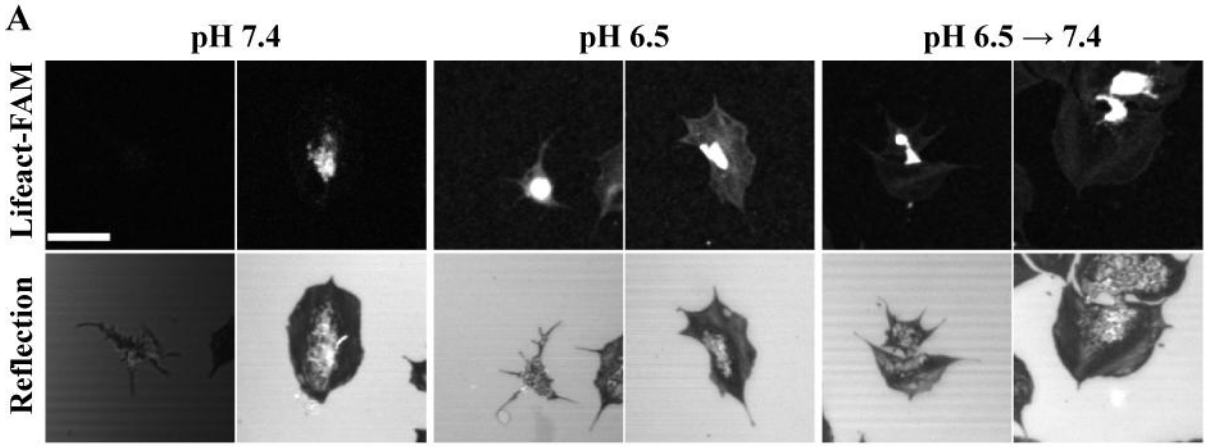

Figure 4.11. Confocal fluorescence and reflection microscopy of human platelets treated with pHLIP-Lifeact. Human platelets (2 x 10^8 mL^{-1}) were resuspended in Tyrode's buffer at pH 6.5 or pH 7.4, as indicated, and treated with pHLIP-Lifeact (6.6 µM, in 0.1 M sodium phosphate buffer with >4 % DMF, DMSO) for 40 min. Platelet suspensions were diluted with Tyrode's buffer to 2 x 10^7 mL^{-1}, the pH was kept constant or increased to pH 7.4 and the platelets were allowed to spread on fibrinogen for 60 min (37 °C, 5 % CO_2) prior to fixation. Confocal fluorescence (*top*) and reflection (*bottom*) images of platelets treated at pH 6.5, pH 6.5 and increased to pH 7.4 and at pH 7.4. Images are representative of more than three experiemnts. Scale bar = 5 µm.

In order to assess the uptake, release and actin labelling of Lifeact delivered using pHLIP, Lifeact-FAM was also conjugated to the fluorescently labelled pHLIP analogue, 550-pHLIP. This conjugation enables visualisation of both pHLIP and Lifeact and their subsequent interactions with human platelets using fluorescence microscopy. Due to the importance of

the pH in dictating uptake, human platelets were incubated with 550-pHLIP-Lifeact in a variety of pH conditions.

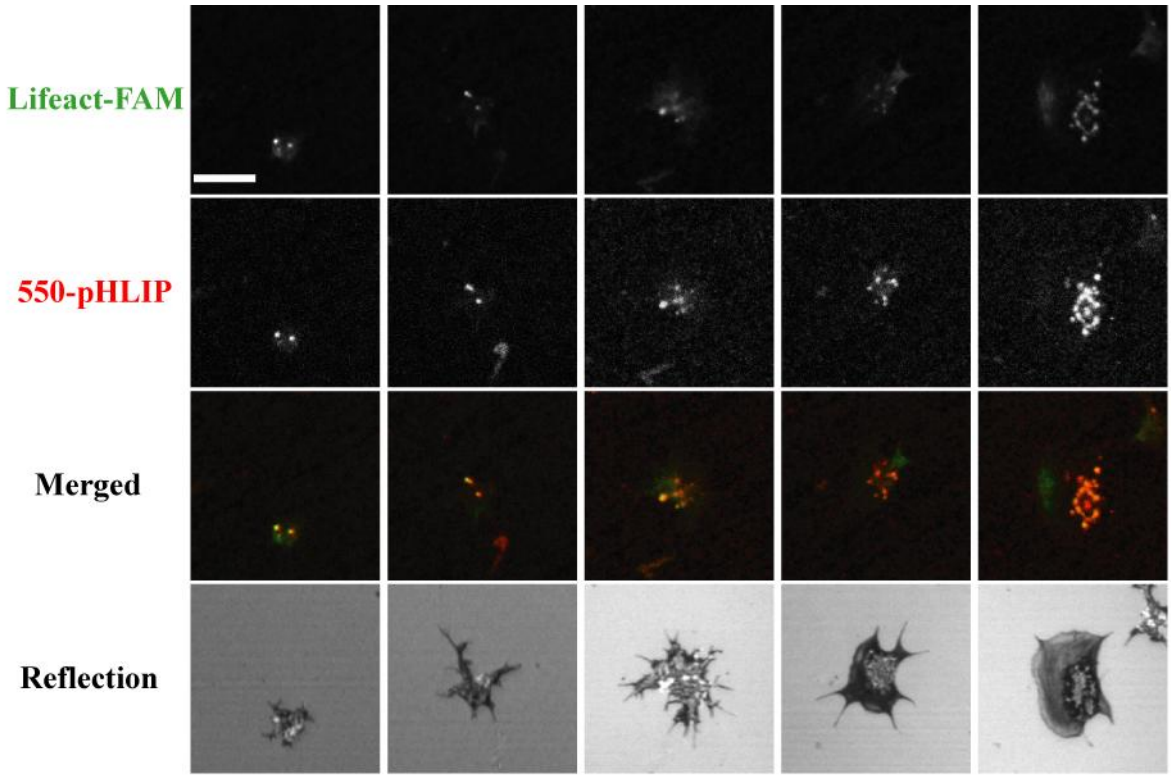

Figure 4.12. Confocal fluorescence and reflection microscopy of human platelets treated with 550-pHLIP-Lifeact at pH 7.4. Human platelets (2 x 10^8 mL^{-1}) were resuspended in Tyrode's buffer (pH 7.4) and treated with 550-pHLIP-Lifeact (6.6 µM, in 0.1 M borate buffer with >4 % DMF) for 40 min. Platelet suspensions were diluted with Tyrode's buffer (pH 7.4) to 2 x 10^7 mL^{-1} and the platelets were allowed to spread on fibrinogen for 60 min (37 °C, 5 % CO_2) prior to fixation. Confocal fluorescence and reflection images of treated platelets. Images are representative of three experiemnts. Scale bar = 5 µm.

Human platelets treated with 550-pHLIP-Lifeact at pH 7.4 exhibited fluorescence from both 550-Dylight and Lifeact-FAM (Figure 4.12). The fluorescent patterns of both labels were similar and showed only patterns of membrane labelling. As previously observed with 550-pHLIP only, labelling was concentrated in the central platelet region. The similar membrane labelling pattern suggests that pHLIP and Lifeact are still conjugated. It is expected that this is

due to pHLIP only being associated with the platelet membrane at neutral pH and as such that Lifeact has not been delivered to the cytoplasm.

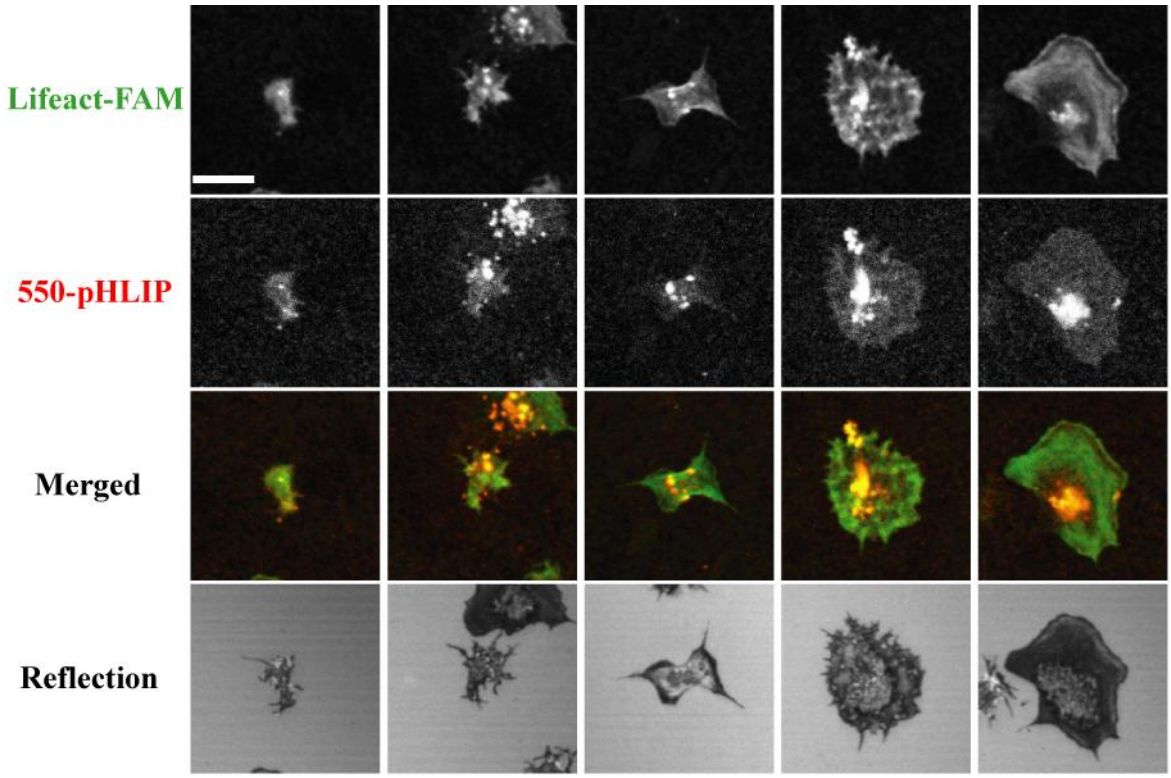

Figure 4.13. Confocal fluorescence and reflection microscopy of human platelets treated with 550-pHLIP-Lifeact at pH 6.5. Human platelets (2 x 10^8 mL^{-1}) were resuspended in Tyrode's buffer (pH 6.5) and treated with 550-pHLIP-Lifeact (6.6 µM, in 0.1 M borate buffer with >4 % DMF) for 40 min. Platelet suspensions were diluted with Tyrode's buffer (pH 6.5) to 2 x 10^7 mL^{-1} and the platelets were allowed to spread on fibrinogen for 60 min (37 °C, 5 % CO_2) prior to fixation. Confocal fluorescence and reflection images of treated platelets. Images are representative of three experiemnts. Scale bar = 5 µm.

Human platelets treated with 550-pHLIP-Lifeact at pH 6.5 exhibited fluorescence from both 550-Dylight and Lifeact-FAM (Figure 4.13). The fluorescent patterns of both labels were distinct, with 550-pHLIP exhibiting membrane labelling and the platelet actin cytoskeleton labelled with Lifeact-FAM. However, a similar pattern of labelling was seen for both fluorophores in the cell centre. This could be due to pHLIP-Lifeact remaining conjugated

within this region. The evident difference in surface labelling with pHlIP and actin labelling with Lifeact, is indicative that Lifeact-FAM has been translocated across the cell membrane by pHLIP and then the disulphide bond cleaved between the two peptides, enabling release of Lifeact into the cytoplasm.

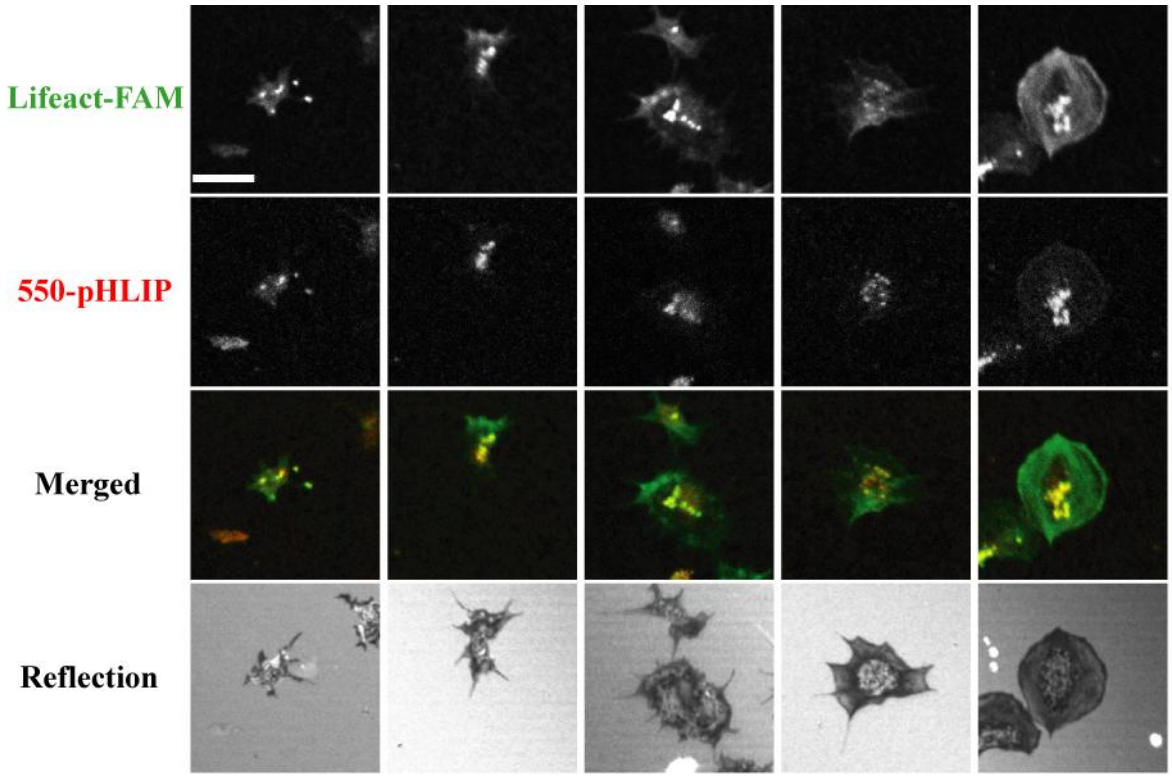

Figure 4.14. Confocal fluorescence and reflection microscopy of human platelets treated with 550-pHLIP-Lifeact at pH 6.5 and increased to pH 7.4. Human platelets (2×10^8 mL^{-1}) were resuspended in Tyrode's buffer (pH 6.5) and treated with 550-pHLIP-Lifeact (6.6 µM, in 0.1 M borate buffer with >4 % *v/v* DMF) for 40 min. Platelet suspensions were diluted with Tyrode's buffer to 2×10^7 mL^{-1}, the pH was increase to pH 7.4 and the platelets were allowed to spread on fibrinogen for 60 min (37 °C, 5 % CO_2) prior to fixation. Confocal fluorescence and reflection images of treated platelets. Images are representative of three experiemnts. Scale bar = 5 µm.

Human platelets were incubated with 550-pHLIP-Lifeact at pH 6.5 and then the pH increased to 7.4 (Figure 4.14). The treated platelets exhibited fluorescence from both 550-Dylight and Lifeact-FAM. Similar to labelling at pH 6.5, the fluorescent patterns of both labels were

distinct, with 550-pHLIP exhibiting membrane labelling and the platelet actin cytoskeleton labelled with Lifeact-FAM. However, membrane labelling with 550-pHLIP was reduced while Lifeact-FAM actin labelling appeared unaffected. Thus demonstrating that restoration of neutral pH is able to remove pHLIP from the platelet membrane. Additionally, if any Lifeact-FAM was still bound to pHLIP this would also be removed therefore reducing background fluorescence.

The central labelling was not reduced following the pH increase suggesting that pHLIP in this region may be protected from the pH change. Such protection could arise as a result of 550-pHLIP-Lifeact residing in vesicles.

Similarly to incubation with pHLIP only, there was no significant difference in the mean cell density of spread platelets, mean platelet area or in the distribution of platelets at various spreading stages for platelets in any pH conditions when compared with their respective solvent control samples (Figure 4.15 *A*-*C*). All platelets exhibited fluorescence from Lifeact-FAM at all pH conditions (Figure 4.15 *D*) but the location of that labelling differed (Figure 4.15 *E*). For all pH conditions, there was labelling of the central region of platelets, as was previously observed for 550-pHLIP only platelet incubation. There was a highly significant decrease in the percentage of platelets with actin labelling for platelets treated at pH 7.4 (6.3 ± 6.2) when compared with those treated at pH 6.5 (71.7 ± 4.4) or varied pH (68.0 ± 6.9). Conversely, the percentage of platelets exhibiting membrane labelling at pH 7.4 (75.7 ± 9.2) was highly significantly greater than at pH 6.5 (23.9 ± 3.2) or varied pH (26.1 ± 5.3). There was a highly significant decrease in the mean fluorescence intensity for platelets treated at pH 6.5 (71.3 ± 1.8) and those at varied pH (39.7 ± 1.6), although, both were highly significantly

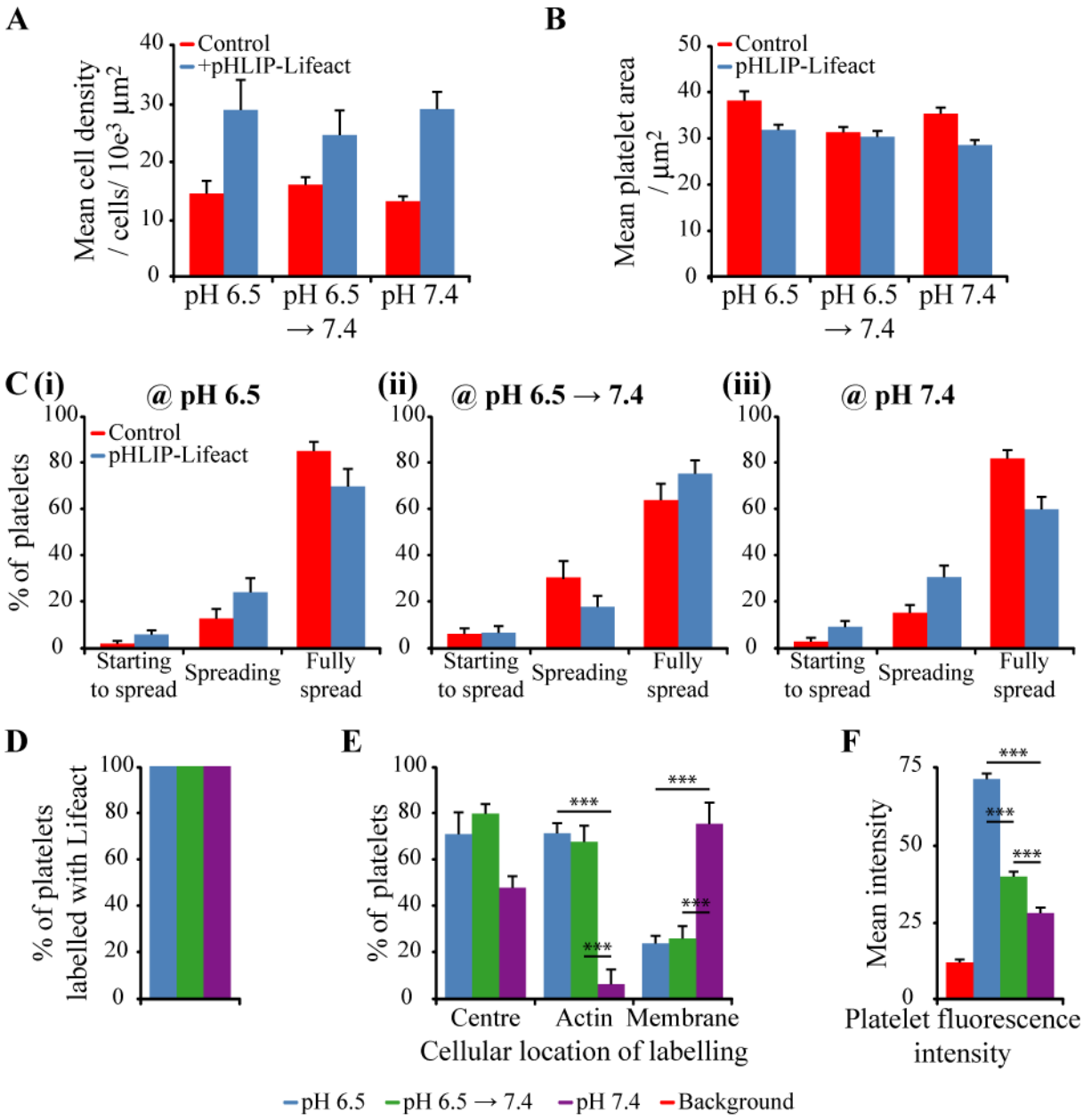

Figure 4.15. Effect of pHLIP-Lifeact on spreading of human platelets. Human platelets (2 x 10^8 mL^{-1}) were resuspended in Tyrode's buffer at pH 6.5 or pH 7.4, as indicated, and treated with solvent control (0.3 % v/v, 0.1 M sodium phosphate buffer with >4 % *v/v* DMF, DMSO) or pHLIP-Lifeact (6.6 µM, in 0.1 M sodium phosphate buffer with >4 % *v/v* DMF, DMSO) for 40 min. Platelet suspensions were diluted with Tyrode's buffer to 2 x 10^7 mL^{-1}, the pH was kept constant or increased to pH 7.4 and the platelets were allowed to spread on fibrinogen for 60 min (37 °C, 5 % CO_2) prior to fixation. (A) Mean cell density. (B) Mean platelet area. (C) Percentage of platelets at various stages of spreading; (i) at pH 6.5, (ii) at pH 6.5 and increased to pH 7.4 and (iii) at pH 7.4. (D) Percentage of platelets labelled with Lifeact. (E) Cellular localisation of Lifeact platelet labelling. (F) Mean platelet fluorescence intensity. A minimum of 30 platelets were analysed per experiment, the results are from more than 5 experiments. Values are shown as ± s.e.m. ***P <0.001.

greater than at pH 7.4 (27.7 ± 1.8) (Figure 4.15 *F*). Since there was no significant difference in the percentage of platelets with actin labelling, the decrease in fluorescence intensity must be as a result of removal of untranslocated pHLIP-Lifeact from the platelet membrane upon increasing the pH.

Similarly to results of platelets incubated with pHLIP only, incubation of human platelets with pHLIP-Lifeact at 6.6 μM does not appear to affect platelet spreading in any of the pH conditions. 70% of human platelets exhibit actin staining indicating uptake of Lifeact-FAM into the platelets when incubated at pH 6.5 is comparable with the 78 % of HeLa cells labelled with dansyl observed by Reshetnyak *et al* at pH 6.5 (Reshetnyak et al., 2006). Additionally, the difference between the percentage of platelets with actin or membrane labelling at the different pH conditions corresponds well with the model for pHLIP properties; at pH 7.4, pHLIP is loosely bound to the membrane so it is expected that less pHLIP would be associated with the membrane than at pH 6.5. The results demonstrate that uptake of Lifeact is pH dependent and, therefore, was delivered by pHLIP.

4.2.5 Effect of pHLIP/ pHLIP-Lifeact on human platelets

The effect of the different experimental pH conditions on platelet spreading was examined (Figure 4.16). There was no significant difference in the mean cell density of spread platelets, mean platelet area nor in the distribution of platelets at various spreading stages for platelets treated at pH 6.5 or pH 6.5 and increased to pH 7.4 compared with platelets treated at the normal pH of 7.4. Therefore, the pH conditions required for pHLIP to deliver cargo

molecules, pH 6.5 or pH 6.5 increased to pH 7.4 following treatment, do not appear to affect platelet spreading.

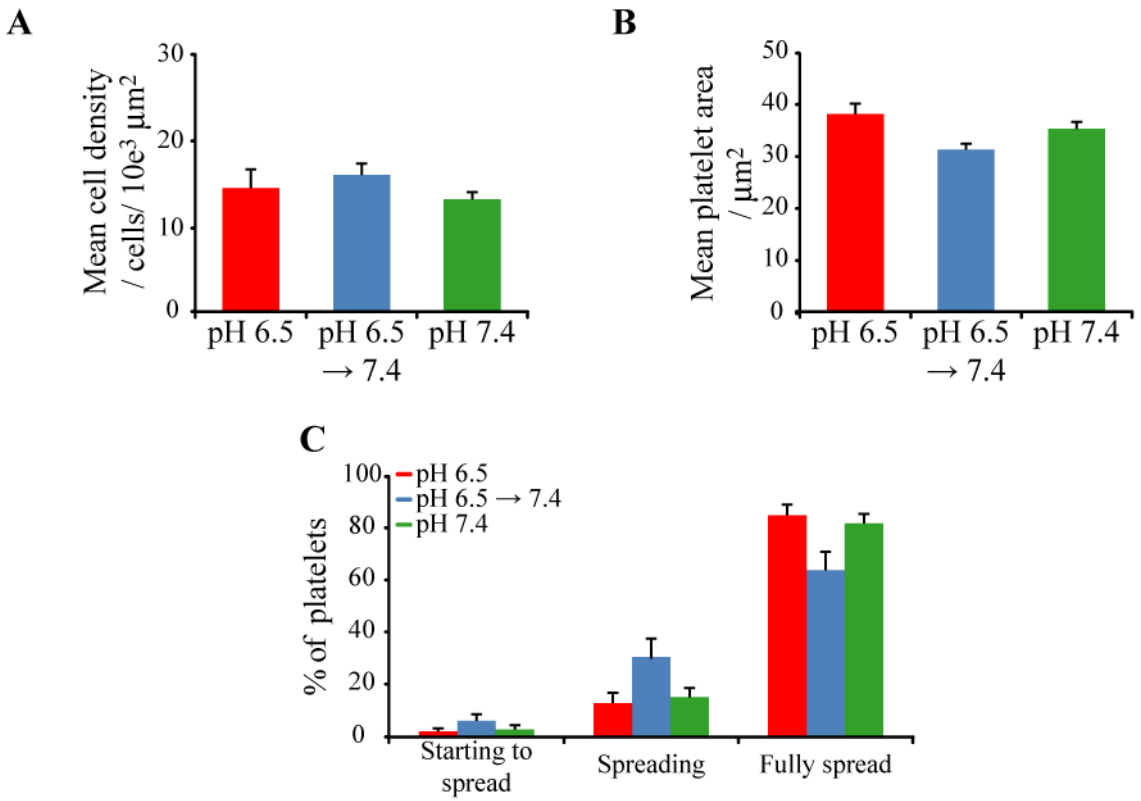

Figure 4.16. Effect of pH conditions on spreading of human platelets. Human platelets (2 x 10^8 mL^{-1}) were resuspended in Tyrode's buffer at pH 6.5 or pH 7.4, as indicated, for 40 min. Platelet suspensions were diluted with Tyrode's buffer to 2 x 10^7 mL^{-1}, the pH was kept constant or increased to pH 7.4 and the platelets were allowed to spread on fibrinogen for 60 min (37 °C, 5 % CO_2) prior to fixation. (A) Mean cell density. (B) Mean platelet area. (C) Percentage of platelets at various stages of spreading. A minimum of 30 platelets were analysed per experiment, the results are from more than 5 experiments. Values are shown ± s.e.m.

Overall, spreading of human platelets on fibrinogen was unaffected by the pH conditions used or incubation with pHLIP or pHLIP-Lifeact (Table 43.1). There was no significant difference in the mean cell density, the mean platelet area or the distribution of platelets at various

spreading stages. These results suggest that low pH mediated delivery of Lifeact into platelets using pHLIP may be a suitable alternative for phalloidin labelling in permeablised cells.

Table 4.1. Summary of platelet properties following treatment with solvent control, pHLIP and pHLIP-Lifeact under the different pH conditions; Human platelets (2 x 10^8 mL^{-1}) were resuspended in Tyrode's buffer at pH 6.5 or pH 7.4, as indicated, and treated with solvent control (0.3 % v/v, 0.1 M sodium phosphate buffer with >4 % *v/v* DMF, DMSO), pHLIP (6.6 µM, in 0.1 M sodium phosphate buffer with 75 % *v/v* DMSO) or pHLIP-Lifeact (6.6 µM, in 0.1 M sodium phosphate buffer with >4 % *v/v* DMF, DMSO) for 40 min. Platelet suspensions were diluted with Tyrode's buffer to 2 x 10^7 mL^{-1}, the pH was kept constant or increased to pH 7.4 and the platelets were allowed to spread on fibrinogen for 60 min (37 °C, 5 % CO_2) prior to fixation. Platelet properties for each treatment at; (a) pH 6.5, (b) pH 6.5 increased to 7.4 and (c) pH 7.4. A minimum of 30 platelets were analysed per experiment, the results are from more than three experiments. Values are shown ± s.e.m.

		Mean cell density / $10e^3$ µm^{-2}	Mean cell area / µm^2	% of platelets; Starting to spread	Spreading	Fully spread
Solvent control (Figure 4.16)	*a*	14.3 ± 2.2	38.0 ± 2.0	1.9 ± 1.2	12.8 ± 4.0	85.3 ± 4.1
	b	15.8 ± 1.3	31.1 ± 1.2	6.1 ± 2.4	30.6 ± 7.8	64.1 ± 7.1
	c	13.0 ± 0.8	35.1 ± 1.4	2.7 ± 1.7	15.2 ± 3.5	82.1 ± 3.7
pHLIP only (Figure 4.6)	*a*	17.0 ± 1.1	32.3 ± 1.2	3.4 ± 1.0	32.7 ± 5.1	65.3 ± 5.3
	b	13.3 ± 0.9	30.6 ± 1.4	4.8 ± 1.8	35.8 ± 5.6	59.5 ± 5.8
	c	18.8 ± 1.0	33.3 ± 1.2	3.5 ± 1.2	22.4 ± 4.2	74.1 ± 4.0
pHLIP-Lifeact (Figure 4.15)	*a*	28.8 ± 5.2	31.7 ± 1.1	5.8 ± 1.8	24.2 ± 6.1	70.0 ± 7.6
	b	24.5 ± 4.4	30.1 ± 1.3	7.1 ± 2.9	17.8 ± 4.7	75.1 ± 5.6
	c	28.9 ± 3.0	28.4 ± 1.1	9.1 ± 2.6	30.8 ± 4.9	60.1 ± 5.4

It is particularly important for live-cell imaging to remove any excess fluorophore in solution in order to reduce background noise and improve cell clarity. In order to remove excess or untranslocated pHLIP-Lifeact from the platelet suspension, the platelets were centrifuged following treatment (Figure 4.17). Prior to spreading, the platelet count was determined for platelets before and after washing for platelets treated at a variety of pHLIP concentrations

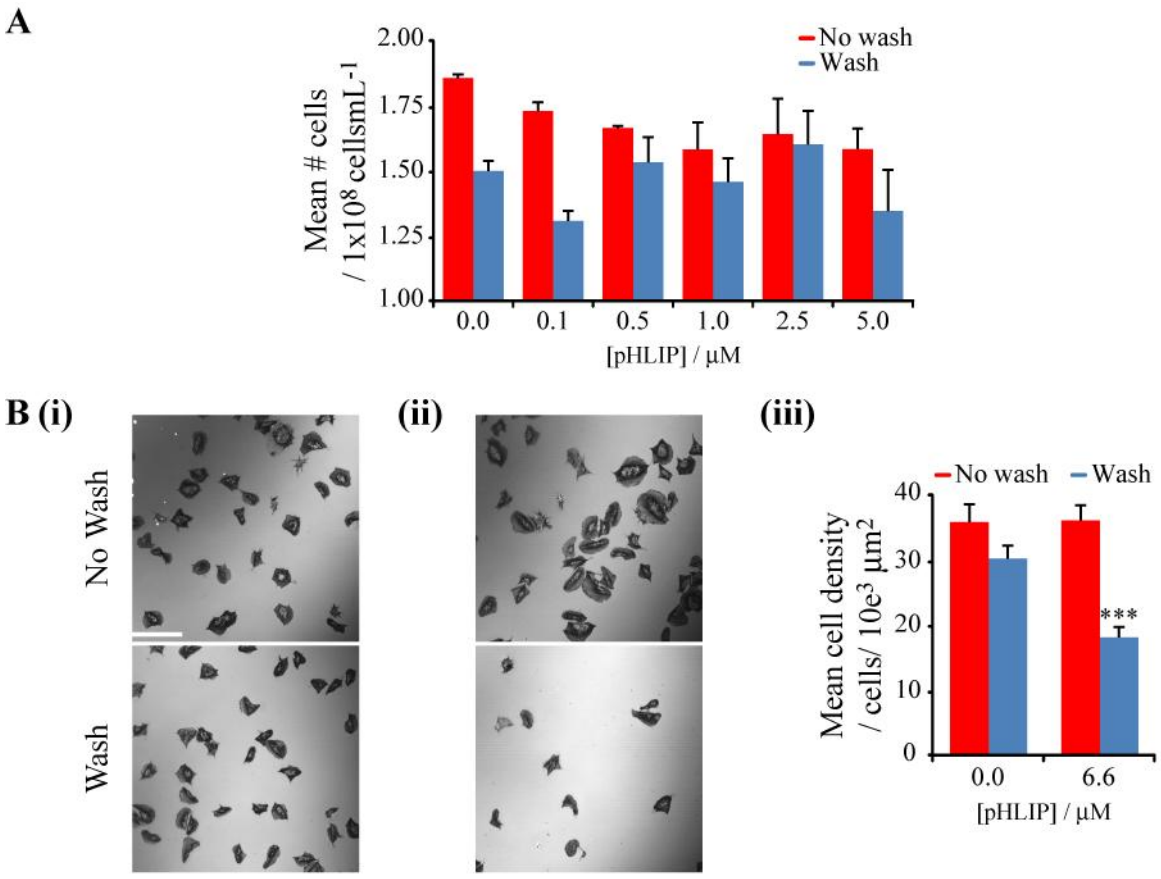

Figure 4.17. Effect of washing following pHLIP treatment. Human platelets (2 x 10^8 mL^{-1}) were resuspended in Tyrode's buffer (pH 6.5) and treated with with various concentrations of pHLIP (in 0.1 M sodium phosphate buffer with 75 % *v/v* DMSO) at pH 6.5 for 10 min. The platelets were washed via centrifugation and resuspended in Tyrode's buffer (pH7.4) to remove untranslocated pHLIP. (A) Following treatment the number of cells in the platelet suspension was measured. The results are from three experiments. (B) Platelet suspensions were diluted with Tyrode's buffer to 2 x 10^7 mL^{-1} and the platelets were then allowed to spread on fibrinogen for 60 min (37 °C, 5 % CO_2) prior to fixation. Confocal reflection images for platelets treated with; (i) 0.0 µM and (ii) 6.6 µM pHLIP. Images are representative of three experiemnts. Scale bar = 20 µm. (iii) Mean cell density. A minimum of 30 platelets were analysed per experiment, the results are from three experiments. Values are shown ± s.e.m.

(Figure 4.17 *A*). There was no significant difference in platelet count between the unwashed/ washed samples for each pHLIP concentration. However, once spread, fixed and imaged, there appeared to be a reduction in the number of spread cells for pHLIP treated and washed platelets (Figure 4.17 *B*). It was found that there was a highly significant decrease in the cell density for pHLIP-treated and washed platelets (18.1 ± 1.7) when compared with washed

control platelets (30.3 ± 2.1). However, there was no significant difference between the unwashed (35.9 ± 2.8) and the washed (30.3 ± 2.1) control platelets.

4.2.6 Live cell imaging of human platelets treated with pHLIP-Lifeact

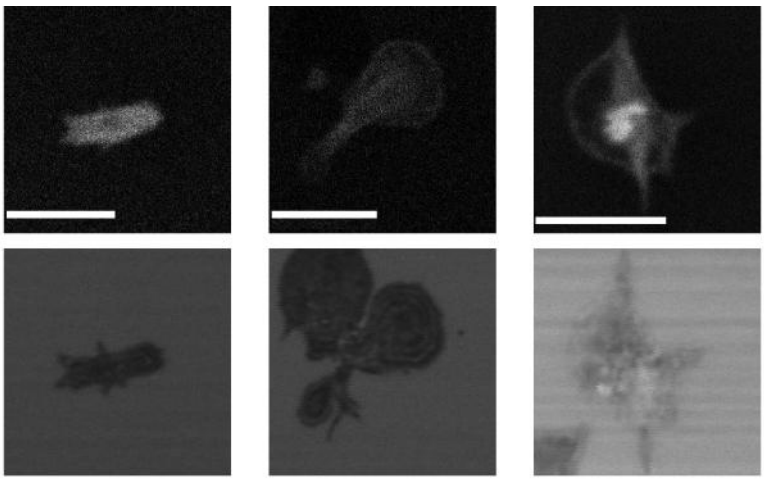

Figure 4.18. Live cell confocal fluorescence and reflection microscopy of human platelets treated with pHLIP-Lifeact. Human platelets (2 x 10^8 mL^{-1}) were resuspended in Tyrode's buffer at pH 6.5 and with pHLIP-Lifeact (8.8 µM, in 0.1 M sodium phosphate buffer with >4 % DMF, DMSO)for 40 min. Platelet suspensions were diluted with Tyrode's buffer to 2 x 10^7 mL^{-1} and the pH increased to pH 7.4. Platelets were allowed to spread on fibrinogen (37 °C) and monitored using real-time confocal fluorescence and reflection microscopy with an image acquired every 2 s. Images are representative of two experiments and show labelling of individual platelets. Scale bar = 5 µm.

Attempts at live cell, real-time confocal fluorescence and reflection microscopy of human platelets treated with pHLIP-Lifeact were unsuccessful (Figure 4.18). Although, some labelled platelets were observed, they were not observed during the spreading process so no real time information can be drawn from them. This was mostly due to restraints of the imaging system which include: Laser scanning is slow, so a smaller area needs to be imaged therefore reducing the probability of imaging a spreading platelet. The computer memory was

not sufficient to enable longer time imaging of the platelets which would have increased the probability of imaging platelets spreading in the field of view.

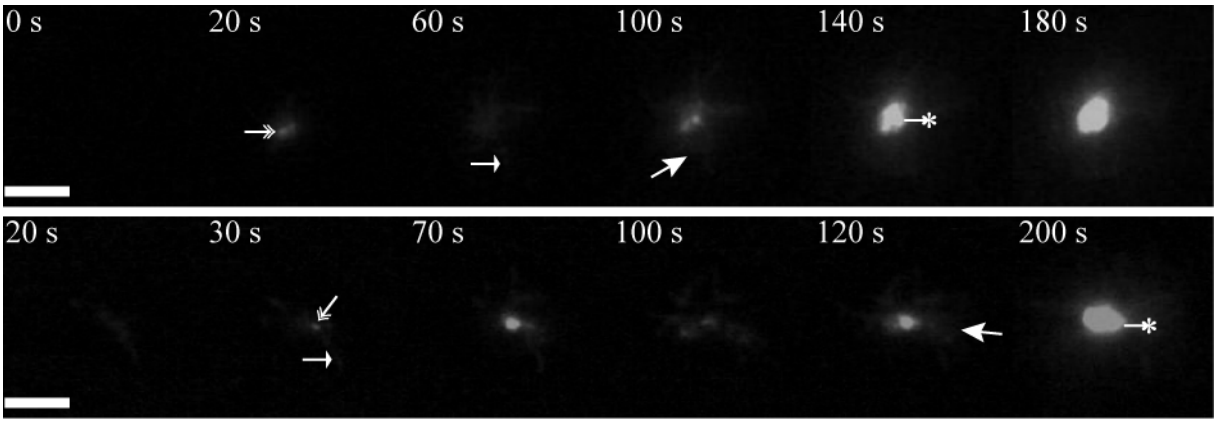

Figure 4.19. Live cell TIRF microscopy of human platelets treated with pHLIP-Lifeact. Human platelets (2 x 10^8 mL^{-1}) were resuspended in Tyrode's buffer at pH 6.5 and with pHLIP-Lifeact (8.8 µM, in 0.1 M sodium phosphate buffer with >4 % DMF, DMSO)for 40 min. Platelet suspensions were diluted with Tyrode's buffer to 2 x 10^7 mL^{-1} and the pH increased to pH 7.4. Platelets were allowed to spread on fibrinogen (37 °C) and monitored using real-time TIRF microscopy with an image acquired every 10 s. Time course of two platelets spreading (*top and bottom*). ↠ indicates nodules, → indicates filopodia, ➔ indicates lamellipodia and →* indicates the strong, non-actin, central labelling. Background subtraction was performed in order to show the platelet clearly. Images are representative of two experiments. Scale bar = 5 µm.

Although, successful labelling and imaging of human platelets was observed using TIRF there were a few issues: Limited numbers of platelets spread in the imaging field of view, possibly due to local heating effects caused by the laser illumination. There is high background fluorescence resulting from excess pHLIP-Lifeact in the cell solution which affects the image clarity. Additionally, the bright labelling of the central region of the platelet greatly affects the ability to image these cells using TIRF. The first two issues could be resolved by increasing the number of platelets added to the imaging chamber and by washing the treated platelets via

centrifugation. However, as previously noted (Figure 4.17), centrifugation of pHLIP treated platelets resulted in dramatic loss of platelet numbers.

4.3 CONCLUSIONS

This work has demonstrated that the fluorescently labelled Lifeact peptide is a suitable actin label for human platelets. Furthermore, it has been shown that the addition of a cysteine residue to the *N*-terminus of Lifeact enables conjugation of Lifeact to pHLIP via a disulphide bond. This then enables rapid cellular uptake and release of Lifeact into human platelets, a cell which has proven difficult to deliver non-permeant molecules into while the cell is unfixed. Consequently, this enables imaging of the actin cytoskeleton in non-permeablised cells.

Incubation of human platelets with 550-pHLIP-Lifeact in various pH conditions demonstrates several important aspects about the pHLIP-Lifeact method (Figure 4.20). Firstly, at all pH conditions some pHLIP is associated with the platelet membrane. Secondly, when the pH is lowered, the membrane labelling is increased, tallying with the increased membrane affinity of pHLIP in low pH conditions. Thirdly, only in low pH conditions is actin labelling discernible, inferring both the successful translocation of Lifeact across the lipid membrane and its cleavage from pHLIP once in the cytoplasm. Finally, increasing the pH back to neutral allows for removal of excess or untranslocated pHLIP-Lifeact from the platelet membrane.

Incubation of human platelets with pHLIP or pHLIP-Lifeact did not appear to affect platelet spreading on fibrinogen for the most part. However, the presence of pHLIP does appear to affect the numbers of platelets able to spread following incubation with pHLIP and centrifugation.

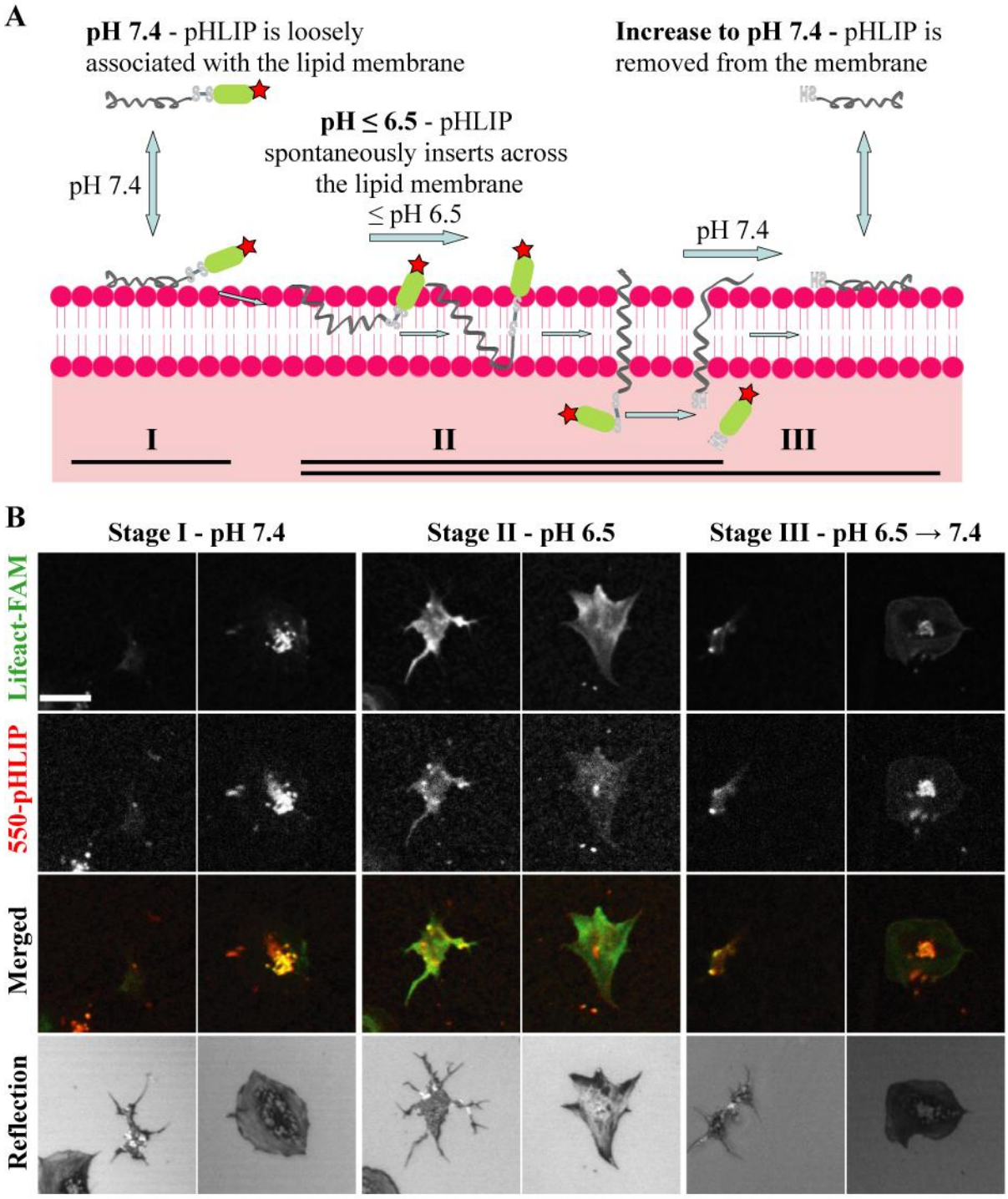

Figure 4.20. pH-dependent cellular uptake of Lifeact-FAM into human platelets. (A) Schematic representation of pH dependent Lifeact-FAM uptake. (B) Representative confocal fluorescence and reflection microscopy images of human platelets treated with 550-pHLIP-Lifeact (6.6 μM) at various pH's for 40 minutes prior to spreading on fibrinogen and fixation. Stages I-III are representative of pH conditions for corresponding insertion stages in (A). Scale bar = 5 μm.

Most importantly, the delivery of Lifeact into platelets using pHLIP has permitted real-time, live-cell microscopy of actin dynamics in human platelets. This represents a significant step forward in the ability to image actin dynamics in human platelets and can provide a stepping stone to further the research of human platelet actin dynamics. Additionally, this method allows for delivery of other fluorescent labels to image the dynamics of other intracellular platelet proteins.

CHAPTER 5

DELIVERY OF LUMINESCENT EUROPIUM COATED GOLD NANOPARTICLES INTO HUMAN PLATELETS USING pH (LOW) INSERTION PEPTIDE

A publication arose from the work presented in this chapter;

Davies, A., Lewis, D. J., Watson, S. P., Thomas, S. G. & Pikramenou, Z. 2012. pH-controlled delivery of luminescent europium coated nanoparticles into platelets. *Proceedings of the National Academy of Sciences,* 109**,** 1862-1867.

5.1 INTRODUCTION

Gold nanoparticles are attractive for use in biological and biomedical applications due to their optical properties and low cellular toxicity (Ghosh et al., 2010). Their tuneable size and high electron density make them attractive for single particle detection, thereby providing greater spatial resolution. Additionally they provide a scaffold upon which multiple moieties may be attached in order to further tailor the nanoparticle properties for specific purposes. The cellular uptake of a great variety of nanoparticles has been investigated, including quantum dots (Popovic et al., 2010, Liu et al., 2008, Smith et al., 2008, Derfus et al., 2004, Gao et al., 2004, Akerman et al., 2002) and cell-penetrating peptide coated nanoparticles (Saha et al., 2011, Nativo et al., 2008). However, many of these rely on endocytic mechanisms of cellular uptake or cell permeablisation through use of surfactants, none of which are suitable for use with platelets.

Methods that allow delivery of optical probes to nonpermeabilized cells, with no loss of

cellular function, will facilitate the application of dynamic live cell imaging which is essential for continual advancement in understanding the molecular mechanisms governing cell activation and cell function. These molecular mechanisms are of particular importance in platelets as they play a critical role in thrombosis and haemostasis. Platelets express a range of surface receptors and signalling peptides, as such, are very sensitive to external stimuli. This sensitivity allows for fulfilment of platelet function via fast platelet activation, aggregation and clot formation following vessel wall damage, thereby restraining blood loss (Nieswandt and Watson, 2003). While an advantage for platelet function, this sensitivity is a disadvantage for *ex vivo* platelet imaging studies which require delivery of optical labels, preventing delivery via permeablisation or microinjection. Furthermore, the anucleate state of platelets prohibits transfection. As a result, live cell studies are limited to transgenic mouse models expressing GFP-fusion proteins (Riedl et al., 2010, Okabe et al., 1997, Schachtner et al., 2012). Such models are time consuming to produce (Lin, 2008) and are not always suitable substitutes for human cells.

To facilitate cellular uptake of nanoparticle labels to enable live cell imaging of platelets, this work introduces the addition of pH (low) insertion peptide, pHLIP, to luminescent gold nanoparticles. pHLIP, a 38 amino acid peptide, has been shown to insert itself, *C*-terminus first, across the plasma membrane upon a reduction in pH from neutral to pH <6.5, thereby translocating any cargo molecule attached to the *C*-terminus across the cell membrane (Reshetnyak et al., 2006). pHLIP has been shown to deliver a variety of cell impermeable compounds including phalloidin and fluorescent molecules, such as Cy5 (An et al., 2010, Reshetnyak et al., 2011). Its ability to deliver fluorescently labelled Lifeact peptide in to human platelets was also demonstrated in **Chapter 4**. Furthermore, attachment of pHLIP to 5

nm gold nanoparticles via the peptide's *N*-terminus to enable detection of tumour cells has been previously investigated (Yao, 2008, Yao et al., 2012). The insertion of pHLIP occurs when the aspartic acid residues are protonated upon a reduction in pH, resulting in the peptide, which is loosely associated with the lipid membrane, undergoing a conformational change enabling it to insert itself across the lipid membrane (Reshetnyak et al., 2008).

In order to optically detect the pHLIP-coated AuNP, the nanoparticles will also be coated with a luminescent lanthanide label since the lanthanide's unique properties are fitting for biological imaging. Such properties include distinctive emission profiles in visible and near infrared spectral regions, large stokes shifts and long luminescence lifetimes (Bunzli, 2010, Montgomery et al., 2009, Moore et al., 2009). The Pikramenou group has previously demonstrated functionalisation of gold nanoparticles with a europium containing lanthanide complex (Lewis et al., 2006) and investigated their effect on cells (Lewis et al., 2010).

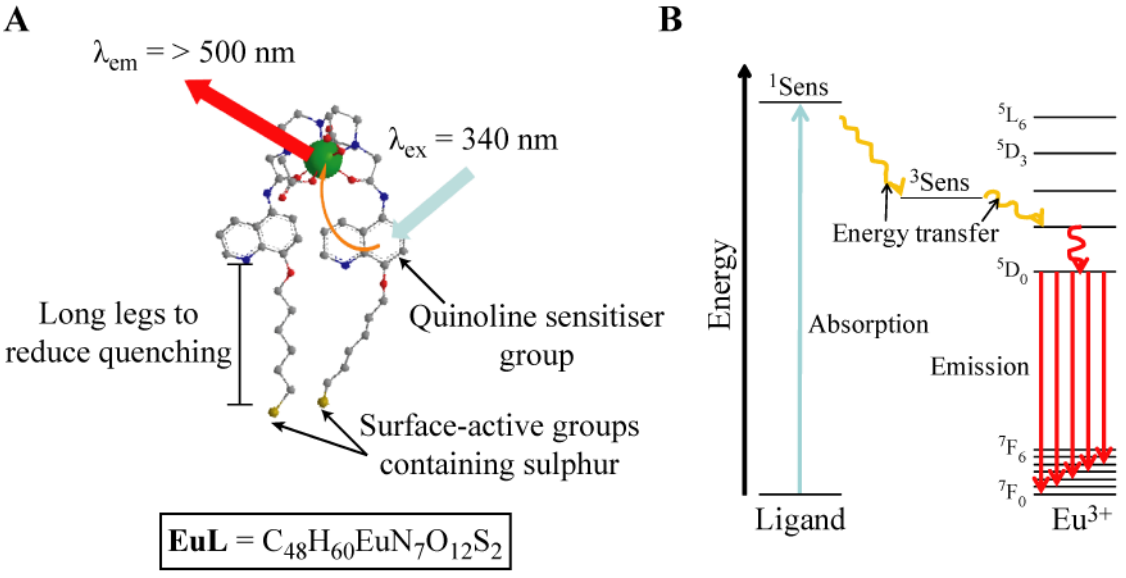

Figure 5.1. Luminescent europium complex. (A) Structure of EuL where ● represents the Eu^{3+} ion. Excitation of Eu^{3+} occurs through the energy transfer between the quinoline sensitiser group and the Eu^{3+} ion. (B) Energy level for sensitised europium luminescence.

Although successful coating was achieved, quenching of the luminescence by the gold resonance was observed (Lewis et al., 2006). To avoid this quenching of the europium luminescence, a complex was designed based on a DTPA-bisamide ligand with a quinoline sensitiser group and surface-active (sulphur containing) groups with 'long legs' (Figure 5.1) (Davies et al., 2012). The advantages of using such a europium complex, EuL, are the neutrality of the complex, its stability (Paulroth and Raymond, 1995), and, unlike the free Eu^{3+} ion, it does not interact with peptide moieties on the nanoparticle surface (Savage and Pikramenou, 2011).

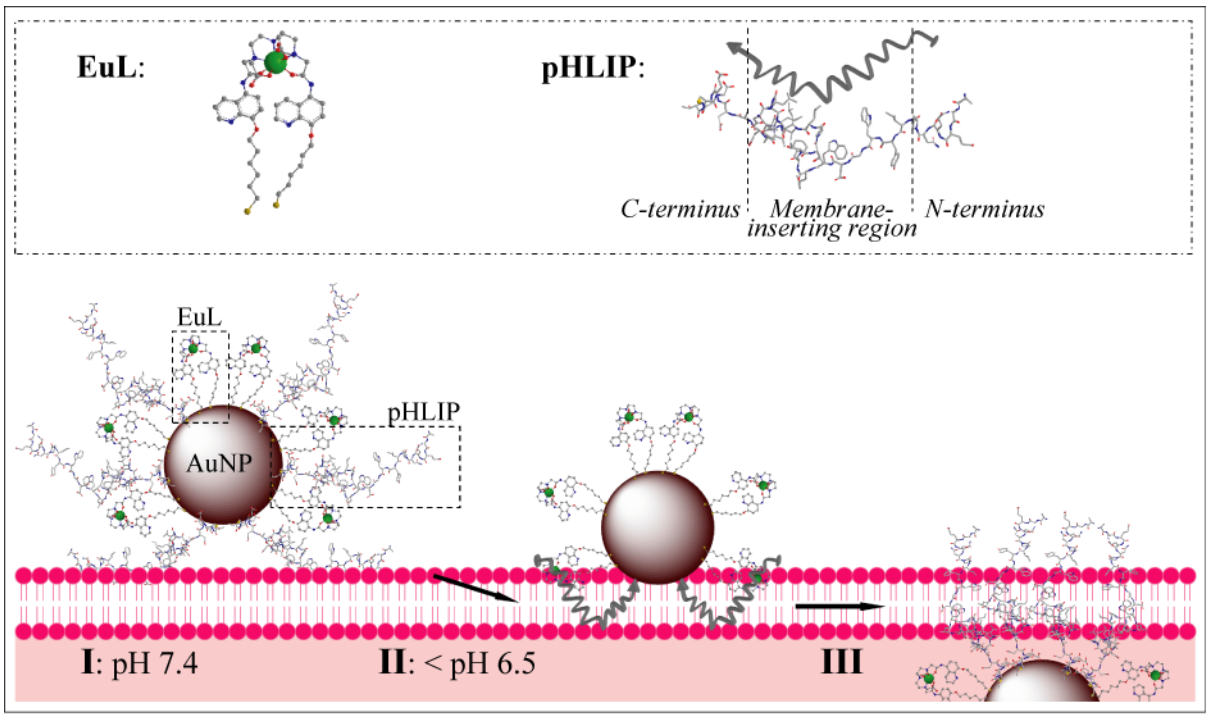

Figure 5.2. Schematic representation of the pH-dependent, pHLIP-mediated translocation of pHLIP•EuL•AuNP into platelets. Stage I: At neutral pH (pH 7.4), pHLIP is loosely associated with the lipid membrane. Stage II: Upon a decrease in pH to < pH 6.5, pHLIP spontaneously folds itself into the lipid membrane. For clarity, only pHLIP molecules (represented as a coiled line) which are interacting with lipid membrane at this point are shown. Stage III: This results in translocation of the luminescent nanoparticles across the lipid membrane into the cell.

The work in this chapter presents a method which enables controlled and rapid cytosolic delivery of luminescent nanoparticles into human platelets. The gold nanoparticles are coated with both a delivery peptide, pHLIP, and a luminescent lanthanide complex, EuL to achieve pH-dependent delivery of pHLIP•EuL•AuNP (Figure 5.2). The attachment of pHLIP to AuNP via its *C*-terminus results in the translocation of pHLIP across the lipid membrane and into the cytoplasm. It demonstrates, that luminescent gold nanoparticles are delivered into the cytoplasm of human platelets using a variety of microscopy techniques and this uptake is due to the low pH induced, conformational change of pHLIP from stage I to III. These results were further verified via comparisons with pHLIP-coated AuNP, pHLIP•AuNP, and EuL-coated AuNP, EuL•AuNP.

5.2 RESULTS & DISCUSSION

5.2.1 Preparation and characterisation of gold nanoparticle samples

Citrate-stabilised gold nanoparticles

Citrate-stabilised gold nanoparticles were synthesised according to Grabar *et al* (Grabar et al., 1995). UV-Vis absorbance spectroscopy was used to determine the characteristic absorbance maximum of the surface plasmon resonance (SPR) band at 518 nm (Figure 5.3 *A*). Transmission electron microscopy (TEM) of the citrate-stabilised AuNP showed mono-dispersed, spherical particles of 13 – 15 nm (Figure 5.3 *B*). Citrate AuNP were found to have a zeta (ζ-) potential of -38 (±5) mV as a result of the negatively charged citrate molecules (Table 5.1).

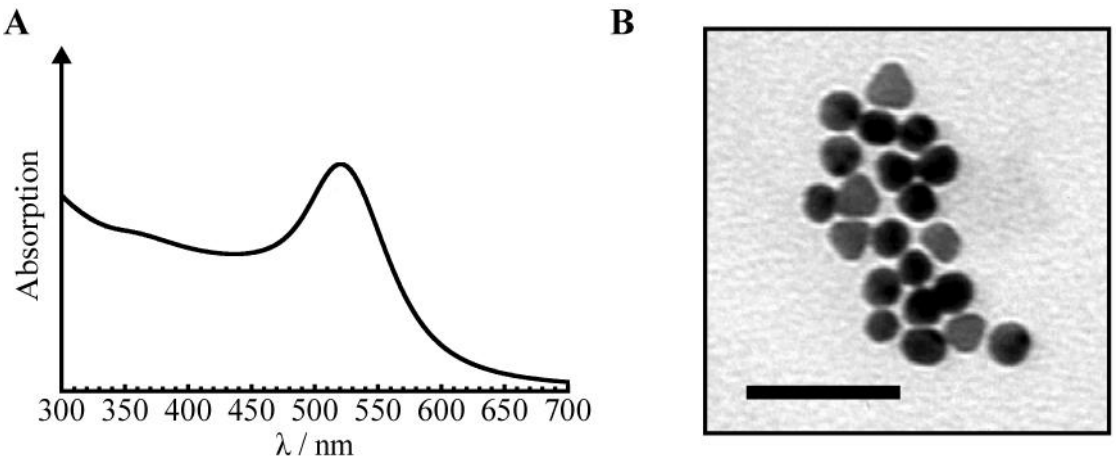

Figure 5.3. Characterisation of citrate-stabilised gold nanoparticles. (A) UV-Vis absorption spectrum of the SPR band of AuNP (9.4 nM in water). (B) Representative TEM image of citrate AuNP. Scale bar = 50 nm.

Europium-coated gold nanoparticles, EuL•AuNP.

A solution of a red luminescent probe, designed for attachment to nanoparticle surfaces

(Davies et al., 2012), EuL (10 mM, in methanol) was titrated into the aqueous suspension of citrate-stabilised AuNP (9.4 nM, in water). This led to an 8 nm red shift in the nanoparticle SPR band confirming the binding of EuL to AuNP via the dithiol anchor points (Figure 5.4 *A*). This shift in the SPR band was concentration-dependent and the levelling off of the SPR peak increase is indicative of fully coating AuNP with EuL. The EuL-coated AuNP, EuL•AuNP, were purified by size-exclusion chromatography to remove any excess, unbound EuL. Following chromatography, the λ_{max} of the SPR band did not shift confirming the unchanged nature of the nanoparticle coating. A solution of EuL•AuNP exhibited the characteristic *f-f* europium luminescence spectrum upon excitation of the quinoline absorption band at 340 nm (Figure 5.4 *B*). An excitation spectrum of EuL•AuNP, monitored at the strongest emission band at 614 nm, demonstrated that energy transfer from the quinoline chromophore to the lanthanide centre is responsible for the population of the Eu^{3+} luminescent state ($^5D_0$). The luminescence lifetime of 287 μs was observed for europium in EuL•AuNP.

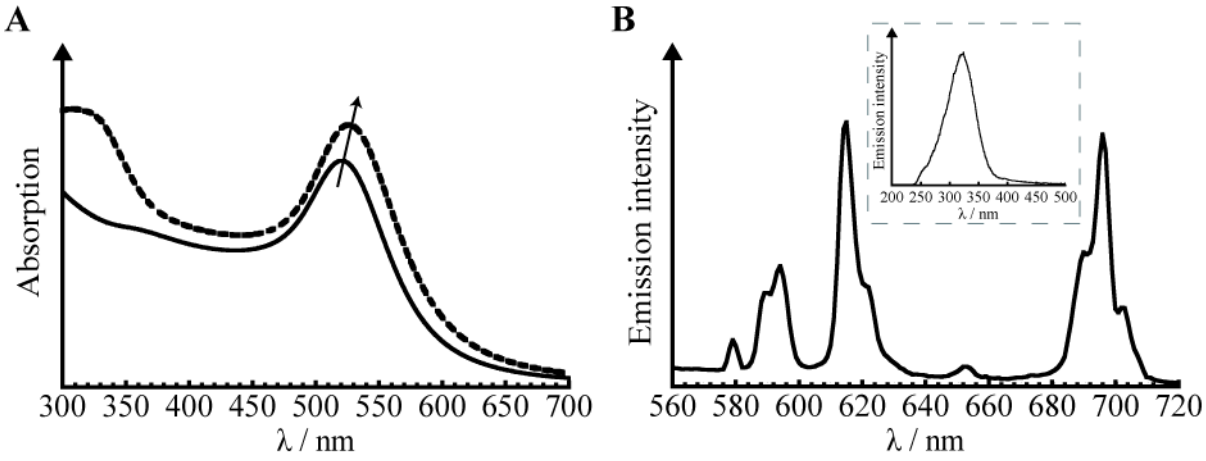

Figure 5.4. Characterisation of EuL coated gold nanoparticles. (A) UV-Vis absorption spectra monitoring the SPR band of AuNP (—; 2.5 mL, 9.4 nM in water), upon addition of EuL (---; 30 μL, 10 mM in methanol). The arrow represents the trend in the shift of the SPR peak during coating. (B) Luminescence emission spectrum of EuL•AuNP (1.2 nM in water). λ_{ex} = 340 nm. *Insert*: Corresponding excitation spectrum of EuL•AuNP. λ_{em} = 614 nm.

Inductively coupled plasma optical emission spectrometry, ICP-OES, was used to determine gold to europium ratio of 80 Au: 1 Eu for EuL•AuNP. Previous work in the Pikramenou group estimates the number of gold atoms per 13 nm AuNP as 106,800 (Lewis et al., 2006). Since there are 80 times fewer Eu present as Au then there are 80 times fewer Eu than Au present per AuNP than there are Au per AuNP. As such, the number of EuL complexes per AuNP is approximated to be 1,335 (Table 5.1). Furthermore, EuL•AuNP were found to have a ζ-potential of -14 (±2) mV indicative of replacement of negatively charge citrates with the neutral EuL molecules.

pHLIP-coated gold nanoparticles, pHLIP•AuNP

A solution of pHLIP (10 mM in 0.1 M sodium phosphate buffer with 75% DMSO) was titrated into an aqueous suspension of citrate-stabilised AuNP (9.4 nM, in water) (Figure 5.5). The red shift in the SPR band confirms the binding of pHLIP to AuNP. The titration was continued until a maximum shift of 5 nm in the AuNP SPR band was observed. This maximum shift is indicative of fully coating of AuNP with pHLIP. The interaction of pHLIP with AuNP is expected to take place via the disulfide linkage of the peptide in the C-terminus area. This is envisaged to be the strongest affinity site for gold (Levy et al., 2004, Nativo et al., 2008, Lewis et al., 2006) and any electrostatic interaction is excluded due to the negative charge on both nanoparticles and peptide (Guo and Gai, 2010).

The pHLIP-coated AuNP, pHLIP•AuNP, were purified by size-exclusion chromatography to remove any excess, unbound pHLIP. Following chromatography, the λ_{max} of the SPR band

did not shift confirming the unchanged nature of the nanoparticle coating. Additionally, pHLIP•AuNP were found to have a ζ-potential of -21 (±1) mV consistent with replacement of the negatively charged citrate molecules with pHLIP (Table 5.1).

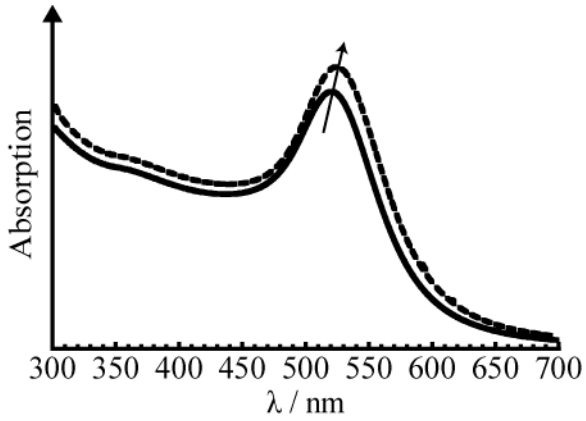

Figure 5.5. Characterisation of pHLIP coated gold nanoparticles. UV-Vis absorption spectra monitoring the SPR band of AuNP (—; 2.5 mL, 9.4 nM in water), upon addition of pHLIP (---; 20 μL, 10 mM in 0.1 M sodium phosphate buffer with 75% DMSO). The arrow represents the trend in the shift of the SPR peak during coating.

pHLIP- and EuL-coated gold nanoparticles, pHLIP•EuL•AuNP

A solution of pHLIP (10 mM in 0.1 M sodium phosphate buffer with 75% DMSO) was titrated into an aqueous suspension of citrate-stabilised AuNP (9.4 nM, in water) (Figure 5.6 *A*). The titration was continued until a maximum shift of 5 nm in the AuNP SPR band was observed, similar to that recorded for pHLIP•AuNP (Figure 5.5). This maximum shift is indicative of fully coating of AuNP with pHLIP. The red shift in the SPR band confirms the binding of pHLIP to AuNP. Subsequently, a solution of EuL (10 mM, in methanol) was titrated in to the pHLIP-coated AuNP suspension which led to a further 4 nm shift in the SPR band confirming the binding of EuL to AuNP (Figure 5.6 *A*). The pHLIP and EuL-coated AuNP, pHLIP•EuL•AuNP, were purified by size-exclusion chromatography to remove any

excess, unbound pHLIP and EuL. Following chromatography, the λmax of the SPR band did not shift confirming the unchanged nature of the nanoparticle coating.

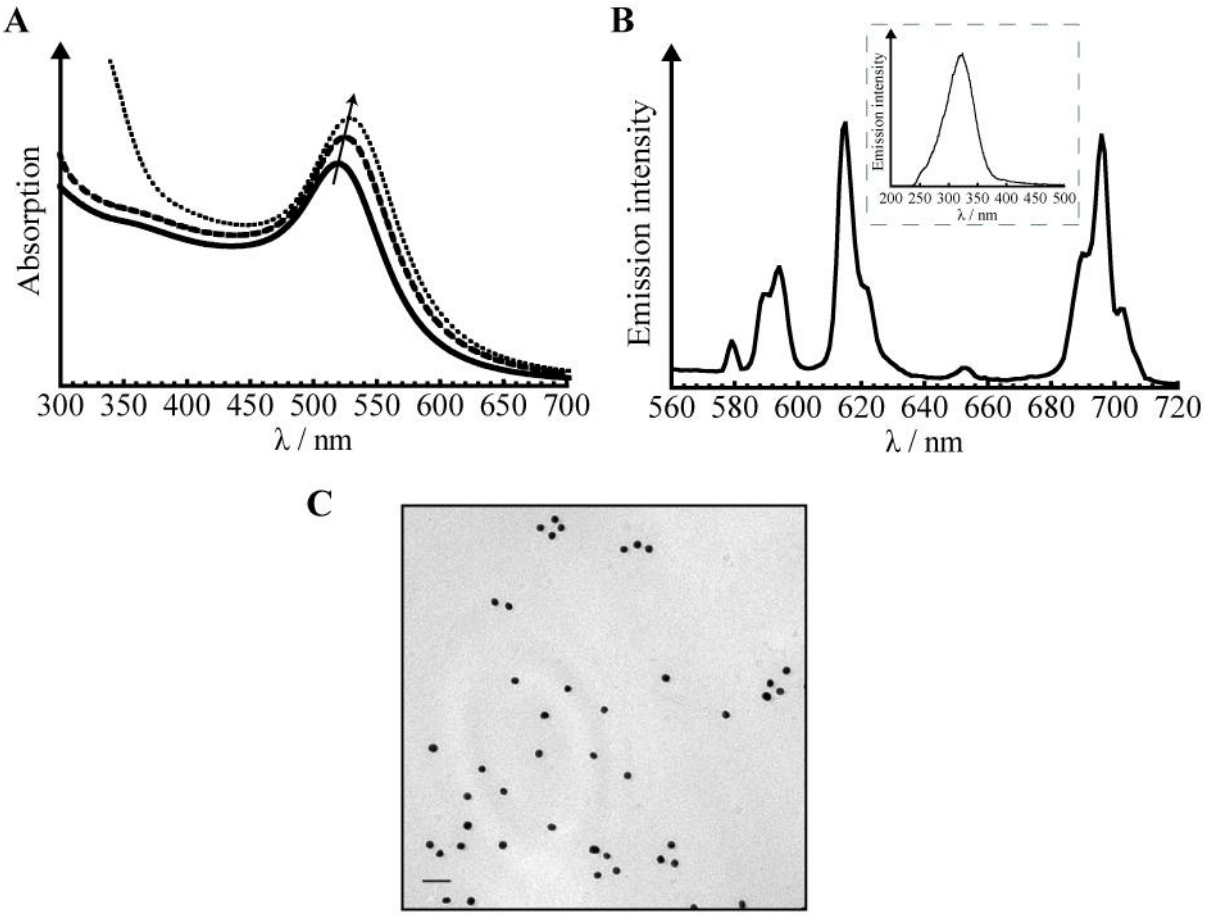

Figure 5.6. Characterisation of pHLIP and EuL coated gold nanoparticles. (A) UV-Vis absorption spectra monitoring the SPR band of AuNP (—; 2.5 mL, 9.4 nM in water), upon addition of pHLIP (---; 20 μL, 10 mM in 0.1 M sodium phosphate buffer with 75% DMSO) and EuL (•••; 84 μL, 10 mM in methanol). The arrow represents the trend in the shift of the SPR peak during coating. (B) Luminescence emission spectrum of pHLIP•EuL•AuNP (1.2 nM in water). λ_{ex} = 340 nm. *Insert*: Corresponding excitation spectrum of pHLIP•EuL•AuNP. λ_{em} = 614 nm. (C) Representative TEM image of EuL•AuNP. Scale bar = 50 nm.

Similarly to EuL•AuNP, an emission spectrum was acquired for pHLIP•EuL•AuNP which also exhibited the characteristic *f-f* europium luminescence when excited at 340 nm (Figure 5.6 *B*). The luminescence lifetime was calculated to be 290 μs, in accord with 287 μs

observed for EuL•AuNP. TEM images showed revealed spherical, mono-disperse nanoparticles with a diameter of 13 - 15 nm (Figure 5.6 *C*).

Furthermore, ICP-OES was used to determine the gold to europium ratio in pHLIP•EuL•AuNP, as previously described for EuL•AuNP. The ratio was found to be approximately 167 Au: 1 Eu which equates to an estimated 640 EuL complexes per AuNP (Table 5.1). The decrease in ζ-potential from -37 mV for citrate AuNP to -29 (±1) mV for pHLIP•EuL•AuNP is indicative of replacement of the negatively charged citrate molecules with pHLIP and EuL.

Table 5.1 summarises the main properties of the citrate AuNP and various coated AuNP. The shift in the SPR band upon addition of either pHLIP or EuL is indicative of their binding to the nanoparticle surface. The values in the table are the maximum shifts that were achieved suggesting the nanoparticles were fully coated with pHLIP or EuL. However, upon titration of EuL into a solution of fully coated pHLIP•AuNP, a further red shift was achieved. The λ_{max} for pHLIP•EuL•AuNP was greater than that for either EuL•AuNP or pHLIP•AuNP indicting that the addition of EuL did not displace pHLIP from the nanoparticle surface. This result was further supported by the ICP-OES result where pHLIP•EuL•AuNP had around half the amount of EuL per AuNP than fully coated EuL•AuNP, 640 and 1,335, respectively. ζ-potential measurements showed that the ζ-potential for pHLIP•EuL•AuNP was an intermediate value (-29 mV) between neutrally coated EuL•AuNP (-14 mV) and entirely negative coatings of citrate AuNP (-38 mV). Similarly, the differences in the ζ-potentials for pHLIP•EuL•AuNP and pHLIP•AuNP, confirm the differences in coating. These results and

the similar Eu^{3+} luminescent lifetimes for pHLIP•EuL•AuNP and pHLIP•AuNP confirm the different coatings of the nanoparticles.

Table 5.1. Summary of nanoparticle properties. *Where applicable values are shown as ± s.e.m.*

	SPR peak (shift) / nm	ζ-potential / mV	Lifetime (at 614 nm) / µs	No. Eu / AuNP
Citrate AuNP	518 (--)	- 37.67 ± 5.5	-----	-----
EuL•AuNP	526 (8)	- 13.81 ± 2.4	287	1335
pHLIP•AuNP	523 (5)	- 21.33 ± 0.9	-----	-----
pHLIP•EuL•AuNP	527 (9)	- 29.67 ± 0.6	290	640

5.2.2 Uptake of gold nanoparticles into human platelets

As optical probes, gold nanoparticles are known to scatter coloured light when illuminated with white light (Yguerabide and Yguerabide, 1998).The side-scatter spectra of the various gold nanoparticles demonstrated this scattering through a range of wavelengths from 400 – 700 nm (Figure 5.7). In particular, strong scattering of light between 450 - 500 nm and 600 - 700 nm was observed. A biological imaging technique which makes use of scattered light is confocal reflection microscopy. The stronger scattering regions of the gold nanoparticles coincide with conventional microscope laser lines of 488 nm and 633 nm and since scattering of light by biological tissues is minimal compared to that of the gold nanoparticles (Kah et al., 2008, Curtis, 1964), making the technique ideal for monitoring gold nanoparticle uptake into

cells.

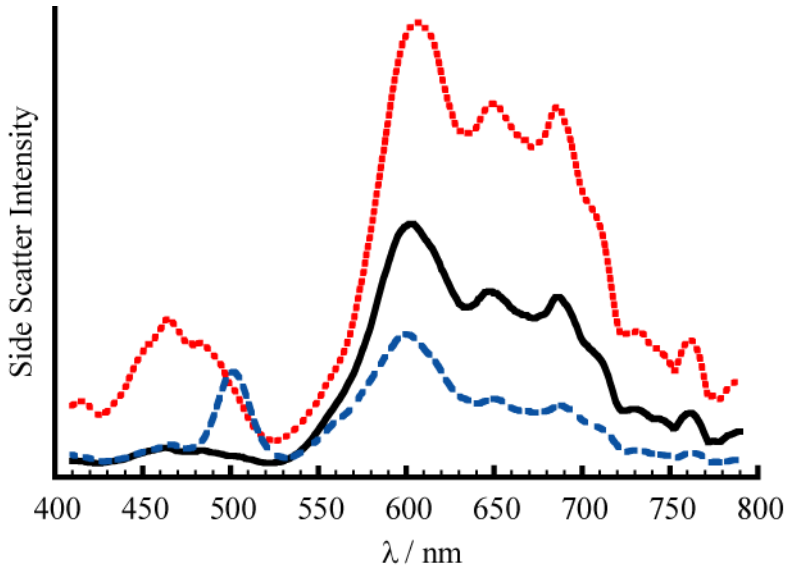

Figure 5.7. Scattering of light by gold nanoparticles. Samples of gold nanoparticles were illuminated and a scattering spectrum detected at 90° to incident illumination in a spectrophotometer. Side-scatter spectrum for citrate-stabilised AuNP (—; 7.4 nM in water), pHLIP•AuNP (---; 7.5 nM in water) and pHLIP•EuL•AuNP (•••; 7.5 nM in water). $\lambda_{ex} = \lambda_{em}$.

Spread platelets were imaged using confocal reflection microscopy with incident light of λ = 488 or 633 nm and collection of reflected light (λ ± 5 nm). Platelets treated with pHLIP•AuNP or pHLIP•EuL•AuNP had high regions of reflection from the gold observed as white spots (Figure 5.8), confirming the presence of nanoparticles in the cells. Untreated platelets and platelets treated with EuL•AuNP did not display these bright regions, indicating the absence of nanoparticles in the cells.

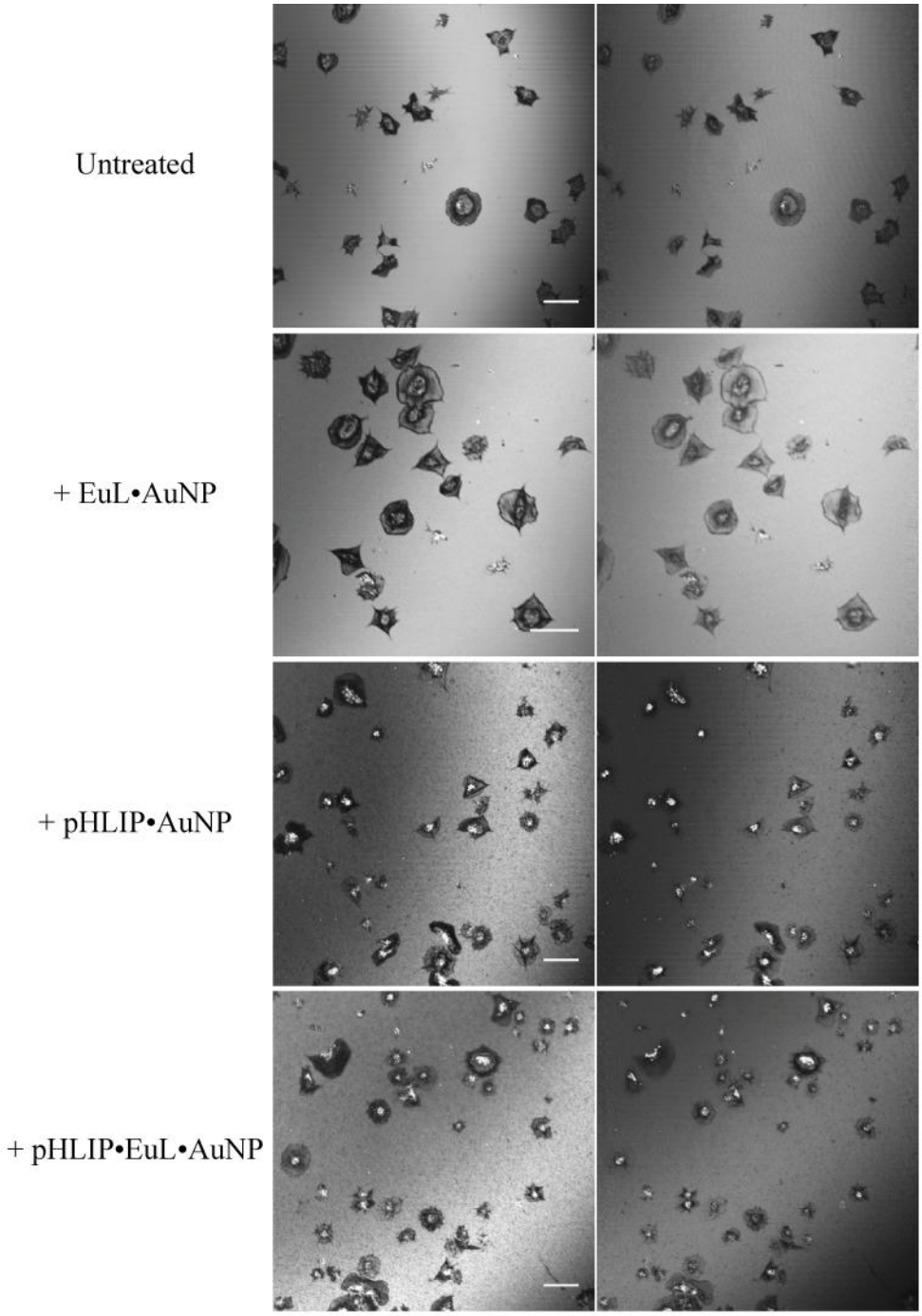

Figure 5.8. Confocal reflection microscopy of human platelets treated with gold nanoparticles. Human platelets (2 x 10^7 mL^{-1}) were resuspended in Tyrode's buffer at pH 6.5 and left untreated (n = 5) or treated with; EuL•AuNP (~40,000 NPs/cell, n = 2), pHLIP•AuNP (~40,000 NPs/cell, n = 4) or pHLIP•EuL•AuNP (~40,000 NPs/cell, n = 5) for 10 min prior to spreading on fibrinogen for 45 minutes (37 °C, 5% CO_2) and fixation. Representative confocal reflection images of platelets imaged with λ_{ex} = 488 nm (*Right*) or 633 nm (*Left*). Scale bar = 10 μm.

The nanoparticles can also be detected via luminescence microscopy due to the presence of EuL on the AuNP. Platelets were treated with EuL•AuNP, pHLIP•AuNP or pHLIP•EuL•AuNP for 10 minutes prior to spreading on fibrinogen and fixation (Figure 5.9). The spread platelets treated with pHLIP•EuL•AuNP exhibited luminescence when imaged with 340 nm excitation wavelength. The large separation between the excitation and emission wavelengths, 340 nm and >510 nm, respectively, removes any background cellular autofluorescence, as such the emission detected can only come from the europium. Untreated wavelengths, 340 nm and >510 nm, respectively, removes any background cellular autofluorescence, as such the emission detected can only come from the europium. Untreated cells and cells treated with EuL•AuNP or pHLIP•AuNP did not exhibit any luminescence, confirming the lack of background autofluorescence and demonstrating no uptake of europium-coated nanoparticles in the absence of pHLIP. In addition, transmitted light images of platelets treated with pHLIP•AuNP or pHLIP•EuL•AuNP have bright regions near the platelet centre which were not apparent in untreated platelets or platelets treated with EuL•AuNP. These bright regions are similar to those seen in confocal reflection microscopy which indicates that it may be as a result of light scattered from the gold nanoparticles in the platelets.

Furthermore, luminescence spectrum acquired from pHLIP•EuL•AuNP treated platelets (Figure 5.10) showed the characteristic *f-f* transition pattern observed for europium, confirming the europium as the source of the emitted light. The luminescence lifetime for EuL was also examined to assess the environment of EuL inside the cell. The platelets treated with pHLIP•EuL•AuNP displayed a luminescence lifetime of 288 μs in spread platelet samples and 277 μs in fixed platelet suspension in buffer, in agreement with the solution of

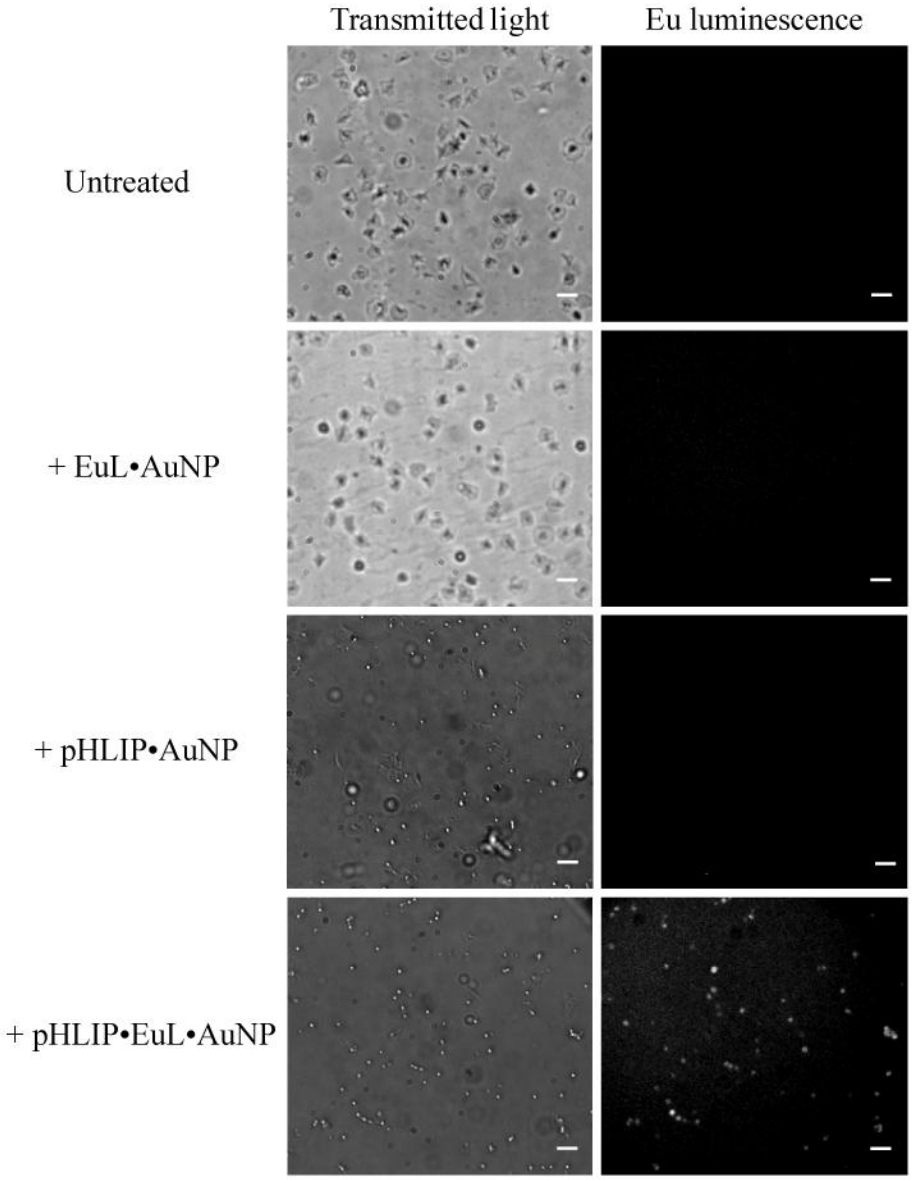

Figure 5.9. Luminescence microscopy of human platelets treated with gold nanoparticles. Human platelets (2 x 10^7 mL^{-1}) were resuspended in Tyrode's buffer at pH 6.5 and left untreated (n = 6) or treated with; EuL•AuNP (~40,000 NPs/cell, n = 2), pHLIP•AuNP (~40,000 NPs/cell, n = 3) or pHLIP•EuL•AuNP (~40,000 NPs/cell, n = 6) for 10 min prior to spreading on fibrinogen for 45 minutes (37 °C, 5% CO_2) and fixation. Representative transmitted light (*Left*) and luminescence (*Right*) images of platelets. The different background signal of the transmitted light images of platelets treated with pHLIP-coated AuNP is due to the lower strength of illumination dictated by the strong signal as a result of scattering of light by AuNP. λ_{ex} = 340 nm, λ_{em} = >510 nm. Scale bar = 10 µm.

pHLIP•EuL•AuNP as reported above. The luminescence lifetime of the Eu signal confirms that the EuL is attached to the nanoparticle and that its coordination environment has not changed. Taken together, these results confirm the presence of pHLIP•EuL•AuNP in the cells.

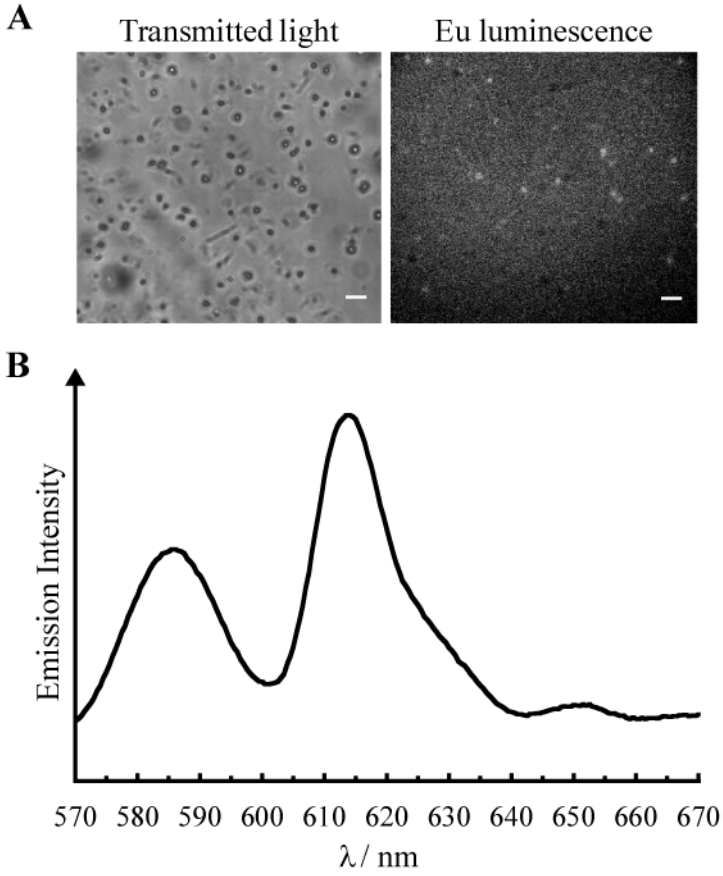

Figure 5.10. Luminescence microscopy and spectroscopy of human platelets treated with pHLIP•EuL•AuNP. Human platelets (2 x 10^7 mL^{-1}) were resuspended in Tyrode's buffer at pH 6.5 and treated with pHLIP•EuL•AuNP (~40,000 NPs/cell, n = 3) for 10 min prior to spreading on fibrinogen for 45 minutes (37 °C, 5% CO2) and fixation. Representative (A) Transmitted light (*Left*) and luminescence (*Right*) images of treated platelets. (B) Corresponding emission spectrum for platelets treated with pHLIP•EuL•AuNP. λ_{ex} = 365 nm, and for luminescence images λ_{em} = >510 nm. Scale bar = 10 μm.

The high electron density of gold makes it a useful label in electron microscopy. In order to determine the localisation of the nanoparticles in the platelets, platelets were either untreated

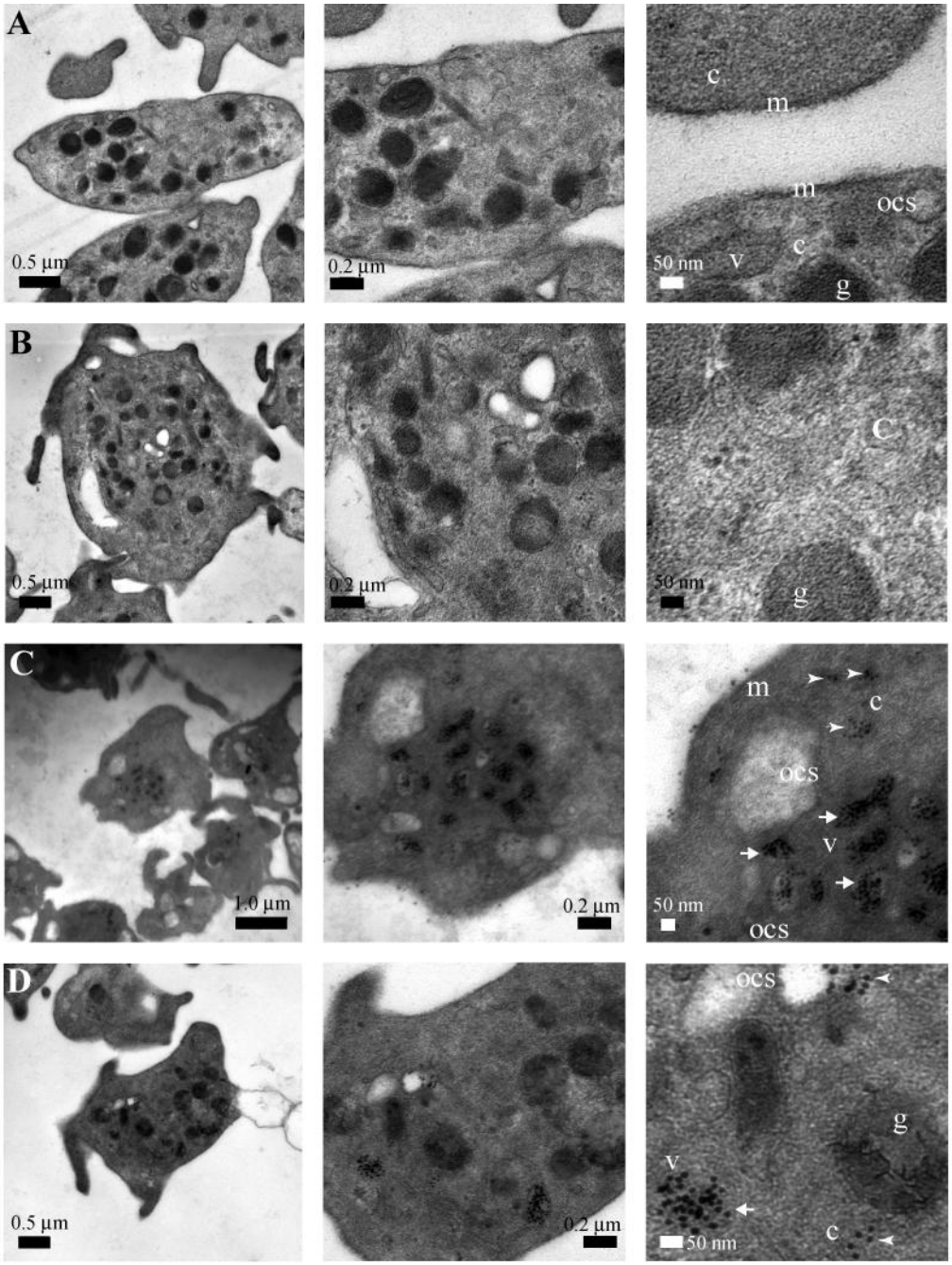

Figure 5.11. Transmission electron microscopy of human platelets treated with gold nanoparticles. Human platelets (2 x 10^7 mL^{-1}) were resuspended in Tyrode's buffer at pH 6.5 and left untreated (n = 3) or treated with; EuL•AuNP (~8,000 NPs/cell, n = 2), pHLIP•AuNP (~8,000 NPs/cell, n = 2) or pHLIP•EuL•AuNP (~8,000 NPs/cell, n = 3) for 10 min prior to spreading on fibrinogen for 45 minutes (37 °C, 5% CO2) and fixation. Representative TEM images of (A) untreated platelets and platelets treated with; (B) EuL•AuNP, (C) pHLIP•AuNP or (D) pHLIP•EuL•AuNP for 10 min prior fixation. Platelets treated with pHLIP•AuNP and pHLIP•EuL•AuNP have AuNP in a variety of platelet membranous structures, including the platelet membrane (m), vesicles (v, arrows), open canalicular system (ocs) and cytoplasm (c, arrowheads) but not in secretory granules (g).

or treated with EuL•AuNP, pHLIP•AuNP or pHLIP•EuL•AuNP for 10 minutes prior to fixation and preparation for transmission electron microscopy, TEM (Figure 5.11). Nanoparticles were mostly visible in membranous regions of the platelet including the internal sides of the platelet membrane, membranes of the open canalicular system and vesicles in platelets treated with pHLIP-coated gold nanoparticles. A small number of nanoparticles were also present in the platelet cytoplasm. Furthermore, no nanoparticles were detected in platelets treated with EuL•AuNP.

Platelets treated with EuL•AuNP, pHLIP•AuNP or pHLIP•EuL•AuNP showed loss of the discoid structure when compared with untreated samples. Since this shape change is apparent in EuL•AuNP treated platelets, where no nanoparticles were detected in the platelet cytoplasm, this suggests that the presence of coated gold nanoparticles in platelet suspension may be causing slight activation of platelets.

Cell membranes are negatively charged and ζ-potential measurements for the various nanoparticle samples were also negative (Table 5.1). Previous work has demonstrated that nanoparticle uptake is charge dependent, with nanoparticles with positive ζ-potentials taken up more efficiently than those with negative ζ-potentials (Arvizo et al., 2010, Liang et al., 2010). pHLIP-coated nanoparticles have more negative ζ-potentials than EuL•AuNP, so if uptake was reliant on the nanoparticle/ membrane charge interaction, it would be expected that EuL•AuNP would be taken up into cells more efficiently. Since, this was not the case the results suggest that cellular uptake of pHLIP-coated nanoparticles was not due to their surface charge.

pHLIP attachment to AuNP is via a gold-sulphur bond which not easily cleavable and intracellular sulphur exchange reactions with glutathione are very slow (Hong et al., 2006). As such, when the nanoparticle is translocated across the cell membrane the nanoparticle should remain at the internal cell membrane. The localisation of pHLIP to membranous regions of the cell, such as membranes of OCS and cell membrane, was shown by TEM (Figure 5.11). Since the nanoparticles are localised to membranes, if the pH of the cell solution was increased to pH 7.4 this should result in removal of the nanoparticles from the inside of the cell (Figure 5.12 *A*).

Platelets were treated, as previously described (**5.2.2**), after 10 minutes incubation with pHLIP•EuL•AuNP the pH was either increased to pH 7.4 or kept at pH 6.5 for a further 10 minutes prior to spreading on fibrinogen, as previous. As a further control platelets were also treated with pHLIP•EuL•AuNP at pH 7.4. In cells treated at pH 7.4 or at pH 6.5 and increased to pH 7.4, there are very small regions of high reflection compared with those cells treated at pH 6.5 only (Figure 5.12 *B*).

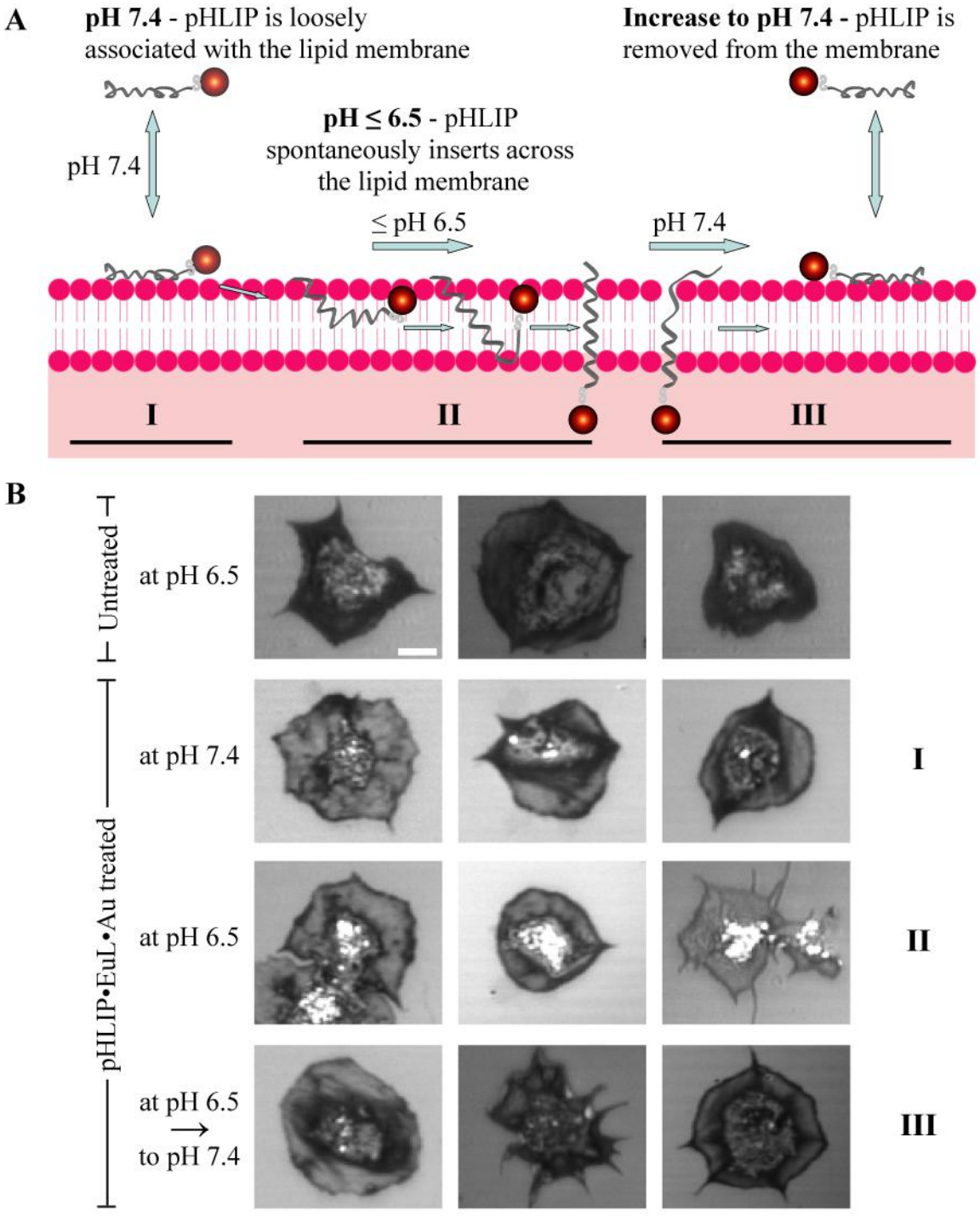

Figure 5.12. pH-dependent uptake of pHLIP-coated gold nanoparticles into human platelets. (A) Schematic representation of pH dependent nanoparticle uptake. (B) Human platelets (2 x 10^7 mL^{-1}) were resuspended in Tyrode's buffer at pH 6.5 or pH 7.4, as indicated, and left untreated (n = 5) or treated with; pHLIP•EuL•AuNP (~40,000 NPs/cell, n = 5) for 10 min. The platelets were washed via centrifugation and resuspended in Tyrode's buffer at pH 6.5 or 7.4, as indicated. Platelets were allowed to rest for 20 min prior to spreading on fibrinogen for 45 minutes (37 °C, 5% CO2) and fixation. Representative confocal reflection images of treated platelets. Stages I - III representative of pH conditions for corresponding insertion stages in (A). λ_{ex} = 488 nm, λ_{em} = 488 ± 5 nm. Scale bar = 2 µm.

5.2.3 Effect of nanoparticle uptake on platelets

Translocation of 13 nm gold nanoparticles across the cell membrane could result in disruption of the platelet membrane or create holes in membrane. Either of these would cause loss of cellular contents. In platelets, loss of cellular contents occurs when platelets are activated and causes an activation signalling cascade; therefore if the nanoparticles punch holes in the cell membrane then this would affect platelet spreading.

In order to assess whether nanoparticle uptake affects membrane integrity, human platelets were loaded with the cell permeant calcium indicator, Oregon-Green BAPTA-1AM prior to treatment with pHLIP•EuL•AuNP. As a control platelet samples were also left untreated and treated with saponin, a membrane pore-forming compound. Calcium was then added to the resulting supernatant from the centrifuged platelet samples and emission spectra acquired (Figure 5.13). The results show that treatment with saponin resulted in loss of BAPTA from the cells into the supernatant, however, this was not the case for untreated or pHLIP•EuL•AuNP treated cells suggesting that uptake of the nanoparticles does not cause disruption to the cell membrane such that loss of cell content occurs.

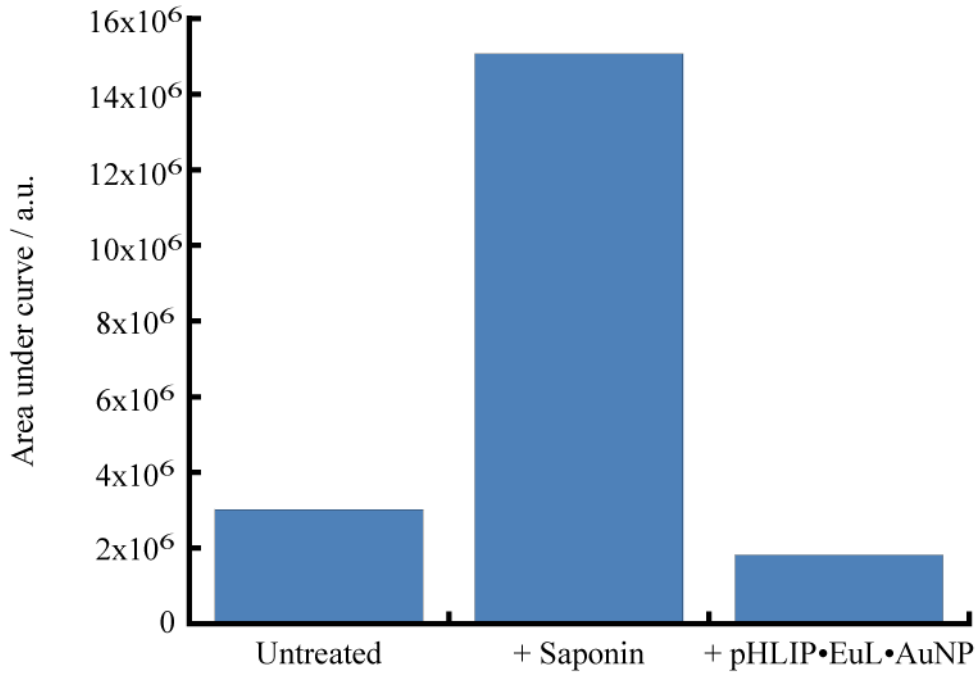

Figure 5.13. Effect of pHLIP•EuL•AuNP treatment on platelet membrane integrity. Human platelets (2 x 10^7 mL^{-1}) were resuspended in Tyrode's buffer (pH 7.4) and loaded with Oregon-Green BAPTA-1 AM (1 μM) in the presence of $CaCl_2$ (200 μM) and Apyrase (2 UmL^{-1}) for 45 mins at 37 °C. Platelets were centrifuged and resuspended in Tyrode's buffer (pH 6.5). pHLIP•EuL•AuNP (~8,000 NPs/cell, n = 3), saponin (10 $mgmL^{-1}$) or Tyrode's buffer were added for 10 min The platelets were centrifuged and the resulting supernatent retained. CaCl2 (50 μM) was added to supernatents prior to fluorescence spectroscopy of the emission of Oregon-Green BAPTA-1 AM. Representative graph of area under curve calculated from emission spectra of Oregon-Green BAPTA-1AM released from untreated, saponin treated and pHLIP•EuL•AuNP treated human platelets. λ_{ex} = 480 nm.

There was no significant difference in the mean cell density of spread platelets, mean platelet area or in the distribution of platelets at various spreading stages for platelets in incubated with pHLIP•EuL•AuNP samples when compared with solvent control samples (Figure 5.15 *A*-*C*). Although there was a significant difference in mean cell density for pHLIP•AuNP treated platelets (41.4 ± 3.6) compared with solvent control (28.0 ± 3.6), there was no significant difference in the mean platelet area or in the distribution of platelets at various spreading stages. Therefore, incubation with pHLIP-coated AuNP and translocation of nanoparticles by pHLIP

into platelets does not appear to affect platelet spreading.

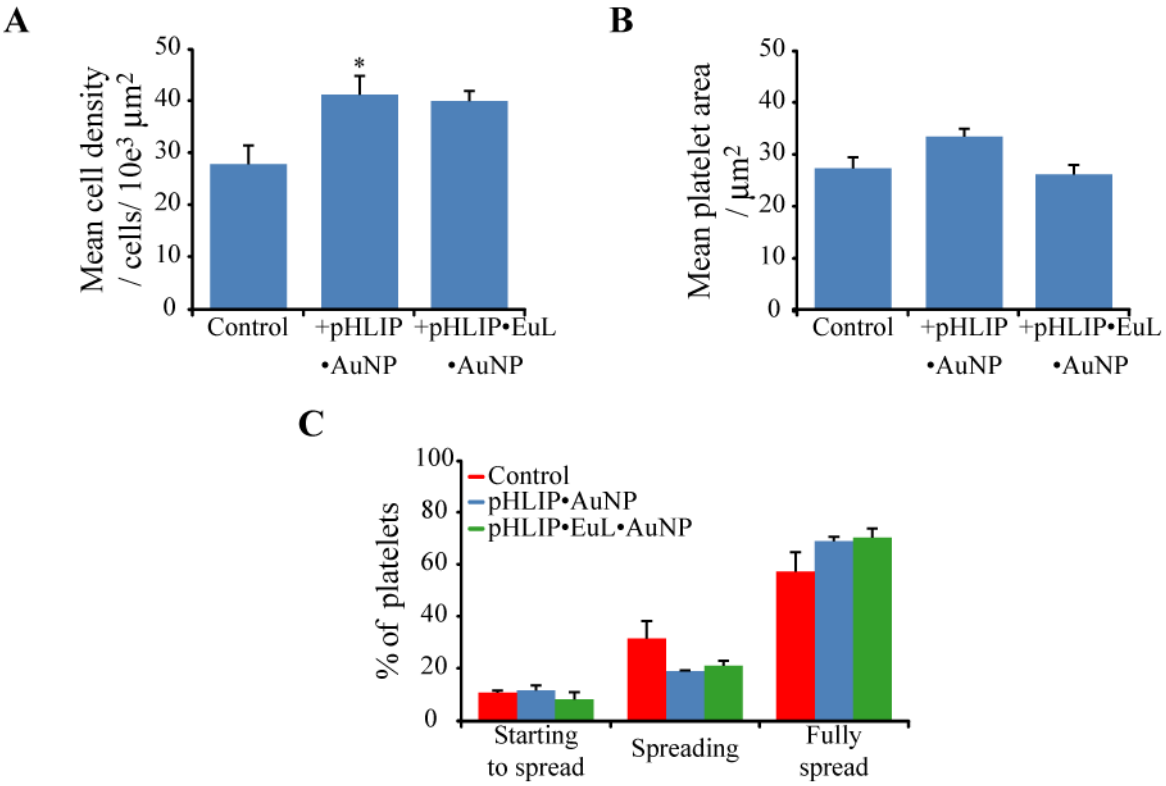

Figure 5.14. Effect of pHLIP•EuL•AuNP treatment on spreading of human platelets. Human platelets (2 x 10^7 mL^{-1}) were resuspended in Tyrode's buffer at pH 6.5 and treated with Tyrode's buffer (control, pH 6.5, n = 5), pHLIP•AuNP (~8,000 NPs/cell, n = 4) or pHLIP•EuL•AuNP (~8,000 NPs/cell, n = 5) for 10 minutes. The platelets were allowed to spread on fibrinogen for 45 minutes (37 °C, 5% CO_2) prior to fixation. Platelets were analysed over five distinct fields with a minimum of 100 platelets were counted per experiment. (A) Mean cell density. (B) Mean platelet area. (C) Percentage of platelets at various stages of spreading. Results are shown as ± s.e.m. *$P < 0.05$ is relative to solvent control.

5.3 CONCLUSIONS

This work has demonstrated that 13 nm gold nanoparticles can be functionalised with pHLIP or with a luminescent europium complex. Furthermore, it has been shown that it is possible to functionalise gold nanoparticles with multiple entities, in the case of this work, a peptide which facilitates non-endocytic uptake of nanoparticles into cells and a luminescent complex which enables detection of the nanoparticles in the cells. This functionalisation allows for the rapid uptake of luminescent gold nanoparticles into human platelets, a cell type which is notoriously difficult to deliver non-permeant molecules into.

Due to the intrinsic properties of pHLIP, uptake into human platelets is pH-dependent and only achievable at a pH of <6.5. This thereby enables not only the ability to deliver nanoparticles non-endocytically but also provides a degree of control over the nanoparticle uptake. The uptake of pHLIP-coated gold nanoparticles into platelets was verified by confocal reflection microscopy, luminescence microscopy and transmission electron microscopy. As hypothesised (Figure 5.1), due the intrinsic properties of pHLIP and the nature of the attachment of pHLIP to AuNP, translocated nanoparticles were localised to membranous regions of the platelet. The presence of these luminescent nanoparticles in platelets did not appear to affect membrane integrity and platelets were able to spread on fibrinogen as normal. Thus, the introduction of pHLIP together with lanthanide label on gold nanoparticles represents a significant step forward in the use of gold nanoparticles as multi-modal imaging labels in biological systems.

CHAPTER 6

DELIVERY OF FLUORESCENT LIFEACT COATED GOLD NANOPARTICLES INTO HUMAN PLATELETS USING pH (LOW) INSERTION PEPTIDE

6.1 INTRODUCTION

In the work presented in **Chapter 5**, successful coating of 13 nm gold nanoparticles with pHLIP and a luminescent label, EuL, was demonstrated (Davies et al., 2012). These nanoparticles were also successfully translocated across the plasma membrane, into the platelet cytoplasm, by pHLIP. However, the luminescent gold nanoparticles remained localised to membranous regions because there is no cleavable bond between pHLIP and the luminescent nanoparticles. Additionally, the luminescent nanoparticles are non-specific labels, so are unable to bind to and label the actin cytoskeleton or any other cellular structure if released into the cytoplasm.

There are various approaches that could be used to enable release of AuNP into the cytoplasm, including glutathione-mediated release, photo-cleavage, peptide cleavage or disulphide bond cleavage. Glutathione-mediated release of molecules bound to gold nanoparticles has been achieved but it is a slow process, occurring over 96 hours or 8 hours if cellular glutathione concentrations are increased (Han et al., 2005, Hong et al., 2006). Photo-cleavage or peptide cleavage has not been reported, to date, for pHLIP mediated delivery. Release of molecules from pHLIP following peptide insertion and cargo translocation has been achieved via the presence of a disulphide bond between pHLIP and the cargo molecule (Reshetnyak et al., 2006, Moshnikova et al., 2013, Wijesinghe et al., 2011, An et al., 2010).

The disulphide bond is cleaved in the reducing environment of the cytoplasm. In **Chapter 4**, this approach was used to successfully release Lifeact into the platelet cytoplasm and enabled imaging of the platelet actin cytoskeleton. Therefore, a disulphide bond between pHLIP and AuNP should enable cytoplasmic release of AuNP.

However, the difficulty with achieving this goal arises from the adsorption of disulphides onto the gold nanoparticle surface and subsequent formation of gold-sulphur bonds and cleavage of sulphur-sulphur bonds. One such way that has been used to achieve disulphides on AuNPs is to conjugate a linker to a fully coated AuNP (Lee et al., 2009).

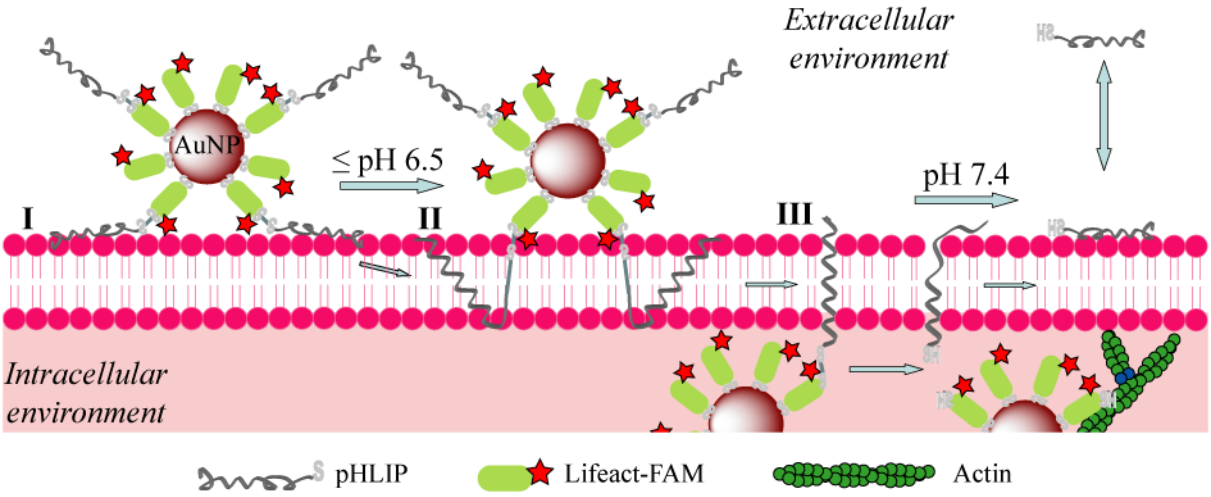

Figure 6.1. Schematic representation of pHLIP mediated cellular delivery of fluorescent Lifeact•AuNP. I, II and III represent the three states that pHLIP adopts; - in solution, associated with the lipid membrane and inserted across the lipid membrane, respectively. Lifeact•AuNP, conjugated to pHLIP's *C*-terminus via a disulphide bond, is translocated across the cell membrane in to the cytoplasm. Reduction of the disulphide bond in the reducing environment inside the cell releases Lifeact•AuNP into the cytoplasm. Thus enabling Lifeact•AuNP to label of the actin cytoskeleton. The low pH induced insertion is completely reversed upon restoration of neutral pH.

The work in this chapter aims to address both the issue of AuNP cytoplasmic release and AuNP label specificity via the introduction of Lifeact-FAM to AuNP, Lifeact•AuNP, with a disulphide bond between pHLIP and Lifeact, pHLIP-S-S-Lifeact•AuNP (Figure 6.1). The presence of Lifeact-FAM on AuNP enables binding to and consequently labelling of the actin cytoskeleton once the nanoparticles have been delivered and released into the cytoplasm. Use of pHLIP-S-S-Lifeact•AuNP in platelets would enable imaging of the actin cytoskeleton with high spatial and temporal resolution: The presence of fluorescently labelled Lifeact allows for live cell imaging of platelet actin dynamics, providing temporal resolution. Following which the same platelets can be fixed and prepared for electron microscopy, providing high spatial resolution of the actin in the same cells. The ability to do this would enable greater understanding of platelet actin dynamics and more particularly that of the platelet actin nodule.

6.2 RESULTS &DISCUSSION

6.2.1 Preparation and characterisation of Lifeact-coated gold nanoparticles

Citrate-stabilised gold nanoparticles

Citrate stabilised gold nanoparticles were synthesised as previously described in **Chapter 5**. See **5.2.1** "**Citrate-stabilised gold nanoparticles**" for details.

Lifeact-coated gold nanoparticles, Lifeact•AuNP

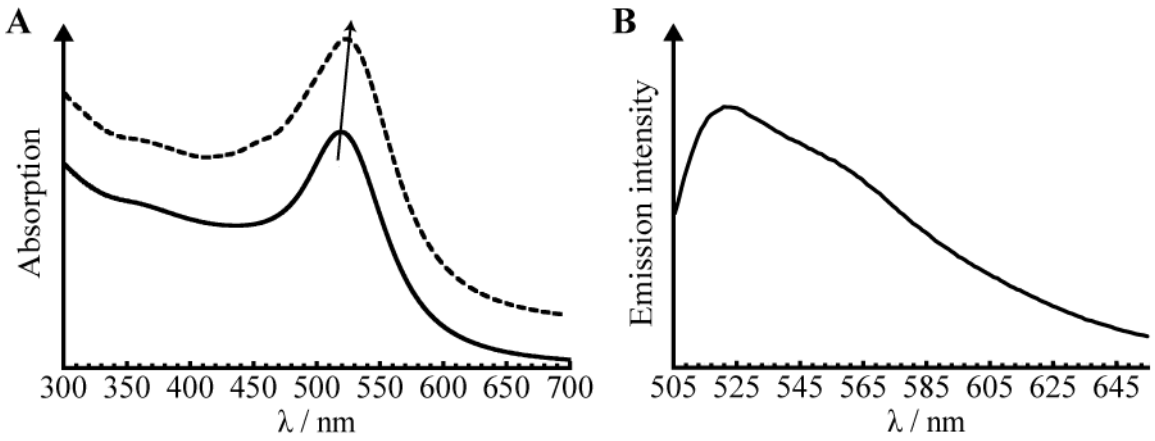

Figure 6.2. Characterisation of Lifeact-FAM coated gold nanoparticles. (A) UV-Vis absorption spectra monitoring the SPR band of AuNP (—; 9.4 nM in water), upon addition of Lifeact-FAM (---; 8 μL, 5 mM, in 0.1 M sodium phosphate buffer with 37 % DMSO). The arrow represents the trend in the shift of the SPR peak during coating. (B) Fluorescence emission spectrum of Lifeact•AuNP (0.47 nM in water). λ_{ex} = 480 nm.

A solution of Lifeact-FAM (5 mM, in 0.1 M sodium phosphate buffer with 37 % DMSO) was titrated into an aqueous suspension of citrate-stabilised AuNP (9.4 nM, in water) (Figure 6.2 *A*). The red shift in the SPR band confirms the binding of Lifeact to AuNP. The titration was continued until a maximum shift of 4.5 nm in the AuNP SPR band was observed. This

maximum shift is indicative of fully coating of AuNP with Lifeact. The interaction of Lifeact with AuNP is expected to take place via the cysteine residue at the *N*-terminus of the peptide. The Lifeact-coated AuNP, Lifeact•AuNP, were purified by size-exclusion chromatography to remove any excess, unbound Lifeact. Following chromatography, the λ_{max} of the SPR band did not shift confirming the unchanged nature of the nanoparticle coating. A solution of Lifeact•AuNP exhibited the characteristic fluorescence emission spectrum for FAM upon excitation at 480 nm (Figure 6.2 *B*). The overlap of AuNP absorption and FAM emission does not appear to result in quenching of the FAM emission.

6.2.2 Labelling of the actin cytoskeleton with Lifeact•AuNP

To assess the ability of Lifeact•AuNP to label the platelet actin cytoskeleton, washed human platelets were allowed to spread on fibrinogen for 45 minutes prior to fixation and permeablisation, then labelled with Lifeact•AuNP. The fixed cells were then imaged using confocal microscopy (Figure 6.3). Similar labelling pattern was observed for platelets labelled with Lifeact or Lifeact•AuNP, indicting labelling of the platelet actin cytoskeleton by Lifeact•AuNP. However, very little reflection corresponding to scattering of light by gold was observed in confocal reflection images. This is most likely due to dispersion of nanoparticles throughout the cell. In **Chapter 5** the nanoparticles were gathered together in membranous locations which resulted in a higher density of light-scattering nanoparticles at the cell surface, in particular, in the centre of the platelet.

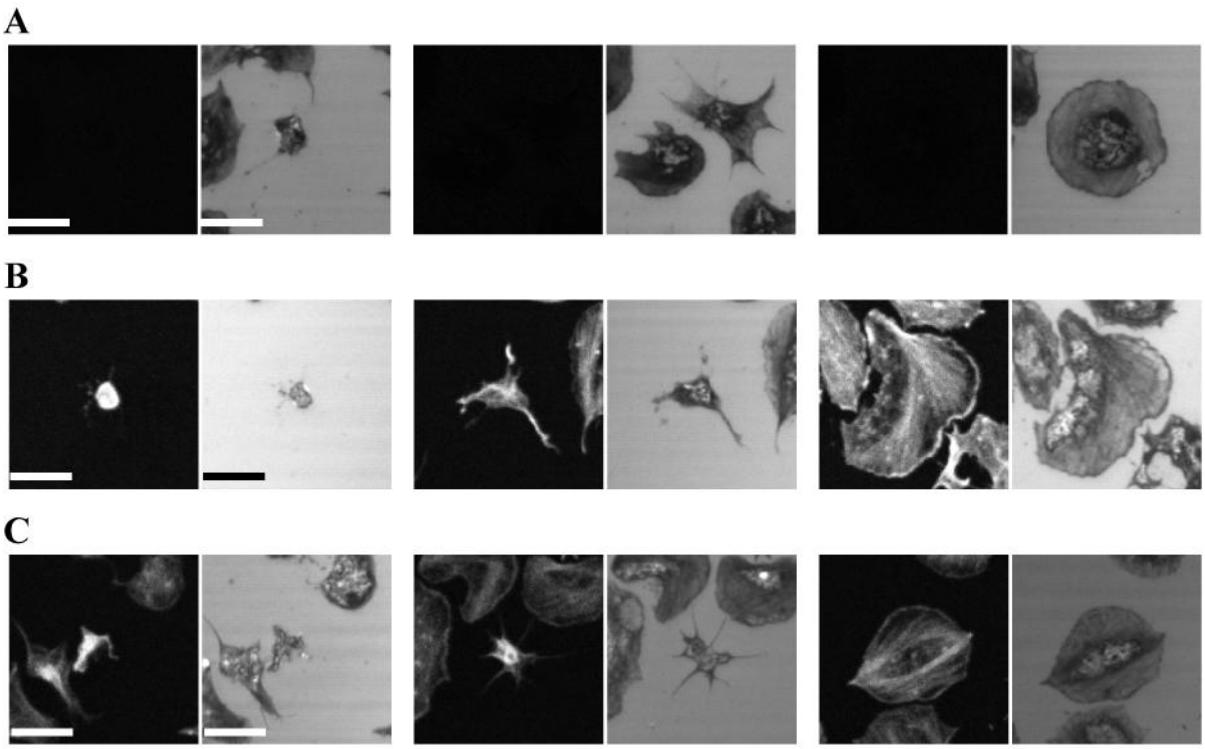

Figure 6.3 Labelling of the platelet actin cytoskeleton with Lifeact•AuNP. Washed human platelets (2 x 10^7 mL^{-1}) were allowed to spread on fibrinogen for 45 min (37 °C, 5 % CO_2) prior to fixation, permeablisation with Triton (0.1 % in PBS) and labelling with Lifeact•AuNP. Confocal fluorescence (*left*) and reflection (*right*) images of: (A) Unlabled platelets. (B) Lifeact-FAM (6.6 pM) labelled platelets. (C) Lifeact•AuNP (30 pM) labelled platelets. Images are representative of three experiments. Scale bar = 5 μm.

6.2.3 Conjugation of pHLIP to Lifeact•AuNP via a disulphide bond

To introduce disulphide bonds between pHLIP and Lifeact•AuNP, use of a disulphide linker, *N*-succinimidyl 3-(2-pyridyldithio) propionate, SPDP, is investigated. SPDP has been successfully used to introduce disulphide bonds on to AuNP to facilitate intracellular release of siRNA from AuNP carrier (Lee et al., 2009). It has also been used to provide a disulphide bond between pHLIP and phalloidin and amanitin (An et al., 2010, Wijesinghe et al., 2011, Moshnikova et al., 2013). SPDP, once conjugated to the *N*-terminus NH_2 group of Lifeact on Lifeact•AuNP will provide a disulphide bond on the nanoparticles (Figure 6.4). Following

SPDP conjugation, pHLIP with it *C*-terminus thiopyridyl group removed, can be conjugated to Lifeact•AuNP via a disulphide bond.

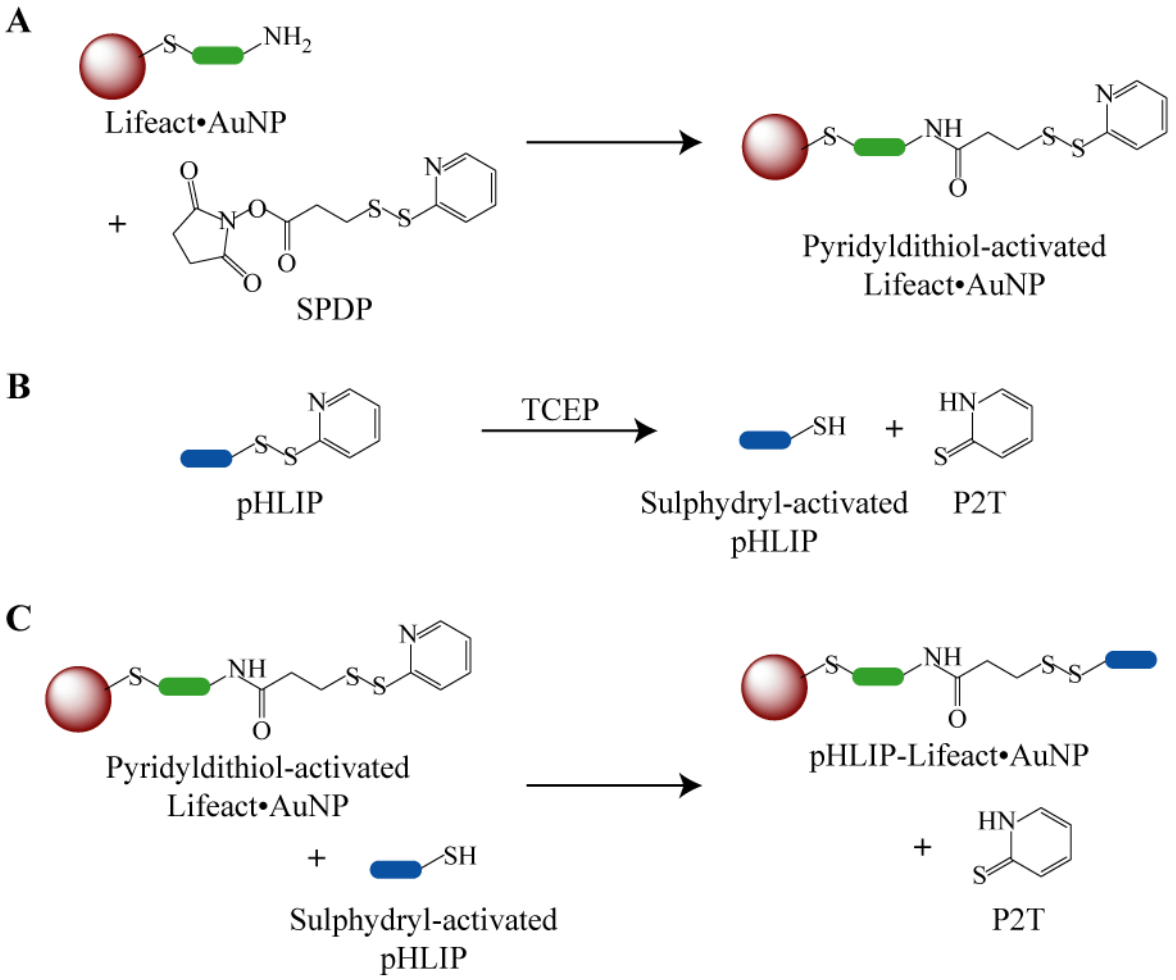

Figure 6.4. Reaction scheme for preparation of pHLIP-Lifeact•AuNP. (A) SPDP is added to Lifeact•AuNP to give a disulphide bond at the *C*-terminus of Lifeact. (B) The disulphide bond at the *C*-terminus of pHLIP is reduced, releasing pyridine 2-thione, P2T. (C) Upon addition of pHLIP to S-S-Lifeact•AuNP a disulphide exchange occurs resulting in formation of a disulphide bond between pHLIP's cysteine and the *C*-terminus sulphur of Lifeact•AuNP,

Lifeact•AuNP and buffer compatibility

A variety of buffers are required during the conjugation reactions. To ensure that the buffers are suitable for use with Lifeact•AuNP and do not cause nanoparticle aggregation, UV-Vis spectroscopy studies were performed. Lifeact•AuNP was centrifuged to remove water and re-

dispersed in PBS, sodium borate buffer or PBS with EDTA, PBS-EDTA. UV-Vis spectroscopy of the SPR band was used to monitor the effect of the buffers on the nanoparticles (Figure 6.5).

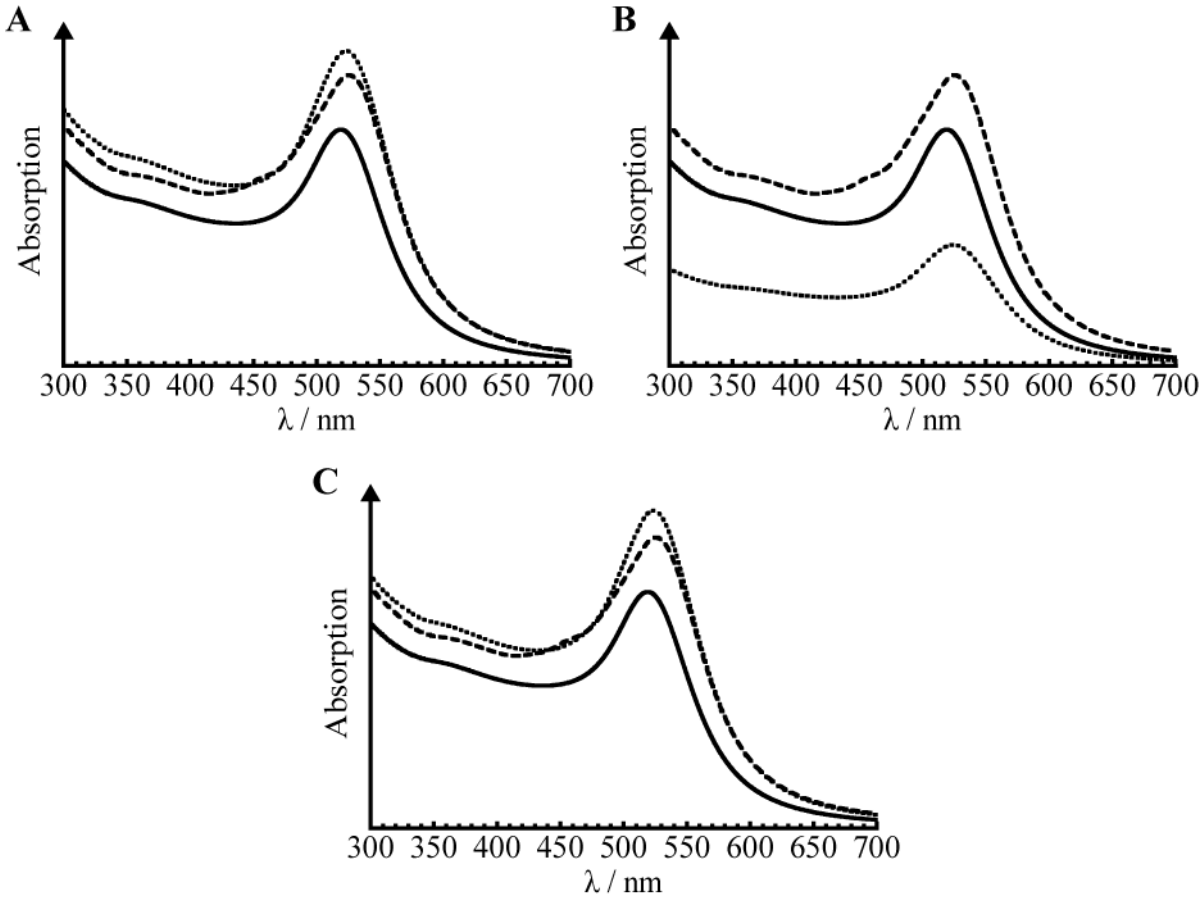

Figure 6.5. Buffer compatibility with Lifeact•AuNP. UV-Vis absorption spectra monitoring the SPR band of Lifeact•AuNP (---; 9.4 nM in water), upon re-dispersal (•••; 9.4 nM) in; (A) PBS, (B) PBS with EDTA and (C) sodium borate buffer. The SPR band of citrate AuNP (—; 9.4 nM in water) is shown for comparison.

There was no shift in the SPR band following buffer replacement for any of the buffers tested. However, there was a reduction in the Lifeact•AuNP concentration when re-dispersed in PBS-EDTA which corresponds with the nanoparticles sticking to the tubes following re-dispersal. This sticking of nanoparticles was not observed for either of the other buffer samples.

Therefore, while PBS-EDTA is not suitable for use with Lifeact•AuNP, PBS and sodium borate buffer appear not to affect the nanoparticles so are suitable for use with nanoparticles.

Conjugation of SPDP to Lifeact•AuNP

As described by Lee *et al*, SPDP (400 μL, 3 mM in PBS with 10 % DMSO) was added to Lifeact•AuNP (400 μL, 30 nM in PBS) and stirred vigorously for 45 minutes at room temperature (Lee et al., 2009). Nanoparticles were found to adhere to the glass vial following addition of SPDP to the nanoparticles. There was a red shift in the λmax for the nanoparticle SPR band indicating a shift in the surface composition of AuNP (Figure 6.6 *A*). This shift was accompanied by a broadening of the SPR band. Also a reduction in the absorbance arises as a result of loss of nanoparticles through adhesion to vial. There was no loss of nanoparticles and no shift in λmax for, or broadening of, the SPR band of Lifeact•AuNP treated with solvent control (400 μL, PBS with 10 % DMSO), indicating that SPDP was responsible for changes to the AuNP properties.

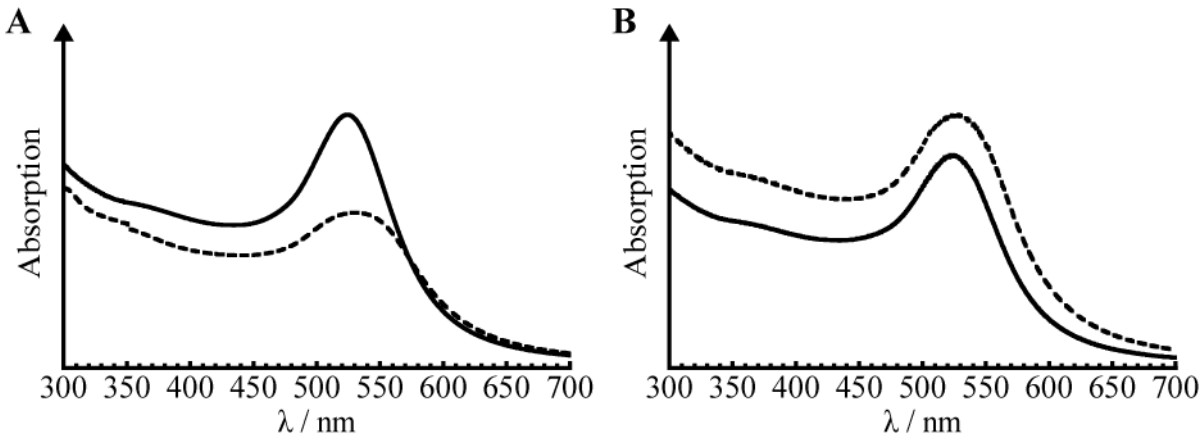

Figure 6.6. Characterisation of SPDP-Lifeact•AuNP. UV-Vis absorption spectra monitoring the SPR band: (A) Following addition of SPDP to Lifeact•AuNP (---; 9.4 nM in PBS) and a solvent control to Lifeact•AuNP (—; 9.4 nM in PBS). (B) Following removal of excess SPDP via centrifugation, SPDP-Lifeact•AuNP (---; 9.4 nM in sodium borate buffer) and solvent control Lifeact•AuNP (—; 9.4 nM in sodium borate buffer).

SPDP-Lifeact•AuNP was centrifuged to remove unconjugated SPDP and the nanoparticles re-dispersed in sodium borate buffer. During washing by centrifugation nanoparticles were observed adhering to vial, this was not the case for solvent control Lifeact•AuNP. Following centrifugation, the λ_{max} of the SPR bands did not shift confirming the unchanged nature of the nanoparticle coating (Figure 6.6 *B*).

pHLIP-Lifeact coated gold nanoparticles, pHLIP-Lifeact•AuNP

The *C*-terminus thiopyridyl group of pHLIP was removed via treatment with TCEP, a disulphide reducing agent, exposing the sulphydryl group, pHLIP-SH. TCEP was selected over other disulphide reducing agents such as, dithiothreitol, DTT, and 2-mercaptoethanol, 2-ME, because it does not contain thiol-groups and therefore does not need to be removed prior to addition to SPDP-Lifeact•AuNP. This reaction was carried out several days before use with AuNP to enable oxidation of TCEP in the phosphate buffer. Additionally pHLIP was dissolved in DMF instead of DMSO since DMSO promotes disulphide formation.

pHLIP-SH (16 μM, in sodium phosphate buffer with 37 % DMF) was added to SPDP-Lifeact•AuNP (15 nM, in sodium borate buffer) and incubated for 18 hours at room temperature. Nanoparticles were found to aggregate during incubation as evidenced by suspension changing colour from a semi-opaque red wine colour to a translucent blue/grey colour. This was also found to be the case when PBS was used as the nanoparticle buffer instead of sodium borate buffer. This suggests that use of SPDP to provide a disulphide bond between pHLIP and Lifeact•AuNP or the method is not suitable.

Lee *et al* re-disperse their nanoparticles in buffers containing the surfactant, Tween20 (Lee et al., 2009). Its presence in the nanoparticle suspension will prevent nanoparticle aggregation since, as an emulsifier, Tween20 saturates binding sites on surfaces. However, Tween20 also lyses cell membranes. Consequently, its presence in the nanoparticle samples negates the need for delivery via pHLIP since nanoparticles would enter the platelets through the disrupted membrane. Additionally, the platelets would no longer be suitable for live cell imaging studies. Therefore, it may not be possible to introduce a disulphide bond on AuNPs without the use of a surfactant.

6.4 CONCLUSIONS

This work has demonstrated that 13 nm gold nanoparticles can be functionalised with fluorescently labelled Lifeact. This functionalisation enables labelling of the actin cytoskeleton in permeablised platelets with both a fluorescent label and a gold nanoparticle. These peptide coated nanoparticles are stable in a variety of cell buffers, so could be suitable for use with live cells. However, it also demonstrates that confocal reflection microscopy may not be a suitable technique for light microscopy imaging of gold nanoparticles which are dispersed throughout the cell. Instead a dark field microscopy technique may be more suitable (Wax and Sokolov, 2009).

Attempts at conjugation of pHLIP to AuNP via a disulphide bond between pHLIP and AuNP-bound Lifeact were unsuccessful. The presence of sulphur groups external to the AuNP surface, resulted in binding of nanoparticles to glass surfaces, as evidenced by adhesion of SPDP-Lifeact•AuNP to vials. Furthermore, when pHLIP-SH was added, the nanoparticle suspension completely aggregated. These results indicate that creation of a disulphide bond on gold nanoparticles may not be possible without the use of a surfactant to prevent aggregation of nanoparticles. Therefore, another method of releasing nanoparticles from pHLIP may be more suitable than disulphide bond cleavage and should be considered in future.

In conclusion, while Lifeact-coated gold nanoparticles may provide a multi-modal imaging label for the actin cytoskeleton, its use in live cells is hampered by the current inability to deliver and release it into the cytoplasm of cell. Conjugation to pHLIP would enable cytoplasmic delivery of Lifeact•AuNP but this work suggests its intracellular release is not possible via a disulphide bond, as previously observed.

CHAPTER 7

GENERAL DISCUSSION

7.1 Summary of results

The work presented in this thesis can be divided into two sections: the first section investigates the role of actin nodules in mouse platelets while the second section focuses on delivery of imaging labels into human platelets to enable investigation of actin nodules in human platelets.

I have demonstrated the ubiquitous presence of actin nodules in early spreading stages of mouse platelets. I have presented evidence for their dynamic nature, i.e. their rapid turnover, as a result of actin polymerisation and depolymerisation. Additionally, I have demonstrated that actin nodule formation requires Arp2/3 complex and calcium ions, while ROCK appears to play a role in the stability of formed nodules. The nodules are stationary, localised to the basal cell membrane and co-localise with integrin clusters.

I have demonstrated the potential of pHLIP as a delivery vector for use in *ex vivo* platelets by the successful delivery of both Lifeact and gold nanoparticles into live cells. Furthermore, I have presented evidence that once translocated across the cell membrane, the disulphide bond between pHLIP and Lifeact is cleaved enabling labelling of the platelet actin cytoskeleton. Incubation of platelets with pHLIP, pHLIP-Lifeact or pHLIP-coated AuNPs does not appear to affect the ability of platelets to spread on a fibrinogen coated surface. I have shown the suitability of the Lifeact peptide as an externally introduced actin label for live cell imaging

studies in platelets. Additionally, I have presented evidence of the suitability and usefulness of gold nanoparticles as a label for multimodal imaging applications.

7.2 The role of actin nodules in platelets

The presence of actin nodules in all platelets during early platelet spreading stages suggest that they play an important role in platelet spreading. Their transient nature, high turnover and localisation to the cell periphery or base of filopodia suggest this role may include mediating the formation of other actin structures such as filopodia and lamellipodia. Furthermore, the location of these nodules at the basal cell membrane, co-localisation with integrin clusters and stationary position allude to a possible role in adhesion of platelets to the exposed ECM. This is supported by their close proximity to the ECM in platelet adhesion under shear stress (Kasirer-Friede et al., 2010). Since focal adhesions are present in platelets when stress fibres are, these transient actin structures may be similar to actin-based adhesion precursors or nascent adhesions which form prior to stress fibre formation (Cerecedo et al., 2006, Choi et al., 2008).

7.3 pHLIP as a delivery vector in human platelets

pHLIP synthesised with a thiopyridyl group on the *C*-terminal cysteine residue enables easy conjugation of a cargo molecule to pHLIP's *C*-terminus. In previous work by Engelman *et al*, extra synthetic steps were required to introduce a linker group to facilitate conjugation via a disulphide bond (Reshetnyak et al., 2006, An et al., 2010). The presence of the thiopyridyl

group served two purposes: Firstly, its presence protects the cysteine residue by preventing disulphide bond formation between cysteine residues on pHLIP and consequently preventing dimerisation of pHLIP in solution. Secondly, the thiopyridyl group provides an efficient leaving group, thus enabling disulphide exchange between the thiopyridyl group and an unprotected –SH group of a cargo molecule. The later function was demonstrated by the conjugation of pHLIP to the fluorescently labelled Lifeact via a disulphide bond in **Chapter 4** and to 13 nm gold nanoparticles via a gold-sulphur bond in **Chapter 5**.

Conjugation to pHLIP enabled successful cytoplasmic delivery of both Lifeact and AuNPs in live human platelets. Immunogold labels and the actin label, phalloidin, have traditionally been introduced via permeablisation of fixed cells. Similarly labelling of other actin regulatory proteins in immunohisochemistry studies is achieved by fixation and permeablisation. Therefore, this represents a major step forward in the ability to undertake live-cell fluorescence imaging studies in human platelets. Conjugation of pHLIP to fluorescently labelled antibodies to actin regulatory proteins, etcetera, via a disulphide bond could enable live-cell imaging of those proteins in human platelets thereby providing detailed understanding of their dynamics and interactions during platelet spreading.

There was a high degree of localisation of pHLIP and pHLIP-cargo to the central region of the platelets. In this region, the disulphide bond between pHLIP and Lifeact appeared to not be cleaved. A similar pattern of cellular localisation has been observed for re-localisation of platelet receptors occurs during platelet spreading resulting in increased concentrations in the granulomere region (Lewis et al., 1990, Kieffer et al., 1992). It may be that there is an excess of pHLIP-cargo on the platelet membrane which has not translocated the platelet membrane

and this excess is re-located to the platelet centre during spreading. Alternatively, the presence of many disulphide isomerases on the platelet surface could result in cleavage of the bond between pHLIP and its cargo (Cho et al., 2008, Essex et al., 1995, Holbrook et al., 2010, Jordan and Gibbins, 2006, Manickam et al., 2008, Robinson et al., 2006). This could result in endocytic uptake of the membrane bound pHLIP and cargo molecules and their localisation to the platelet granulomere. This may account for the few nanoparticles observed in vesicles.

Incubation of platelets with <10 μM pHLIP does not appear to affect platelets in suspension. However, following incubation in suspension, washing of platelets via centrifugation to remove pHLIP or excess cargo, results in loss of platelets. This suggests that the presence of pHLIP on the platelet membrane may cause slight activation of the platelets. TEM images of platelets treated with pHLIP-coated nanoparticles (**Chapter 5**) showed that the discoid shape of the platelets is not maintained suggesting activation of the platelets, although it is not clear whether this is due to pHLIP or the nanoparticles. Nevertheless, platelets appear to spread normally following pHLIP treatment.

Therefore, pHLIP has potential as an intracellular delivery agent for *ex vivo* platelets. However, further investigation is required to fully explore the effect of pHLIP on platelets and to reduce the high localisation to the platelet granulomere which currently impedes live cell imaging studies.

7.4 Labelling and imaging actin in human platelets

The actin cytoskeleton plays a fundamental role in platelet spreading and aggregation and in cellular processes in other cells, including cell division and migration (Cande et al., 1977, Wehland et al., 1977). Additionally, impairments in cytoskeletal function are implicated in diseases including Alzheimer's and cancer (Bamburg and Bloom, 2009, Suresh, 2007). Staining and imaging of actin has been vital in studying the actin cytoskeleton. In platelets, actin labelling is achieved using fluorescently labelled phalloidin which is introduced via permeablisation of the membrane of fixed platelets. Introduction of Lifeact peptide into fixed human platelets via permeablisation, produced similar labelling to phalloidin (**Chapter 4**). Therefore Lifeact peptide could be used as an alternative to phalloidin in fixed cell studies in platelets and other cells. Its small size (17 aa) means it could be easily and cheaply synthesised whereas phalloidin is generally extracted from *Amanita phalloides*, a procedure which is expensive and elaborate, since it has proved difficult to synthesize (Wieland et al., 1983).

For live cell studies Lifeact has been expressed as a GFP-fusion protein in cultured cells and mouse models (Era et al., 2009, Riedl et al., 2008, Godin et al., 2011, Riedl et al., 2010, Schachtner et al., 2012). Platelets from a Lifeact-GFP mouse model have enabled imaging of platelet actin dynamics during spreading. Although this has previously been achieved using platelets from GFP-actin mice, there is evidence that Lifeact-GFP does not affect actin dynamics to the same degree as actin-GFP(Deibler et al., 2011).

However, platelets are non-transfectable, as are primary neutrophils and other cells such as, oocytes, are difficult to transfect. While introduction of Lifeact peptide to these cells may be

possible via microinjection or scrape loading, these methods are inefficient, labelling only a few cells, or causing damage to the cells (McNeil et al., 1984, Li et al., 2008). Conjugation of the Lifeact peptide to pHLIP presents a method which enables uptake into non transfectable cells. Lifeact delivered thusly was able to label the human platelet actin cytoskeleton in live cells. However, in platelets, this method requires further investigation since currently a high degree of labelling of the central region of the platelet hampers the ability to image the cells spreading. pHLIP has been successfully used to deliver *C*-terminally conjugated cargo molecules to a variety of cells including HeLa and mouse prostate (TRAMPC1) and breast (JC) cancer cell lines (Reshetnyak et al., 2006). Therefore, pHLIP may provide a suitable method to enable live cell imaging of actin cytoskeleton dynamics in many cell types through Lifeact labelling.

7.5 Gold nanoparticles as imaging labels in human platelets

Gold nanoparticles have been traditionally used in immunogold labelling for electron microscopy studies in platelets. However, gold nanoparticles are also suitable for light microscopy studies due to their ability to scatter light (Kah et al., 2008, Wax and Sokolov, 2009). Additionally, their functionalisation with fluorescent labels provides another application in fluorescence microscopy. Functionalisation of 13 nm gold nanoparticles with a luminescent europium complex (**Chapter 5**) or fluorescently labelled Lifeact peptide (**Chapter 6**) enables visualisation of the nanoparticles in human platelets via fluorescence or luminescence microscopy, confocal reflection microscopy and transmission electron microscopy, thus demonstrating their potential as imaging labels for multimodal imaging. Furthermore, having demonstrated pHLIP-mediated cytosolic delivery of europium coated

nanoparticles into platelets, replacement of the europium ion with another lanthanide such as gadolinium, transforms these nanoparticle labels from luminescent ones to magnetic resonance imaging, MRI, labels.

With the rise in popularity of correlative light and electron microscopy techniques to provide dynamic and temporal resolution and high spatial resolution, respectively, of cellular process, gold nanoparticles provide an ideal label for such applications (Sartori et al., 2007, Cortese et al., 2009, Vicidomini et al., 2009). In platelets, this technique has been used to study fibrinogen receptor movement (Olorundare et al., 1992). Intracellular delivery of nanoparticles by pHLIP could provide an ideal system of labelling for correlative light and electron microscopy in human platelets.

7.6 Final thoughts

In this thesis, I have further characterised the actin nodule and their ubiquitous in the early platelet spreading stages suggest their importance in platelet shape change. However, their precise role is not known and further research is required to gain a greater understanding of the role of actin nodules in both human and mouse platelet spreading. Additionally, I have demonstrated the potential of pHLIP as a delivery vector for human platelets. Although, successful intracellular, cytoplasmic delivery of Lifeact and luminescent nanoparticles was achieved, this method still needs further research, particularly to address the excess accumulation of pHLIP and its cargo in the central region of platelets.

REFERENCES

ABERCROMBIE, M. 1980. The Croonian Lecture, 1978: The Crawling Movement of Metazoan Cells. *Proceedings of the Royal Society of London. Series B. Biological Sciences,* 207**,** 129-147.

ABERCROMBIE, M., HEAYSMAN, J. E. & PEGRUM, S. M. 1970. The locomotion of fibroblasts in culture. II. "RRuffling". *Exp Cell Res,* 60**,** 437-44.

ABES, R., ARZUMANOV, A. A., MOULTON, H. M., ABES, S., LVANCIVA, G. D., LVERSEN, P. L., GAIT, M. J. & LEBLEU, B. 2007. Cell-penetrating-peptide-based delivery of oligonucleotides: an overview. *Biochemical Society Transactions,* 35**,** 775-779.

AKERMAN, M. E., CHAN, W. C. W., LAAKKONEN, P., BHATIA, S. N. & RUOSLAHTI, E. 2002. Nanocrystal targeting in vivo. *Proceedings of the National Academy of Sciences of the United States of America,* 99**,** 12617-12621.

ALI, L. M., GUTIERREZ, M., CORNUDELLA, R., MORENO, J. A., PINOL, R., GABILONDO, L., MILLAN, A. & PALACIO, F. 2013. Hemostasis disorders caused by polymer coated iron oxide nanoparticles. *J Biomed Nanotechnol,* 9**,** 1272-85.

AN, M., WIJESINGHE, D., ANDREEV, O. A., RESHETNYAK, Y. K. & ENGELMAN, D. M. 2010. pH-(low)-insertion-peptide (pHLIP) translocation of membrane impermeable phalloidin toxin inhibits cancer cell proliferation. *Proceedings of the National Academy of Sciences of the United States of America,* 107**,** 20246-20250.

ANDREEV, O. A., DUPUY, A. D., SEGALA, M., SANDUGU, S., SERRA, D. A., CHICHESTER, C. O., ENGELMAN, D. M. & RESHETNYAK, Y. K. 2007. Mechanism and uses of a membrane peptide that targets tumors and other acidic

tissues in vivo. *Proceedings of the National Academy of Sciences of the United States of America,* 104**,** 7893-7898.

ANDREEV, O. A., ENGELMAN, D. M. & RESHETNYAK, Y. K. 2009. Targeting acidic diseased tissue New technology based on use of the pH (Low) Insertion Peptide (pHLIP). *Chimica Oggi-Chemistry Today,* 27**,** 34-37.

ANDREEV, O. A., KARABADZHAK, A. G., WEERAKKODY, D., ANDREEV, G. O., ENGELMAN, D. M. & RESHETNYAK, Y. K. 2010. pH (low) insertion peptide (pHLIP) inserts across a lipid bilayer as a helix and exits by a different path. *Proceedings of the National Academy of Sciences of the United States of America,* 107**,** 4081-4086.

ANDREIADIS, E. S., DEMADRILLE, R., IMBERT, D., PECAUT, J. & MAZZANTI, M. 2009. Remarkable tuning of the coordination and photophysical properties of lanthanide ions in a series of tetrazole-based complexes. *Chemistry,* 15**,** 9458-76.

ARIYOSHI, H. & SALZMAN, E. W. 1996. Association of localized Ca2+ gradients with redistribution of glycoprotein IIb-IIIa and F-actin in activated human blood platelets. *Arterioscler Thromb Vasc Biol,* 16**,** 230-5.

ARVIZO, R. R., MIRANDA, O. R., THOMPSON, M. A., PABELICK, C. M., BHATTACHARYA, R., ROBERTSON, J. D., ROTELLO, V. M., PRAKASH, Y. S. & MUKHERJEE, P. 2010. Effect of Nanoparticle Surface Charge at the Plasma Membrane and Beyond. *Nano Letters,* 10**,** 2543-2548.

ASLAN, J. E., BAKER, S. M., LOREN, C. P., HALEY, K. M., ITAKURA, A., PANG, J., GREENBERG, D. L., DAVID, L. L., MANSER, E., CHERNOFF, J. & MCCARTY, O. J. 2013. The PAK system links Rho GTPase signaling to thrombin-mediated platelet activation. *Am J Physiol Cell Physiol,* 305**,** C519-28.

BAMBURG, J. R. & BLOOM, G. S. 2009. Cytoskeletal pathologies of Alzheimer disease. *Cell Motil Cytoskeleton,* 66**,** 635-49.

BARCZYK, M., CARRACEDO, S. & GULLBERG, D. 2010. Integrins. *Cell Tissue Res,* 339**,** 269-80.

BARDEN, J. A., MIKI, M., HAMBLY, B. D. & DOS REMEDIOS, C. G. 1987. Localization of the phalloidin and nucleotide-binding sites on actin. *Eur J Biochem,* 162**,** 583-8.

BARNES, A. 2011. *Hepatitis C virus entry receptor dynamics and studies of platelet actin dynamics using lifeact-gfp: a potential role for actin nodules in filopodia formation.* M.Res., University of Birmingham.

BARRERA, F. N., WEERAKKODY, D., ANDERSON, M., ANDREEV, O. A., RESHETNYAK, Y. K. & ENGELMAN, D. M. 2011. Roles of Carboxyl Groups in the Transmembrane Insertion of Peptides. *Journal of Molecular Biology,* 413**,** 359-371.

BAZZONI, G., DEJANA, E. & DEL MASCHIO, A. 1991. Platelet-neutrophil interactions. Possible relevance in the pathogenesis of thrombosis and inflammation. *Haematologica,* 76**,** 491-9.

BEGG, D. A., RODEWALD, R. & REBHUN, L. I. 1978. The visualization of actin filament polarity in thin sections. Evidence for the uniform polarity of membrane-associated filaments. *J Cell Biol,* 79**,** 846-52.

BENNETT, J. S., BERGER, B. W. & BILLINGS, P. C. 2009. The structure and function of platelet integrins. *J Thromb Haemost,* 7 Suppl 1**,** 200-5.

BERNARD, E., PARTHASARATHI, L., CHO, M. K., AYLWARD, K., RAAB, M., DAXECKER, H., O'DUSHLAINE, C. T., SHIELDS, D. C., DEVOCELLE, M., KEYES, T., COSGRAVE, L., O'NEILL, S., MOK, K. H. & MORAN, N. 2009.

Ligand switching in cell-permeable peptides: manipulation of the alpha-integrin signature motif. *ACS Chem Biol,* 4**,** 457-71.

BERNDT, M. C., SHEN, Y., DOPHEIDE, S. M., GARDINER, E. E. & ANDREWS, R. K. 2001. The vascular biology of the glycoprotein Ib-IX-V complex. *Thrombosis and Haemostasis,* 86**,** 178-188.

BEST, D., SENIS, Y. A., JARVIS, G. E., EAGLETON, H. J., ROBERTS, D. J., SAITO, T., JUNG, S. M., MOROI, M., HARRISON, P., GREEN, F. R. & WATSON, S. P. 2003. GPVI levels in platelets: relationship to platelet function at high shear. *Blood,* 102**,** 2811-8.

BICKFORD, L. R., AGOLLAH, G., DREZEK, R. & YU, T. K. 2010. Silica-gold nanoshells as potential intraoperative molecular probes for HER2-overexpression in ex vivo breast tissue using near-infrared reflectance confocal microscopy. *Breast Cancer Research and Treatment,* 120**,** 547-555.

BLOCK, M. R., BADOWSKI, C., MILLON-FREMILLON, A., BOUVARD, D., BOUIN, A. P., FAUROBERT, E., GERBER-SCOKAERT, D., PLANUS, E. & ALBIGES-RIZO, C. 2008. Podosome-type adhesions and focal adhesions, so alike yet so different. *European Journal of Cell Biology,* 87**,** 491-506.

BOLLAG, G. & MCCORMICK, F. 1991. REGULATORS AND EFFECTORS OF RAS PROTEINS. *Annual Review of Cell Biology,* 7**,** 601-632.

BOLTE, S. & CORDELIÈRES, F. P. 2006. A guided tour into subcellular colocalization analysis in light microscopy. *Journal of Microscopy,* 224**,** 213-232.

BOTTCHER, R. T., WIESNER, S., BRAUN, A., WIMMER, R., BERNA, A., ELAD, N., MEDALIA, O., PFEIFER, A., ASZODI, A., COSTELL, M. & FASSLER, R. 2009.

Profilin 1 is required for abscission during late cytokinesis of chondrocytes. *Embo Journal,* 28**,** 1157-1169.

BOUSCHE, O., BRAIMAN, M., HE, Y. W., MARTI, T., KHORANA, H. G. & ROTHSCHILD, K. J. 1991a. Vibrational spectroscopy of bacteriorhodopsin mutants. Evidence that ASP-96 deprotonates during the M----N transition. *J Biol Chem,* 266**,** 11063-7.

BOUSCHE, O., SONAR, S., KREBS, M. P., KHORANA, H. G. & ROTHSCHILD, K. J. 1992. Time-resolved Fourier transform infrared spectroscopy of the bacteriorhodopsin mutant Tyr-185-->Phe: Asp-96 reprotonates during O formation; Asp-85 and Asp-212 deprotonate during O decay. *Photochem Photobiol,* 56**,** 1085-95.

BOUSCHE, O., SPUDICH, E. N., SPUDICH, J. L. & ROTHSCHILD, K. J. 1991b. Conformational changes in sensory rhodopsin I: similarities and differences with bacteriorhodopsin, halorhodopsin, and rhodopsin. *Biochemistry,* 30**,** 5395-400.

BOYLES, J., FOX, J. E., PHILLIPS, D. R. & STENBERG, P. E. 1985. Organization of the cytoskeleton in resting, discoid platelets: preservation of actin filaments by a modified fixation that prevents osmium damage. *The Journal of Cell Biology,* 101**,** 1463-1472.

BRETSCHNEIDER, T., DIEZ, S., ANDERSON, K., HEUSER, J., CLARKE, M., MULLER-TAUBENBERGER, A., KOHLER, J. & GERISCH, G. 2004. Dynamic actin patterns and Arp2/3 assembly at the substrate-attached surface of motile cells. *Current Biology,* 14**,** 1-10.

BRUNNER, A., MINAMITAKE, Y. & GOPFERICH, A. 1998. Labelling peptides with fluorescent probes for incorporation into degradable polymers. *European Journal of Pharmaceutics and Biopharmaceutics,* 45**,** 265-273.

BRUST, M., WALKER, M., BETHELL, D., SCHIFFRIN, D. J. & WHYMAN, R. 1994. SYNTHESIS OF THIOL-DERIVATIZED GOLD NANOPARTICLES IN A 2-PHASE LIQUID-LIQUID SYSTEM. *Journal of the Chemical Society-Chemical Communications***,** 801-802.

BUBB, M. R., SENDEROWICZ, A. M. J., SAUSVILLE, E. A., DUNCAN, K. L. K. & KORN, E. D. 1994. JASPLAKINOLIDE, A CYTOTOXIC NATURAL PRODUCT, INDUCES ACTIN POLYMERIZATION AND COMPETITIVELY INHIBITS THE BINDING OF PHALLOIDIN TO F-ACTIN. *Journal of Biological Chemistry,* 269**,** 14869-14871.

BUGYI, B. & CARLIER, M. F. 2010. Control of actin filament treadmilling in cell motility. *Annu Rev Biophys,* 39**,** 449-70.

BUNCH, T. A. 2010. Integrin alpha IIb beta 3 Activation in Chinese Hamster Ovary Cells and Platelets Increases Clustering Rather than Affinity. *Journal of Biological Chemistry,* 285**,** 1841-1849.

BUNZLI, J. C. G. 2010. Lanthanide Luminescence for Biomedical Analyses and Imaging. *Chemical Reviews,* 110**,** 2729-2755.

BURKEL, B. M., VON DASSOW, G. & BEMENT, W. M. 2007. Versatile fluorescent probes for actin filaments based on the actin-binding domain of Utrophin. *Cell Motility and the Cytoskeleton,* 64**,** 822-832.

CALAMINUS, S. D. J., THOMAS, S., MCCARTY, O. J. T., MACHESKY, L. M. & WATSON, S. P. 2008. Identification of a novel, actin-rich structure, the actin nodule, in the early stages of platelet spreading. *Journal of Thrombosis and Haemostasis,* 6**,** 1944-1952.

CANDE, W. Z., LAZARIDES, E. & MCINTOSH, J. R. 1977. A comparison of the distribution of actin and tubulin in the mammalian mitotic spindle as seen by indirect immunofluorescence. *J Cell Biol,* 72**,** 552-67.

CARLIER, M. F., DUCRUIX, A. & PANTALONI, D. 1999. Signalling to actin: the Cdc42-N-WASP-Arp2/3 connection. *Chem Biol,* 6**,** R235-40.

CARLIER, M. F., JEAN, C., RIEGER, K. J., LENFANT, M. & PANTALONI, D. 1993. Modulation of the interaction between G-actin and thymosin beta 4 by the ATP/ADP ratio: possible implication in the regulation of actin dynamics. *Proc Natl Acad Sci U S A,* 90**,** 5034-8.

CARLIER, M. F. & PANTALONI, D. 1997. Control of actin dynamics in cell motility. *J Mol Biol,* 269**,** 459-67.

CERECEDO, D., MONDRAGON, R., CISNEROS, B., MARTINEZ-PEREZ, F., MARTINEZ-ROJAS, D. & RENDON, A. 2006. Role of dystrophins and utrophins in platelet adhesion process. *Br J Haematol,* 134**,** 83-91.

CHALFIE, M., TU, Y., EUSKIRCHEN, G., WARD, W. W. & PRASHER, D. C. 1994. Green fluorescent protein as a marker for gene expression. *Science,* 263**,** 802-5.

CHARBONNIERE, L., MAMERI, S., KADJANE, P., PLATAS-IGLESIAS, C. & ZIESSEL, R. 2008. Tuning the coordination sphere around highly luminescent lanthanide complexes. *Inorg Chem,* 47**,** 3748-62.

CHARBONNIERE, L. J., WEIBEL, N., RETAILLEAU, P. & ZIESSEL, R. 2007. Relationship between the ligand structure and the luminescent properties of water-soluble lanthanide complexes containing bis(bipyridine) anionic arms. *Chemistry,* 13**,** 346-58.

CHAUHAN, A., TIKOO, A., KAPUR, A. K. & SINGH, M. 2007. The taming of the cell penetrating domain of the HIV Tat: myths and realities. *J Control Release,* 117**,** 148-62.

CHO, J., FURIE, B. C., COUGHLIN, S. R. & FURIE, B. 2008. A critical role for extracellular protein disulfide isomerase during thrombus formation in mice. *Journal of Clinical Investigation,* 118**,** 1123-1131.

CHOI, C. K., VICENTE-MANZANARES, M., ZARENO, J., WHITMORE, L. A., MOGILNER, A. & HORWITZ, A. R. 2008. Actin and alpha-actinin orchestrate the assembly and maturation of nascent adhesions in a myosin II motor-independent manner. *Nat Cell Biol,* 10**,** 1039-50.

CHOIDAS, A., JUNGBLUTH, A., SECHI, A., MURPHY, J., ULLRICH, A. & MARRIOTT, G. 1998. The suitability and application of a GFP-actin fusion protein for long-term imaging of the organization and dynamics of the cytoskeleton in mammalian cells. *Eur J Cell Biol,* 77**,** 81-90.

CHUNG, J. W., LEE, K., NEIKIRK, C., NELSON, C. M. & PRIESTLEY, R. D. 2012. Photoresponsive coumarin-stabilized polymeric nanoparticles as a detectable drug carrier. *Small (Weinheim an der Bergstrasse, Germany),* 8**,** 1693-700.

CHUNG, Y. C., CHEN, I. H. & CHEN, C. J. 2008. The surface modification of silver nanoparticles by phosphoryl disulfides for improved biocompatibility and intracellular uptake. *Biomaterials,* 29**,** 1807-1816.

CLEMETSON, K. J. & CLEMETSON, J. M. 2001. Platelet collagen receptors. *Thrombosis and Haemostasis,* 86**,** 189-197.

COBBE, S. M. & POOLE-WILSON, P. A. 1982. Continuous coronary sinus and arterial pH monitoring during pacing-induced ischaemia in coronary artery disease. *Br Heart J,* 47**,** 369-74.

COOPER, G. M. 2000. *The Cell: A Molecular Approach.*, Sinauer Associates.

COOPER, J. A. 1987. Effects of cytochalasin and phalloidin on actin. *J Cell Biol,* 105**,** 1473-8.

CORTESE, K., DIASPRO, A. & TACCHETTI, C. 2009. Advanced correlative light/electron microscopy: current methods and new developments using Tokuyasu cryosections. *J Histochem Cytochem,* 57**,** 1103-12.

COSEN-BINKER, L. I. & KAPUS, A. 2006. Cortactin: the gray eminence of the cytoskeleton. *Physiology (Bethesda),* 21**,** 352-61.

COVIC, L., GRESSER, A. L., TALAVERA, J., SWIFT, S. & KULIOPULOS, A. 2002a. Activation and inhibition of G protein-coupled receptors by cell-penetrating membrane-tethered peptides. *Proc Natl Acad Sci U S A,* 99**,** 643-8.

COVIC, L., MISRA, M., BADAR, J., SINGH, C. & KULIOPULOS, A. 2002b. Pepducin-based intervention of thrombin-receptor signaling and systemic platelet activation. *Nat Med,* 8**,** 1161-5.

COX, S., ROSTEN, E., MONYPENNY, J., JOVANOVIC-TALISMAN, T., BURNETTE, D. T., LIPPINCOTT-SCHWARTZ, J., JONES, G. E. & HEINTZMANN, R. 2012. Bayesian localization microscopy reveals nanoscale podosome dynamics. *Nat Methods,* 9**,** 195-200.

CRAMER, L. P., SIEBERT, M. & MITCHISON, T. J. 1997. Identification of novel graded polarity actin filament bundles in locomoting heart fibroblasts: implications for the generation of motile force. *J Cell Biol,* 136**,** 1287-305.

CURTIS, A. S. G. 1964. Mechanism of adhesion of cells to glass - Study by interference reflection microscopy. *Journal of Cell Biology,* 20**,** 199-&.

DASARY, S. S. R., RAI, U. S., YU, H. T., ANJANEYULU, Y., DUBEY, M. & RAY, P. C. 2008. Gold nanoparticle based surface enhanced fluorescence for detection of organophosphorus agents. *Chemical Physics Letters,* 460**,** 187-190.

DAUMAR, P., WANGER-BAUMANN, C., PILLARSETTY, N., FABRIZIO, L. A., CARLIN, S. D., RESHETNYAK, Y. K., ANDREEV, O. A. & LEWIS, J. S. 2012. Efficient [18F]-Labeling of Large 37-Amino Acid pHLIP Peptide Analogues and their Biological Evaluation. *Bioconjugate Chemistry*.

DAVID, T., OHLMANN, P., ECKLY, A., MOOG, S., CAZENAVE, J. P., GACHET, C. & LANZA, F. 2006. Inhibition of adhesive and signaling functions of the platelet GPIb-V-IX complex by a cell penetrating GPIbalpha peptide. *J Thromb Haemost,* 4**,** 2645-55.

DAVIES, A., LEWIS, D. J., WATSON, S. P., THOMAS, S. G. & PIKRAMENOU, Z. 2012. pH-controlled delivery of luminescent europium coated nanoparticles into platelets. *Proceedings of the National Academy of Sciences,* 109**,** 1862-1867.

DEIBLER, M., SPATZ, J. P. & KEMKEMER, R. 2011. Actin Fusion Proteins Alter the Dynamics of Mechanically Induced Cytoskeleton Rearrangement. *Plos One,* 6**,** 5.

DERFUS, A. M., CHAN, W. C. W. & BHATIA, S. N. 2004. Intracellular delivery of quantum dots for live cell labeling and organelle tracking. *Advanced Materials,* 16**,** 961-+.

DEROSSI, D., JOLIOT, A. H., CHASSAING, G. & PROCHIANTZ, A. 1994. The third helix of the Antennapedia homeodomain translocates through biological membranes. *J Biol Chem,* 269**,** 10444-50.

DIMITRIOU, A. A., STATHOPOULOS, P., MITSIOS, J. V., SAKARELLOS-DAITSIOTIS, M., GOUDEVENOS, J., TSIKARIS, V. & TSELEPIS, A. D. 2009. Inhibition of platelet activation by peptide analogs of the beta(3)-intracellular domain of platelet integrin alpha(IIb)beta(3) conjugated to the cell-penetrating peptide Tat(48-60). *Platelets,* 20**,** 539-47.

DOBROVOLSKAIA, M. A., PATRI, A. K., SIMAK, J., HALL, J. B., SEMBEROVA, J., DE PAOLI LACERDA, S. H. & MCNEIL, S. E. 2012. Nanoparticle size and surface charge determine effects of PAMAM dendrimers on human platelets in vitro. *Mol Pharm,* 9**,** 382-93.

DOS REMEDIOS, C. G., CHHABRA, D., KEKIC, M., DEDOVA, I. V., TSUBAKIHARA, M., BERRY, D. A. & NOSWORTHY, N. J. 2003. Actin binding proteins: Regulation of cytoskeletal microfilaments. *Physiological Reviews,* 83**,** 433-473.

EDWARDS, K. A., DEMSKY, M., MONTAGUE, R. A., WEYMOUTH, N. & KIEHART, D. P. 1997. GFP-moesin illuminates actin cytoskeleton dynamics in living tissue and demonstrates cell shape changes during morphogenesis in Drosophila. *Developmental Biology,* 191**,** 103-117.

ERA, A., TOMINAGA, M., EBINE, K., AWAI, C., SAITO, C., ISHIZAKI, K., YAMATO, K. T., KOHCHI, T., NAKANO, A. & UEDA, T. 2009. Application of Lifeact reveals F-actin dynamics in Arabidopsis thaliana and the liverwort, Marchantia polymorpha. *Plant and Cell Physiology***,** pcp055.

ERNI, R., ROSSELL, M. D., KISIELOWSKI, C. & DAHMEN, U. 2009. Atomic-Resolution Imaging with a Sub-50-pm Electron Probe. *Physical Review Letters,* 102**,** 4.

ESSEX, D. W., CHEN, K. & SWIATKOWSKA, M. 1995. LOCALIZATION OF PROTEIN DISULFIDE-ISOMERASE TO THE EXTERNAL SURFACE OF THE PLATELET PLASMA-MEMBRANE. *Blood,* 86**,** 2168-2173.

EVANS, C. W., RASTON, C. L. & IYER, K. S. 2010. Nanosized luminescent superparamagnetic hybrids. *Green Chemistry,* 12**,** 1175-1179.

FAIX, J. & ROTTNER, K. 2006. The making of filopodia. *Current Opinion in Cell Biology,* 18**,** 18-25.

FALET, H., HOFFMEISTER, K. M., NEUJAHR, R. & HARTWIG, J. H. 2002. Normal Arp2/3 complex activation in platelets lacking WASp. *Blood,* 100**,** 2113-22.

FAN, Z. L. & JIN, W. R. 2007. A method for visualization of biomolecules labeled by a single quantum dot in living cells by a combination of total internal reflection fluorescence microscopy and intracellular fluorescence microscopy. *Talanta,* 72**,** 1114-1122.

FAULSTICH, H., SCHAFER, A. J. & WECKAUF, M. 1977. The dissociation of the phalloidin-actin complex. *Hoppe Seylers Z Physiol Chem,* 358**,** 181-4.

FENG, Z. Q., CHEN, W. N., LEE, P. V. S., LIAO, K. & CHAN, V. 2005. The influence of GFP-actin expression on the adhesion dynamics of HepG2 cells on a model extracellular matrix. *Biomaterials,* 26**,** 5348-5358.

FILLER, T. J. & PEUKER, E. T. 2000. Reflection contrast microscopy (RCM): a forgotten technique? *Journal of Pathology,* 190**,** 635-638.

FLAUMENHAFT, R. 2004. Platelet permeabilization. *In:* GIBBINS, J. M. & MAHAUT-SMITH, M. P. (eds.) *Methods Mol Biol.* 2004/08/17 ed.: Humana Press.

FOX, J. E. B. 2001. Cytoskeletal proteins and platelet signaling. *Thrombosis and Haemostasis,* 86**,** 198-213.

FRENS, G. 1973. Controlled nucleation for the regulation of the particle size in monodisperse gold suspensions. *Nature,* 241**,** 20-22.

FURUKAWA, R., MASELLI, A., THOMSON, S. A. M., LIM, R. W. L., STOKES, J. V. & FECHHEIMER, M. 2003. Calcium regulation of actin crosslinking is important for function of the actin cytoskeleton in Dictyostelium. *Journal of Cell Science,* 116**,** 187-196.

FUTAKI, S., NAKASE, I., TACLOKORO, A., TAKEUCHI, T. & JONES, A. T. 2007. Arginine-rich peptides and their internalization mechanisms. *Biochemical Society Transactions,* 35**,** 784-787.

GAO, G., CHEN, L., DONG, B., GU, H., DONG, H., PAN, Y., GAO, Y. & CHEN, X. 2009. RhoA effector mDia1 is required for PI 3-kinase-dependent actin remodeling and spreading by thrombin in platelets. *Biochem Biophys Res Commun,* 385**,** 439-44.

GAO, X. H., CUI, Y. Y., LEVENSON, R. M., CHUNG, L. W. K. & NIE, S. M. 2004. In vivo cancer targeting and imaging with semiconductor quantum dots. *Nature Biotechnology,* 22**,** 969-976.

GAWDEN-BONE, C., ZHOU, Z., KING, E., PRESCOTT, A., WATTS, C. & LUCOCQ, J. 2010. Dendritic cell podosomes are protrusive and invade the extracellular matrix using metalloproteinase MMP-14. *J Cell Sci,* 123**,** 1427-37.

GHOSH, P., YANG, X. C., ARVIZO, R., ZHU, Z. J., AGASTI, S. S., MO, Z. H. & ROTELLO, V. M. 2010. Intracellular Delivery of a Membrane-Impermeable Enzyme in Active Form Using Functionalized Gold Nanoparticles. *Journal of the American Chemical Society,* 132**,** 2642-2645.

GODIN, L. M., VERGEN, J., PRAKASH, Y. S., PAGANO, R. E. & HUBMAYR, R. D. 2011. Spatiotemporal dynamics of actin remodeling and endomembrane trafficking in

alveolar epithelial type I cell wound healing. *American Journal of Physiology-Lung Cellular and Molecular Physiology,* 300**,** L615-L623.

GOGGS, R., SAVAGE, J. S., MELLOR, H. & POOLE, A. W. 2013. The small GTPase Rif is dispensable for platelet filopodia generation in mice. *Plos One,* 8**,** e54663.

GOH, W. I., SUDHAHARAN, T., LIM, K. B., SEM, K. P., LAU, C. L. & AHMED, S. 2011. Rif-mDia1 interaction is involved in filopodium formation independent of Cdc42 and Rac effectors. *J Biol Chem,* 286**,** 13681-94.

GOUTAYER, M., DUFORT, S., JOSSERAND, V., ROYERE, A., HEINRICH, E., VINET, F., BIBETTE, J., COLL, J. L. & TEXIER, I. 2010. Tumor targeting of functionalized lipid nanoparticles: Assessment by in vivo fluorescence imaging. *European Journal of Pharmaceutics and Biopharmaceutics,* 75**,** 137-147.

GRABAR, K. C., FREEMAN, R. G., HOMMER, M. B. & NATAN, M. J. 1995. PREPARATION AND CHARACTERIZATION OF AU COLLOID MONOLAYERS. *Analytical Chemistry,* 67**,** 735-743.

GROSS, B. S., WILDE, J. I., QUEK, L., CHAPEL, H., NELSON, D. L. & WATSON, S. P. 1999. Regulation and Function of WASp in Platelets by the Collagen Receptor, Glycoprotein VI. *Blood,* 94**,** 4166-4176.

GUO, L. & GAI, F. 2010. Heterogeneous Diffusion of a Membrane-Bound pHLIP Peptide. *Biophysical Journal,* 98**,** 2914-2922.

HALEY, B. & FRENKEL, E. 2008. Nanoparticles for drug delivery in cancer treatment. *Urol Oncol,* 26**,** 57-64.

HALL, A. 1994. SMALL GTP-BINDING PROTEINS AND THE REGULATION OF THE ACTIN CYTOSKELETON. *Annual Review of Cell Biology,* 10**,** 31-54.

HALLETT, A. J., CHRISTIAN, P., JONES, J. E. & POPE, S. J. A. 2009. Luminescent, water-soluble gold nanoparticles functionalised with (MLCT)-M-3 emitting rhenium complexes. *Chemical Communications***,** 4278-4280.

HAN, G., CHARI, N. S., VERMA, A., HONG, R., MARTIN, C. T. & ROTELLO, V. M. 2005. Controlled recovery of the transcription of nanoparticle-bound DNA by intracellular concentrations of glutathione. *Bioconjugate Chemistry,* 16**,** 1356-1359.

HARTWIG, J. & ITALIANO, J., JR. 2003. The birth of the platelet. *J Thromb Haemost,* 1**,** 1580-6.

HARTWIG, J. H. 1992. Mechanisms of actin rearrangements mediating platelet activation. *The Journal of Cell Biology,* 118**,** 1421-1442.

HARTWIG, J. H. & ITALIANO, J. J. E. 2006. Cytoskeletal mechanisms for platelet production. *Blood Cells, Molecules, and Diseases,* 36**,** 99-103.

HARTWIG, J. H. & KWIATKOWSKI, D. J. 1991. Actin-binding proteins. *Curr Opin Cell Biol,* 3**,** 87-97.

HESSA, T., KIM, H., BIHLMAIER, K., LUNDIN, C., BOEKEL, J., ANDERSSON, H., NILSSON, I., WHITE, S. H. & VON HEIJNE, G. 2005. Recognition of transmembrane helices by the endoplasmic reticulum translocon. *Nature,* 433**,** 377-81.

HOLBROOK, L. M., WATKINS, N. A., SIMMONDS, A. D., JONES, C. I., OUWEHAND, W. H. & GIBBINS, J. M. 2010. Platelets release novel thiol isomerase enzymes which are recruited to the cell surface following activation. *British Journal of Haematology,* 148**,** 627-637.

HONG, R., HAN, G., FERNANDEZ, J. M., KIM, B. J., FORBES, N. S. & ROTELLO, V. M. 2006. Glutathione-mediated delivery and release using monolayer protected nanoparticle carriers. *Journal of the American Chemical Society,* 128**,** 1078-1079.

HOON, J. L., WONG, W. K. & KOH, C. G. 2012. Functions and regulation of circular dorsal ruffles. *Mol Cell Biol,* 32**,** 4246-57.

HUNT, J. F., EARNEST, T. N., BOUSCHE, O., KALGHATGI, K., REILLY, K., HORVATH, C., ROTHSCHILD, K. J. & ENGELMAN, D. M. 1997a. A biophysical study of integral membrane protein folding. *Biochemistry,* 36**,** 15156-15176.

HUNT, J. F., RATH, P., ROTHSCHILD, K. J. & ENGELMAN, D. M. 1997b. Spontaneous, pH-dependent membrane insertion of a transbilayer alpha-helix. *Biochemistry,* 36**,** 15177-15192.

HYNES, R. O. 2002. Integrins: bidirectional, allosteric signaling machines. *Cell,* 110**,** 673-87.

IBARRA, N., POLLITT, A. & INSALL, R. H. 2005. Regulation of actin assembly by SCAR/WAVE proteins. *Biochem Soc Trans,* 33**,** 1243-6.

ILINSKAYA, A. N. & DOBROVOLSKAIA, M. A. 2013a. Nanoparticles and the blood coagulation system. Part I: benefits of nanotechnology. *Nanomedicine (Lond),* 8**,** 773-84.

ILINSKAYA, A. N. & DOBROVOLSKAIA, M. A. 2013b. Nanoparticles and the blood coagulation system. Part II: safety concerns. *Nanomedicine (Lond),* 8**,** 969-81.

ISENBERG, G., AEBI, U. & POLLARD, T. D. 1980. An actin-binding protein from Acanthamoeba regulates actin filament polymerization and interactions. *Nature,* 288**,** 455-9.

JACCOB, M., RAJARAMAN, G. & TOTTI, F. 2012. On the kinetics and thermodynamics of S-X (X = H, CH3, SCH3, COCH3, and CN) cleavage in the formation of self-assembled monolayers of alkylthiols on Au(111). *Theoretical Chemistry Accounts,* 131**,** 11.

JOHANSSON, P. I., SORENSEN, A. M., PERNER, A., WELLING, K. L., WANSCHER, M., LARSEN, C. F. & OSTROWSKI, S. R. 2012. High sCD40L levels early after trauma are associated with enhanced shock, sympathoadrenal activation, tissue and endothelial damage, coagulopathy and mortality. *J Thromb Haemost,* 10**,** 207-16.

JONES, A. T. & SAYERS, E. J. 2012. Cell entry of cell penetrating peptides: tales of tails wagging dogs. *Journal of Controlled Release,* 161**,** 582-591.

JORDAN, P. A. & GIBBINS, J. M. 2006. Extracellular disulfide exchange and the regulation of cellular function. *Antioxidants & Redox Signaling,* 8**,** 312-324.

JURASZ, P., ALONSO-ESCOLANO, D. & RADOMSKI, M. W. 2004. Platelet--cancer interactions: mechanisms and pharmacology of tumour cell-induced platelet aggregation. *Br J Pharmacol,* 143**,** 819-26.

KAH, J. C. Y., OLIVO, M. C., LEE, C. G. L. & SHEPPARD, C. J. R. 2008. Molecular contrast of EGFR expression using gold nanoparticles as a reflectance-based imaging probe. *Molecular and Cellular Probes,* 22**,** 14-23.

KAHNER, B. N., KATO, H., BANNO, A., GINSBERG, M. H., SHATTIL, S. J. & YE, F. 2012. Kindlins, integrin activation and the regulation of talin recruitment to alphaIIbbeta3. *Plos One,* 7**,** e34056.

KAHR, W. H. A. 2009. Granules and thrombus formation. *Blood,* 114**,** 932-933.

KANCHANAWONG, P., SHTENGEL, G., PASAPERA, A. M., RAMKO, E. B., DAVIDSON, M. W., HESS, H. F. & WATERMAN, C. M. 2010. Nanoscale architecture of integrin-based cell adhesions. *Nature,* 468**,** 580-4.

KARABADZHAK, A. G., WEERAKKODY, D., WIJESINGHE, D., THAKUR, M. S., ENGELMAN, D. M., ANDREEV, O. A., MARKIN, V. S. & RESHETNYAK, Y. K.

2012. Modulation of the pHLIP Transmembrane Helix Insertion Pathway. *Biophysical Journal,* 102**,** 1846-1855.

KARAKOSE, E., SCHILLER, H. B. & FASSLER, R. 2010. The kindlins at a glance. *J Cell Sci,* 123**,** 2353-6.

KASIRER-FRIEDE, A., RUGGERI, Z. M. & SHATTIL, S. J. 2010. Role for ADAP in shear flow-induced platelet mechanotransduction. *Blood,* 115**,** 2274-2282.

KATOH, K., KANO, Y., AMANO, M., ONISHI, H., KAIBUCHI, K. & FUJIWARA, K. 2001. Rho-kinase--mediated contraction of isolated stress fibers. *J Cell Biol,* 153**,** 569-84.

KELLUM, J. A., SONG, M. & LI, J. 2004. Science review: extracellular acidosis and the immune response: clinical and physiologic implications. *Crit Care,* 8**,** 331-6.

KIEFFER, N., GUICHARD, J. & BRETON-GORIUS, J. 1992. Dynamic redistribution of major platelet surface receptors after contact-induced platelet activation and spreading. An immunoelectron microscopy study. *Am J Pathol,* 140**,** 57-73.

KIELIAN, M. & JUNGERWIRTH, S. 1990. Mechanisms of enveloped virus entry into cells. *Mol Biol Med,* 7**,** 17-31.

KIMLING, J., MAIER, M., OKENVE, B., KOTAIDIS, V., BALLOT, H. & PLECH, A. 2006. Turkevich method for gold nanoparticle synthesis revisited. *Journal of Physical Chemistry B,* 110**,** 15700-15707.

KOBSAR, A. & EIGENTHALER, M. 2006. The Cytoskeleton of the Platelet. *In:* BITTAR, E. E. & SEEMA, K. (eds.) *Advances in Molecular and Cell Biology.* Elsevier.

KUMAR, S., GANDHI, K. S. & KUMAR, R. 2007. Modeling of formation of gold nanoparticles by citrate method. *Industrial & Engineering Chemistry Research,* 46**,** 3128-3136.

LACERDA, S. H., SEMBEROVA, J., HOLADA, K., SIMAKOVA, O., HUDSON, S. D. & SIMAK, J. 2011. Carbon nanotubes activate store-operated calcium entry in human blood platelets. *ACS Nano,* 5**,** 5808-13.

LEE, D., FONG, K. P., KING, M. R., BRASS, L. F. & HAMMER, D. A. 2012. Differential Dynamics of Platelet Contact and Spreading. *Biophysical Journal,* 102**,** 472-482.

LEE, D. W., WU, X., EISENBERG, E. & GREENE, L. E. 2006. Recruitment dynamics of GAK and auxilin to clathrin-coated pits during endocytosis. *J Cell Sci,* 119**,** 3502-12.

LEE, J. S., GREEN, J. J., LOVE, K. T., SUNSHINE, J., LANGER, R. & ANDERSON, D. G. 2009. Gold, Poly(beta-amino ester) Nanoparticles for Small Interfering RNA Delivery. *Nano Letters,* 9**,** 2402-2406.

LENG, L., KASHIWAGI, H., REN, X. D. & SHATTIL, S. J. 1998. RhoA and the function of platelet integrin alphaIIbbeta3. *Blood,* 91**,** 4206-15.

LEROUEIL, P. R., BERRY, S. A., DUTHIE, K., HAN, G., ROTELLO, V. M., MCNERNY, D. Q., BAKER, J. R., JR., ORR, B. G. & HOLL, M. M. 2008. Wide varieties of cationic nanoparticles induce defects in supported lipid bilayers. *Nano Lett,* 8**,** 420-4.

LEVY, R., THANH, N. T. K., DOTY, R. C., HUSSAIN, I., NICHOLS, R. J., SCHIFFRIN, D. J., BRUST, M. & FERNIG, D. G. 2004. Rational and combinatorial design of peptide capping Ligands for gold nanoparticles. *Journal of the American Chemical Society,* 126**,** 10076-10084.

LEWIS, D. J., BRUCE, C., BOHIC, S., CLOETENS, P., HAMMOND, S. P., ARBON, D., BLAIR-REID, S., PIKRAMENOU, Z. & KYSELA, B. 2010. Intracellular synchrotron nanoimaging and DNA damage/genotoxicity screening of novel lanthanide-coated nanovectors. *Nanomedicine,* 5**,** 1547-1557.

LEWIS, D. J., DAY, T. M., MACPHERSON, J. V. & PIKRAMENOU, Z. 2006. Luminescent nanobeads: attachment of surface reactive Eu(III) complexes to gold nanoparticles. *Chemical Communications***,** 1433-1435.

LEWIS, D. J., MORETTA, F. & PIKRAMENOU, Z. 2012. Controlled assembly of heterometallic lanthanide(III) macrocycles: incorporation of photoactive and highly paramagnetic metal centres within a single complex. *Supramolecular Chemistry,* 24**,** 135-142.

LEWIS, J. C., HANTGAN, R. R., STEVENSON, S. C., THORNBURG, T., KIEFFER, N., GUICHARD, J. & BRETON-GORIUS, J. 1990. Fibrinogen and glycoprotein IIb/IIIa localization during platelet adhesion. Localization to the granulomere and at sites of platelet interaction. *Am J Pathol,* 136**,** 239-52.

LI, H. B., GUO, F. L., RUBINSTEIN, B. & LI, R. 2008. Actin-driven chromosomal motility leads to symmetry breaking in mammalian meiotic oocytes. *Nature Cell Biology,* 10**,** 1301-U101.

LI, N., YIN, L., THEVENIN, D., YAMADA, Y., LIMMON, G., CHEN, J. Z., CHOW, V. T. K., ENGELMAN, D. M. & ENGELWARD, B. P. 2013. Peptide targeting and imaging of damaged lung tissue in influenza-infected mice. *Future Microbiology,* 8**,** 257-269.

LI, X., WANG, J., SUN, L. & WANG, Z. 2010a. Gold nanoparticle-based colorimetric assay for selective detection of aluminium cation on living cellular surfaces. *Chem. Commun.,* 46**,** 988-990.

LI, X. K., WANG, J. N., SUN, L. L. & WANG, Z. X. 2010b. Gold nanoparticle-based colorimetric assay for selective detection of aluminium cation on living cellular surfaces. *Chemical Communications,* 46**,** 988-990.

LIANG, M., LIN, I. C., WHITTAKER, M. R., MINCHIN, R. F., MONTEIRO, M. J. & TOTH, I. 2010. Cellular Uptake of Densely Packed Polymer Coatings on Gold Nanoparticles. *ACS Nano,* 4**,** 403-413.

LIMOZIN, L. & SENGUPTA, K. 2009. Quantitative reflection interference contrast microscopy (RICM) in soft matter and cell adhesion. *Chemphyschem,* 10**,** 2752-68.

LIN, J., ZHANG, H., CHEN, Z. & ZHENG, Y. 2010. Penetration of lipid membranes by gold nanoparticles: insights into cellular uptake, cytotoxicity, and their relationship. *ACS Nano,* 4**,** 5421-9.

LIN, J. H. 2008. Applications and limitations of genetically modified mouse models in drug discovery and development. *Curr Drug Metab,* 9**,** 419-38.

LINDER, S. 2007. The matrix corroded: podosomes and invadopodia in extracellular matrix degradation. *Trends Cell Biol,* 17**,** 107-17.

LINDER, S. & AEPFELBACHER, M. 2003. Podosomes: adhesion hot-spots of invasive cells. *Trends in Cell Biology,* 13**,** 376-385.

LINDER, S. & KOPP, P. 2005. Podosomes at a glance. *Journal of Cell Science,* 118**,** 2079-2082.

LINDER, S., WIESNER, C. & HIMMEL, M. 2011. Degrading devices: invadosomes in proteolytic cell invasion. *Annu Rev Cell Dev Biol,* 27**,** 185-211.

LIU, B. R., LO, S. Y., LIU, C. C., CHYAN, C. L., HUANG, Y. W., ARONSTAM, R. S. & LEE, H. J. 2013. Endocytic Trafficking of Nanoparticles Delivered by Cell-penetrating Peptides Comprised of Nona-arginine and a Penetration Accelerating Sequence. *Plos One,* 8**,** e67100.

LIU, W., HOWARTH, M., GREYTAK, A. B., ZHENG, Y., NOCERA, D. G., TING, A. Y. & BAWENDI, M. G. 2008. Compact biocompatible quantum dots functionalized for cellular imaging *J. Am. Chem. Soc.,* 130**,** 1274-1284.

LIZARRAGA, F., POINCLOUX, R., ROMAO, M., MONTAGNAC, G., LE DEZ, G., BONNE, I., RIGAILL, G., RAPOSO, G. & CHAVRIER, P. 2009. Diaphanous-Related Formins Are Required for Invadopodia Formation and Invasion of Breast Tumor Cells. *Cancer Research,* 69**,** 2792-2800.

LOFTUS, J. C., CHOATE, J. & ALBRECHT, R. M. 1984. PLATELET ACTIVATION AND CYTOSKELETAL REORGANIZATION - HIGH-VOLTAGE ELECTRON-MICROSCOPIC EXAMINATION OF INTACT AND TRITON-EXTRACTED WHOLE MOUNTS. *Journal of Cell Biology,* 98**,** 2019-2025.

LUNDBERG, P. & LANGEL, U. 2003. A brief introduction to cell-penetrating peptides. *J Mol Recognit,* 16**,** 227-33.

MACHOLL, S., MORRISON, M. S., IVESON, P., ARBO, B. E., ANDREEV, O. A., RESHETNYAK, Y. K., ENGELMAN, D. M. & JOHANNESEN, E. 2012. In Vivo pH Imaging with Tc-99m-pHLIP. *Molecular Imaging and Biology,* 14**,** 725-734.

MAEDA, H., NAKAMURA, H. & FANG, J. 2013. The EPR effect for macromolecular drug delivery to solid tumors: Improvement of tumor uptake, lowering of systemic toxicity, and distinct tumor imaging in vivo. *Adv Drug Deliv Rev,* 65**,** 71-9.

MANICKAM, N., SUN, X. H., LI, M. R., GAZITT, Y. & ESSEX, D. W. 2008. Protein disulphide isomerase in platelet function. *British Journal of Haematology,* 140**,** 223-229.

MARCHISIO, P. C., CIRILLO, D., NALDINI, L., PRIMAVERA, M. V., TETI, A. & ZAMBONIN-ZALLONE, A. 1984. Cell-substratum interaction of cultured avian osteoclasts is mediated by specific adhesion structures. *J Cell Biol,* 99**,** 1696-705.

MARUYAMA, K. 2011. Intracellular targeting delivery of liposomal drugs to solid tumors based on EPR effects. *Adv Drug Deliv Rev,* 63**,** 161-9.

MATA, J. E., DYAL, L. A., SLAUSON, M. E., SUMMERTON, J. E., LOEHR, C., TYSON, A. R., RODRIGUEZ-PROTEAU, R. & GUSTAFSON, S. B. 2007. Tumor imaging using technetium-99m bound to pH-sensitive peptides. *Nanomedicine-Nanotechnology Biology and Medicine,* 3**,** 297-305.

MATTILA, P. K. & LAPPALAINEN, P. 2008. Filopodia: molecular architecture and cellular functions. *Nat Rev Mol Cell Biol,* 9**,** 446-54.

MCCARTY, O. J. T., LARSON, M. K., AUGER, J. M., KALIA, N., ATKINSON, B. T., PEARCE, A. C., RUF, S., HENDERSON, R. B., TYBULEWICZ, V. L. J., MACHESKY, L. M. & WATSON, S. P. 2005. Rac1 is essential for platelet Lamellipodia formation and aggregate stability under flow. *Journal of Biological Chemistry,* 280**,** 39474-39484.

MCNEIL, P. L., MURPHY, R. F., LANNI, F. & TAYLOR, D. L. 1984. A method for incorporating macromolecules into adherent cells. *J Cell Biol,* 98**,** 1556-64.

MELLOR, H. 2010. The role of formins in filopodia formation. *Biochim Biophys Acta,* 1803**,** 191-200.

MERRIFIELD, C. J., FELDMAN, M. E., WAN, L. & ALMERS, W. 2002. Imaging actin and dynamin recruitment during invagination of single clathrin-coated pits. *Nat Cell Biol,* 4**,** 691-8.

MILLIS, B. A. 2012. Evanescent-wave field imaging: an introduction to total internal reflection fluorescence microscopy. *Methods Mol Biol,* 823**,** 295-309.

MITSIOS, J. V., PREVOST, N., KASIRER-FRIEDE, A., GUTIERREZ, E., GROISMAN, A., ABRAMS, C. S., WANG, Y., LITVINOV, R. I., ZEMLJIC-HARPF, A., ROSS, R. S. & SHATTIL, S. J. 2010. What is vinculin needed for in platelets? *J Thromb Haemost,* 8**,** 2294-304.

MONTGOMERY, C. P., MURRAY, B. S., NEW, E. J., PAL, R. & PARKER, D. 2009. Cell-Penetrating Metal Complex Optical Probes: Targeted and Responsive Systems Based on Lanthanide Luminescence. *Accounts of Chemical Research,* 42**,** 925-937.

MOORE, E. G., SAMUEL, A. P. S. & RAYMOND, K. N. 2009. From Antenna to Assay: Lessons Learned in Lanthanide Luminescence. *Acc. Chem. Res.,* 42**,** 542-552.

MORI, J., WANG, Y. J., ELLISON, S., HEISING, S., NEEL, B. G., TREMBLAY, M. L., WATSON, S. P. & SENIS, Y. A. 2012. Dominant Role of the Protein-Tyrosine Phosphatase CD 148 in Regulating Platelet Activation Relative to Protein-Tyrosine Phosphatase-1B. *Arteriosclerosis Thrombosis and Vascular Biology,* 32**,** 2956-+.

MOSER, M., NIESWANDT, B., USSAR, S., POZGAJOVA, M. & FASSLER, R. 2008. Kindlin-3 is essential for integrin activation and platelet aggregation. *Nat Med,* 14**,** 325-30.

MOSHNIKOVA, A., MOSHNIKOVA, V., ANDREEV, O. A. & RESHETNYAK, Y. K. 2013. Antiproliferative Effect of pHLIP-Amanitin. *Biochemistry,* 52**,** 1171-1178.

MOULTON, H. M., FLETCHER, S., NEUMAN, B. W., MCCLOREY, G., STEIN, D. A., ABES, S., WILTON, S. D., BUCHMEIER, M. J., LEBLEU, B. & IVERSEN, P. L. 2007. Cell-penetrating peptide-morpholino conjugates alter pre-mRNA splicing of

DMD (Duchenne muscular dystrophy) and inhibit murine coronavirus replication in vivo. *Biochemical Society Transactions,* 35**,** 826-828.

MÜHLPFORDT, H. 1982. The preparation of colloidal gold particles using tannic acid as an additional reducing agent. *Experientia,* 38**,** 1127-1128.

MUNSIE, L. N., CARON, N., DESMOND, C. R. & TRUANT, R. 2009. Lifeact cannot visualize some forms of stress-induced twisted f-actin. *Nature Methods,* 6**,** 317-317.

MUSIAL-SIWEK, M., KARABADZHAK, A., ANDREEV, O. A., RESHETNYAK, Y. K. & ENGELMAN, D. M. 2010. Tuning the insertion properties of pHLIP. *Biochimica Et Biophysica Acta-Biomembranes,* 1798**,** 1041-1046.

NAGHAVI, M., JOHN, R., NAGUIB, S., SIADATY, M. S., GRASU, R., KURIAN, K. C., VAN WINKLE, W. B., SOLLER, B., LITOVSKY, S., MADJID, M., WILLERSON, J. T. & CASSCELLS, W. 2002. pH Heterogeneity of human and rabbit atherosclerotic plaques; a new insight into detection of vulnerable plaque. *Atherosclerosis,* 164**,** 27-35.

NARITA, A., TAKEDA, S., YAMASHITA, A. & MAEDA, Y. 2006. Structural basis of actin filament capping at the barbed-end: a cryo-electron microscopy study. *EMBO J,* 25**,** 5626-33.

NATIVO, P., PRIOR, I. A. & BRUST, M. 2008. Uptake and intracellular fate of surface-modified gold nanoparticles. *ACS Nano,* 2**,** 1639-1644.

NIESWANDT, B. & WATSON, S. P. 2003. Platelet-collagen interaction: is GPVI the central receptor? *Blood,* 102**,** 449-61.

OKABE, M., IKAWA, M., KOMINAMI, K., NAKANISHI, T. & NISHIMUNE, Y. 1997. 'Green mice' as a source of ubiquitous green cells. *Febs Letters,* 407**,** 313-319.

OKAMURA, Y., SCHMIDT, R., RASCHKE, I., HINTZE, M., TAKEOKA, S., EGNER, A. & LANG, T. 2011. A few immobilized thrombins are sufficient for platelet spreading. *Biophys J,* 100**,** 1855-63.

OLORUNDARE, O. E., SIMMONS, S. R. & ALBRECHT, R. M. 1992. Cytochalasin D and E: effects on fibrinogen receptor movement and cytoskeletal reorganization in fully spread, surface-activated platelets: a correlative light and electron microscopic investigation. *Blood,* 79**,** 99-109.

PANCHUK-VOLOSHINA, N., HAUGLAND, R. P., BISHOP-STEWART, J., BHALGAT, M. K., MILLARD, P. J., MAO, F. & LEUNG, W. Y. 1999. Alexa dyes, a series of new fluorescent dyes that yield exceptionally bright, photostable conjugates. *J Histochem Cytochem,* 47**,** 1179-88.

PANG, K. M., LEE, E. & KNECHT, D. A. 1998. Use of a fusion protein between GFP and an actin-binding domain to visualize transient filamentous-actin structures. *Curr Biol,* 8**,** 405-8.

PAULROTH, C. & RAYMOND, K. N. 1995. Amide functional-group contribution to the stability of Gadolinium(III) complexes - DTPA derivatives. *Inorganic Chemistry,* 34**,** 1408-1412.

PELLEGRIN, S. & MELLOR, H. 2007. Actin stress fibres. *J Cell Sci,* 120**,** 3491-9.

PETERSON, L. J., RAJFUR, Z., MADDOX, A. S., FREEL, C. D., CHEN, Y., EDLUND, M., OTEY, C. & BURRIDGE, K. 2004. Simultaneous stretching and contraction of stress fibers in vivo. *Mol Biol Cell,* 15**,** 3497-508.

PHILLIPS, D. R., NANNIZZI-ALAMIO, L. & PRASAD, K. S. S. 2001. beta 3 tyrosine phosphorylation in alpha IIb beta 3 (platelet membrane GP IIb-IIIa) outside-in integrin signaling. *Thrombosis and Haemostasis,* 86**,** 246-258.

PITKEATHLY, W. T., POULTER, N. S., CLARIDGE, E. & RAPPOPORT, J. Z. 2012. Auto-align - multi-modality fluorescence microscopy image co-registration. *Traffic,* 13**,** 204-17.

POOGA, M., HALLBRINK, M., ZORKO, M. & LANGEL, U. 1998. Cell penetration by transportan. *FASEB J,* 12**,** 67-77.

POPOVIC, Z., LIU, W., CHAUHAN, V. P., LEE, J., WONG, C., GREYTAK, A. B., INSIN, N., NOCERA, D. G., FUKUMURA, D., JAIN, R. K. & BAWENDI, M. G. 2010. A Nanoparticle Size Series for In Vivo Fluorescence Imaging. *Angew. Chem. Int. Ed.,* 49**,** 8649-8652.

PRASHER, D. C., ECKENRODE, V. K., WARD, W. W., PRENDERGAST, F. G. & CORMIER, M. J. 1992. Primary structure of the Aequorea victoria green-fluorescent protein. *Gene,* 111**,** 229-33.

PURBHOO, M. A., LIU, H. B., ODDOS, S., OWEN, D. M., NEIL, M. A. A., PAGEON, S. V., FRENCH, P. M. W., RUDD, C. E. & DAVIS, D. M. 2010. Dynamics of Subsynaptic Vesicles and Surface Microclusters at the Immunological Synapse. *Science Signaling,* 3.

PYTELA, R., PIERSCHBACHER, M. D., GINSBERG, M. H., PLOW, E. F. & RUOSLAHTI, E. 1986. Platelet membrane glycoprotein IIb/IIIa: member of a family of Arg-Gly-Asp--specific adhesion receptors. *Science,* 231**,** 1559-62.

RADLER, J. O., FEDER, T. J., STREY, H. H. & SACKMANN, E. 1995. Fluctuation analysis of tension-controlled undulation forces between giant vesicles and solid substrates. *Physical Review E,* 51**,** 4526-4536.

RESHETNYAK, Y. K., ANDREEV, O. A., LEHNERT, U. & ENGELMAN, D. M. 2006. Translocation of molecules into cells by pH-dependent insertion of a transmembrane

helix. *Proceedings of the National Academy of Sciences of the United States of America,* 103**,** 6460-6465.

RESHETNYAK, Y. K., ANDREEV, O. A., SEGALA, M., MARKIN, V. S. & ENGELMAN, D. M. 2008. Energetics of peptide (pHLIP) binding to and folding across a lipid bilayer membrane. *Proceedings of the National Academy of Sciences of the United States of America,* 105**,** 15340-15345.

RESHETNYAK, Y. K., SEGALA, M., ANDREEV, O. A. & ENGELMAN, D. M. 2007. A monomeric membrane peptide that lives in three worlds: In solution, attached to, and inserted across lipid bilayers. *Biophysical Journal,* 93**,** 2363-2372.

RESHETNYAK, Y. K., YAO, L., ZHENG, S., KUZNETSOV, S., ENGELMAN, D. M. & ANDREEV, O. A. 2011. Measuring Tumor Aggressiveness and Targeting Metastatic Lesions with Fluorescent pHLIP. *Molecular Imaging and Biology,* 13**,** 1146-1156.

REUTER, M., SCHWIEGER, C., MEISTER, A., KARLSSON, G. & BLUME, A. 2009. Poly-L-lysines and poly-L-arginines induce leakage of negatively charged phospholipid vesicles and translocate through the lipid bilayer upon electrostatic binding to the membrane. *Biophysical Chemistry,* 144**,** 27-37.

RICHARD, J. P., MELIKOV, K., VIVES, E., RAMOS, C., VERBEURE, B., GAIT, M. J., CHERNOMORDIK, L. V. & LEBLEU, B. 2003. Cell-penetrating peptides - A reevaluation of the mechanism of cellular uptake. *Journal of Biological Chemistry,* 278**,** 585-590.

RIEDL, J. 2011. *Development and Characterization of Lifeact - a versatile marker for the visualization of F-actin.* Dissertation, LMU München: .

RIEDL, J., CREVENNA, A. H., KESSENBROCK, K., YU, J. H., NEUKIRCHEN, D., BISTA, M., BRADKE, F., JENNE, D., HOLAK, T. A., WERB, Z., SIXT, M. &

WEDLICH-SOLDNER, R. 2008. Lifeact: a versatile marker to visualize F-actin. *Nature Methods,* 5**,** 605-607.

RIEDL, J., FLYNN, K. C., RADUCANU, A., GARTNER, F., BECK, G., BOSL, M., BRADKE, F., MASSBERG, S., ASZODI, A., SIXT, M. & WEDLICH-SOLDNER, R. 2010. Lifeact mice for studying F-actin dynamics. *Nature Methods,* 7**,** 168-169.

RIVERA, J., LOZANO, M. L., NAVARRO-NUNEZ, L. & VICENTE, V. 2009. Platelet receptors and signaling in the dynamics of thrombus formation. *Haematologica,* 94**,** 700-11.

ROBINSON, A., O'NEILL, S., KIERNAN, A. S., O'DONOGHUE, N. & MORAN, N. 2006. Bacitracin reveals a role for multiple thiol isomerases in platelet function. *British Journal of Haematology,* 132**,** 339-348.

SAHA, K., BAJAJ, A., DUNCAN, B. & ROTELLO, V. M. 2011. Beauty is Skin Deep: A Surface Monolayer Perspective on Nanoparticle Interactions with Cells and Bio-macromolecules. *Small,* 7**,** 1903-1918.

SARTORI, A., GATZ, R., BECK, F., RIGORT, A., BAUMEISTER, W. & PLITZKO, J. M. 2007. Correlative microscopy: bridging the gap between fluorescence light microscopy and cryo-electron tomography. *J Struct Biol,* 160**,** 135-45.

SAVAGE, A. C. & PIKRAMENOU, Z. 2011. Peptide coated gold nanoparticles that bind lanthanide ions. *Chemical Communications,* 47**,** 6431-6433.

SCHACHTNER, H., CALAMINUS, S. D. J., SINCLAIR, A., MONYPENNY, J., BLUNDELL, M. P., LEON, C., HOLYOAKE, T. L., THRASHER, A. J., MICHIE, A. M., VUKOVIC, M., GACHET, C., JONES, G. E., THOMAS, S. G., WATSON, S. P. & MACHESKY, L. M. 2013. Megakaryocytes assemble podosomes that degrade matrix and protrude through basement membrane. *Blood,* 121**,** 2542-2552.

SCHACHTNER, H., LI, A., STEVENSON, D., CALAMINUS, S. D. J., THOMAS, S. G., WATSON, S. P., SIXT, M., WEDLICH-SOLDNER, R., STRATHDEE, D. & MACHESKY, L. M. 2012. Tissue inducible Lifeact expression allows visualization of actin dynamics in vivo and ex vivo. *European Journal of Cell Biology,* 91**,** 923-929.

SCHMIDT, N., MISHRA, A., LAI, G. H. & WONG, G. C. 2010. Arginine-rich cell-penetrating peptides. *FEBS Lett,* 584**,** 1806-13.

SCHOENWAELDER, S. M., ONO, A., NESBITT, W. S., LIM, J., JARMAN, K. & JACKSON, S. P. 2010. Phosphoinositide 3-Kinase p110 beta Regulates Integrin alpha(IIb)beta(3) Avidity and the Cellular Transmission of Contractile Forces. *Journal of Biological Chemistry,* 285**,** 2886-2896.

SCHOUMACHER, M., GOLDMAN, R. D., LOUVARD, D. & VIGNJEVIC, D. M. 2010. Actin, microtubules, and vimentin intermediate filaments cooperate for elongation of invadopodia. *J Cell Biol,* 189**,** 541-56.

SCHWARZE, S. R., HO, A., VOCERO-AKBANI, A. & DOWDY, S. F. 1999. In vivo protein transduction: delivery of a biologically active protein into the mouse. *Science,* 285**,** 1569-72.

SEGALA, J., ENGELMAN, D. M., RESHETNYAK, Y. K. & ANDREEV, O. A. 2009. Accurate Analysis of Tumor Margins Using a Fluorescent pH Low Insertion Peptide (pHLIP). *International Journal of Molecular Sciences,* 10**,** 3478-3487.

SEMBEROVA, J., DE PAOLI LACERDA, S. H., SIMAKOVA, O., HOLADA, K., GELDERMAN, M. P. & SIMAK, J. 2009. Carbon nanotubes activate blood platelets by inducing extracellular Ca2+ influx sensitive to calcium entry inhibitors. *Nano Lett,* 9**,** 3312-7.

SEVERIN, S., NASH, C. A., MORI, J., ZHAO, Y., ABRAM, C., LOWELL, C. A., SENIS, Y. A. & WATSON, S. P. 2012. Distinct and overlapping functional roles of Src family kinases in mouse platelets. *Journal of Thrombosis and Haemostasis,* 10**,** 1631-1645.

SHIMOMURA, O., JOHNSON, F. H. & SAIGA, Y. 1962. Extraction, Purification and Properties of Aequorin, a Bioluminescent Protein from the Luminous Hydromedusan, Aequorea. *Journal of Cellular and Comparative Physiology,* 59**,** 223-239.

SINGER, V. L. & JOHNSON, I. D. Year. Fluorophore Characteristics: Making Intelligent Choices in Application-Specific Dye Selection. *In:* Eighth International Symposium on Human Identification - 1997, 1997. Promega.

SMALL, J., ROTTNER, K., HAHNE, P. & ANDERSON, K. I. 1999. Visualising the actin cytoskeleton. *Microsc Res Tech,* 47**,** 3-17.

SMITH, A. M., DUAN, H., MOHS, A. M. & NIE, S. 2008. Bioconjugated quantum dots for in vivo molecular and cellular imaging. *Adv. Drug Delivery Rev.,* 60**,** 1226-1240.

SOCOL, M., LEFROU, C., BRUCKERT, F., DELABOUGLISE, D. & WEIDENHAUPT, M. 2010. Synchronization of Dictyostelium discoideum adhesion and spreading using electrostatic forces. *Bioelectrochemistry,* 79**,** 198-210.

SOSUNOV, E. A., ANYUKHOVSKY, E. P., SOSUNOV, A. A., MOSHNIKOVA, A., WIJESINGHE, D., ENGELMAN, D. M., RESHETNYAK, Y. K. & ANDREEV, O. A. 2013. pH (low) insertion peptide (pHLIP) targets ischemic myocardium. *Proceedings of the National Academy of Sciences,* 110**,** 82-86.

SPENCE, H. J., TIMPSON, P., TANG, H. R., INSALL, R. H. & MACHESKY, L. M. 2012. Scar/WAVE3 contributes to motility and plasticity of lamellipodial dynamics but not invasion in three dimensions. *Biochem J,* 448**,** 35-42.

STEPHENS, D. J. & ALLAN, V. J. 2003. Light microscopy techniques for live cell Imaging. *Science,* 300**,** 82-86.

STUBBS, M., MCSHEEHY, P. M. J., GRIFFITHS, J. R. & BASHFORD, C. L. 2000. Causes and consequences of tumour acidity and implications for treatment. *Molecular Medicine Today,* 6**,** 15-19.

SUETSUGU, S., YAMAZAKI, D., KURISU, S. & TAKENAWA, T. 2003. Differential roles of WAVE1 and WAVE2 in dorsal and peripheral ruffle formation for fibroblast cell migration. *Dev Cell,* 5**,** 595-609.

SURESH, S. 2007. Biomechanics and biophysics of cancer cells. *Acta Biomater,* 3**,** 413-38.

TAKADA, Y., YE, X. & SIMON, S. 2007. The integrins. *Genome Biol,* 8**,** 215.

TAKAGI, S., SATO, S., OH-HARA, T., TAKAMI, M., KOIKE, S., MISHIMA, Y., HATAKE, K. & FUJITA, N. 2013. Platelets Promote Tumor Growth and Metastasis via Direct Interaction between Aggrus/Podoplanin and CLEC-2. *Plos One,* 8**,** e73609.

TANG, Y. Q., YEAMAN, M. R. & SELSTED, M. E. 2002. Antimicrobial peptides from human platelets. *Infect Immun,* 70**,** 6524-33.

THANH, N. T. K. & GREEN, L. A. W. 2010. Functionalisation of nanoparticles for biomedical applications. *Nano Today,* 5**,** 213-230.

THEVENIN, D., AN, M. & ENGELMAN, D. M. 2009. pHLIP-Mediated Translocation of Membrane-Impermeable Molecules into Cells. *Chemistry & Biology,* 16**,** 754-762.

THOMAS, S. G., CALAMINUS, S. D., AUGER, J. M., WATSON, S. P. & MACHESKY, L. M. 2007. Studies on the actin-binding protein HS1 in platelets. *Bmc Cell Biology,* 8**,** 8.

TREUEL, L., JIANG, X. & NIENHAUS, G. U. 2013. New views on cellular uptake and trafficking of manufactured nanoparticles. *J R Soc Interface,* 10**,** 20120939.

TSIEN, R. Y. 1998. The green fluorescent protein. *Annual Review of Biochemistry,* 67**,** 509-544.

TURKEVICH, J., STEVENSON, P. C. & HILLIER, J. 1951. A STUDY OF THE NUCLEATION AND GROWTH PROCESSES IN THE SYNTHESIS OF COLLOIDAL GOLD. *Discussions of the Faraday Society***,** 55-&.

VALLENIUS, T. 2004. *Characterization of actin stress fibers: involvement of PDZ-LIM adapter proteins and the novel Clik1 kinase.* University of Helsinki, Finland.

VAN DER HONING, H. S., VAN BEZOUWEN, L. S., EMONS, A. M. C. & KETELAAR, T. 2011. High expression of Lifeact in Arabidopsis thaliana reduces dynamic reorganization of actin filaments but does not affect plant development. *Cytoskeleton,* 68**,** 578-587.

VANDEKERCKHOVE, J., DEBOBEN, A., NASSAL, M. & WIELAND, T. 1985. The phalloidin binding site of F-actin. *EMBO J,* 4**,** 2815-8.

VARGA-SZABO, D., PLEINES, I. & NIESWANDT, B. 2008. Cell adhesion mechanisms in platelets. *Arteriosclerosis Thrombosis and Vascular Biology,* 28**,** 403-412.

VAVERE, A. L., BIDDLECOMBE, G. B., SPEES, W. M., GARBOW, J. R., WIJESINGHE, D., ANDREEV, O. A., ENGELMAN, D. M., RESHETNYAK, Y. K. & LEWIS, J. S. 2009. A Novel Technology for the Imaging of Acidic Prostate Tumors by Positron Emission Tomography. *Cancer Research,* 69**,** 4510-4516.

VERMA, A., UZUN, O., HU, Y. H., HU, Y., HAN, H. S., WATSON, N., CHEN, S. L., IRVINE, D. J. & STELLACCI, F. 2008. Surface-structure-regulated cell-membrane penetration by monolayer-protected nanoparticles. *Nature Materials,* 7**,** 588-595.

VERSCHUEREN, H. 1985. Interference reflection microscopy in cell biology: methodology and applications. *J Cell Sci,* 75**,** 279-301.

VICIDOMINI, G., GAGLIANI, M. C., CORTESE, K., KRIEGER, J., BUESCHER, P., BIANCHINI, P., BOCCACCI, P., TACCHETTI, C. & DIASPRO, A. 2009. A novel approach for correlative light electron microscopy analysis. *Microscopy Research and Technique,* 9999**,** NA.

VINZENZ, M., NEMETHOVA, M., SCHUR, F., MUELLER, J., NARITA, A., URBAN, E., WINKLER, C., SCHMEISER, C., KOESTLER, S. A., ROTTNER, K., RESCH, G. P., MAEDA, Y. & SMALL, J. V. 2012. Actin branching in the initiation and maintenance of lamellipodia. *Journal of Cell Science,* 125**,** 2775-2785.

WAGNER, C. L., MASCELLI, M. A., NEBLOCK, D. S., WEISMAN, H. F., COLLER, B. S. & JORDAN, R. E. 1996. Analysis of GPIIb/IIIa receptor number by quantification of 7E3 binding to human platelets. *Blood,* 88**,** 907-14.

WANG, J. N., DUAN, T. C., SUN, L. L., LIU, D. J. & WANG, Z. X. 2009. Functional gold nanoparticles for studying the interaction of lectin with glycosyl complex on living cellular surfaces. *Analytical Biochemistry,* 392**,** 77-82.

WANG, N. & SUO, Z. 2005. Long-distance propagation of forces in a cell. *Biochem Biophys Res Commun,* 328**,** 1133-8.

WANG, R. E., COSTANZA, F., NIU, Y., WU, H., HU, Y., HANG, W., SUN, Y. & CAI, J. 2012. Development of self-immolative dendrimers for drug delivery and sensing. *J Control Release,* 159**,** 154-63.

WANG, W., ZOU, M. & CHEN, K. Z. 2010. Novel Fe3O4@YPO4:Re (Re = Tb, Eu) multifunctional magnetic-fluorescent hybrid spheres for biomedical applications. *Chemical Communications,* 46**,** 5100-5102.

WATSON, S. P. & HARRISON, P. 2007. The Vascular Function of Platelets. *In:* A. VICTOR HOFFBRAND, D. C. E. G. D. T. (ed.) *Postgraduate Haematology (Fifth Edition).*

WAX, A. & SOKOLOV, K. 2009. Molecular imaging and darkfield microspectroscopy of live cells using gold plasmonic nanoparticles. *Laser & Photonics Reviews,* 3**,** 146-158.

WEERAKKODY, D., MOSHNIKOVA, A., THAKUR, M. S., MOSHNIKOVA, V., DANIELS, J., ENGELMAN, D. M., ANDREEV, O. A. & RESHETNYAK, Y. K. 2013. Family of pH (low) insertion peptides for tumor targeting. *Proceedings of the National Academy of Sciences of the United States of America,* 110**,** 5834-5839.

WEHLAND, J., OSBORN, M. & WEBER, K. 1977. Phalloidin-induced actin polymerization in the cytoplasm of cultured cells interferes with cell locomotion and growth. *Proc Natl Acad Sci U S A,* 74**,** 5613-7.

WEHLAND, J. & WEBER, K. 1981. Actin rearrangement in living cells revealed by microinjection of a fluorescent phalloidin derivative. *Eur J Cell Biol,* 24**,** 176-83.

WEKSLER, B. B. 1983. Platelets and the inflammatory response. *Clin Lab Med,* 3**,** 667-76.

WESTPHAL, M., JUNGBLUTH, A., HEIDECKER, M., MUHLBAUER, B., HEIZER, C., SCHWARTZ, J. M., MARRIOTT, G. & GERISCH, G. 1997. Microfilament dynamics during cell movement and chemotaxis monitored using a GFP-actin fusion protein. *Curr Biol,* 7**,** 176-83.

WHITE, J. & CLAWSON, C. 1980. The surface-connected canalicular system of blood platelets--a fenestrated membrane system. *Am J Pathol,* 101**,** 353-364.

WIELAND, T., MIURA, T. & SEELIGER, A. 1983. Analogs of phalloidin. D-Abu2-Lys7-phalloin, an F-actin binding analog, its rhodamine conjugate (RLP) a novel fluorescent

F-actin-probe, and D-Ala2-Leu7-phalloin, an inert peptide. *Int J Pept Protein Res,* 21**,** 3-10.

WIJESINGHE, D., ENGELMAN, D. M., ANDREEV, O. A. & RESHETNYAK, Y. K. 2011. Tuning a Polar Molecule for Selective Cytoplasmic Delivery by a pH (Low) Insertion Peptide. *Biochemistry,* 50**,** 10215-10222.

WIWANITKIT, V., SEREEMASPUN, A. & ROJANATHANES, R. 2009. Gold nanoparticles and a microscopic view of platelets: a preliminary observation Short Communication. *Cardiovascular Journal of Africa,* 20**,** 142-143.

WOLFENSON, H., LAVELIN, I. & GEIGER, B. 2013. Dynamic regulation of the structure and functions of integrin adhesions. *Dev Cell,* 24**,** 447-58.

WOLINSKY, J. B., COLSON, Y. L. & GRINSTAFF, M. W. 2012. Local drug delivery strategies for cancer treatment: gels, nanoparticles, polymeric films, rods, and wafers. *J Control Release,* 159**,** 14-26.

WONG, C. H., JENNE, C. N., PETRI, B., CHROBOK, N. L. & KUBES, P. 2013. Nucleation of platelets with blood-borne pathogens on Kupffer cells precedes other innate immunity and contributes to bacterial clearance. *Nat Immunol,* 14**,** 785-92.

WOOLLEY, R., ROY, S., PRENDERGAST, U., PANZERA, A., BASABE-DESMONTS, L., KENNY, D. & MCDONAGH, C. 2013. From particle to platelet: optimization of a stable, high brightness fluorescent nanoparticle based cell detection platform. *Nanomedicine,* 9**,** 540-9.

WU, C., ASOKAN, SREEJA B., BERGINSKI, MATTHEW E., HAYNES, ELIZABETH M., SHARPLESS, NORMAN E., GRIFFITH, JACK D., GOMEZ, SHAWN M. & BEAR, JAMES E. 2012. Arp2/3 Is Critical for Lamellipodia and Response to Extracellular Matrix Cues but Is Dispensable for Chemotaxis. *Cell,* 148**,** 973-987.

WULF, E., DEBOBEN, A., BAUTZ, F. A., FAULSTICH, H. & WIELAND, T. 1979. Fluorescent phallotoxin, a tool for the visualization of cellular actin. *Proc Natl Acad Sci U S A*, 76**,** 4498-502.

YAMADA, S., POKUTTA, S., DREES, F., WEIS, W. I. & NELSON, W. J. 2005. Deconstructing the cadherin-catenin-actin complex. *Cell*, 123**,** 889-901.

YANG, H. C. & PON, L. A. 2002. Actin cable dynamics in budding yeast. *Proceedings of the National Academy of Sciences of the United States of America*, 99**,** 751-756.

YAO, L. 2008. *Fabrication, characterization and application of the novel bionanomaterials.* PhD, University of Rhode Island.

YAO, L., DANIELS, J., WIJESINGHE, D., ANDREEV, O. A. & RESHETNYAK, Y. K. 2013. pHLIP (R)-mediated delivery of PEGylated liposomes to cancer cells. *Journal of Controlled Release*, 167**,** 228-237.

YAO, L., DANNIELS, J., MOSHNIKOVA, A., KUZNETSOV, S., AHMED, A., ENGELMAN, D. M., RESHETNYAK, Y. K. & ANDREEV, O. A. 2012. pHLIP peptide targets nanogold particles to tumors. *Proceedings of the National Academy of Sciences*.

YGUERABIDE, J. & YGUERABIDE, E. E. 1998. Light-scattering submicroscopic particles as highly fluorescent analogs and their use as tracer labels in clinical and biological applications - I. Theory. *Analytical Biochemistry*, 262**,** 137-156.

YIN, H. L. & STOSSEL, T. P. 1979. Control of cytoplasmic actin gel-sol transformation by gelsolin, a calcium-dependent regulatory protein. *Nature*, 281**,** 583-6.

YOON, Y., PITTS, K. & MCNIVEN, M. 2002. Studying cytoskeletal dynamics in living cells using green fluorescent protein. *Mol Biotechnol*, 21**,** 241-50.

YOSHIKAWA, T. 1991. Changes in cytoskeletal structure during adhesion of human platelets: A transmission electron microscope study. *Journal of the Osaka City Medical Center,* 40**,** 613-643.

ZHANG, Q., TANG, J., FU, L., RAN, R., LIU, Y., YUAN, M. & HE, Q. 2013. A pH-responsive alpha-helical cell penetrating peptide-mediated liposomal delivery system. *Biomaterials,* 34**,** 7980-93.

ZHANG, W., SONG, J. J., ZHANG, B. Z., LIU, L. W., WANG, K. R. & WANG, R. 2011. Design of Acid-Activated Cell Penetrating Peptide for Delivery of Active Molecules into Cancer Cells. *Bioconjugate Chemistry,* 22**,** 1410-1415.

ZHAO, M., KIRCHER, M. F., JOSEPHSON, L. & WEISSLEDER, R. 2002. Differential conjugation of tat peptide to superparamagnetic nanoparticles and its effect on cellular uptake. *Bioconjugate Chemistry,* 13**,** 840-844.

ZHONG, C. J., BRUSH, R. C., ANDEREGG, J. & PORTER, M. D. 1999. Organosulfur monolayers at gold surfaces: Reexamination of the case for sulfide adsorption and implications to the formation of monolayers from thiols and disulfides. *Langmuir,* 15**,** 518-525.